Deciphering the key conditions required to build a 3D biomimetic vascularized and innervated skeletal muscle-on-chip

Manh-Louis Nguyen

PSL UNIVERSITÉ PARIS

THÈSE DE DOCTORAT
DE L'UNIVERSITÉ PSL

Préparée à l'Institut Curie et à l'Institut Pierre Gilles de Gennes pour la Microfluidique

Deciphering the key conditions required to build a 3D biomimetic vascularized and innervated skeletal muscle-on-chip

Etude des éléments clefs nécessaires à la création d'un muscle squelettique 3D biomimétique et vascularisé sur puce microfluidique

Soutenue par

Manh-Louis NGUYEN

Le 15 Mars 2022

Ecole doctorale n° 388

Chimie Physique et Chimie Analytique Paris Centre

Spécialité

Ingénierie Tissulaire, organe-sur-puce et microfluidique

Composition du jury :

Danijela, VIGNJEVIC Directeur de recherche, Institut Curie	*Président*
Cécile, LEGALLAIS Directeur de recherche, Université de technologie de Compiègne	*Rapporteur*
Xavier, GIDROL Directeur de recherche, Commissariat à l'énergie atomique et aux énergies alternatives, Grenoble	*Rapporteur*
Olivier, BENVENISTE Professeur universitaire – Praticien Hospitalier, Hôpital Pitié-Salpêtrière, service de médecine interne et immunologie clinique	*Examinateur*
Laurent, MALAQUIN Directeur de recherche, Laboratoire d'analyse et d'architecture des systèmes, Toulouse	*Examinateur*
Edgar, GOMES Directeur de recherche, Institut de Médecine Moléculaire de Lisbonne, Portugal	*Examinateur*
Stéphanie, DESCROIX Directeur de recherche. Institut curie	Directeur *de thèse*

institutCurie | PSL

A mon père et ma mère

To my father and my mother

« If you think you are too small to make a difference, try sleeping with a mosquito"
Dalai Lama

Remerciements

Il y a beaucoup de personnes que j'aimerais remercier, et que je remercie encore pour m'avoir donné la possibilité d'être ce que je suis aujourd'hui. Je remercie remercie mon père, ma mère et mes deux frères de m'avoir soutenu depuis ma tendre enfance, de toujours avoir mis au premier plan mon éducation, mon bien être et de m'avoir transmis cette richesse qu'est ma double culture franco-vietnamienne.

Je remercie mes professeurs qui m'ont tant marqué au collège, au lycée et durant mes études supérieures. Après une période de lycée où je me suis beaucoup épanouï sur le plan personnel, sans que les notes ne suivent obligatoirement, je me suis retroussé les manches et ai redoublé d'effort pour réussir mon concours de première année de médecine à l'Université Pierre et Marie Curie en 2009. Durant mes études de médecine, je m'estime chanceux d'avoir rencontré de formidables médecins, compétents et humains, qui sont devenus pour moi des modèles à suivre.
Après le concours de l'internat de médecine en 2015, j'ai choisi de rester à Paris dans une spécialité médicale méconnue mais loin d'être inintéressante : la génétique médicale. Tantôt au lit du patient, tantôt en paillasse analysant son génome, cette spécialité en pleine expansion m'a permis d'allier le soin et la recherche. Cependant, après avoir sauté dans le train de la médecine, j'avais l'intime conviction qu'il y avait une voie que je désirais explorer. Cette voie, c'était la Physique.

En 2017, j'ai donc décidé de reprendre mes études, en Master 2 de Physique spécialisé en microfluidique, une branche de la mécanique des fluides. Je voudrais remercier tout particulièrement Marie-Caroline Jullien, à l'époque responsable de ce master 2 et professeur de mécanique des fluides à l'ESPCI. Je me rappelle encore de sa question : « mais dîtes-moi, ça fait combien de temps que vous n'avez pas fait de physique ? ». Dès lors, après l'hôpital et ce toutes les nuits, je reprenais les cours de physique et de mathématiques de terminale, de licence, puis de master. Je m'arrangeais pour venir à ses cours lors que je pouvais, et participais activement à la résolution des exercices. Marie-Caroline, je te remercie donc de m'avoir fait confiance et de m'avoir accepté au Master 2 de Microfluidique !

J'aimerais également remercier Stéphanie Descroix, qui a depuis toujours été là pour moi. D'abord en stage de Master, puis en thèse, tu m'as toujours fait confiance. Le laboratoire que tu diriges est unique en son genre, et tu y es pour beaucoup. Je pense sincèrement que l'environnement de recherche que tu instaures au laboratoire nous permet d'être nous-même et nous donne la volonté de nous surpasser à chaque instant. Merci Stéphanie pour ta patience, ta bienveillance et tes bons conseils !

Enfin j'aimerais remercier ma fiancée, Sérina Demetz, sage-femme, avec qui j'ai maintenant passé 10 merveilleuses années. Je remercie tous mes amis, mes collègues de bureau, mes collègues de laboratoire et mes collègues musicaux ! C'est aussi grâce à vous que ma personnalité se forge tous les jours.

TABLE OF CONTENTS

PREAMBLE

Have you ever wondered how many muscles we have in our body? From the muscles that move our toes to the ones that move our eyes, there are approximately more than 600 muscles we can voluntarily contract [1]. All human activities rely on them. If not for them, there wouldn't be The Beatles or great artists such as Leonardo da Vinci. Animals can move quickly, to flee, to hunt and to travel long distances to conquer new territories. Muscles are crucial in evolution. They already existed in ancestral animals that lived more than 500 million years ago, the Cnidarians (Figure 1) [2]. Are there any animals without any muscles at all? We could amusingly wonder if such animals exist (and they do) but let's talk about muscles.

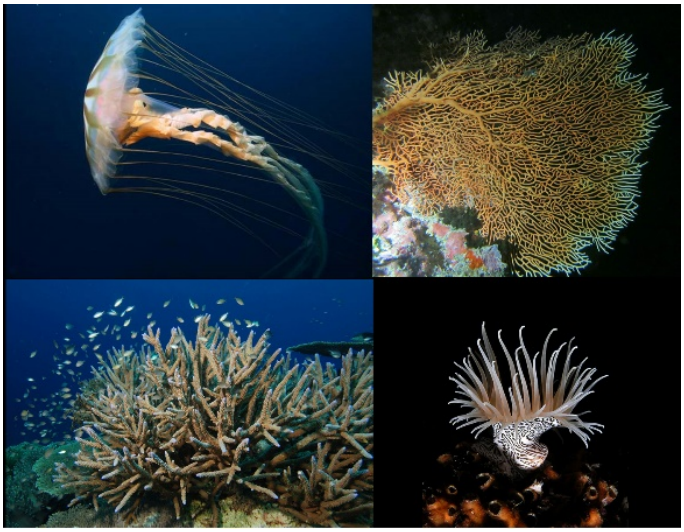

Figure 1 : Some examples of Cnidarian animals. From wikipedia.org.

What is a muscle? In our daily life, muscles appear in many ways: the meat we eat, our heart beating, people going to the gym lifting weights or when we run trying to catch the bus. Every one of these things have a common point: muscle activity. On the other hand, many situations result in the lack of muscle function such as: starvation, traumatic surgeries, injuries, and medical conditions. Obviously, these situations are extremely debilitating. It is therefore of a major importance to deeply understand how muscles work in order to restore the functionality when it's lost.

As we will discuss in detail below, there is an increasing need to develop new *in vitro* skeletal muscle models. Hereditary myopathies, ageing and bio prosthetics are not the only concerned fields: soft robotics and food industry start to seriously consider bio engineered skeletal muscles. Animal models and petri dish cultures have proven their limits to recapitulate *in vivo* human skeletal muscles. Bio engineered skeletal muscles are therefore currently shifting toward more complex 3D structures.

I had the opportunity to work within the MyoChip project[a] that was funded in the late 2018 by the European Commission. The aim of the MyoChip project is to gather human and financial resources to tackle the tough scientific challenge of building a 3D vascularized skeletal muscle that is innervated by neurons on a microfluidic chip. The MyoChip consortium gathers four research teams (Figure 2): Instituto de Medicina Molecular (Lisbon, Portugal), Institut Curie (Paris, France), The University of Edinburgh (Edinburgh, UK) and Fluigent Company (Paris, France).

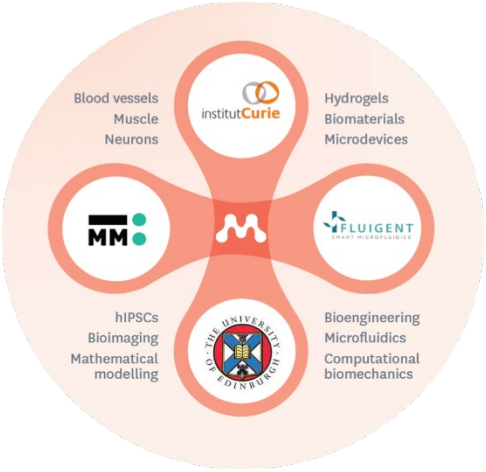

Figure 2: MyoChip partners: Instituto de Medicina Molecular (IMM, Lisbon, Portugal), Institut Curie (Paris, France), The University of Edinburgh (Edinburgh, UK) and Fluigent Company (Paris, France).

Together, they proposed a strategy to face this scientific challenge. First, we will have to find the optimal conditions to separately cultivate muscle, vessel, and neuronal constructs on-chip as they will be the fundamental building blocks (Figure 3). Secondly, a proper scaffold must be created. Finally, each building blocks are assembled to make a vascularized and innervated muscle (Figure 4).

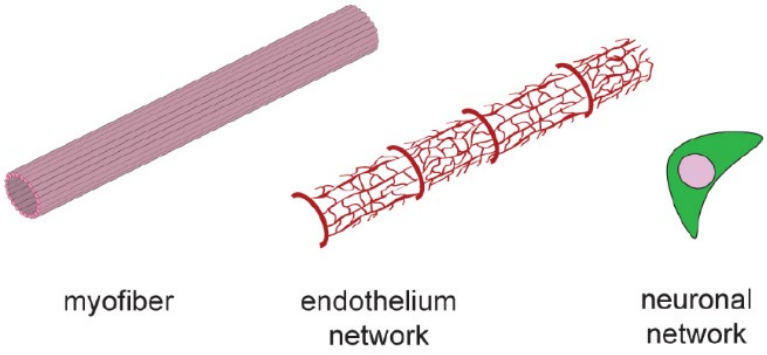

Figure 3: Generating the building blocks for muscle construction.

The key point of this project is to embrace complete 3D vascularized and innervated muscle construction in the most biomimetic environment as possible. Thus, one relevant geometry was conceptualized as parallel multi tubular system (Figure 4). This will not only allow to generate blood vessel-like structures, but muscle cells will also have physical cues to growth along the tube axis,

[a] https://cordis.europa.eu/project/id/801423

hence generating muscles fibers. The biocompatible scaffold will also host the neuronal network. Finally, the device must be connected to a fluidic interface to perfuse the system. As we can see, this is a tough scientific challenge. Bringing the expertise of each team within this interdisciplinary consortium is then critical.

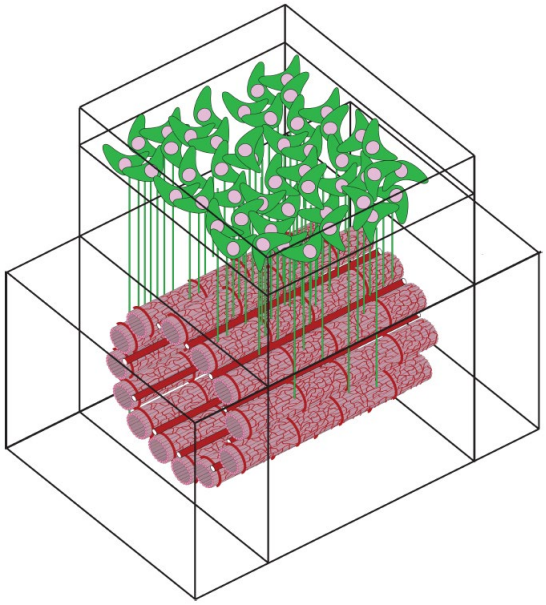

Figure 4: Assembling the building blocks to generate a 3D vascularized and innervated muscle.

Within the Institut Curie's team, and especially at the Institut Pierre Gilles de Gennes pour la microfluidique (IPGG), I built the parallel multi tubular system within the biomimetic scaffold. Then, the system was used to cultivate different cell types on-chip. Each time, I tried to decipher the optimal conditions for on-chip cell culture. Finally, with all the knowledge gathered from these experiments, I tried to co-cultivate muscle cells with different other cell types to build a biomimetic skeletal muscle on-chip.

This thesis is going to articulate as following:

- **Chapter 1** is an introduction about skeletal muscles. Herein, I will talk about the particularities of the muscle tissue and discuss about current *in vitro* models that exist and why it is important to develop new ones.
- **Chapter 2** gathers all the information about my experimental workflow. I will discuss about the chip microfabrication and the details about on-chip cell culture.
- **Chapter 3** shows the results about on-chip skeletal muscle cells cultures. Herein, I will discuss about the optimizations made to reach a differentiated skeletal muscle tissue on-chip, and will characterize it.
- **Chapter 4** shows the results of other cell type cultures on-chip, and their co-culture with muscle cells. I will discuss the successful technology transfer to collaborators at Institut Curie that resulted in micro-vessel on-chip generation, and how we took advantage of these results for co-cultures with muscle cells.
- **Perspectives and conclusion** chapter discusses about collaborative projects using the MyoChip device, such as the one with Institut Necker Enfants Malades (Paris) for bronchi-on-chip generation to study cystic fibrosis, as well as other projects.

CHAPTER 1: INTRODUCTION

1. Muscles and society

About 40 % of all our body weight is made of skeletal muscles [3], the ones we voluntarily contract, unlike the heart muscle or the smooth muscles that surround our blood vessels. While skeletal muscles allow us to breathe (thanks to the diaphragm muscle) and move, they also have a very important metabolic function. It is a source of heat when the weather is cold [4] and of energy in times of starvation [3]. It maintains the body posture and allows precise movements. Hence, there is no doubts that studying skeletal muscles is very interesting from many perspectives.

- **Sports**

We all know that exercising can improve muscle functions. Stamina training (e.g., swimmers) not only enhances the cardiovascular system, but also help skeletal muscles to develop. But it will develop toward a muscle fiber type called "slow-twitch muscle" that can endure longer effort but with little force generated [5]. On the other hand, strength and power training (e.g., weight lifters or sprinters) tend to develop muscles toward a muscle fiber type called "fast-twitch muscle", sustaining short burst of efforts [5].

These fast and slow-twitch muscles are distinguishable macroscopically and microscopically. Slow-twitch muscles consumes a significant amount of oxygen. To maintain this aerobic oxidative respiration through time, muscles synthesize more myoglobin to store more oxygen, mitochondria density and vascularization are much higher. This molecule gives the red color of these oxidative muscles. Fast-twitch muscles, consume *in situ* glucose through an anaerobic glycolysis. With repetitive training, muscle cells store more glucose within glycogen grains. That gives the white color of these glycolytic muscles. There is a large spectrum between these two types of muscles depending on their molecular contents (i.e., different isoforms of myosin heavy chain protein). Switching from one type to another depends on the type of training. It has been recently shown that epigenetic modifications and micro RNA are involved in that switch [6]. Hence, better understanding these modifications can help us fight against muscle waste during medical conditions and enhance patients' quality of life.

- **Artificial meat**

Recently, food industry got interested in muscle engineering for the purpose of developing "artificial meat" or "cultured meat" [7]. It especially aims to cultivate meats in labs from animal biopsies. They then isolate stem cells and cultivate them until reaching a critical mass [8]. According to MarketsandMarkets Research Company, the meat substitutes market is estimated at USD 1.6 billion in 2019, and is projected to reach USD 3.5 billion by 2026[b].

[b] https://www.marketsandmarkets.com/Market-Reports/meat-substitutes-market-979.html

Artificial meat actually has four main branches: meat substitutes, *in vitro* meat, genetically modified organisms and cloned animals. Meat substitutes are currently the most commercialized as meat replacement products. The process extracts alternative proteins from soy, wheat proteins or mycoproteins. *In vitro* meat recently got more attention in 2013 when the first eatable meat-in-lab was produced in 2013 by Mark Post's lab in the Netherlands (Figure 5) [9].

Figure 5: Sample of in-vitro meat held by Mark Post. Source : https://www.nytimes.com/2013/08/06/science/a-lab-grown-burger-gets-a-taste-test.html

It cost more than 300,000$ to produce and got financially helped by Google Company. Of course this is a very controversial and hot topic [10]. *In* vitro meat defenders see advantages: less impact on the climate change in comparison to conventional meat industry [11] even though not everyone agrees [12], less killed and abused animals; more food in an overpopulated world. But artificial meats have lots of drawbacks. A lot of reagents derived from animal and a lot of antibiotics are currently used for *in vitro* meat.

Recently, for the first time in history, lab-grown meat is available for delivery. In Singapore, we can now order *in vitro* chicken meat from the company Eat Just[c]. In July 2021, the company Nestlé announced a partnership with the startup Future Meat Technologies to explore lab-grown meat[d]. Although there is still a way to go before reaching the dream of making clean meat without killing animals, it is obvious that this market is growing exponentially.

- **Bio-prosthetics**

Engineering also makes use of muscle biology understanding. Prosthetics field in itself does already an astonishing work. Some celebrities already benefit from prosthetics limbs that significantly enhances their life, such as celebrity Angel Giuffria from the Hunger Games TV show (Figure 6). The robotics field is especially very creative. Thus, making robotic actuators with a biological tissue and electronically contract them with electrodes to mimic a human arm has been achieved (Figure 7) [13].

[c] https://www.cnbc.com/2021/03/01/eat-just-good-meat-sells-lab-grown-cultured-chicken-in-world-first.html
[d] https://www.nestle.com/media/news/nestle-explores-emerging-technologies-cultured-meat

Figure 6: Actress Angel Giuffria from the TV show Hunger Games, holding a box with a prosthetic arm.

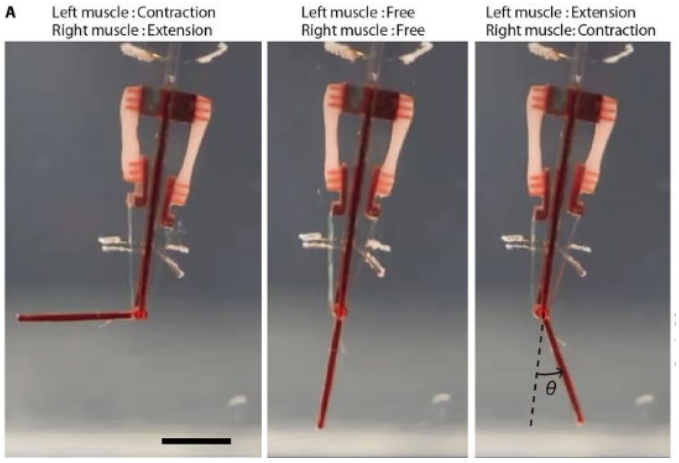

Figure 7: Motions of bio hybrid robot powered by skeletal muscle tissue [13]. Scale bar is 5 mm.

As soft implantable microelectrodes field of research is growing fast [14] in parallel with some remarkable applications (Parkinson's disease [15]), bio-prosthetics can highly benefit from a better understanding of skeletal muscle generation. In the future, if combining prosthetic engineering with tissue engineering is reached, it is thrilling to imagine what we would be able to do. This can bring medicine and surgery to new horizons.

2. Muscles and medicine

Physicians deal with all kinds of diseases on a daily basis. While genetic diseases such as muscle dystrophies obviously affect skeletal muscles, there is actually a larger spectrum of medical conditions that affect the skeletal muscles as well [16], [17].

- **Skeletal muscle wasting**

While caring for the acute diseases, it's also critical to fight against physical deconditioning. Indeed, as a patient is healing on hospital's bed, "muscle wasting" occurs. This phenomenon is characterized by a loss of muscle mass and it affects both acute diseases and nearly every chronic

diseases our society faces nowadays such as diabetes or cancers [18]. This phenomenon has been largely studied to develop therapies specifically designed to decrease muscle wasting. While complex molecular pathways are involved, muscle waste fundamentally results from intra cellular myofibril proteins damages [17]. Those proteins are the one involved in muscle contraction and constitute more than 70% of muscle proteins. These molecular mechanisms have mainly been studied in animal models or in petri dish cultured cells. Although the only current validated treatment is physical rehabilitation and exercising, some drugs have been reported to decrease muscle waste [17], [18]. Therefore, developing new biomimetic skeletal muscle models that allow human cells to be cultivated within can greatly improve drug screening.

Sarcopenia is another skeletal muscle waste condition, associated with ageing even without disease [18]. As the life expectancy is increasing in most of the developed countries, the global population is also aging. According to the World Health Organization (WHO), the world's population aged over 60 years will double from 900 million people to 2 billion people in 2050[e]. Sarcopenia leads to higher mortality and morbidity in elderly people [19]. It results in loss of independence, to institutionalizations or prolonged hospitalizations. As the world's population is ageing, sarcopenia increases health costs and is a major burden to society. Indeed, ageing biology is key to understand why organisms degrade through time. Nonetheless, new skeletal muscle models can uncover new fields of research in ageing biology. Being able to cultivate patients' muscle tissue from biopsies on biomimetic micro devices will allow studying the mechanisms of sarcopenia in real time. These new models will be more physiologic than model animals or petri dish cultures.

- **Muscular dystrophies (MD)**

Muscular dystrophies are a heterogeneous group of genetically inherited degenerative disorders of muscle defined by progressive muscle weakness and by pathologic features on muscle biopsy. Although the most common one is the Duchenne muscular dystrophy (DMD), that affects about 7.1 per 100 000 males worldwide in 2020 [20], there are more than 30 different types of muscular dystrophies associated with different gene mutation [21].
While dystrophies are considered as rare diseases (i.e., affecting less than 1/2000 persons[f]), they have an enormous socioeconomical impact and are a burden for the health system. For instance, DMD healthcare cost is about (per year per patient) 40 000 € in the US [22], 30 000 € in the UK, 50 000 € in France and 100 000 € in Germany [23]. As a comparison, healthcare for cardiovascular diseases, that are the first cause of death worldwide, costs about 76 000 € when taking into consideration absolutely all the medical interventions [24]. The main reason for that is because there is currently no curative treatment for dystrophies even though some clinical trials are promising [21].

The main hindrance of drug studies is the poor transposability of the results from animals to humans [25], since the mouse model is the most extensively used model for muscular dystrophies studies [26]. For instance, one main feature of DMD is the poor regenerative capacity of muscle in human, that is not reproduced in the standard mouse model [25]. Better skeletal muscle models are

[e] https://www.who.int/news-room/fact-sheets/detail/ageing-and-health
[f] https://www.orpha.net/consor/cgi-bin/Education_AboutRareDiseases.php?lng=EN

therefore required to closer mimic human *in vivo* physiology.

- **Pre-clinical drug trials**

Pre-clinical drug trials gather all the experiments done on animals to assess if a treatment or procedure is likely to be useful, before anything is tested on humans[g]. Animal models and especially mouse model, are widely used in biomedical research. Even after mouse studies suggest that a treatment will be efficient, it fails with a rate of 80% when tested on people [27]. It has been reported that it may be due to both poor pre-clinical studies design and physiologic differences between animal and humans [28], [29]. For instance in amyotrophic lateral sclerosis disease, it has been stated that this led to a loss of confidence in the relevance of these models [30]. As we previously mentioned, some features exhibited in human DMD are not well recapitulated in mouse models [25] and the necessity of more human-relevant skeletal models are now greatly emphasized.

In conclusion, skeletal muscles are substantially part of our daily life. Whether it is to make meat without killing animals, for bio-prosthetics, to better understand muscles behavior in sports or to create models for diseases studying and drug screening, I hope it now appears obvious that studying skeletal muscle is crucial and requires new approaches. To do so, our knowledge first start with *in vivo* observation and understanding. We will thus in the next part, examine the structure of *in vivo* skeletal muscle.

3. *In vivo* skeletal muscle tissue

Skeletal muscle macroscopic structure is like Russian dolls, each structure being nested within the other [31]. If we look at a longitudinal section of a skeletal muscle (Figure 8), several elongated muscle cells (myotubes, or myofibers) are gathered into structures called fascicles. Then, several fascicles gather together to constitute the whole muscle. Each of these structures are all linked together by a rich and complex network of extra cellular matrix.

3.1. Extra cellular matrix (ECM)

- **Structure and components**

Traditionally, the skeletal muscle ECM is subdivided into three interconnected main part [5], [31]. Each muscle cells are surrounded by the endomysium. Fascicles are surrounded by the perimysium. Finally, the whole muscle is surrounded by the epimysium (Figure 8). Intra muscular ECM has multiple functions [5]. It provides a biomechanical support for forces transmission to tendons and bones during a contraction, as well as a scaffold for blood vessels and nerves. It is also a support for cell-matrix interactions and can affect muscle regeneration through the basement membrane [25].

[g] https://www.cancer.gov/publications/dictionaries/cancer-terms/def/preclinical-study

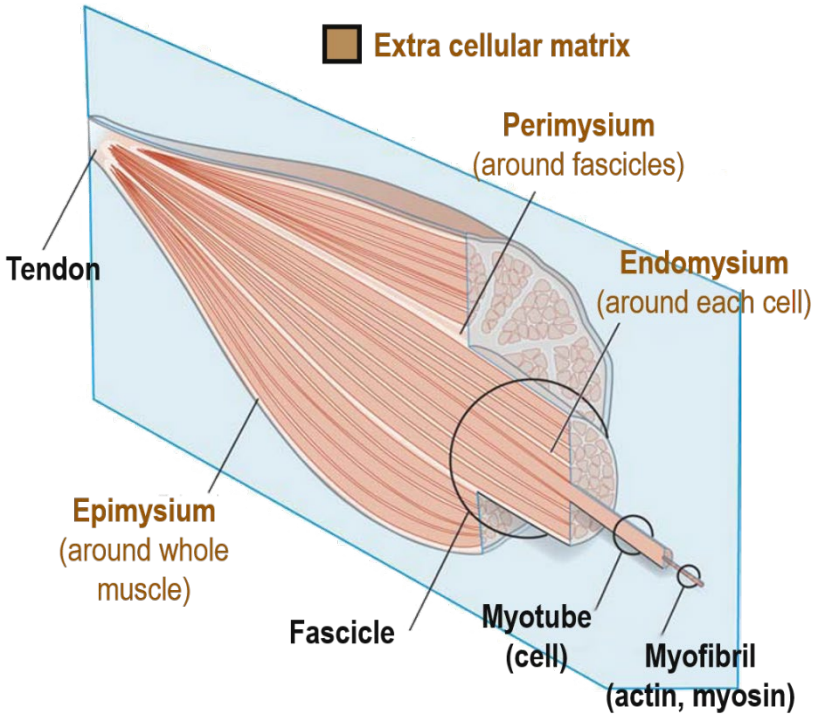

Figure 8: Skeletal muscle macroscopic structure, longitudinal section. The whole muscle is linked to bones at each end by tendons. Several muscle cells (myotubes) are gathered together within fascicles. Several fascicles gathered together constitute the whole muscle. Each of these structures are linked together by rich network of extracellular matrix. From [31].

While containing different proteins such as proteoglycans, glycoproteins and elastin, ECM is predominantly composed by collagen [32]. Up to 7 different types have been identified among which collagen type I has been reported to be the most common one [32]. The basement membrane, which is the layer separating muscle cells from the ECM, is mainly composed of laminin and collagen IV [31], [33]. Fibronectin is also part of this basement membrane and helps organizing the inter connection between all other proteins [5]. Obviously, the ECM has a much more complex organization with a lot more different proteins that maintain skeletal muscle homeostasis *in vivo*. But focusing on the main components will allows us to more efficiently build a model.

Skeletal muscle ECM is a very dynamic structure and its composition can greatly change throughout several circumstances such as exercising, disease, diet and age [5]. Continuous ECM degradation and synthesis are in equilibrium thanks to matrix remodeling enzymes that are secreted by skeletal muscle cells, but also by other cell types such as fibroblasts [34]–[36]. These cells reside in the extracellular matrix, between muscle cells and fascicles [25].

- **Fibroblasts**

Fibroblasts are the main type of cells of the ECM, producing the majority of ECM components [33], [37]. Although muscle cells also secrete some ECM components such as collagen I, it has been reported that the presence of fibroblasts is crucial for the assembly of this collagen into functional ECM [33], [38].

Skeletal muscle fibroblasts are involved in crucial processes such as muscle myogenesis, differential muscle fiber types development, regeneration and fibrosis [25], [33], [39], [40]. Upon injury, immune cells migrate toward the wound via the vascular system and secrete inflammatory factors

such as TGF-β and IL-1β that activate fibroblasts. They hence start to differentiate into myofibroblasts. Myofibroblasts are characterized by an increase proliferation rate, an increase in focal adhesion proteins (paxillin, vincullin, tensin) and an enhanced contractility with the expression of α-smooth-muscle actin (αSMA) [41], [42]. When αSMA stress fibers contract, they exert mechanical tension on the ECM hence the name 'myofibroblast'. Reconstructed 3D images from electron microscopy images show that fibroblasts wrap around collagen cables, thus displaying close relationships [33]. Myofibroblasts synthetize more collagen I compare to normal fibroblasts, hence contributing to fibrosis, which is an excessive accumulation of ECM that can impair muscle regeneration [25], [42]. A subpopulation of progenitors called fibro-adipogenic progenitors (FAP) can differentiate into fibroblast upon muscle injury [43], [44]. Their major contribution to muscle regeneration as well as to muscle dystrophy has attracted a considerable attention since their discovery. Indeed, cross-talks between FAPs and muscle stem cells (satellite cells) have been demonstrated [45].

- **Satellite cells**

Satellite cells (SC) are located just underneath the basement membrane, in really close contact with the muscle cell plasma membrane (Figure 9 [46]).

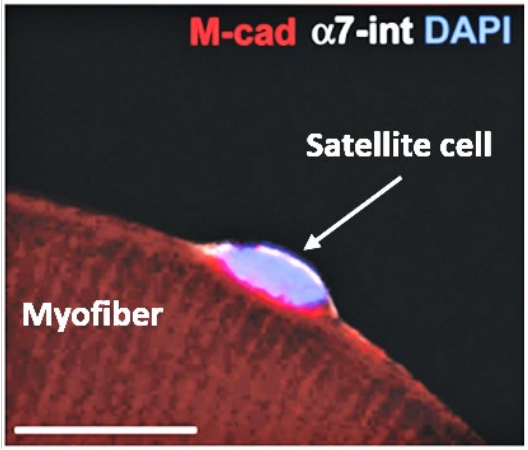

Figure 9: Human satellite cell stained with DAPI (blue) for the nucleus, M-cadherin (red) on supra nuclear side and α7 integrin (white) at infra nuclear side. From [46].

They are the muscle stem cells that mediate muscle regeneration [46], [47]. The main marker for is Pax7 that is ubiquitously express in all SC in a wide variety of species, but several cell surface membrane proteins have been identified as markers as well, such as M-cadherin, α7 and β1 integrins, CD34, vascular cell adhesion molecule-1 (VCAM1) and neural cell adhesion molecule-1 (NCAM1) [46]. They are normally quiescent in a healthy and undamaged adult muscle, but become activated in response to injury. They undergo a symmetrical division, maintaining the pool of SC. Some SC undergo asymmetrical division resulting in another pool of cells that differentiate into myogenic progenitors. It has been reported a proliferative exhaustion of SC in muscular dystrophies and with ageing with decrease regenerative capability [44]. However, removing SC from a dystrophic environment reveals that their regenerative capacity remains intact and is similar to SC derived from healthy muscle [48]. Host environment is therefore critical for controlling SC functions.

We saw that ECM is a complex structure, which is crucial for skeletal muscle homeostasis. It

also has an extremely organized architecture allowing skeletal muscle cells to be highly aligned, hence efficiently transmitting forces generated to tendons and bones. Some studies reported mechanical investigations of stiffness on whole mouse skeletal muscle, using tensile test on excised rats soleus muscles [49] or on mice extensor digitorum longus (EDL) and soleus muscles [50] yielding stiffness values around 150 kPa for healthy animals. Another work focused on the stiffness at the cultured cells scale, using C2C12 myoblasts and atomic force microscopy (AFM) yielding stiffness values around 45 kPa for differentiated cells [51]. Reyna *et al.* performed decellularization of the flexor digitorum profundus muscle from chicken to only retrieve the ECM [52]. They subsequently measured the extracted ECM stiffness using a tensile method. Stiffness values extracted from their data was around 300 kPa. Therefore, it appears that the skeletal muscle stiffness depends on the scale we are looking at. Our project aiming to recapitulate the skeletal muscle at the fascicle scale, and based on the literature, range of values around 45 kPa seems to be relevant for our MyoChip system.

3.2. Skeletal muscle cells

Skeletal muscle cells make up about 95% of a muscle's cross sectional area [33]. Indeed, skeletal muscles are composed of linear arrays of multinucleated muscle cells (also called 'muscle fibers', 'myofibers', or 'myotubes' at early stages of development [25]). These cells are post-mitotic cells, meaning they are differentiated and do not proliferate anymore. Each cells contain specialized structures called sarcomeres, which convert chemical energy to mechanical energy. Skeletal muscles, which contractions are mediated by motor neurons signals, need lots of energy. They therefore need a very dense network of vascularization [5]. Myogenesis is extremely complex and I won't go into details of this mechanism. However, we will see the main features of a mature skeletal muscle so we can have references while generating our own model.

3.2.1. Mature skeletal muscle criterions

- **A highly aligned structure**

Muscle cells are all aligned toward the long axis of the muscle, encapsulated within their ECM as shown in the Figure 10 [53]. This is a longitudinal section of a mammalian skeletal muscle stained with hematoxylin and eosin (H&E). It clearly shows aligned muscle cells (in pink), with a network of capillary network (arrows).

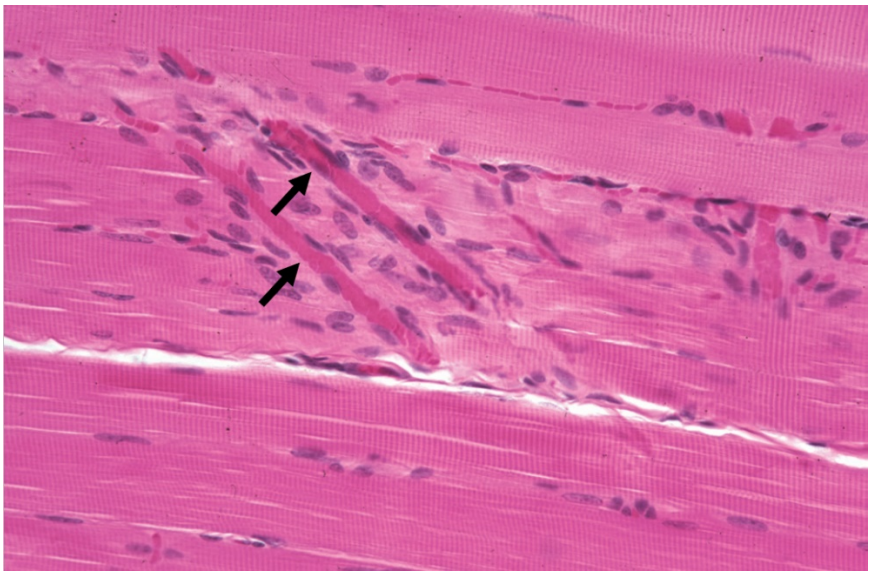

Figure 10: H&E staining of mammalian skeletal muscle, longitudinal section. Note the myofibers striations (pink), the peripherally located nuclei (dark blue) and the extensive capillary network (arrow). From [53].

A cross-section view shows the arrangement of the muscle cell (Figure 11 [54]). A mature muscle cell has an average diameter of several tens of μm and has a shape sometimes described as hexagonal, cylindrical or elliptical. We also see that several muscle cells gather into one fascicle (dashed black line). Fascicle's diameter is few hundreds of μm. Its length is few millimeters [55]. Each fascicle is separated to another by a slightly thicker ECM, corresponding to the perimysium. We can also note that blood vessels are located within the ECM (Figure 11, arrows).

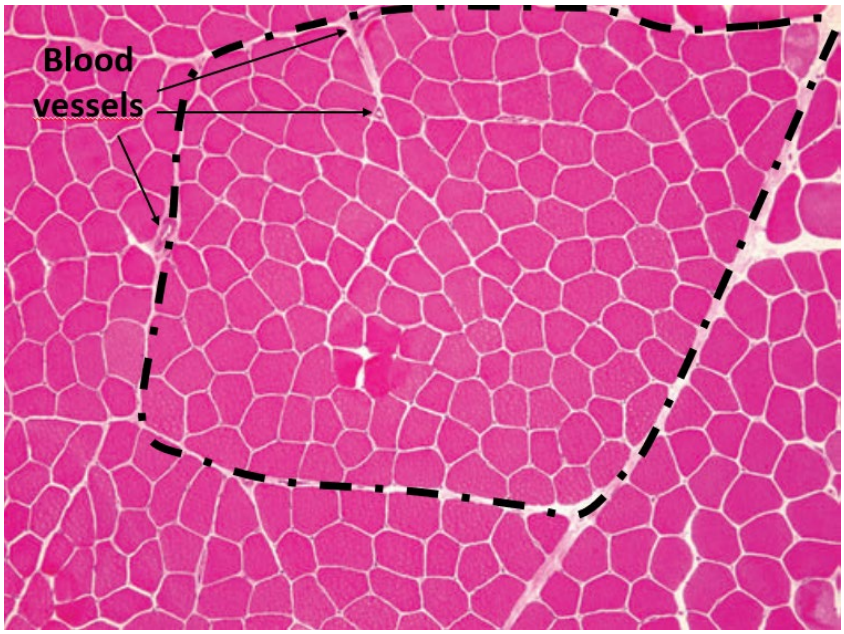

Figure 11: H&E staining of normal human adult skeletal muscle, cross section, ×100. The dashed black line represents one fascicule, which gathers several myofibers. Each myofibers had an average diameter of tens of μm. Blood vessels are located in the ECM. From [54].

When examining with higher magnification, another element reflecting cell alignment is the outstanding endomysium organization surrounding each single myofiber as shown in Figure 12 [56].

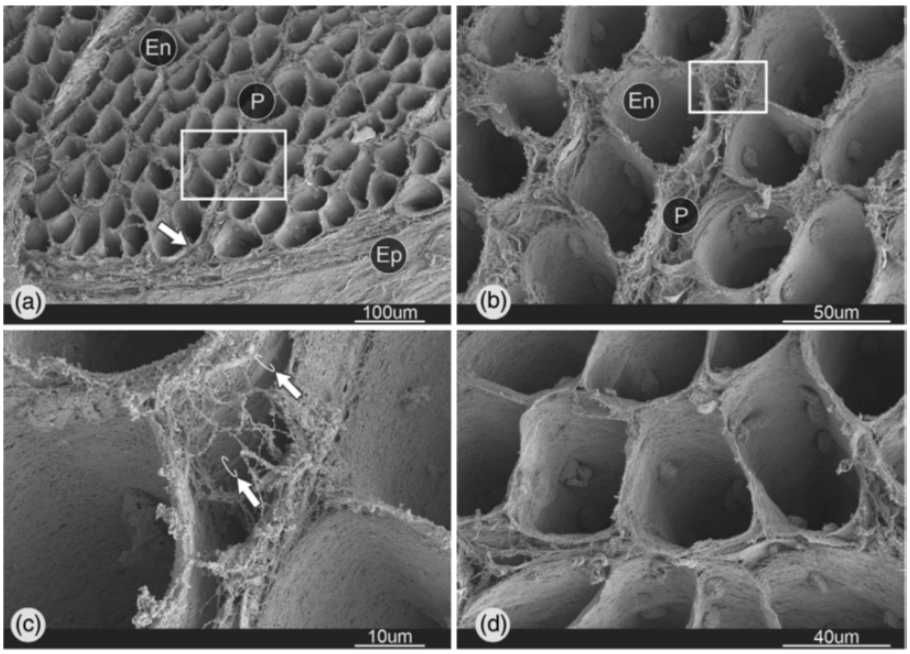

Figure 12: Scanning electron microscopy of the collagenous ECM after sample preparation and muscle cell digestion thus letting only the collagenous ECM in place. From [56].

It is a scanning electron microscopy image, took after muscle cells have been dissolved, thus only letting collagenous ECM in place. Endomysium overview (Figure 12.a) reveals an array of 'tubes' into which myofibers insert. This *in vivo* geometry is partly what inspired the MyoChip device fabrication, as we'll see in chapter 2.

A striking element is the complex continuous collagen network that span the entire cross section of skeletal muscles. Indeed, endomysium closely surrounds each myofiber. It then links to perimysium, located in thicken ECM part, that ultimately links to epimysium at the periphery of the muscle.

- **Multinucleated cells**

Skeletal muscle cells nuclei tell us a lot about their health state. When looking more specifically at nuclei, we see that they are specifically localized at the periphery of the cell, underneath the plasma membrane (Figure 13 [57]). Plus, myofibers are multinucleated cells as seen in Figure 10. Indeed, these unique characteristics derive from early stages of embryonic development, through myogenesis, where multiple myocytes fuse together to later constitute myofibers [1]. Skeletal muscle nuclei movement and positioning has been studied in more details recently. It is a unique feature in mammalian organisms [58]–[60]. Nuclei malposition can reflect various muscle state, such as regeneration, muscle waste or other diseases.

Some interesting parameters about skeletal muscle nuclei have been studied in *in vivo* mouse [61]. Using labelled DNA injection directly inside mice myofibers of anesthetized mouse, *in vivo* live imaging techniques and 3D reconstruction analysis, nuclei position could be precisely determined.

Dimensions. A nucleus has an average diameter of 10 μm, a long axis of about 18 ±2 μm and a short axis of about 5 ±1 μm. It is hence elongated, and strictly parallel to the myofiber axis in the *extensor digitorum longus* muscle, but deviates a bit from the cell axis in the soleus muscle.

Distribution. Along the length of myofibers, there was an average of 5 nuclei per 100 μm. Nuclei are regularly spaced, and their displacement is not significant through time.

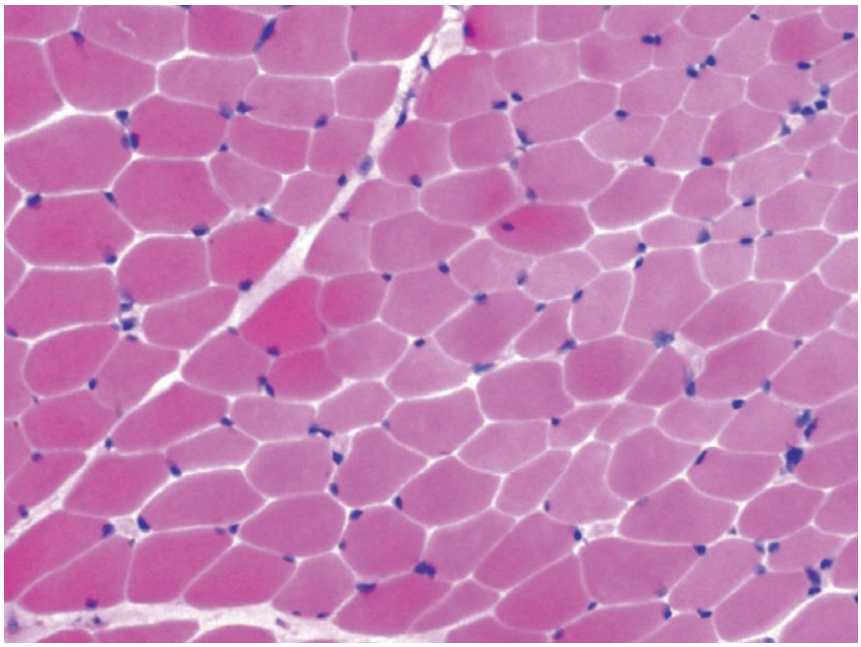

Figure 13: H&E stain of normal muscle. Note that nuclei (in blue) are all located at the periphery of cells. From [57].

The center-to-center distance between neighboring nuclei is 30 to 32 μm. Interestingly, nuclei were closer when neighboring neuromuscular junction or toward the myotendinous area.

Density. The nuclear density ranges from 30 to 77 nuclei per myofiber mm (hence about 3 to 7 nuclei per 100 μm of myofiber).

Nuclear positioning has been shown to depend on some specific proteins: nesprins and centrosomal proteins such as pericentrin [62]. Nesprins are transmembrane proteins that can be localized at the perinuclear space as well as in the cytoplasm. Indeed, it has been shown in mouse myoblasts (C2C12) that nesprin-1 signal is weak in undifferentiated cells and becomes prominent in at the nuclear envelope in differentiated myotubes [62]. On the other hand, nesprin-2 signal is important at the nuclear envelope in undifferentiated cells, and becomes weaker and mostly cytoplasmic in differentiated myotubes (Figure 14, Figure 15 [62]). This in turn leads to centrosomal proteins relocalization to the nuclear envelope. Thus, pericentrin signal is much more intense at the nuclear envelope in differentiated myotubes.

These nuclei characteristics found in mature skeletal muscle cells should be kept in mind while generating our model, to have landmarks for cell differentiation analysis. Another hallmark of these skeletal muscles, beside their unique nuclei features, are these striations we saw in Figure 10. That feature, found in skeletal and heart muscles, give them the 'striated muscle' aspect, as we sometimes called them. These striations are the contractile unit of the myofibers, called sarcomeres.

- **Sarcomeres (sarcomeric striations)**

Sarcomeres are the functional unit mediating forces generation in skeletal muscles [5]. Despite its very small size compared to the muscle, a single sarcomere only measuring about 2 μm in length [63], its molecular structure is very complex.

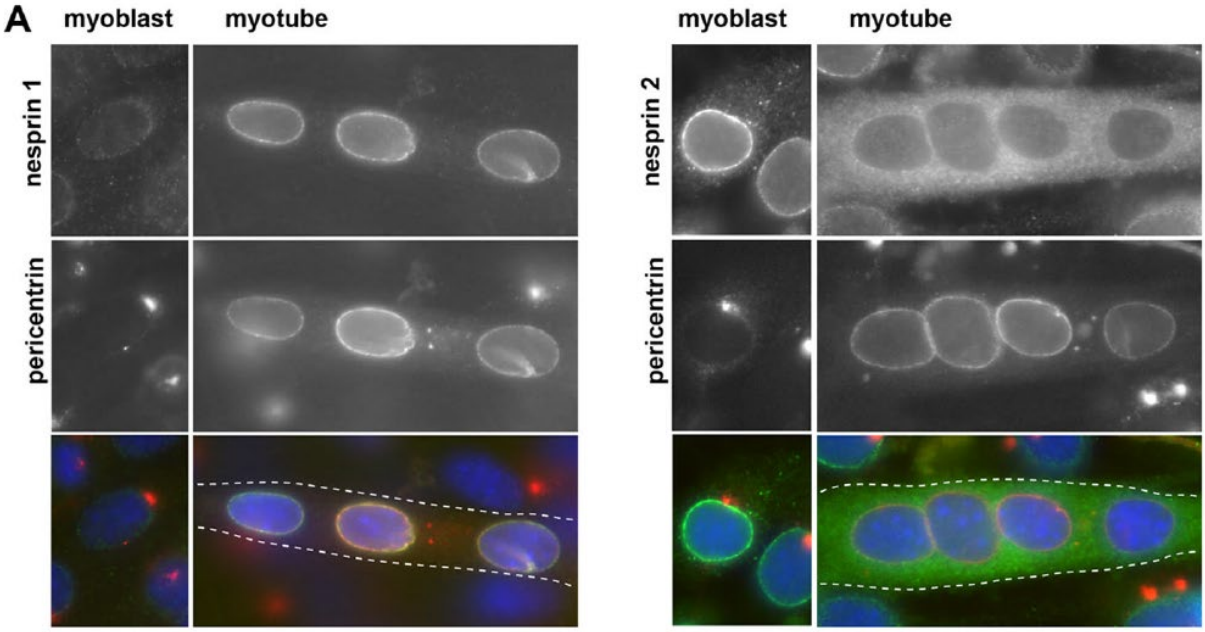

Figure 14: Localization of nesprins and pericentrin during C2C12 differentiation. Immunolocalization of nesprin-1 , nesprin-2 and pericentrin in proliferating myoblasts and in differentiated myotubes (green). Cell nucleus is stained in DAPI (blue). From [62].

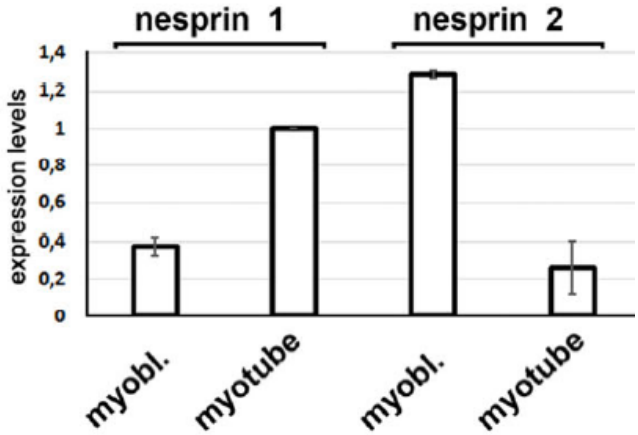

Figure 15: Total RNA RT-qPCR of nesprin-1 and nesprin-2 cDNA in myoblasts and differentiating myotubes. From [62].

In Figure 16.A[h], striations pattern are clearly visible in light microscopy imagng. But electron microscopy image below (Figure 16.B) shows a repetitive unit making these striations (small black rectangle).

A higher magnification (Figure 17[h]) shows that one sarcomere spans between two Z-bands, connecting it to the adjacent sarcomeres. Due to its alternating myofibrillar protein composition, alternated spaced I-bands (isotropic, lighter in light microscopy) and A-bands (anisotropic, darker in light microscopy) gives this striated aspect.

[h] Ovalle, W. K., & Nahirney, P. C. (2020). Netter's Essential Histology. Elsevier Health Sciences.

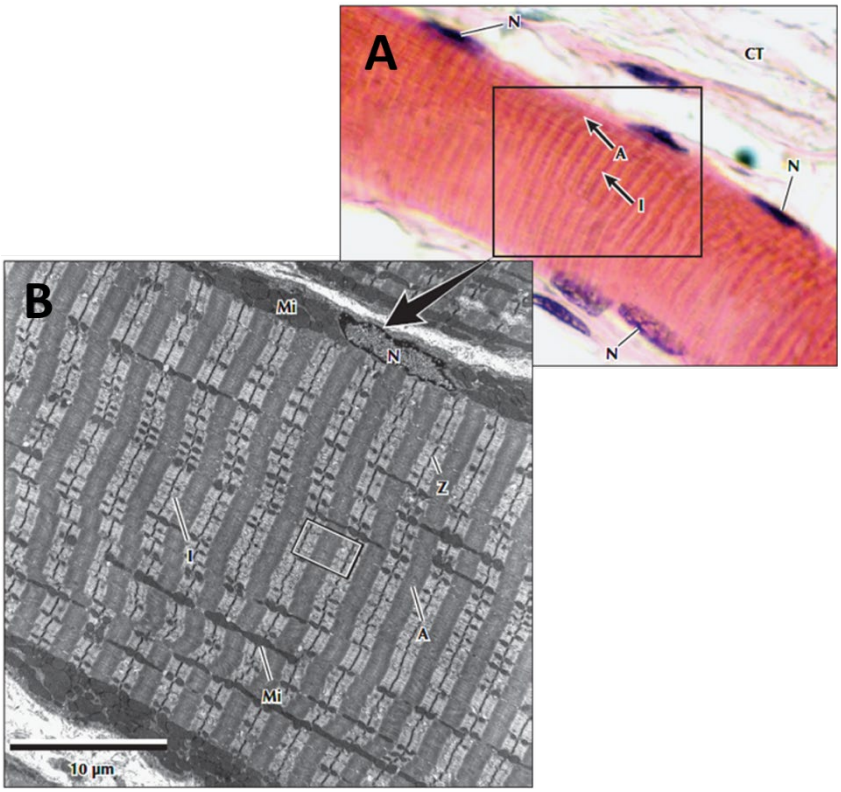

Figure 16: (A) Light microscopy image of part of a myofiber, longitudinal section. Note the regular striation pattern. N: nucleus. CT: connective tissue. A: sarcomere A bands. I: sarcomere I bands. (B) Electron microscopy image of the square area in light microscopy image. Striations appears to be a repetitive unit (small black rectangle). Mi: mitochondria. Z: sarcomeres Z lines.

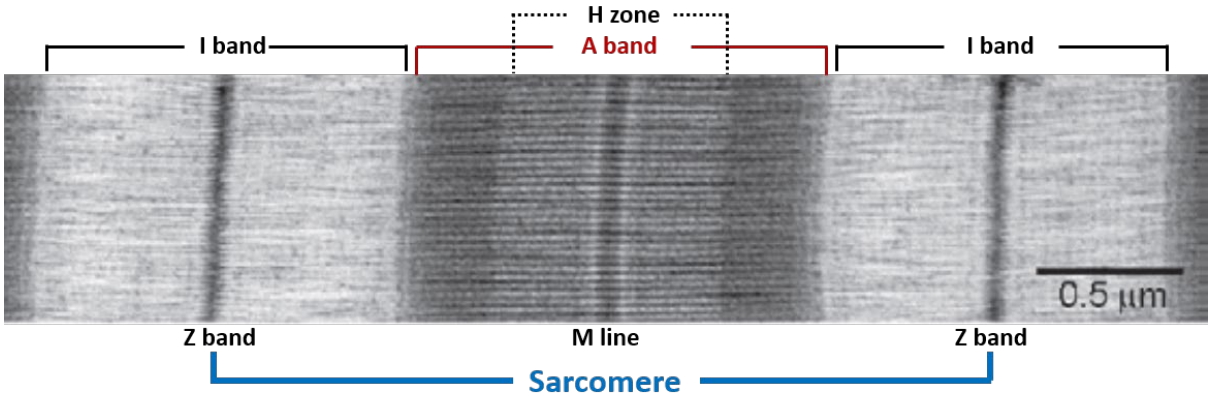

Figure 17: High magnification electron microscopy image centered on one sarcomere, showing its main limits. A sarcomere spans between two Z-bands, connecting sarcomeres together. Due to its alternating myofibrillar protein composition, alternated I-band (isotropic, lighter in light microscopy) and A -band (anisotropic, darker in light microscopy) gives this striated aspect.

Moving one step further into the sarcomere structure allows us to distinguish the main myofibrils (Figure 18). Sarcomere's myofibrils are thin actin filaments, and thick myosin filaments (Figure 18.B). Actin filaments of adjacent sarcomeres are linked by α-actinin protein in Z-bands.
Whole muscle contraction is actually the addition of all sarcomere's contraction along the muscle axis, with actin filaments sliding on thick filaments [64].

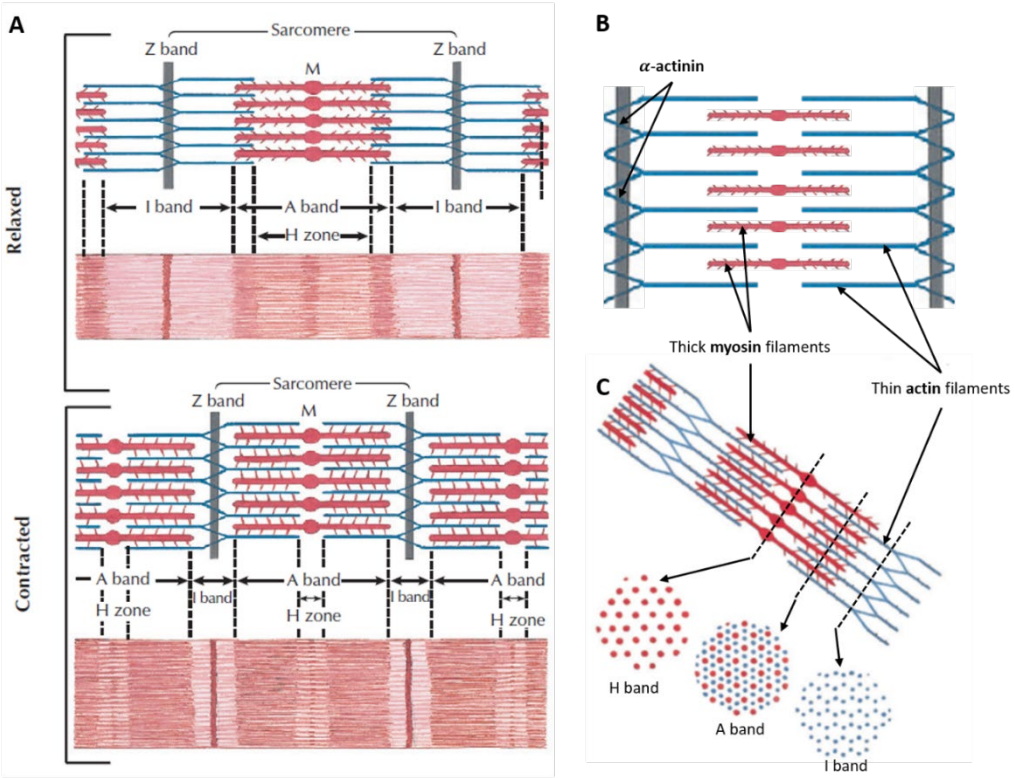

Figure 18: (A) Sarcomere schematics showing interdigitation of thick myosin filament and thin actin filaments, in relaxed state and contracted state. During contraction, thin actin filaments slide on thick myosin filaments: A-bands remain unchanged in length, I-bands and H-zones shorten. (B) Detailed view of the main myofibrils. (C) Cross sections of a sarcomere, showing the myofibrils composition of H band, A band and I band.

Sarcomere structure contains more proteins and the mechanism of contraction involve myosin filament heavy chain unit binding to actin filaments in a complex yet very elegant manner [65]. But I won't go into details in this work. Instead, we will keep in mind the main features for the skeletal muscle on-chip analysis: actin filaments, myosin filament and α-actinin protein, all displayed in a striated way.

- **Forces**

Skeletal muscle generates movement. Thus, one sign of maturation if also the forces generated by the tissue. Few studies investigates forces generated by *in vivo* human skeletal muscles, or in *ex-vivo* mouse skeletal muscles It is interesting to note that in these studies, human skeletal muscles generated about 150 up to 3000 N [66]. Forces measurement on mouse skeletal muscle have been reported, with values ranging from 40 mN to 5 N [67]–[69]. However, forces measurement on human was realized on real persons at whole muscle scale. Mouse's muscles on the other hand were took off a sacrificed mouse. If we were to measure forces in our device, it would be impossible to compare with these data. Therefore, at this stage, I won't consider it as a relevant output analysis for the MyoChip device.

Up to now, we have described the specificities of the ECM and some unique features of skeletal muscle cells. Nevertheless, we must not forget that it is also a high vascularized tissue, particularly when an effort must be made. And what makes the skeletal muscle stands out from the heart muscle and smooth muscle, is its innervation from motor neurons, we can voluntarily control.

3.2.2. Vascularization and motor innervation

- **Vascularization**

Skeletal muscles have a dense capillary network that bring them nutrients and oxygen. But this also serves as waste metabolites and heat removal, especially during an effort [70]. Micro vascularization of skeletal muscle has been studied since long ago, deciphering the overall organization one step at a time. It has been observed that, from arteries parallel to muscle axis, the arterioles emerged perpendicularly at constant intervals [71], [72].

In the Figure 19 [72], we clearly see the *in vivo* microvascular organization of the skeletal muscle at high magnification.

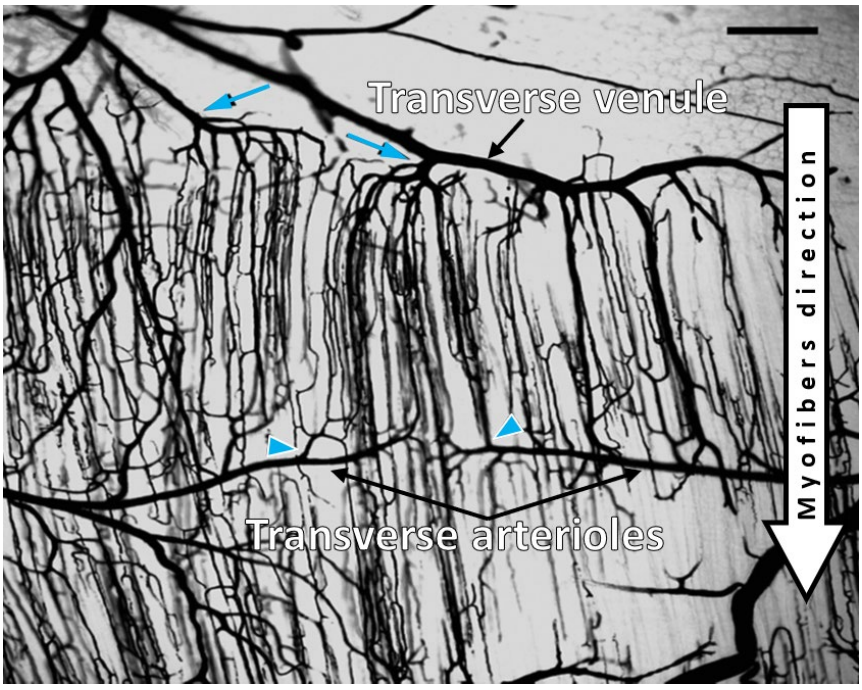

Figure 19: Light microscopy image showing microvascular organization in mouse gluteus maximus muscle. Blue arrowheads indicate two of the several terminal arterioles, arising perpendicularly from the transverse arterioles. Blue arrows indicate two collecting venules. Scale bar is 250 µm. From [72].

From main arteries parallel to muscle axis, they divide perpendicularly into arterioles as they deeply penetrate through the ECM between myofibers. Terminal arterioles then emerge from transverse arteriole, irrigating the portion of myofiber they are in close contact with. Exhausted blood is then drained by collecting venules up to main veins.

Figure 20 [73] illustrates this unique microvascular feature. Blood flow comes from longitudinal primary arteries along the outer side of the epimysium. Then feed arteries divide perpendicularly from them and penetrate the muscle before branching into arterioles. Arterioles keep branching through several orders until reaching terminal arterioles. Micro capillaries detached from these terminal arterioles and are in close contact with myofibers.

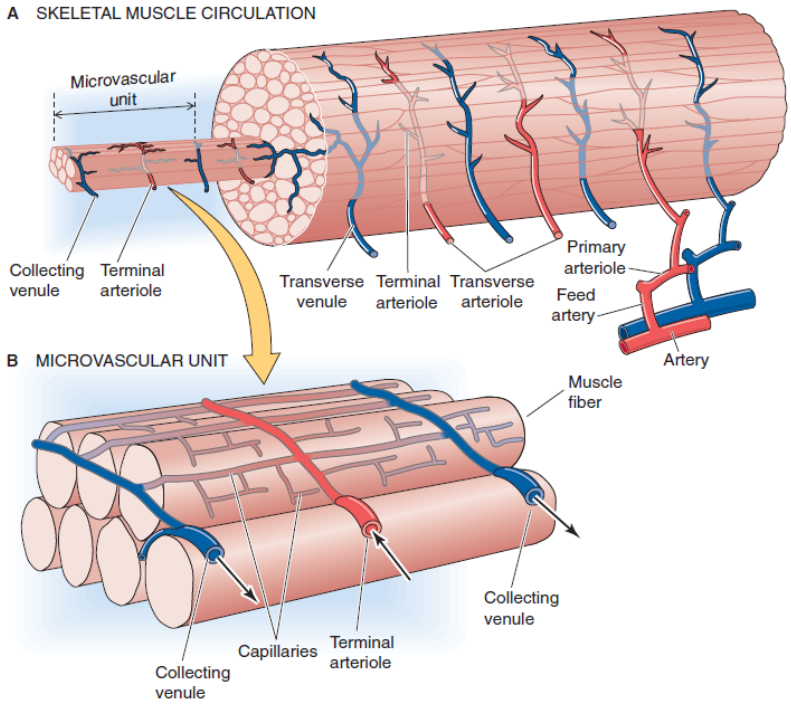

Figure 20: Schematics of skeletal muscle vascularization. (A) Arterioles detach from main arteries parallel to muscle axis. They divide perpendicularly as they penetrate through the ECM between myofibers. Terminal arteriole then emerge from transverse arterioles irrigating portion of the myofiber in contact with. Exhausted blood is drained by collecting venules. A microvascular unit is thus defined as an area of vascularization between one terminal arteriole and two collecting venules. From [73].

Lengths and diameters of arteries in mammals have been studied [73]–[76]. The average diameters are about few hundreds of µm for arteries, tens of µm for arterioles and few µm for capillaries. Therefore, by varying the diameter of the vessel, we can decide to study these different sub-branches of vascularization in the MyoChip device. It will of course also depend of technological limits. Another feature to consider is that those blood vessels divide into a dense micro capillary network embedded in the ECM that is close to myofibers (Figure 21). This therefore justifies the MyoChip parallel multi tubular design where each tissue will be close to each other, separated by ECM.

Finally, another cell type to consider for skeletal muscle modeling are the motor neurons, also visible on the Figure 21 as nerve embedded in ECM. This is crucial for skeletal muscle movement controls. Motor neurons therefore communicate with skeletal muscle through a specialized junction called the neuromuscular junction.

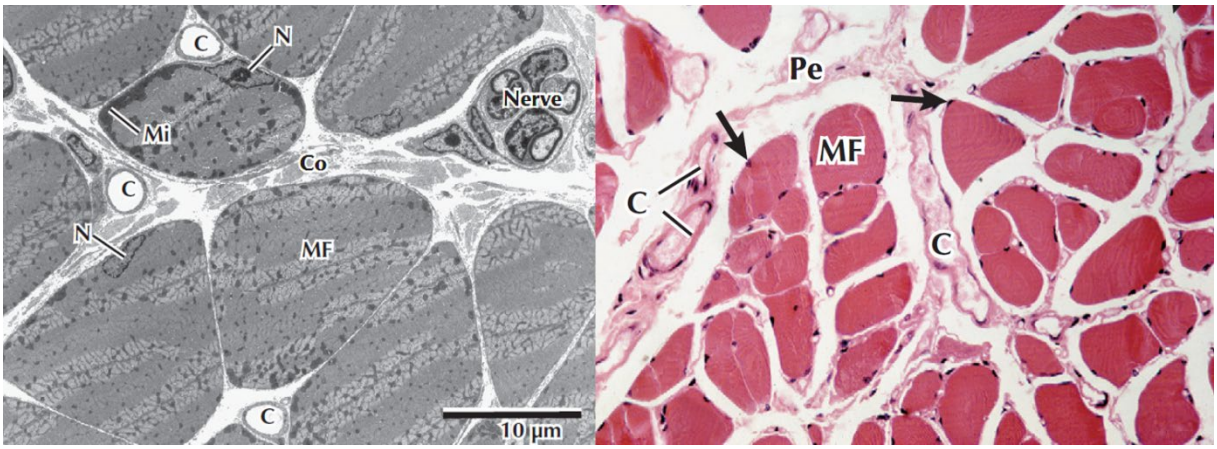

Figure 21: electron microscopy of skeletal muscle in transverse section. (MF) is a myofiber in close contact with micro capillaries (C). We observe peripheral nuclei (N), and the endomysium with collagen (Co). Source: Netter's Essential Histology.

- **Neuromuscular junction (NMJ)**

Neuromuscular junction is again, a unique feature of skeletal muscle cells. Voluntary movement starts in the brain where cortical neurons project their axons through the spinal cord until they make synapse with alpha motor neurons. These alpha motor neurons then project their axons reaching muscles [77]. The whole nervous system mediating movements would deserve a whole section due to its extraordinary complexity yet extremely logical organization. I will here only focus on the main features we need for the MyoChip project.

The NMJ is unique to the muscle (Figure 22 [78]). Four main protagonists gather to generate it: the myofiber, the motor neuron, the basement membrane that is particular at this location, and the Schwann cell [78]. Schwann cells are a type of peripheral nervous system cells that are non-neurons (glial cells). They wrap around axons, making the myelin sheath of myelinated fibers [79]. This myelin is essential for rapid propagation of action potentials, through saltatory conduction.

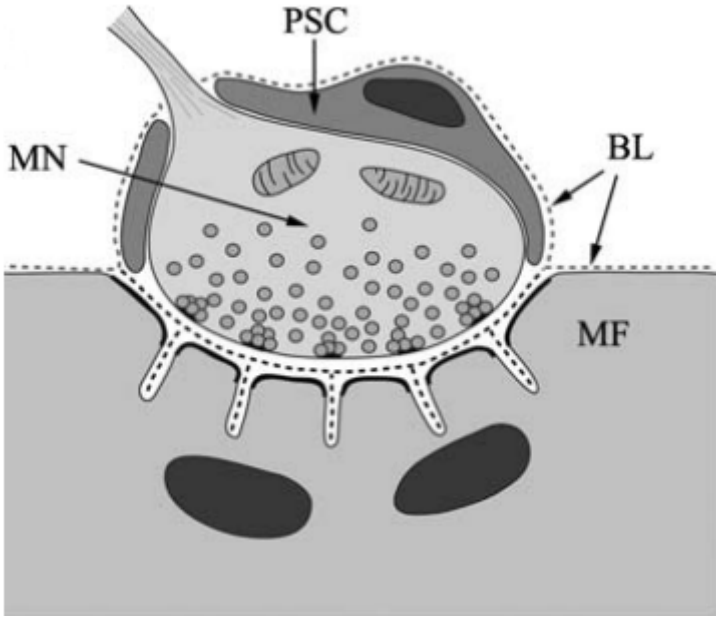

Figure 22: Structure of the vertebrate neuromuscular junction. (MN) is the motor neuron axon termination. (MF) is the myofiber. (PSC) is a peri synaptic Schwann cell. (BL) is the basal lamina. Dark ovals in the myofiber are the peripheral nuclei. From [78].

Schwann cells cover the NMJ and have a regulatory role by secreting trophic factors such as fibroblasts growth factors (FGF), ciliary neurotrophic factors (CNTF), insulin-like growth factors (IGF) or glial-derived growth factor (GDNF) [78]. There, the basement membrane of the myofiber splits (Figure 22). One part covers the synaptic depression in close contact with the myofiber and the motor neuron, the other part covers the Schwann cells and the motor neuron termination. The NMJ is often described as having a pretzel shape (Figure 23 [80]).

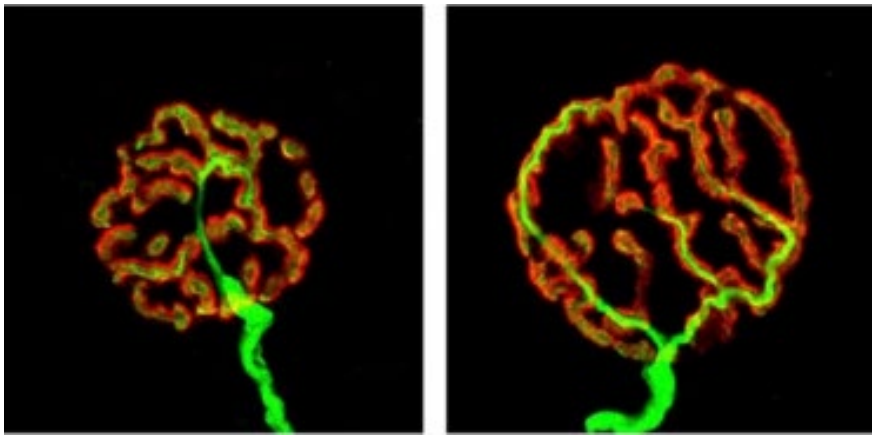

Figure 23: Pretzel shape of neuromuscular junction. Red staining is acetylcholine receptors. Green staining is axonal terminations. From [80].

The myofiber contraction mechanism from the cortex neuron is complex, further details can be found in this article [5]. Briefly, motor neurons axon tip contains presynaptic vesicles with a neurotransmitter: acetylcholine (Ach). Voluntary movement starts from the efferent action potential, which depolarizes the axon tip. This depolarization will fuse those vesicles to the axon plasma membrane, submerging the synaptic cleft with Ach. Myofiber plasma membrane has Ach receptors (AchR). The binding of Ach to AchR allows the action potential to pursue its path toward the myofiber, reaching the endoplasmic reticulum containing a lots of calcium ions. Release of calcium ions inside myofiber cytoplasm will in turn enable sliding interactions between actin filaments on myosin filaments, as previously saw, resulting in muscle contraction.

To stain the NMJ and study it, we can either use antibody against AchR, or a specific drug that binds to AchR known as α bungarotoxin [78]. Therefore, the presence of AchR is not only a sign of muscle cell maturation, but also of neuromuscular junction formation.

We now have the knowledge to start going from *in vivo* to *in vitro* skeletal muscle models on a microfluidic chip. It is however interesting to see what has been developed until now to recapitulate skeletal muscle *in vitro*. Knowing the advantages and the limits of each model will enrich our knowledge and lead us toward new possibilities.

4. *In vitro* skeletal muscle tissue

According to the number of articles on PubMed, 'skeletal muscle engineering' research only started to take off in late 1990. The expression 'engineered skeletal muscle' has been published for the first time in research in 1996, when a team subcutaneously implanted an engineered mouse

skeletal muscle organoid to directly deliver recombinant growth hormone [81]. Another team used for the first time the exact same cells and matrix we are going to use to engineer a skeletal muscle, with C2C12 cells embedded in collagen type I [82]. To align these cells, they cast cells-laden collagen I inside capillary glass of submillimeter diameter. They succeeded to generate aligned multinucleated cells. However, Shansky *et al.* was the first team to implement skeletal muscle engineering on small devices back in 1997 [83]. The device geometry was a rectangular silicon well (Figure 24A).

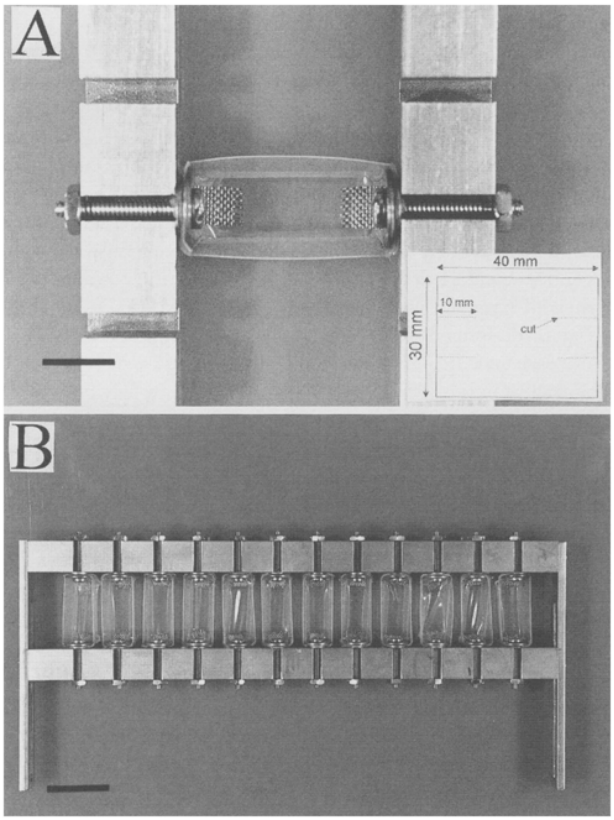

Figure 24: (A) Rectangular silicon culture device (20 ×10 ×10 mm) secured to aluminum brackets. Stainless steel mesh at each end tip provides a surface for cell attachment. (B) Each aluminum bracket holds 12 culture devices. Scale bars: 10 mm (A) and 25 mm (B). From [83].

Device's surface was sprayed with collagen I, providing ECM attachment cues for cells. Medium was then added into the well, then cells suspension was added. Using avian or neonatal mouse myoblasts, they featured tissue anchoring at each end tips with stainless steel mesh (Figure 24A). After 5 days of culture, the skeletal muscle tissue self-organized and detached from the bottom of the silicon device, therefore generating a suspended skeletal muscle tissue between two steel meshes (Figure 25). Immunostaining showed striated aligned multinucleated myotubes.

As we will see, this pioneer experiment with this anchoring feature will lead to very successful *in vitro* skeletal muscle models later on. Hence, let's explore in the next part how skeletal muscle modeling has evolved from 2D models to 3D models, as tissue engineering developed and organ-on-chip technologies emerged in-between. Then, we will discuss about how the MyoChip project can bring new features.

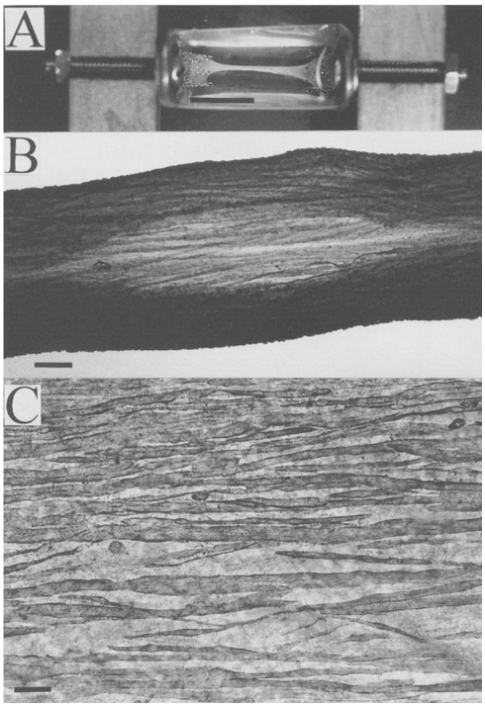

Figure 25: Skeletal muscle tissue generated on-device. (A) Tissue detachment from the bottom of the device but maintained at each extremity. (B) Higher magnification on the central part of the tissue, showing it wrapped on itself after detachment. (C) Aligned myotubes within the tissue. Scale bars: 10 mm (A), 200 µm (B) and 50 µm (C).

4.1. 2D Skeletal muscles-on-chip

In vitro models based on 2D conditions present the advantage of being limited to a cell monolayer (or only few) grown on the substrate. It is hence much easier to track and image cells than in 3D configuration even if their biomimetic properties remain limited. The main feature these devices initially focused on was myocytes alignment.

- **Surface micropatterning**

In 1999, Evans *et al.* worked on myoblasts alignment to topographical cues, using microgrooves patterns with different widths and depth [84]. The substrate was a fused-silica microscope slide, and reactive ion etching technology was used to directly etch the substrate. They showed that primary mouse myoblasts aligned much more to the groove's axis for all groove widths from 5 to 100 µm, but with a preference for groove depth of 5 or 12 µm compared to submicrometric or higher 25 µm depth. They mainly focused on isolated myoblasts. The culture lasted for 5 days and no cell fusion nor myotubes studied were conducted.

In another work, Clark *et al.* showed that adhesion molecules coated on substrates are required for long term myoblasts culture [85]. One main drawback of skeletal muscle modeling was the tissue detachment from the substrate few days after differentiation due to lack of adhesive molecules. On an untreated glass, they built regularly spaced hydrophobic tracks. Attachment factors from serum preferentially adhered to the untreated-glass tracks. Therefore, when plating myoblasts, they aligned on untreated-glass patterns. However, in absence of adhesive molecules such as laminin or collagen I, cells detached after few days. Coating the tracks with laminin resulted in preferential adhesion of laminin onto hydrophobic tracks.

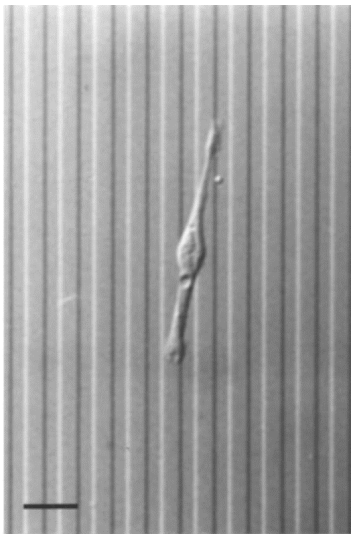

Figure 26: A single C2C12 cell plated on the 'micro groove' patterned substrate. Scale bar is 20 μm. From [84].

Plating myoblasts therefore resulted on cells adhering on laminin tracks, myotubes formation and survival after 8 days of culture. Interestingly, they show that myotubes diameter was constant (about 12 μm) either on 5 μm or on 100 μm width tracks. While only one myotube could form on 5 μm width, several myotubes of the same diameter formed on 100 μm width, without forming one bigger myotube (Figure 27).

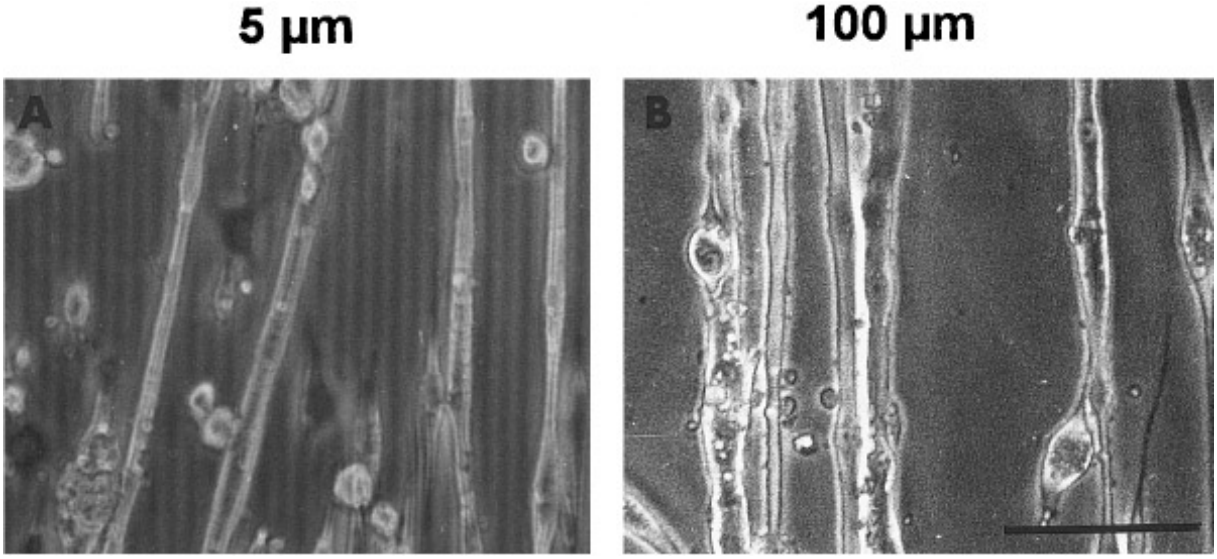

Figure 27: Myotubes after 8 days of culture in differentiation conditions, on laminin pre-coated patterns. (A) 5 μm width tracks. (B) 100 μm width tracks. Note that in 5 μm width tracks, only single myotubes formed onto the tracks, whereas many myotubes formed onto 100 μm tracks, but all having the same diameter. From [85].

They also observed that, even though some myocytes aligned at 45°C to the pattern axis, very few myotubes formed in that direction compared to myotubes formed aligned to the patterned axis. These observations tend to reinforce the assumption that myoblasts only fuse end-to-end and not laterally. To further investigate these observations, they conducted another study, using nanogrooves (130 nm wide, 210 nm deep) [86]. These nanogrooves showed to strongly align fibroblasts and epithelial cells with very low lateral movement [87]. By inhibiting lateral cell movements, they indeed showed that myocytes movements were mainly parallel to the groove's

axis. They ended up fusing and making myotubes. When cells deviated from the groove's axis, they mainly formed aggregates without fusing. However, they noticed that myotubes formed along groove's axis were short with few nuclei, hence immature. While their work highlighted the importance of cell adhesiveness for long term culture, and cell alignment for myotube formation, it is not sufficient to generate more mature myotubes. Finding constant myotubes diameter at 12 μm is a sign of non-maturation since we know that mature ones should measure several tens of microns.

Lam *et al.* emphasized on the importance of continuous curvature over sharped angles grooves in biomimicking skeletal muscle architecture [88]. Using polydimethylsiloxane (PDMS) rectangular sheet, they managed to generate wavy patterns on the surface with oxygen plasma (Figure 28). Tuning the oxygen plasma machine, they achieved various wavy patterns wavelengths (3, 6 and 12 μm) and depths (400 nm up to 1.7 μm). The substrate was coated with laminin. Mouse cell line was used (C2C12) and cultures were kept 12 days.

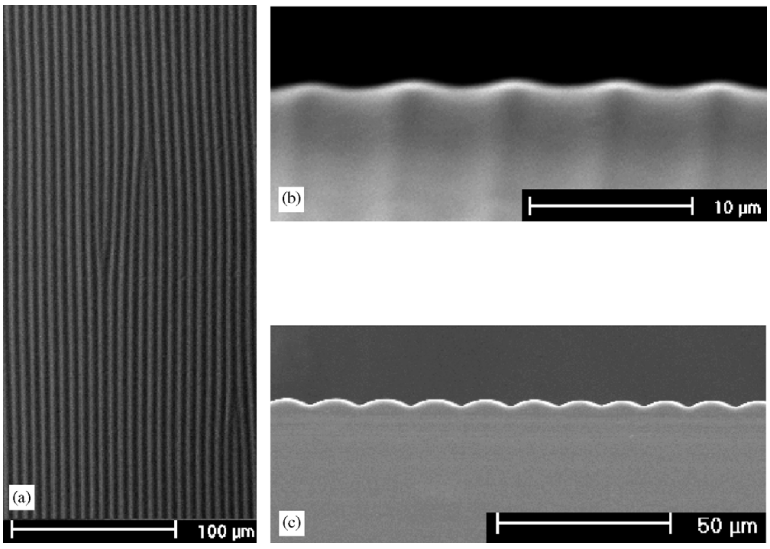

Figure 28: Scanning electron microscope of wavy PDMS substrates showing smooth and continuous features. (a) Top view. (b) and (c) cross section. Wavelengths are 6 μm (b) and 12 μm (c). From [88].

They showed that cells were more aligned along the groove's axis when plated on 6 μm waves, which is roughly the size of a single cell, compared to 3 or 12 μm waves. Showing fluorescent images stained with actin filament and nucleus, they claimed that on 6 μm waves pattern, myotubes had peripherally located nuclei elongated and aligned with groove's axis. But there was no quantitative data on that claim, and their images were not that much convincing (Figure 29). They however pointed out the importance of cell seeding density, obtaining better alignment results with 6 μm waves and cell density of 0.25×10^6 cells\cm² rather than with higher concentrations. But they attributed this to cells stacking on each other since the wavy patterns was already completely covered with a layer of cells. Even though curvatures can be interesting to study in skeletal muscles, their device didn't bring many innovations from what we already saw.

Shimizu *et al.* developed a simple stencil PDMS membrane with arrays of aligned rectangular holes [89]. This membrane was passivated with bovine serum albumin, preventing cell adhesion. The principle is elegant. Briefly, when myoblasts are cultivated on a normal flat surface, they proliferate until confluence.

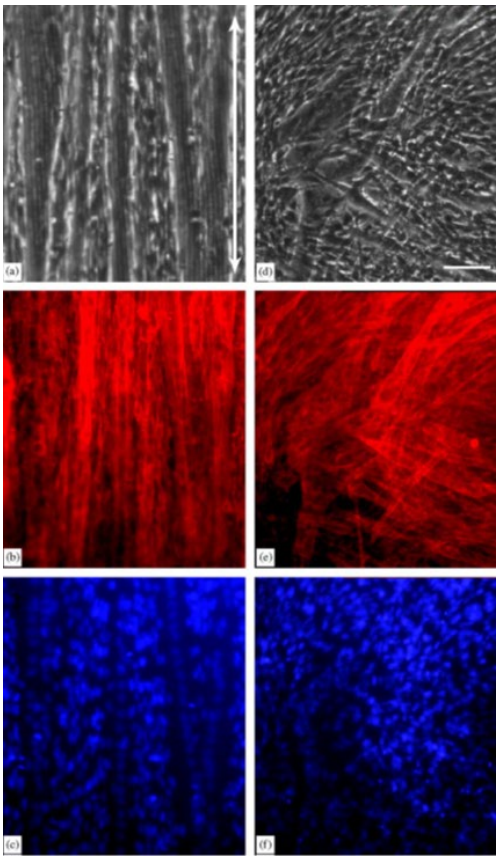

Figure 29: Optical microscopy images of C2C12 on 6 µm waves. (a) Stained for actin filaments. (b) Stained for nucleus. Scale bar is 100 µm. From [88].

At some point, when sufficient myoblasts are aligned end-to-end to fuse, myotubes are formed and orient randomly. But using the membrane, it restrains the culture space into already aligned rectangle wells, that forces cells to align, thus imposing cell fusion and myotube formation (Figure 30A, B). Interestingly, they quantified the number of myotubes with respect to the width of rectangular holes. They found a higher myotubes density for higher constrains (meaning 30 to 50 µm rectangular holes compared with 200 µm) (Figure 30C). This suggests that cells confinement could affect myoblasts behavior.

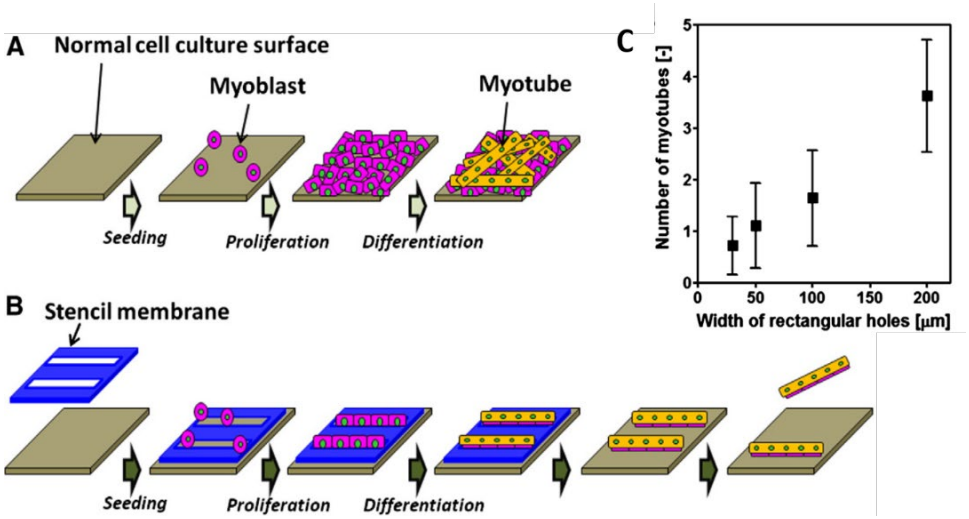

Figure 30: Schematics of cell differentiation with membrane methods. (A) Process of myoblasts differentiation on flat surface. (B) Controlled-myotube formation with the membrane. From [89].

Another team was interested in cultivating myoblasts on hydrogel substrates instead of classic plastic or PDMS substrate. Hosseini *et al.* built microgrooves made of gelatin methacrylate (GelMA) and used C2C12 mouse myoblasts to generate myotubes [90]. Grooves had a width of 100 µm and a depth of 40 µm. Each groove is separated by ridges, of 50 µm or 100 µm width. After 14 days of culture, they showed that myotubes covered more substrate surface and exhibited larger diameter when ridges width was 50 µm, meaning when cells were closer. But myotube length and alignment did not show significant differences between 50 and 100 µm width grooves. One interesting feature here was electrical stimulations performed on the cultivated tissue. Indeed, they reported an enhancement in myotubes maturation reflected by the apparition of sarcomeric striations when electrical stimulations were performed, compared to controls (Figure 31).

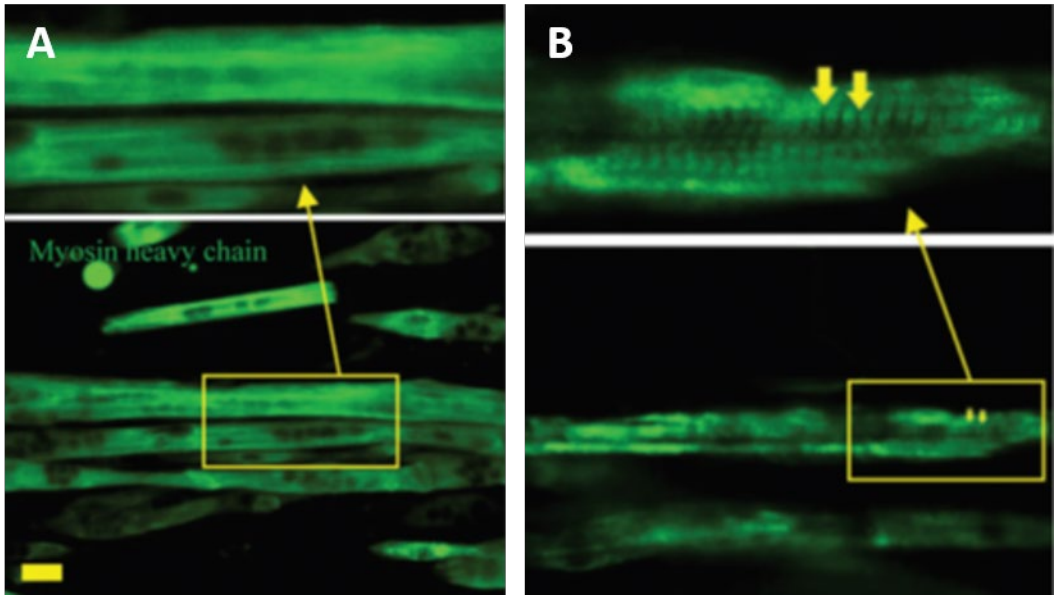

Figure 31: Immunofluorescent images of myosin heavy chain staining in myotubes cultured in GelMA for 8 days (A) without electrical stimulation and (B) with electrical stimulation. Note that myotubes exhibited striations aspect after electrical stimulation. Scale bar is 50 µm. From [90].

- **Muscle thin film approach**

Grosberg *et al.* built an array of elastic films using PDMS that are micro patterned with fibronectin to align cells on it [91]. One tip of the elastic film is attached to the substrate while the other is free to bend. Implementing electrodes to electrically stimulate the skeletal tissue attached on the elastic film, they succeeded in contracting the whole muscle film. They hence called their technology 'muscular thin film' (Figure 32). Electric stimulation not only enhances cell maturation, that exhibited striations aspect (Figure 32c), but cell contraction induced thin film bending displacement that could be measured (Figure 32b, d). Knowing the stiffness of the film material, it is possible to compute the stresses generated by the tissue construct (Figure 32e).

This muscular thin film technology has been used to build a model of Duchene muscular dystrophy (DMD). Nesmith *et al.* cultivated human healthy and dystrophic myoblasts on the device [92]. After 6 days of culture, they showed that DMD myoblasts align less, that DMD myotubes were less mature with less peripherical nuclei compared to healthy myoblasts (Figure 33).

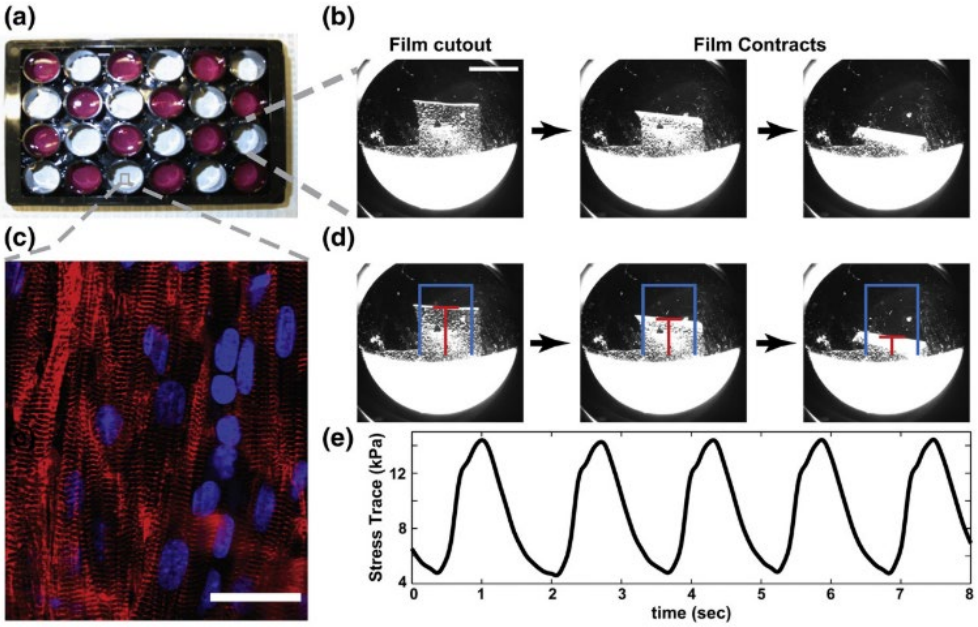

Figure 32: (a) Home-made 24 wells plate, each containing their muscular thin film (b). When stimulated electrically, cells become more mature (c) and contract so the thin film bending displacement is measure (d). Knowing the stiffness of the material, it is possible to compute the stresses generated by the tissue construct (e). Scale bar is 30 μm. From [91].

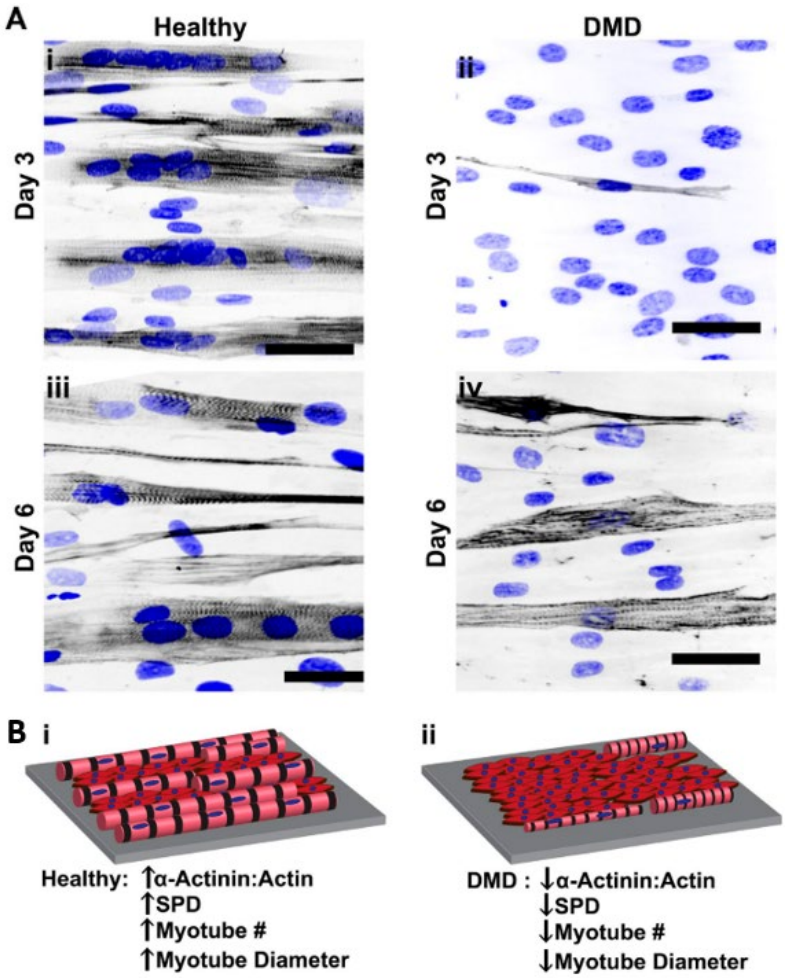

Figure 33: (A) Healthy and DMD myoblasts cultivated using muscular thin film technologies. DMD myoblasts formed less myotubes, and that are less mature than healthy myoblasts. (B) Schematic representation of healthy (i) and DMD (ii) tissues with main observed features. From [92].

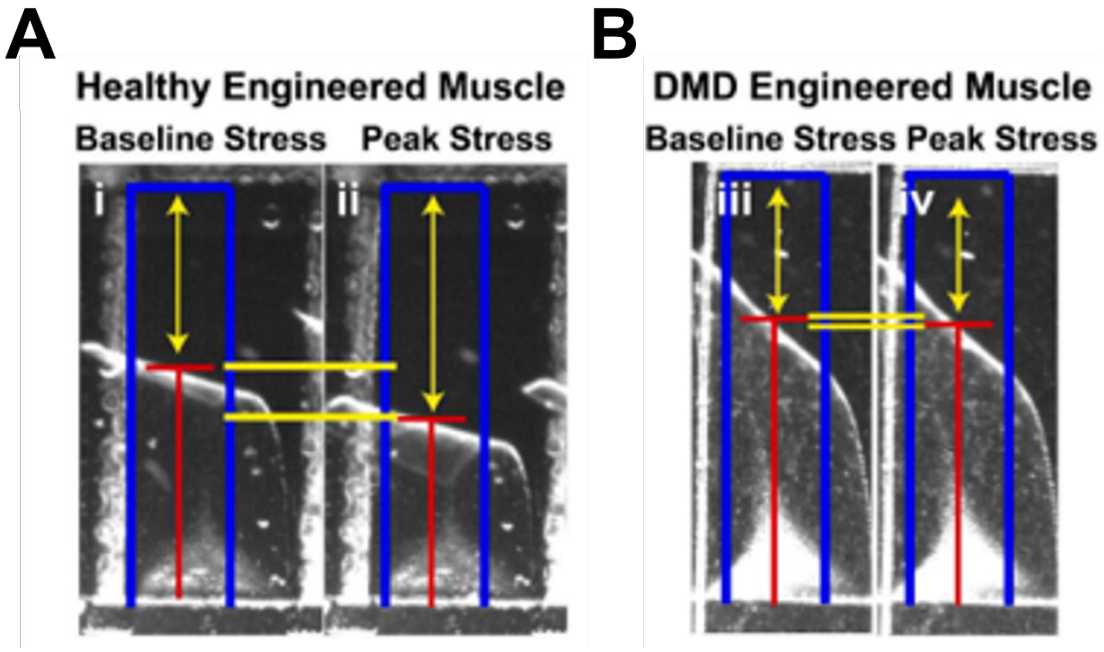

Figure 34: Images of cultivated skeletal muscle tissue bending the thin film for healthy engineered muscle (A) or a model of Duchenne muscular dystrophy muscle (DMD) (B) either when no electrical stimulation is applied (Baseline stress), or with electrical stimulation such that the film bending reaches a plateau (Peak stress). Note that DMD engineered muscle bends less the film. From [92].

Not only they succeeded in showing morphological differences between DMD myoblasts and healthy myoblasts, but using the muscular thin film technology, they also clearly showed that DMD tissue-construct always contracted worse compared to healthy tissue (Figure 34). This model is quite interesting because it is clinically relevant with clear outputs, so further studies can be carried out with drug studies. This thin film technology is remarkable and brings enormous innovation to 2D skeletal muscle models. But the process is extraordinary time consuming, requiring a lot of steps with specific machines. It is therefore not transposable at all to a common hospital or biological laboratory.

- **Layer by layer cell technology**

Some teams tackle the skeletal muscle engineering in a different way. Their ultimate goal being to create 3D muscle cell structures. To generate such structures, Takahashi *et al.* cultivated human myoblasts on hydrophilic patterned stripes of 50 µm [93]. These patterned stripes were linked to the substrates by a thermo responsive polymer, the poly(N-isopropylacrylamide) (Figure 35).

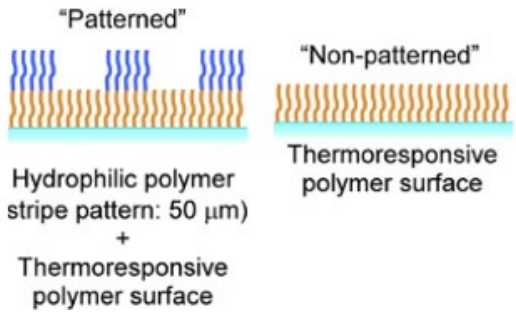

Figure 35: Cells adhere to hydrophilic stripes pattern (in blue), which are link to the substrate by a thermo responsive polymer. From [93].

When myotubes are formed, lower the temperature allows the thermo responsive polymer to detach from the cell sheet the substrate, maintaining the whole cell-sheet construct structure for 3 weeks. Polymerizing gelatin on top of the cell sheet and using a plunge, the cell sheet can be transferred to another culture plate. Using that technique, several cells monolayer-sheets of 20 × 20 mm can thus be cultivated on top of each other. By layering multiple cell-sheets, they interestingly showed that the orientation of one cell-sheet is influenced by the other cell-sheets. When a randomly oriented cell-sheet is on top or beneath an oriented cell-sheet, it reorients toward the oriented cell-sheet within 18 hours (Figure 36). This self-organization was also observed in several layered more than two. But this effect was lessening the more layered were added.

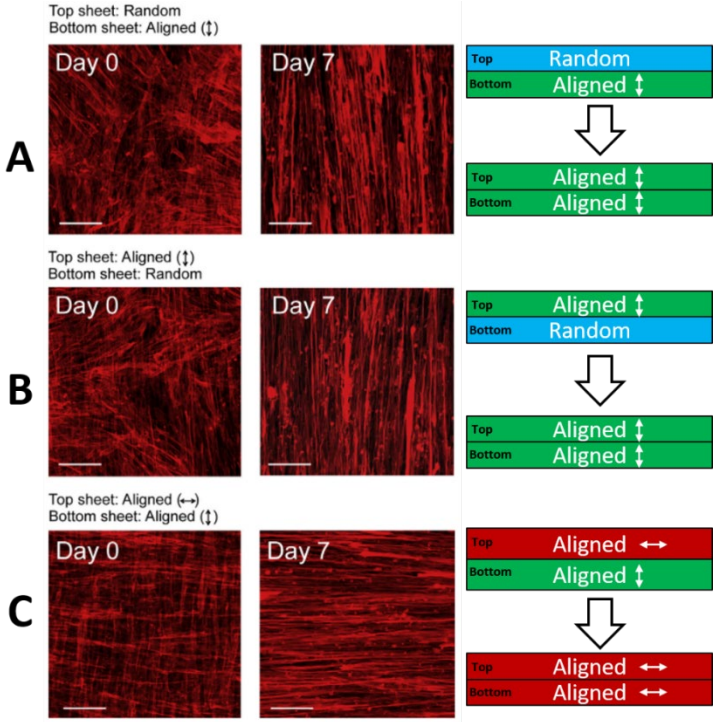

Figure 36: Confocal microcopy images of two layered cell-sheets, stained for actin filaments. (A) Randomly oriented cells-sheet on vertically aligned cells-sheet. (B) Vertically oriented cells-sheet on top of a randomly oriented cells-sheet. (C) Horizontally oriented cells-sheet on top of a vertically aligned cells-sheet. After 7 days of culture, randomly oriented cells-sheet re orient toward the upper or beneath initially oriented cells-sheet (A and B), whereas the upper cells-sheet orientation was imposed when layering two perpendicularly oriented cells-sheet (C). From [93].

This 'layering effect' was also observed by Engler *et al.* by using micro stamp technology to pattern stripes of collagen I on a polyacrylamide substrate, they seeded a first layer of C2C12 myoblasts on it [94]. After a day of two, a second layer of C2C12 myoblasts were seeded on top of the previous one. They observed that overtime the lower layer of myotubes develops no striations, whereas 80% of the upper of layer of myotubes develop actin and myosin striations (Figure 37).

They studied the influence of percentage of striated myotubes with respect to the substrate stiffness. After 4 week of culture, C2C12 cells exhibited diffuse actin and myosin staining on very soft substrate (< 5 kPa) or very stiff ones (glass, ~ GPa). On the other hand, they show actin and myosin striations when cultivated on intermediate polyacrylamide stiffness (8-11 kPa). They concluded that the optimal substrate stiffness should be around 12 kPa for myotubes to generate striations.

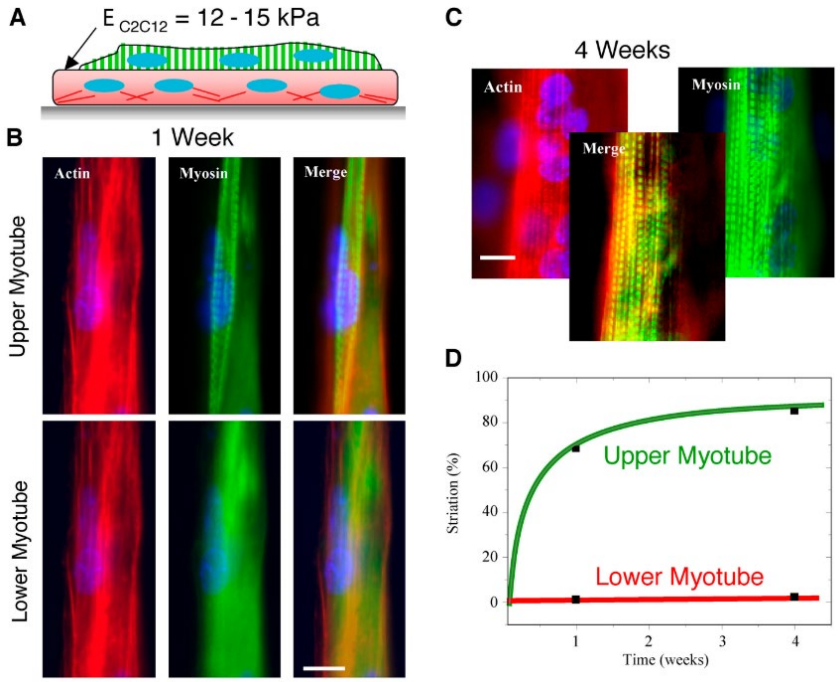

Figure 37: (A) Schematics of the multi layered cells. (B) Confocal images of upper myotubes and lower myotubes after 1 week of culture. (C) Upper myotubes after 4 weeks of culture. (D) Percentage of striated myotubes overtime in upper and lower myotubes. Scale bars are 10 µm. From [94].

In the same line, Sasagawa *et al.* developed a multilayered co cultured device [95]. Using the thermo responsive polymer poly(N-isopropylacrylamide), they cultivated cells-sheets of human skeletal myoblasts and layered them on top of each other. But instead of only stacking myoblasts-sheets, they added endothelial cells in-between, using human umbilical vein endothelial cells (HUVEC). After 3 days of culture, immunostaining showed a self-organized network of vessel-like structures. To investigate if this construct has the ability of neovascularization *in vivo*, they performed a dorsal subcutaneous graft on rat. Two sets of graft the were assessed: 5 layers of human myoblasts without HUVEC, or with HUVEC between each layer. One week after grafting, red blood cells were observed inside the first graft configuration, coming from the host. Immunostaining of grafted myoblasts and HUVEC showed their survival within the host, and new vessels inside the graft. These results highlighted the high angiogenic potential of this tissue-construct.

Altogether, these works highlighted the influence of the substrate stiffness for myotube maturation and the possibility to generate a skeletal muscle *in vitro* layer by layer in a sequential way. It also showed the possibility to co cultivate skeletal muscle cells with endothelial cells, further mimicking the *in vivo* tissue.

While some of these 2D models showed great results and were promising at that time, the biomimicry is still lacking. Many points can be underlined. Cultivating cells on a micropatterned substrate only allows cells to adhere on that substrate, which is substantially different from them having adhesive cues coming as well from the top and from the sides. We know myofibers have basement membrane all around (endomysium), giving them adhesive cues while maintaining them well aligned. One other drawback is the lack co-culturing scaffold. We saw that Sasagawa *et al.*

injected endothelial cells between each cells-sheets. But from *in vivo* tissue, vascularization is not randomly organized and that's a matter of nutrients and oxygen diffusion efficiency. On 2D surfaces, building specific scaffold for each cell subtype simply cannot be done. Implementing relevant co-cultures with more than 2 cell types becomes therefore very limited on these devices. And last but not least, all of these devices are air opened with no means to precisely control any perfusion flow, diffusion gradients of molecules or to compartmentalize cells in specific regions.

But years have passed and people started to get interested in tissue engineering. A quite new field of research has emerged within tissue-engineering: organ-on-chip (OoC) technologies [96]–[100]. This allowed new horizons to be explored and 3D skeletal models started to became more numerous. Organ-on-chip can be defined as a 'microfluidic cell culture device created with microchip manufacturing methods that contains continuously perfused chambers inhabited by living cells arranged to simulate tissue- and organ- level physiology' [100]. A lot of different organs were studied using this OoC approach, the skeletal muscle being one of them. Let's have a look at some novelties brought by OoC technologies in 3D skeletal muscle modeling.

4.2. 3D Skeletal muscles-on-chip

3D Skeletal muscle OoC can be classified into subgroups based on their main feature used to align muscle cells on-chip.

- **Cell-laden Hydrogel**

When considering working in 3D, the scaffold becomes crucial. The biomaterial used for cell culture will determine cell behavior in the 3D environment. GelMA has been widely used as a material for tissue engineering applications because of its affordable fabrication process and the ease to tune its mechanical properties by simply changing the reagents concentration [101]. It is synthesized by direct reaction of gelatin with methacrylic anhydride, substituting amine and hydroxyl groups of the amino acids residues by methacryloyl groups. GelMA can subsequently be covalently cross-linked with UV, in a radical polymerization using a photo initiator. Therefore, the main drawback is its cytotoxicity due to reactive oxygen species, leading to long mandatory steps of washing after photo polymerization.
In 2010, Aubin *et al.* encapsulated various cells and in particular, muscle cells (10×10^6 cells/ml) in micro engineered 5% GelMA hydrogel [102]. They exposed the cells-laden hydrogel to UV through a mask that create aligned patterns with various width (50, 100 and 200 µm) (Figure 38). After 5 days of culture, they showed a higher nuclei alignment toward the 50 µm width patterned axis, with a decrease nuclear circularity reflecting an elongated nuclei shape. While this work is interesting on showing that C2C12 cells, NIH 3T3 fibroblasts cells and HUVEC cells can survive and align in 5% GelMA after UV crosslinking, it doesn't specifically focus on skeletal muscle cell and no myotubes maturation was assessed.

This same GelMA was also used by Ostrovidov *et al.* in 2017 to co culture C2C12 myoblasts with PC12 cells (extracted from rat pheochromocytoma, usually used as a neuron-like model) [103]. They first generated 20% GelMA aligned patterns (heigh 50 µm × widths of 50 µm or 100 µm) using PDMS stamp technology.

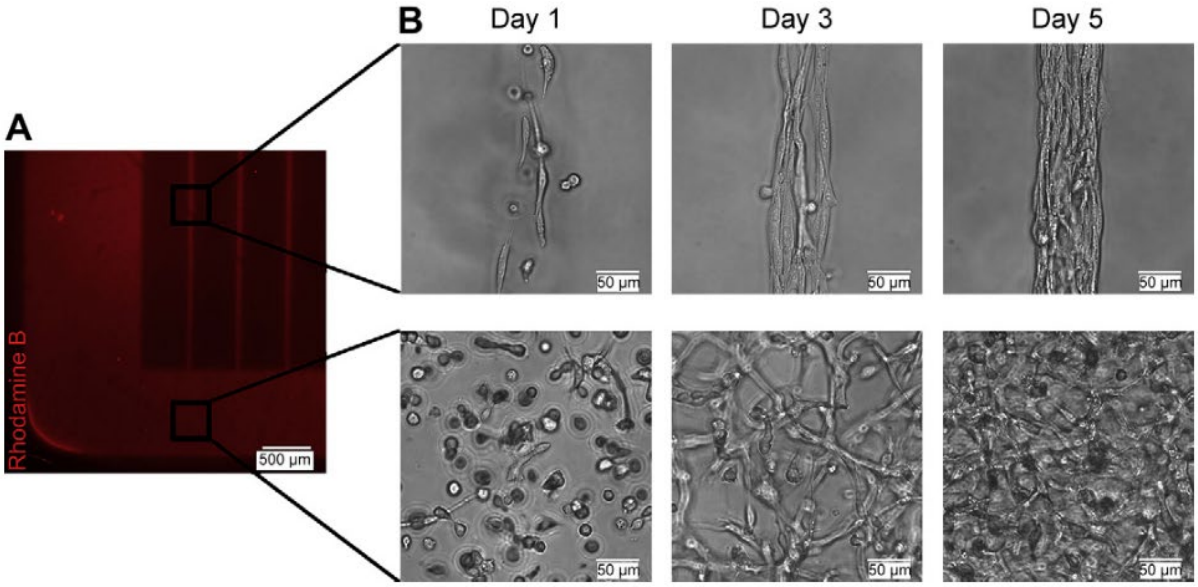

Figure 38: Mouse fibroblasts (NIH 3T3) cultivated on patterned surface (top) compared to unpattern surface (bottom) over time showing cell survival after UV exposure and cell alignment along the patterned axis. From [102].

C2C12 myoblasts and PC12 cells were re suspended at 30×10^6 cells/ml before encapsulation within 5% GelMA, either one cell type at a time, either together. Cells-laden co culture hydrogel was cast on top of the micropatterns rectangular wells, and forced to go inside the wells using a plastic piece. The device was subsequently exposed to UV (Figure 39). Cells were co-cultivated for 5 days in growth medium (DMEM, 10% FBS, 1% PS, 20 mM of HEPES), then for 7 days in differentiation medium (DMEM, 2% HS, 1% PS, 20 mM of HEPES).

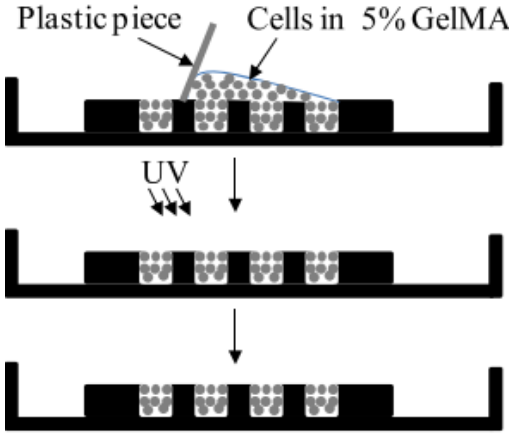

Figure 39: Schematic process for cells-laden GelMA casting in micropatterned mold. From [103].

Electrical stimulation was implemented using two platinum wires (6V, 1Hz, 1 ms of duration, square wave pulse) and was applied for 2 more days after. RT-qPCR was performed on several genes: GAPDH housekeeping gene, C2C12 myoblasts maturation marker (myogenin, Myf-5, Mef2c, MLP), mouse muscle fibers maturation marker (sarcomeric actin, α-actinin, MHC-pn, MHC-IId/x, MHC-IIa, MHC-IIb) and rat neuromuscular junction marker (AchR-ϵ and AChE). Alignment and maturation were assessed with confocal microscope and nucleus, actin filaments and cytoplasmic staining.

Interestingly, PC12 and C2C12 co culture resulted in more elongated nuclei compared to C2C12 monoculture, although myotubes alignment (within 10° angle along the pattern axis) was higher in

C2C12 monoculture.
They also showed that electrical stimulation further improved myotubes maturation in coPC12 and C2C12 co-cultures, with more aligned myotubes and longer myotubes with higher coverage area. The mRNA expression analysis showed an overall upregulation of all maturation markers cited above, comforting the idea that co-culture improves skeletal tissue maturation. Although they mentioned neurite outgrowth, images are not fully convincing and there is no AchR immunostaining and neuromuscular junction analysis.

Shimizu *et al.* encapsulated C2C12 myoblasts (10×10^6 cells/ml) within collagen I (3 mg/ml) and injected that cells-laden hydrogel inside a culture microchannel (150 µm height × 500 µm width) (Figure 40A and C, the microchannel for culture being tagged as 'MC-C') [104].

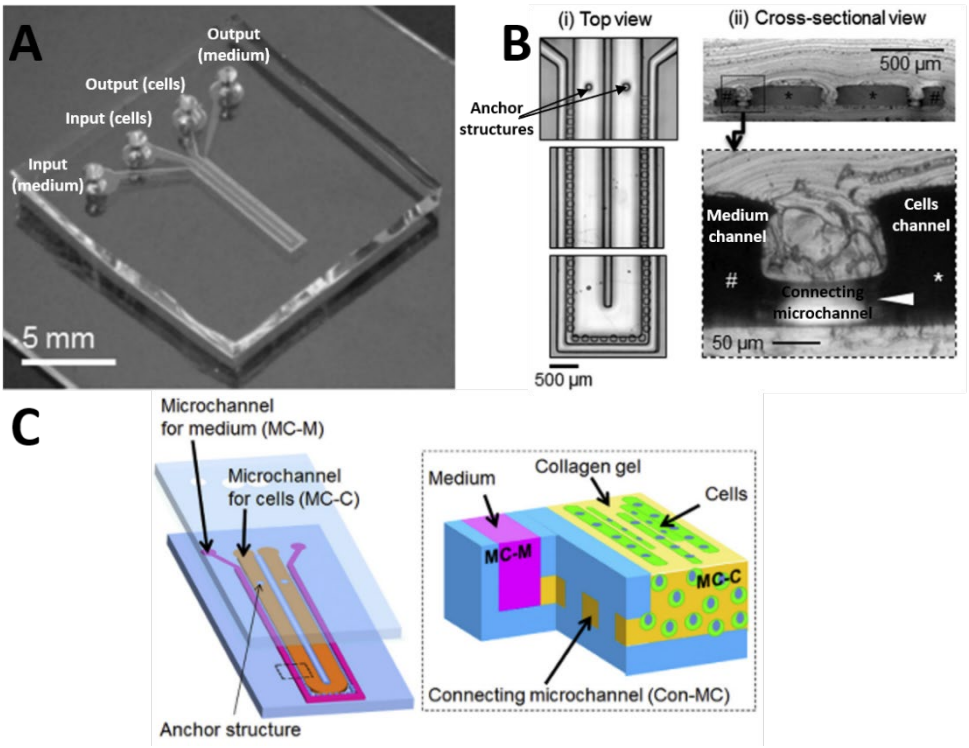

Figure 40: (A) Photograph of the chip with microchannels inputs and outputs. (B) Top view of the channel (i), showing lateral perpendicular short microchannels (ii, white arrowhead) for the medium to diffuse inside the cells compartment. (C) Schematic of the chip showing the different channels. From [104].

To prevent tissue collapsing under forces generated by myotubes, they designed anchors made of PDMS pillars at each end (Figure 40B and C). Differentiation medium (DMEM containing 2% of HS and 1% of PS) was then directly flowed inside medium channels right after collagen polymerization (Figure 40C, microchannel for medium being tagged as 'MC-M'), diffusing to the cells compartment through short lateral connecting microchannels. After 6 days of culture, hydrogel detach from the surface and started to form a cylindrical construct (Figure 41) with multinucleated cells. To investigate the function of the skeletal muscle construct, gold electrodes were inserted in the input and output of medium channels. Electrical pulses (±20V, 10 of pulse width, rectangular waveform) were applied. Contractions were observed and exhibited both twitch (1 Hz) and tetanus (50 Hz) behaviors. This behavior is called the 'positive force-frequency' of the muscle, as the generated forces become higher with higher electrical frequencies, until it reaches tetanus.

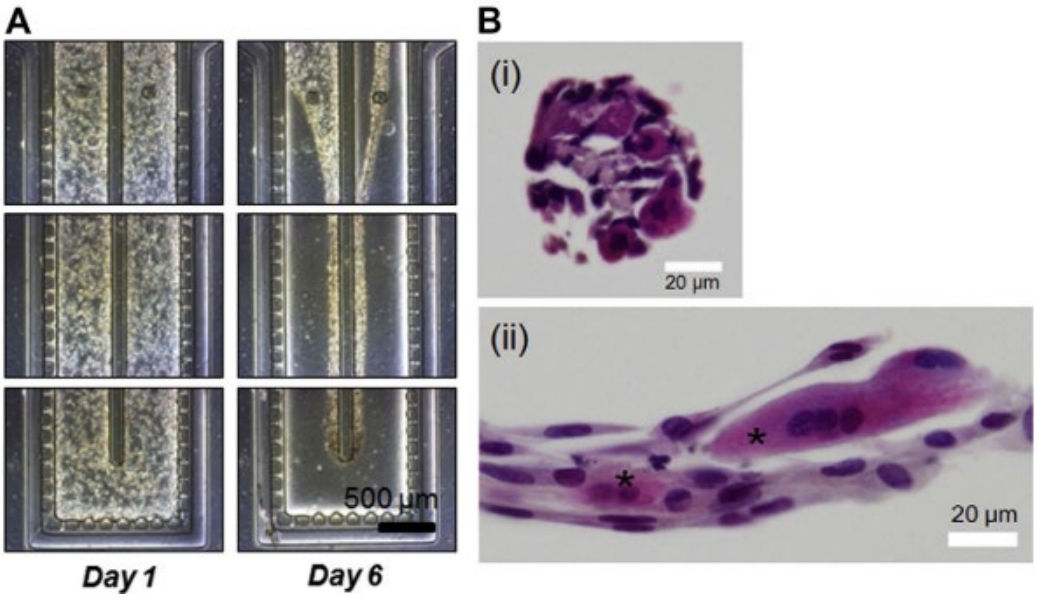

Figure 41: (A) C2C12-laden collagen I hydrogel construct inside microchannel stained with H&E, detaching from the channel at day 6 and making cylindrical construct (B, i) with multinucleated cells indicated with (*) (B, ii). From [104]

This device is interesting, because tissue maturation can be assessed by imaging, but also by forces measurement. The medium microchannel also allows perfusion of different drugs. The anchor structures also help the muscle tissue not to collapse on itself. The main drawback would be the absence of separated compartment for co cultures, such as endothelium cells. But with a redesign mold, it would be possible to implement such co culture compartment.

Costantini *et al.* studied the influence of hydrogel stiffness and geometrical confinement on skeletal muscle maturation [105]. Encapsulating C2C12 myoblasts (20×10^6 cells/ml) in different concentration of GelMA hydrogel (3% up to 8 % w/v of GelMA in PBS). Strain-stress mechanical data were obtained by performing compressive deformations. The GelMA elastic modulus spanned from 1 kPa to 16 kPa. They showed that optimal GelMA concentration was around 4%, resulting in an elastic modulus of around 3 kPa. Casting cells-laden 4% GelMa hydrogel inside rectangular wells, they observed a better cell alignment for 500×500 µm wells (compared to larger). But no myotubes maturation was assessed. Interestingly, this work showed an optimal GelMA concentration that yields an elastic modulus of 3 kPa, 5-folds smaller than what Engler *et al.* observed in their work [94]. But considering the GelMA photopolymerization process that goes along with toxicity, the hindrance could also be attributed to cell death. Indeed, Engler *et al.* did not encapsulated cells inside the photo polymerizable substrate, but plated cells on top of it.

- **Anchoring**

We previously described the pioneer concept of anchoring using a silicon mold with stainless steel meshes at each extremity developed by Shansky *et al.* in 1997. This concept was then revisited and improved by many groups around the world as it allows long term cell culture without skeletal muscle tissue collapsing and detaching. In this line, Huang *et al.* developed in 2005 a simple device to cultivate rat primary myoblasts embedded in fibrin gel (Figure 42, [106]). Anchors were made by pinning 6 mm long pieces of surgical silk suture, spaced by 12 mm.

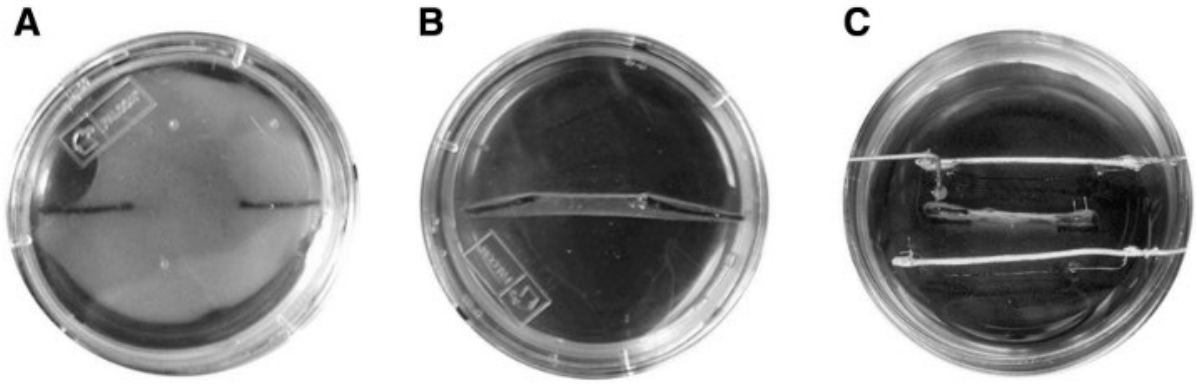

Figure 42: (A) Day 2 of culture, myoblasts were seeded on top of a fibrin gel. (B) Day 7 of culture, myotubes contractions induce fibrin gel contraction that are maintained with these silk suture anchor. (C) Day 10 of culture, 2 parallel platinum wire electrodes are mounted. Forces are measured using a high-resolution force transducer. From [106]).

Myoblasts were plated on top of a fibrin gel (Figure 42A). After 7 days, growth medium was changed for differentiation medium (DMEM, 6% heat-inactivated FBS, 1% PS) to promote myotube formation. The muscle-construct then contracts and self-organize, inducing fibrin gel contraction but still maintained between the anchors (Figure 42B). After 10 days, Pt wire electrodes are mounted to later stimulate the muscle construct, and forces are measured using a high-resolution force transducer. Besides passive forces measurement, contractile properties were measured at days 14 and 21 of culture (single 1.2 ms pulse at 15V for muscle twitch, 1 s train of 1.2 ms pulses at 150 Hz, 15V for tetanus). The authors showed that cells align themselves along the long axis formed by the contracted fibrin gel (Figure 43). However, alignment quantification was not performed.

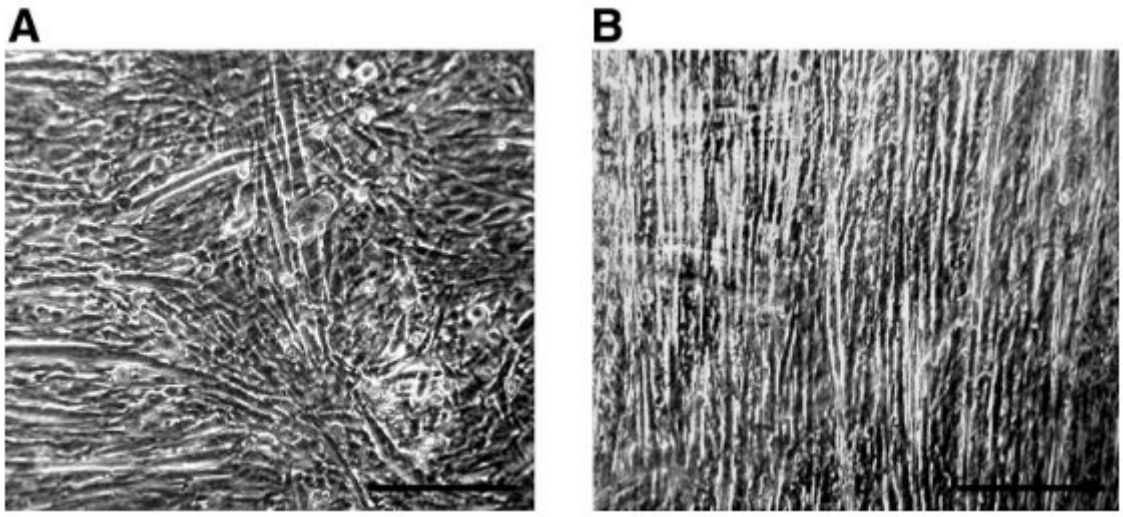

Figure 43: (A) Cells and myotubes seeded on top of fibrin gel, with randomly oriented angles. (B) When the fibrin gel contracts, myotubes reorganize along the line of force between the two anchors, hence strongly aligned parallel to each other. From [106]

Cross section of the construct showed positive staining for myosin heavy chain type II, reflecting differentiated myotube. Electron microscopy of a longitudinal section showed sarcomere structures. The muscle-construct exhibited an average diameter of 180 μm for a length of 12 mm and forces measurement on it showed values of about 300 μN for twitch and about 700 μN for tetanus. An interesting point is when adding growth factor IGF-1, twitch forces increased but not proportionally. They attribute that to a downregulation of IGF-1 receptors within myocytes, as it

has already been reported [107]. They also reported a positive force frequency, achieving tetanus above 80 Hz.
This work brings great innovations on forces measurement with a quite simple device. Although they have electron microscopy images, they didn't investigate nuclei positioning or myotubes diameters.

It is worth mentioning another work with the similar device by Lam *et al.* [108] although with a slightly different approach. The actually combined 2D patterned PDMS as described previously [88], with the pin anchors. Briefly, a wavy patterned PDMS sheet was coated with laminin (10 μg/ml). Rat primary myoblasts (5×10^5 cells) were plated on that wavy laminin-coated PDMS sheet, promoting cell alignment. After 2-3 days of culture, they pinned through the cell sheet, two silk sutures spaced by 12 mm. Fibrin was then casted on top, allowing myotubes to slowly transfer to that hydrogel when laminin was totally degraded by cells over time. The cells-laden fibrin hydrogel adopted the same construct as seen previously, i.e., detaching from the PDMS substrate and contracting into a cylinder, anchored between the pins. Forces measurement were assessed in the same way with electrodes and a force transducer. They found about 200 μN for twitch forces, and about 400 μN for tetanus forces, values in the same order of magnitude than Huang *et al.* ones.

Powell *et al.* built a device for skeletal muscle culture where mechanical deformations could be directly applied to the construct (Figure 44A [109]).

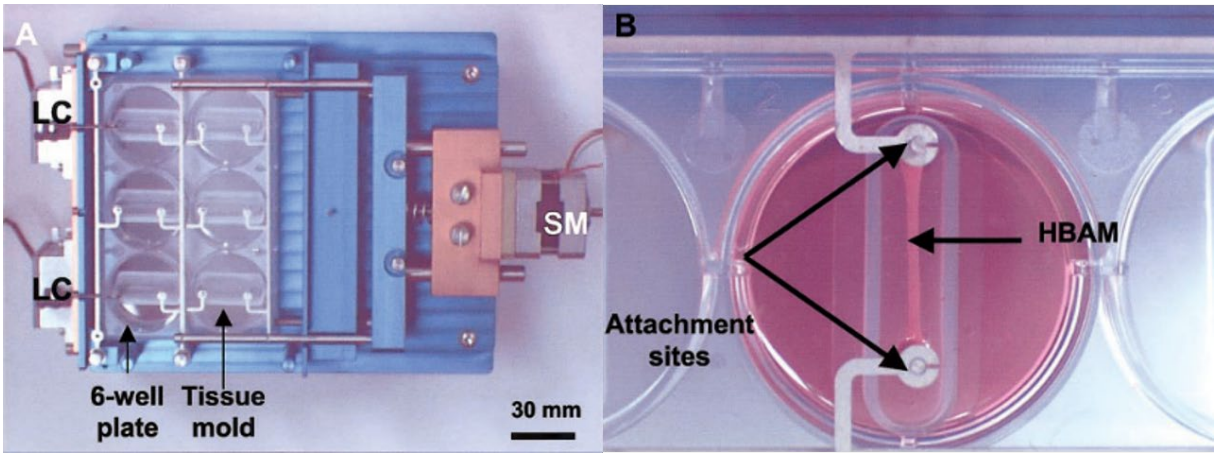

Figure 44: (A) Apparatus for mechanical deformations fitting a 6-wells plate. Two Omega ultra-low-capacity bending beam load cells were located in the left (LC), and the step motor was on the right (SM). (B) Zoom in a well showing the human bioartificial muscle (HBAM) suspended between the two pins, connected to the apparatus. From [109].

Two 2 mm stainless pins, spaced by 20 mm, were immersed into each silicon mold, acting as anchors for skeletal muscle construct (called 'human bioartificial muscle (HBAM)' in their article) (Figure 44A). One pin was connected to the apparatus, where a step motor could apply controlled deformation to all 6 constructs simultaneously. For two constructs, the other pin was connected to an ultra-low-capacity bending beam load cells (LC), acting as a force transducer. For the other four constructs, the other pin was immobile. Human myoblasts from biopsies were mixed within rat tail collagen I (0.8 mg/ml) and MATRIGEL (1:6 v/v Matrigel:collagen) in growth medium (MGM, 15% FBS). After 24h post seeding, cells-laden hydrogel contracted and detached from the mold, being suspended between the two pins (Figure 44B). Unidirectional stretching then began for 4 days, at a rate of 500 μm/day. Muscle constructs were then held at the new extended length

for 3 days (7 days post seeding) and repetitive stretch/relaxation then began (8 days post seeding). During this second cycle of mechanical stimulation, muscle constructs were stretched and relaxed at different strains: 5% for 2 days (10 days post seeding) then 10% for 2 days (12 days post seeding) then 15% for 4 days (16 days post seeding).

Thanks to this versatile device, the authors showed that the second cycle of mechanical stimulations improved myotube maturation with an increased diameter by 12% (6.4 μm to 7.1 μm) and myotube coverage area in cross section by 40% (7.8% to 10.9% of the total cross section coverage by myotubes). Passive forces measurement from the construct showed increased values overtime, with a maximum value of about 600 μN at day 11 post seeding. It is surprising that even with mechanical stimulation, they only reached myotube diameter of 7 μm, while 2D works with micropattern alignment resulted in 12 μm myotube diameter. They attributed that to the lack of innervation. While their apparatus is incredibly useful, they did not further investigate any other signs of skeletal muscle maturation, such as nuclei behavior, striations aspect or gene expression. They merely showed images of fixed construct and stained for sarcomeric myosin and a cross section with myotubes (Figure 45). Moreover, they noted that in contrary to *in vivo* skeletal muscle where the ECM only represents few percent of the whole muscle, their construct failed in that ECM occupies too much space in cross-section view (Figure 45B). I think they could have seeded with a high cell density. But cell seeding concentration was not reported in their work.

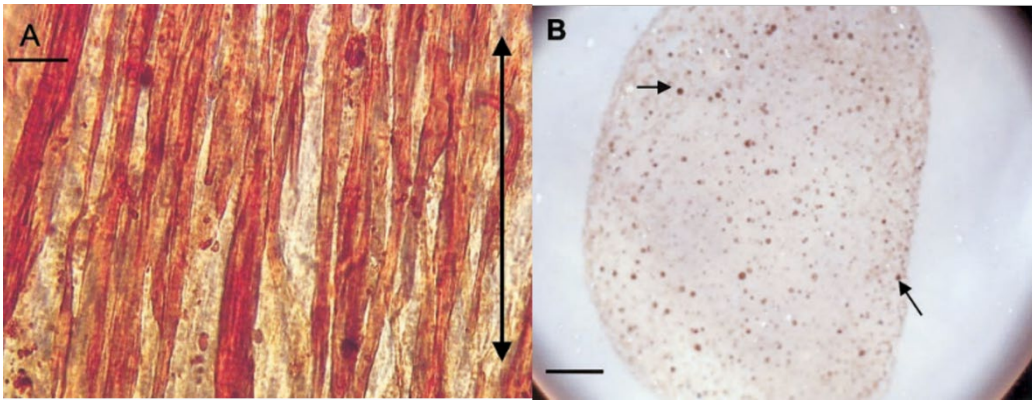

Figure 45: (A) Muscle construct after 2 weeks of culture, fixed and stained for sarcomeric myosin (brown staining). Double headed arrow reflects the long axis of the construct. (B) Cross section of the construct showing dispersed myotubes within the hydrogel. From [109].

By keeping the anchoring concept but by varying the means to achieve it, Hinds *et al.* studied the impact of different ECM composition on skeletal muscle construct maturation [34]. Their device was smartly designed. A silicone tubing (4.7 mm in diameter) was cut longitudinally, resulting in a half-cylinder silicon culture chamber of 25 mm long. Both ends were sealed with PDMS. The tubing was then coated to prevent cell adhesion, and placed into a commercial 6-wells plate. Velcro tabs, acting as gel attachment sites, were positioned at each end of the silicon culture chamber, secured with stainless steel pins (Figure 46A). Mixtures of rat primary myoblasts (15×10^6 cells/ml) with different hydrogels (collagen I at 1.4 mg/ml or fibrinogen at 2, 4 and 6 mg/ml) and Matrigel (10, 20 or 40% v/v) were prepared and seeded in the culture well. Thrombin was added to polymerize the fibrinogen into fibrin gel. After 5 days of cultivation in growth medium (DMEM, 10% FBS, 1% PS, 5 μg/ml gentamycin), they switched to differentiation medium (DMEM, 3% HS, 1% PS, 5 μg/ml gentamycin) until day 14.

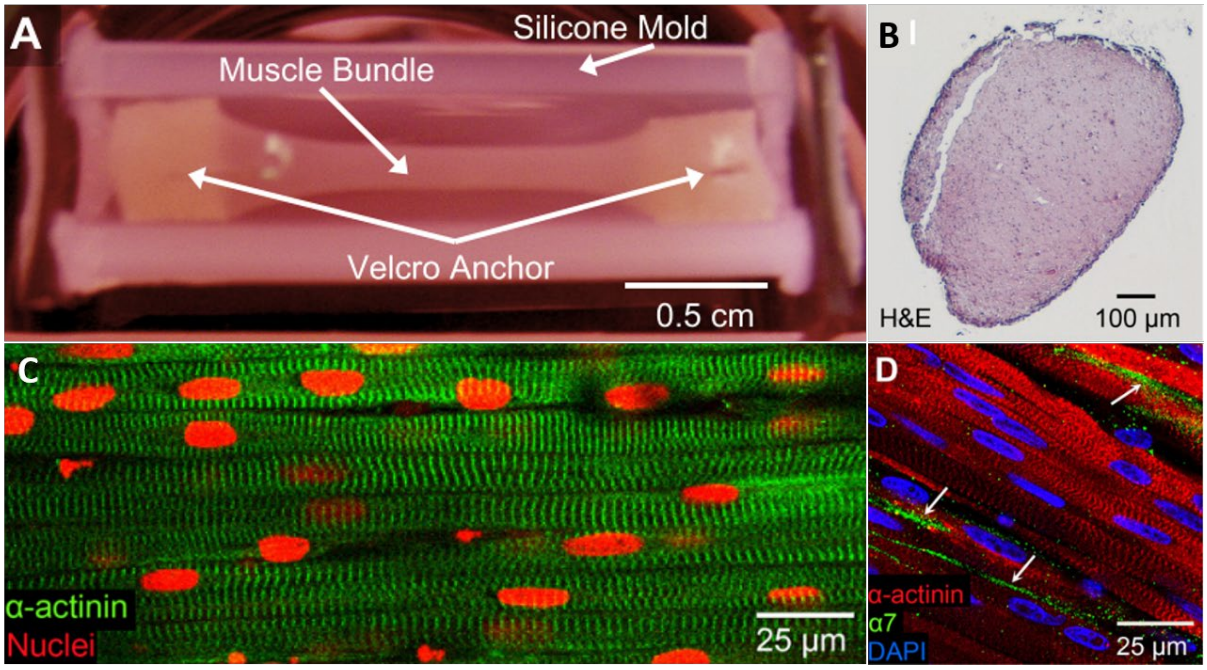

Figure 46: (A) A muscle construct (called 'muscle bundle') in the silicone mold, attached at each end to velcro anchors. (B) Cross section of 14 days muscle construct stained with H&E, showing mainly laterally located myotubes (darker region). (C) Longitudinal section 20 µm below the muscle construct surface, showing α actinin striations (green) and nuclei (red). D) Another longitudinal section showing striations and $\alpha 7$ integrins (green) along myotube plasma membrane. From [34].

At day 14, muscle construct was removed from the silicon culture chamber and transferred to another home-made chamber. The construct was then set to a tissue holder at one end while the other tissue extremity was connected to an optical force transducer. After 10 min of equilibration, the initial length of the construct was set to be the baseline length L_0. Every 2 min, the construct was elongated by $0.02 \times L_0$, then an electrical pulse was applied (3V/mm, 10 ms) that induced a muscle twitch. Tetanus was reached by stimulating the construct every 2 min at increasing frequencies (1 – 50 Hz).

Due to the muscle construct by itself, arising from a layer of myoblasts, contracting into a cylinder shape, myotubes were mainly localized at the periphery of the construct (Figure 46B). However, the muscle construct showed aligned multinucleated myotubes with α actinin striations, with some peripherally located nuclei (Figure 46C, D). Collagen I based construct exhibited higher rate of rupture within the first 7 days of culture compared to fibrin gel, that lasted 5 weeks without rupturing. They also observed that fibrin-based construct generated contractile forces up to 3-fold higher than collagen I-based construct. The optimal matrix composition they found was 4 mg/ml fibrin-based hydrogel with 40 % of Matrigel, yielding in contractile forces of about 2.8 mN, which is one order of magnitude higher than all the studies we have seen until now. This could mean that the muscle-construct in their system reached a further state of maturation than the other studies. Interestingly, this configuration resulted in the lowest stiffness compared to all other configuration (about 4 kPa). For the same construct, this configuration also resulted in higher total protein mass over DNA (ratio of about 12) and higher myotube diameter (about 15 µm). Positive force-frequency was also showed. I think that this device is very promising, as it is easy to make, and can assessed skeletal muscle construct maturation with a lot of modalities. Some drawbacks can

however be underlined. First, as they showed in Figure 46B, the myotubes are mainly localized at the periphery of the cylindrical construct. Although they generated a much more mature muscle construct able of generating up to mN forces, it might had been more relevant if they succeeded in filling the center of the construct with a higher myotube density. Plus, their device doesn't include room for co-culture, vascularization of innervation. This might have improved muscle maturation.

Madden *et al.* used the same system to cultivate human myoblasts, replacing the Velcro patches by a square nylon frames, and the half-cylinder silicon by a PDMS molds containing two half cylinders [110]. After 4 weeks of culture, they successfully generated a mature muscle construct, with aligned multinucleated striated myotubes of about 20 µm diameter, with peripherally localized nuclei and generating forces of mN scales. They however brought new features. Protein semi-quantification of myosin, α-actinin and muscle creatine kinase was performed by western blot, showing an increase over time. Drug influence on the muscle construct was also assessed, showing reduced muscle functions with higher muscle-toxic-known drugs.

Drug toxicity assessment was also performed by Agrawal *et al* [111] using a similar approach. Combining anchoring technique with cells-laden GelMA hydrogel, they built a closed-microfluidic device that is perfusable, although through a long and complex process of microfabrication (Figure 47).

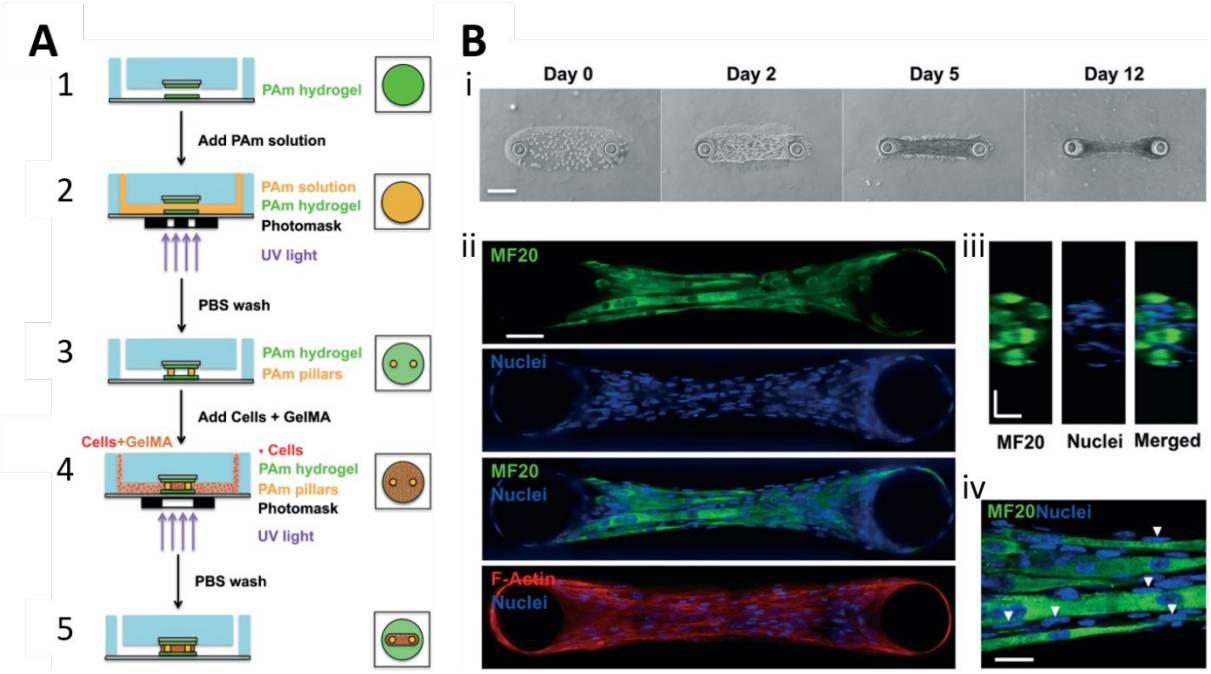

Figure 47: (A) Microfabrication process of the device. Left view is a cross section view, right view is a top view of the central region of interest. 1 – Round shape polyacrylamide (PAm) gel was generated on a glass cover slip, and sealed within a PDMS chip. 2 and 3 – Pam were generated by injecting a solution of PAm with a photo initiator inside the chip, to UV exposed the solution through a mask with pillars shape. 4 – Cells-laden GelMA was injected inside the chip and UV exposed around the pillars. 5 – Several rincing with PBS were performed. Scale bars are 150 µm (B, i), 50 µm (B, ii) and 20 µm (B, iii and iv). From [111].

Muscle construct was cultivated in growth medium for 24 hours, then in differentiation medium until 12 days. Forces generated by the muscle construct were measured by embedding fluorescent particles in the PAm hydrogels and computing 2D beads displacement.

After 12 days of culture, the cells-laden hydrogel contracted between the two pillars (Figure 47B, i). Confocal imaging on fixed samples showed multinucleated myotubes, manly aligned along the axis formed by the two pillars (Figure 47B, ii) with positive myosin heavy chain marker. Some myotubes had peripherally localized and elongated nuclei (Figure 47C, D). Pillars geometry variation showed interesting results on myotubes alignment and fusion. Two sets of experiments were performed. First, inter pillar distance was kept constant at 500 μm while their diameters varied at 100, 200 and 300 μm. Resulting aspect ratios were 1:5, 2:5 and 3:5. Secondly, pillars diameter was kept constant at 100 μm; while inter pillar distance varied at 500, 1000 and 1500 μm. Resulting aspect ratios were 1:5, 1:10 and 1:15.

Observations showed that the aspect ratio 1:5 (100 μm diameter pillars spaced by 500 μm) exhibited the best myotube alignment with about 90% of all myotubes aligned along the major axis (Figure 48A) and with the highest fusion index at about 32% (Figure 48B).

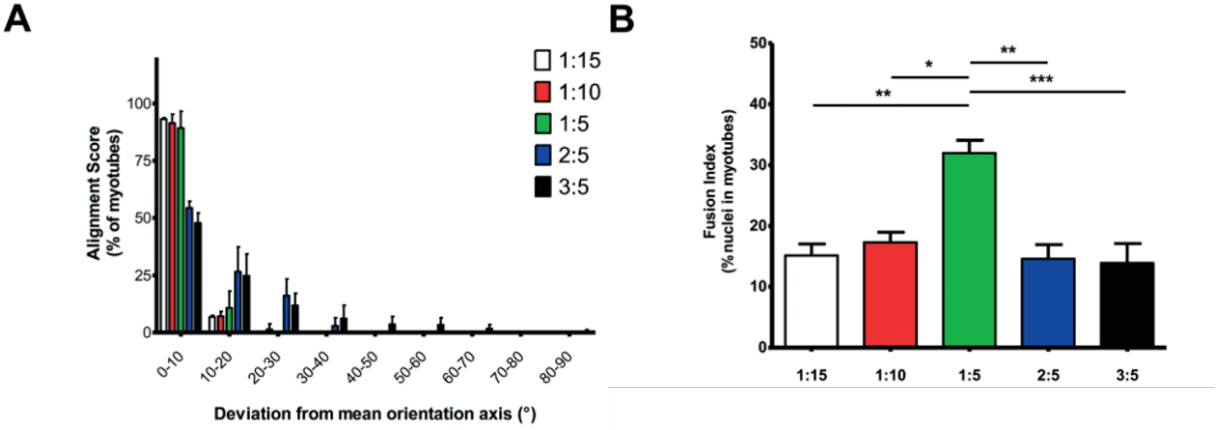

Figure 48: (A) Myotubes alignment and (B) cell fusion with respect to the different set of experiments with various inter pillar distance and inter pillar diameters ratios. From [111].

Fusion index reflects cell fusion and was computed as the number of nuclei within multinucleated myotubes containing three of more nuclei, over the total number of nuclei within the sample. To further assess their model as medically relevant, they evaluated drug toxicity on the muscle construct. Cardiotoxin (CTX) is known to be toxic for muscles. They thus showed a dose-dependent response of the muscle construct to 24 hours CTX exposition, completely dismantling the muscle construct at high doses. Forces measurement showed a clear decrease when increasing CTX doses, overtime (about 8 μN down to 1 μN with 0.5 μM CTX exposure) due to the cytoskeletal disruption.

This work interestingly highlighted the optimal pillar diameter and inter pillar distance, to be 100 μm and 500 μm respectively, using C2C12 mouse myoblasts. Although they did assess muscle construct maturation with myosin heavy chain immunostaining nuclei shape and alignment, and forces generation, they did not investigate striation aspect with more markers, such as α actinin of higher magnification of actin filaments. However, according to the other maturation readouts, it is highly probable that they would see striations. What is more incredible is that, only using simple C2C12 cell line, they succeeded in creating a medically relevant skeletal muscle model. This is very powerful because C2C12 cells are extremely easy to handle. Yet, the main drawback of their device is the extremely complex microfabrication process.

Osaki *et al.* built a very nice device to co-cultivate skeletal muscle cells with neurons on-chip [112]. A PDMS chamber containing pillars was designed to compartmentalize the chip for optimal co-culture (Figure 49A and B).

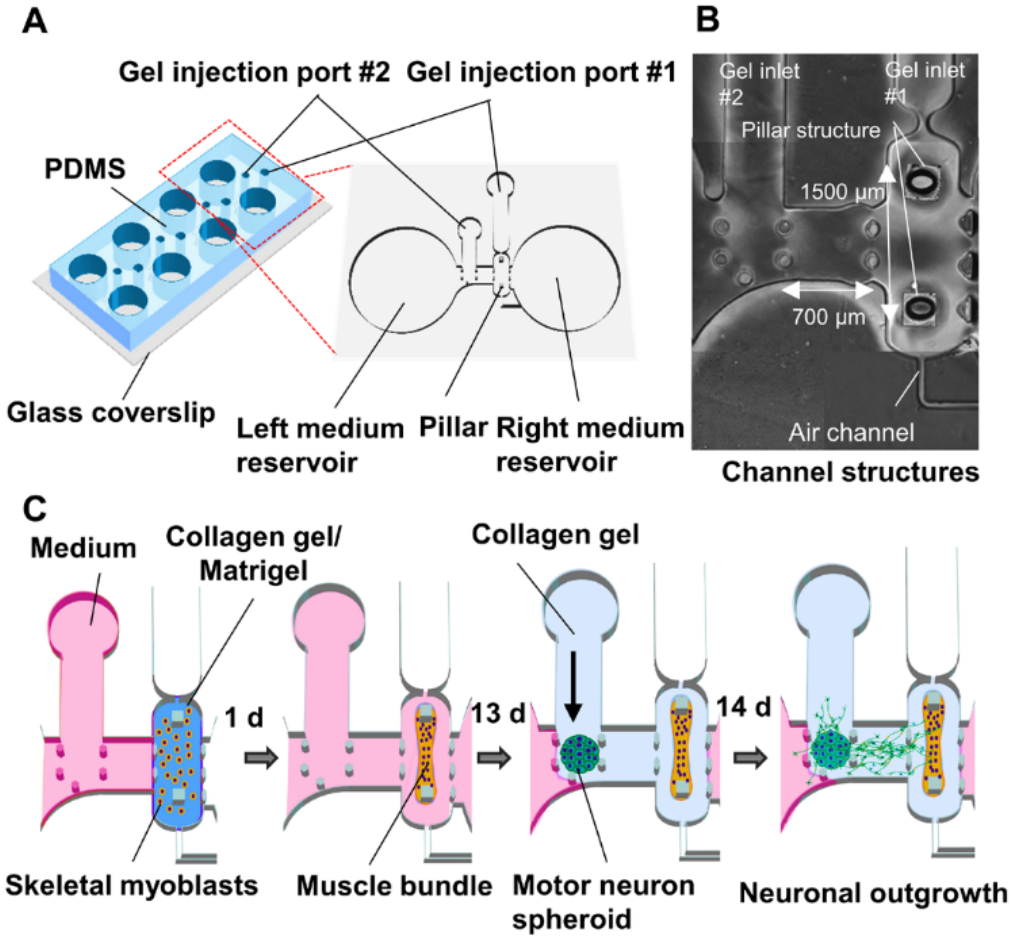

Figure 49: (A) Microfabricated PDMS chip schematics. (B) Actual picture of the central region of an individual chip. (C) Cell seeding process. From [112].

A mixture growth medium, skeletal muscle cells (C2C12 or iPSC-derived skeletal muscle cells) with collagen I (2.4 mg/ml) and 10% Matrigel was injected into gel port #1 (Figure 49A). Within 24 hours, the muscle construct was formed and anchored to both PDMS pillars, separated by 1500 µm. Muscle construct was cultivated on-chip for 13 days in differentiation medium. After 13 days, a human iPSC derived (motor neuron (MN) spheroid mixed in collagen I (2.4 mg/ml) into the gel injection port #2. Neuron medium was injected in the left reservoir, while muscle medium was injected in the right reservoir. Cultures lasted 28 days. Generated forces by the muscle construct were measure optically by pillars displacement.

After 21 days, they successfully generated aligned multinucleated striated highly maturated myotubes (Figure 50), with a high fusion index (around 70 %) and upregulated muscle-specific genes such as MyoD and myogenin by 4-fold and 16-fold compared to GAPDH housekeeping gene. Measured contractility showed generated forces reaching µN scales.

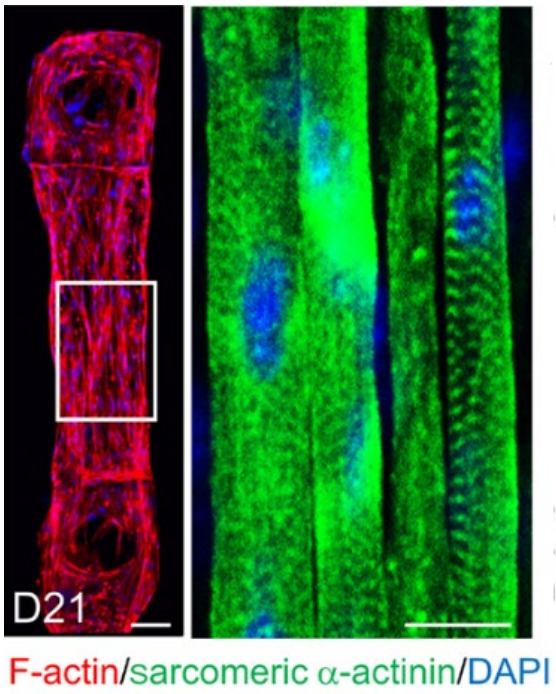

Figure 50: Muscle construct showing aligned multinucleated myotubes with *α*-actinin striations at day 21 of culture. Scale bars are 50 µm. From [112].

Positive force-frequency was observed. MN spheroid exhibited neurites elongation in collagen gel toward the muscle construct at day 4, with thick neurite fiber bundles shown with neuron-specific microtubule marker (Tuj1) (Figure 51A, B). Choline acetyltransferase (ChAT) and islet1 marker reflected MN maturation (Figure 51C), with a mature muscle construct within the co culture (Figure 51D). Neurite terminal attachment to the muscle construct with NMJ formation were then observed (Figure 51E).

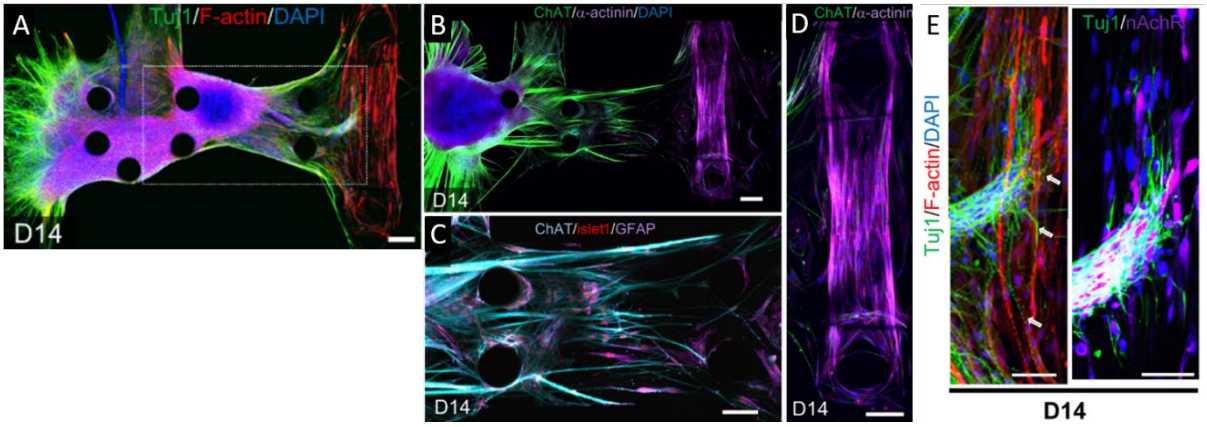

Figure 51: (A) MN neurite elongation toward the muscle construct at day 14. (B) Thick neural fibers were observed, with Tuj1 microtubule marker. (C) Choline acetyltransferase (ChAT) and islet1 marker reflecting MN maturation. (D) Mature muscle construct expressing *α*-actinin within the co culture. (E) Images revealing neurite terminal attachment and NMJ formation.

Once the NMJ was in place, MN stimulation with glutamic acid allowed muscle construct contraction after day 4. But when MN were exposed for 7 days of glutamic acid, muscle construct started to lose its function, with decreased contractibility.

This device is a highly versatile and well-designed by combining all the advantages we previously described. Pillars allowed long term culture of muscle construct, that was embedded in collagen I matrix. Compartmentalization allowed co-culture of muscle construct with MN spheroid. Generated forces were assessed by pillars displacement. Various readouts were performed, assessing the innervated-skeletal muscle maturation. Plus, human cells are used, thus further mimicking the *in vivo human* skeletal muscle. A model of ALS was created and some tested drugs showed good results of reversing the phenotype. This is really promising for drug screening and myology research.

- **Cells on wire**

Another strategy consists in cultivating muscle cells on wire. Neumann *et al.* used arrays of polymer fiber to grow C2C12 cells onto it [113]. A home-made apparatus holds parallel several fibers (polypropylene 10-15µm in diameter). Fibers are aligned, positioned within each lateral combs' grooves (Figure 52A and C).

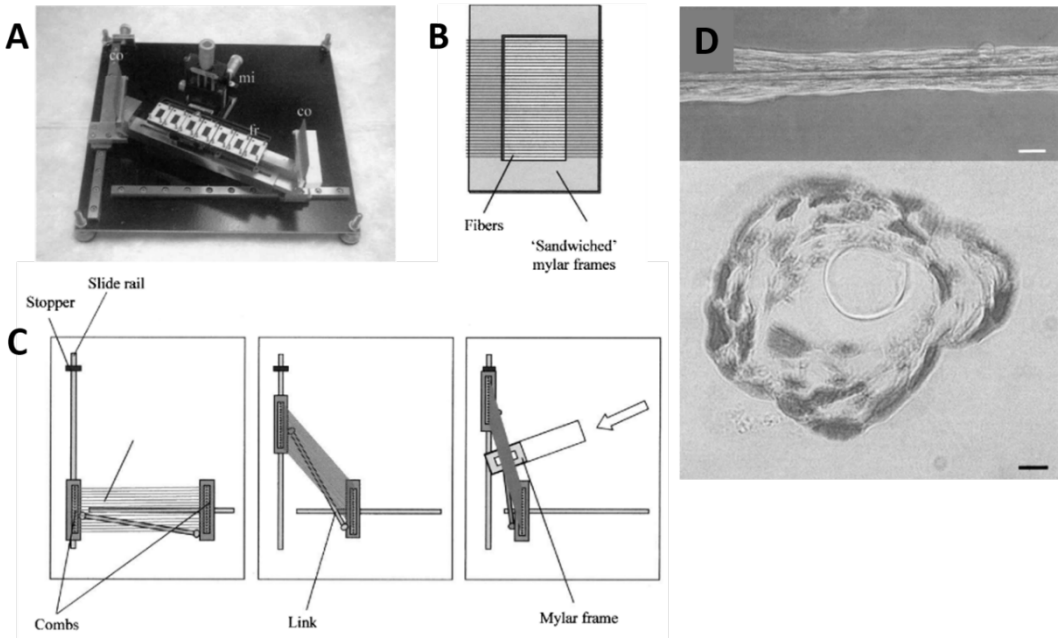

Figure 52: Fiber array fabrication. (A) Home-made apparatus with combs structures at each side (co), and an array of frames (fr) in the center, that can move up and reach the fibers with a stage microcontroller (mi). (B) Schematics of several fibers, stuck between two frames. (C) Schematics of how to control fiber inter distance, by moving the combs, and sandwiching the frames. (D) A single laminin coated fiber with C2C12 attached around, after 21 days of culture. Cross section views, fixed and stained with H&E. Scaler bars are 50 µm. From [113].

An array of sticky frames is positioned in the center below the fibers, and can move up to the fibers, thanks to a stage microcontroller. (Figure 52A, B). Fiber interspace is controlled by moving each comb separately (Figure 52C). Fibers were coated with laminin and C2C12 myoblasts suspension was then casted in the culture dish containing the frame. They investigated three situations: a) cultivating C2C12 cells on single fibers, b) assessing the influence of fiber spacing and c) creating a large cell sheet. For a) and b), C2C12 were plated with only growth medium for 21 days and fibers spacing from 30 up to 90 µm were assessed. For c) 150 fibers were fixed approximately spaced at 20-100 µm apart. C2C12 were plated in growth medium for 35 days, then in differentiation medium for 7 days and finally into growth medium again until day 69 of culture.

They managed to cultivate C2C12 around those fibers for 21 days showing many concentrical

layers of muscle cells around the fiber. Fiber spacing influence of C2C12 culture showed gaps of 30 to 55 μm were completely filled with cells whereas gaps of 70 μm didn't close after 28 days. Finally, large cells sheet experiment showed striations aspect after 10 weeks of culture (Figure 53A), with a 150 μm thick cell sheet in cross section view (Figure 53B). They reported myotubes of 3 mm long and 20 μm diameter at the surface. Although they did not quantify the muscle construct maturation by any readout usually used previously, their work has some very fascinating aspects. It is the unique published paper that cultivate skeletal muscle cells on fiber.

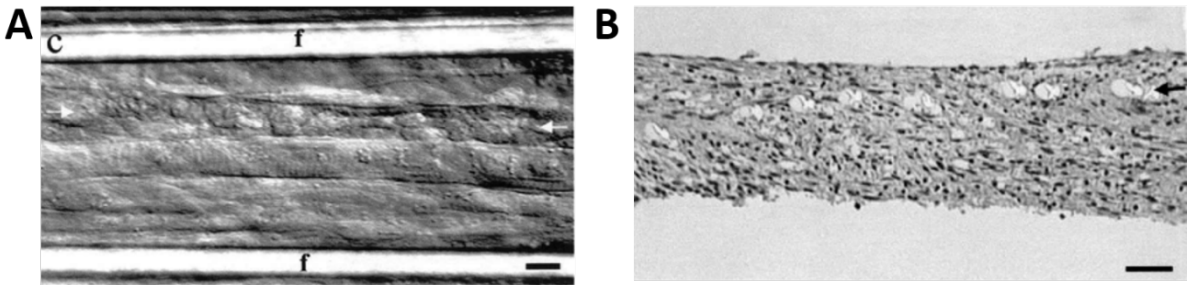

Figure 53: (A) Phase contrast images of the muscle construct, 10 weeks after, showing striations patterns in surface myotubes. (B) Cross section view of fixed and H&E stained showing a 150 μm thick cell sheet. Scale bars are 50 μm. From [113].

This is extremely innovative, because this central fiber can mimic the bone. Plus, by changing the fiber material, a lot of different experiment can be achieved, such as elastic fibers and stretching, different fiber stiffness. During my PhD, this paper got me inspired to try cultivating C2C12 on wires. Few experiments were tried with natural silk fibers of 10 μm diameter, with cells successfully attached onto it (data not shown). Other material was also assessed, such as rubber fiber, which inhibit cell attachment on it.

It is worth mentioning that other groups also cultivated cells on the surface or within tubes. Silberzan *et al.* studied kidney cells (MDCK) migration on glass wires [114] and Caterina *et al.* studied cells behavior as a function of the curvature, confining the same cell type in tubes made of alginate [115].

- **Cylindrical geometry**

In vivo skeletal muscle structure, myofibers are embedded in ECM sheath that resembles a tube. It is therefore natural to think of a cylindrical geometry when trying to model skeletal muscle. In 2014, Neal *et al.* got me inspired for the MyoChip device. They introduced an innovative way to generate a muscle construct, called 'sacrificial outer molding' [116]. Holes were drilled on the sides of an aluminum piece, with a central milled pocket (Figure 54A).

Steel pins are inserted through the holes and spanned the milled pocket, with PDMS casted on top of them, filling the central pocket (Figure 54B). After pins removal, a PDMS slab is peeled off, and is cut into individual chips (Figure 54C, D). An individual PDMS chip is bonded on glass, and pins are inserted again into the seeding wells (Figure 54E). The three wells were 5 mm diameter, separated by 3 mm distance. The central well is for medium, the two lateral wells are for cells seeding. Muscle construct molding process is thus quite complex but elegant (Figure 55). Pins were inserted back into the PDMS device.

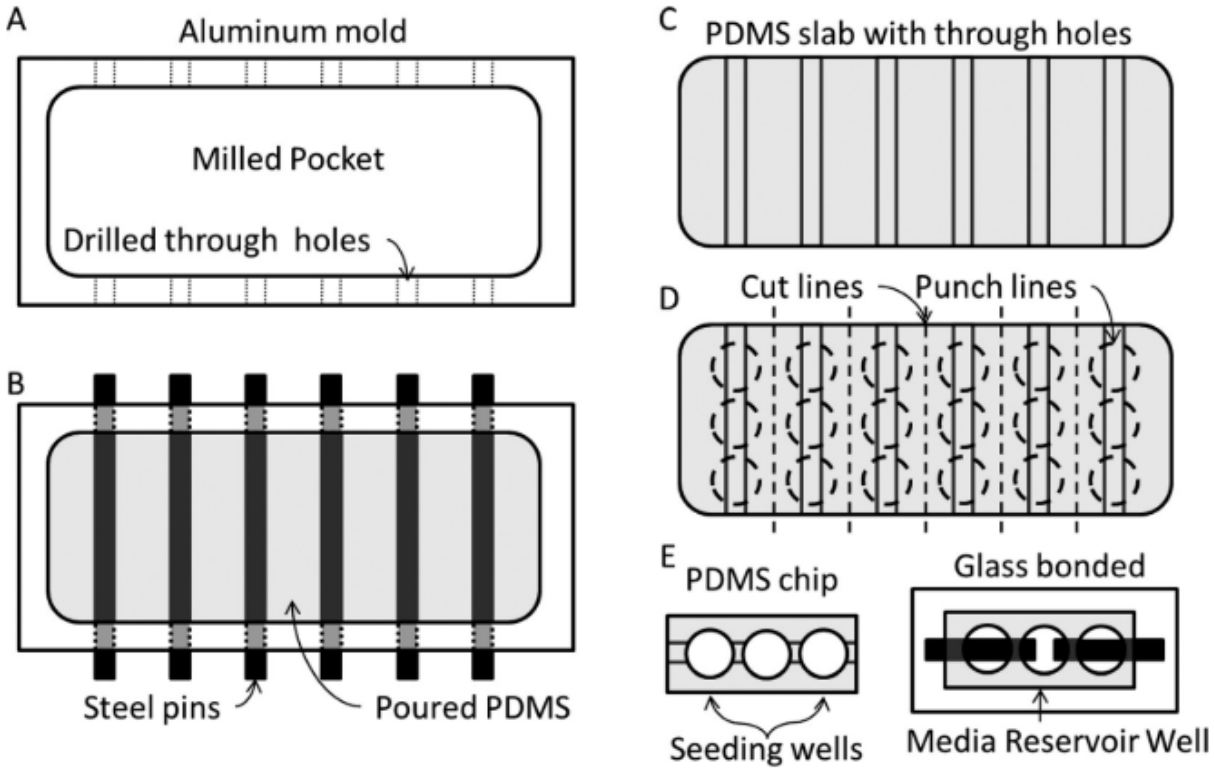

Figure 54: Schematics of the device fabrication. (A) A machined aluminum mold consisting of an aluminum bar with a milled pocket and several drilled through holes. (B) Steel pins spanning the milled pocket with PDMS casted over it, filling the central pocket. (C) PDMS slab after steel pins removal. (D) Cut and punch lines for individual chips. € Individual PDMS chip and final device, consisting of PDMS chip bonded to glass with steel pins inserted into the seeding wells. From [116].

Gelatin solution containing gelling agents (thrombin) was then injected in the lateral seeding wells, and the device was cooled at 4°C to polymerize gelatin. Pins were then removed, generating a hollow tube. Cells-laden hydrogel (C2C12 in growth medium, Matrigel at 20% v/v and fibrinogen) was injected into the tube. The device was then re heated at 37°C, melting the outer gelatin gel and releasing the gelling agent (thrombin) which induced the cells-laden hydrogel to polymerize inside the tube. Outer liquid gelatin was then replaced with growth medium. The newly formed muscle construct was then cultivated for 14 days.

With their device, they successfully generate muscle construct with aligned cells and nuclei, with α-actinin striations (Figure 56A-D, E). They assessed whether two anchoring ends were important or not for the muscle construct, by disconnecting one end. They found that disconnecting one end resulted in a much less mature construct, exhibiting lower α-actinin protein density (Figure 56G-J). The whole construct always contracted over time, the diameter reduction reaching 60% at day 10.

This device introduced a novel technique with the 'sacrificial outer mold', using gelatin suspension containing thrombin, that melt when heating up from 4°C to 37°C. Inversely, the inner tube is made of cells-laden fibrinogen that polymerized at 37°C, when the thrombin is released from the surrounding gelatin. They though didn't investigate forces generation by the construct, nor gene expression through time.

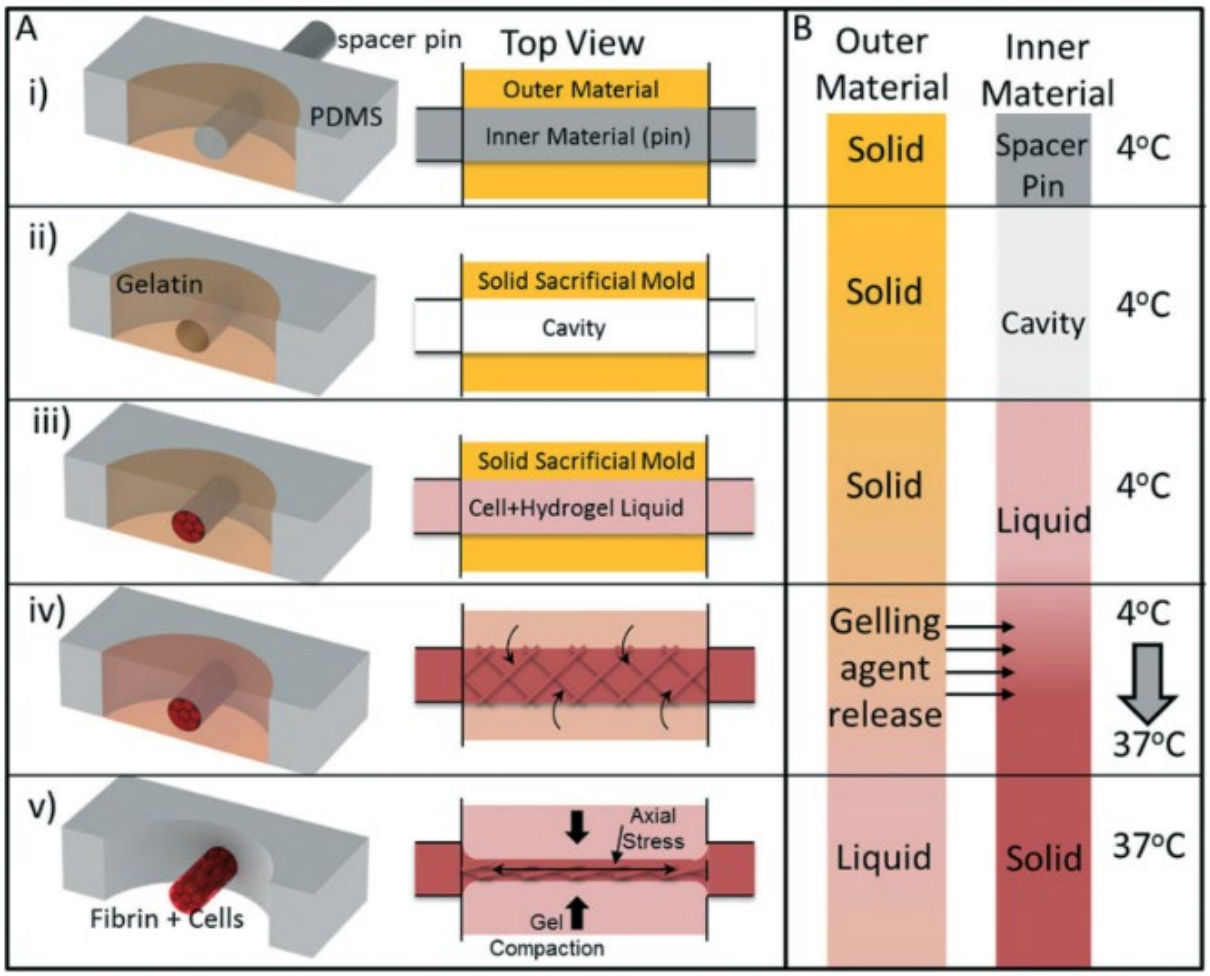

Figure 55: Muscle construct technique. (A) Schematic cross section view and top view of the molding process. (B) When heating a 37°C, the gelatin melts and the hydrogel begins to solidify, as gelling agents dissolved in the gelatin are released into the hydrogel. Finally, cell-mediated gel compaction generates anisotropic stress. From [116].

Their muscle construct, although showing striations and elongated aligned nuclei, still does not exhibit a fully filled tube with myotubes as shown in Figure 56F. Interestingly they noticed that the highest α-actinin volumetric density are observed with smaller diameter (80 µm at day 10). Yet, their construct lacks co culture, which might have improved myotubes maturation. But the device only had one channel.

In a similar way to the anchoring technique by Shansky *et al.* that became a very popular technique, this hydrogel molding technique with needles will also become quite common for any tubular organ (muscle, vessel, kidney, gut). Bersini *et al.* used that needle molding technique to build a muscle construct for fibrosis studying [117]. The novelty they brought was co cultivating human skeletal muscle cells with endothelial cells and human fibroblasts. To create the muscle construct, three steel rods (600 µm in diameter) were inserted back in the arch-shaped structure. Using the same 'sacrificial outer mold' technique with outer gelatin and inner cells-laden fibrinogen, they generated a cylindrical muscle construct. After this muscle construct generation, surrounding gelatin was discarded and a second mixture of cells-laden gelatin was casted around, ringing other cells types.

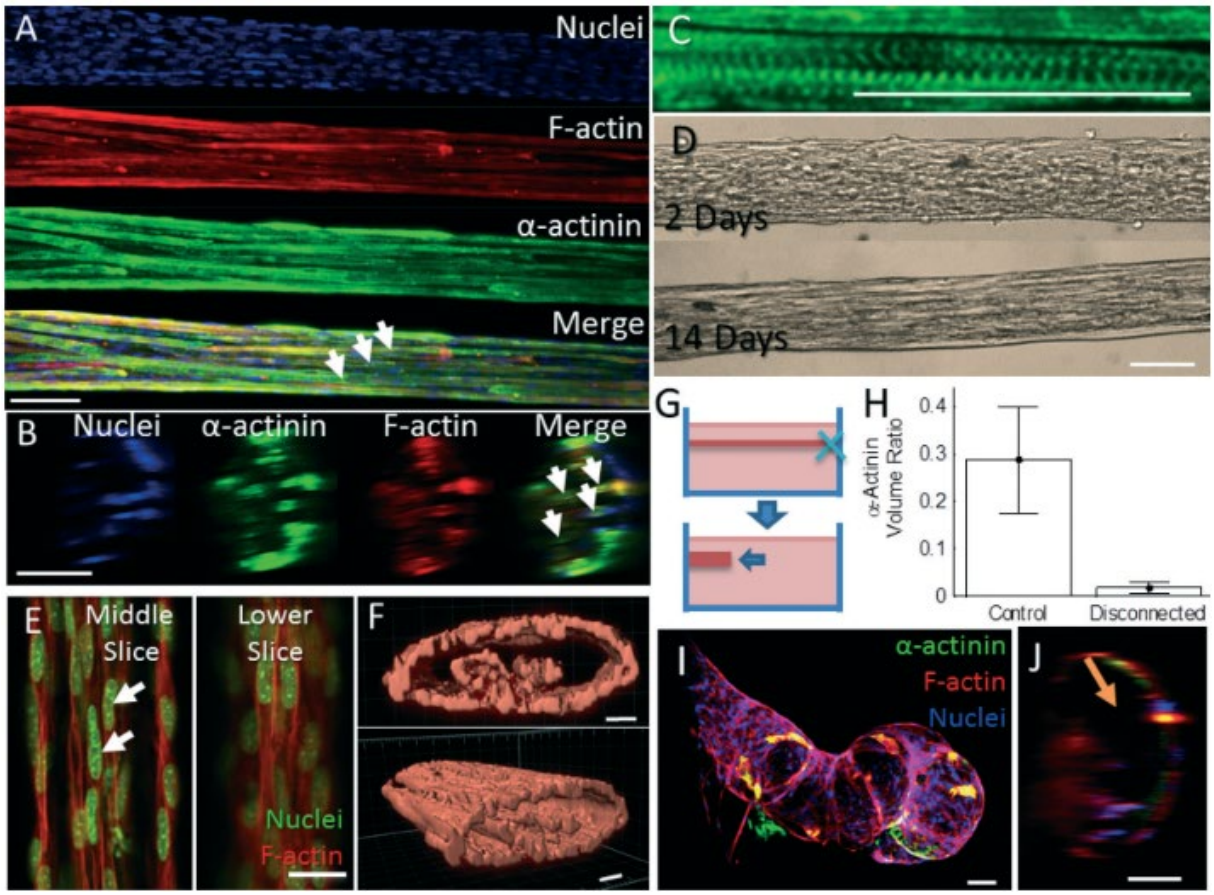

Figure 56: (A) Longitudinal stack and (B) axial stack confocal images of muscle construct. (C) *α*actinin striations. (D) Phase contrast images of the construct at day 2 and day 14. (E) 2-photon microscope images, showing actin alignment and elongated and aligned nuclei. (F) Imaris 3D reconstructions of actin filaments. (G) Schematic sideview of seeding well with a construct having one end disconnected. (H) Volumetric density of *α*-actinin with both ends anchored vs. one end disconnected. -I) Longitudinal stack and (J) axial stack of muscle construct when one end is disconnected, showing poor myotube formation and a large central region void of cells. Scale bars: 50 μm (A-E, I and J) and 10 μm (F). From [116].

Starting at 600 μm, the muscle construct contracted to a diameter of around 70 μm at day 34. Skeletal muscle cells were alive at day 34 and exhibited myosin heavy chain marker. Histological section of the muscle construct showed aligned myotubes, that has been reported to closely resembling the *in vivo* human skeletal tissue architecture, although it is difficult to tell by eye. Co cultures with endothelial cells upregulated some skeletal muscle specific gene, such as desmin and *Myf5*. They also observed the formation of a microvascular network with some lumen-like structures. Muscle cells – endothelial cells – fibroblasts or mesenchymal stem cells tri co-cultures showed a higher length/diameter ratio of the vascular network, reflecting a denser vascular network. They investigated whether endothelial cells expressed muscle-specific endothelial cells genes when co-cultivated with skeletal muscle, such as TSPAN7 or PPARG, by performing RT q-PCR. Their results showed an upregulation of these genes by co-culture, reflecting a differentiation of those endothelial cells toward a muscle-specific type. Tri co culture with muscle-derived fibroblasts showed a 100% increase of fibroblast recruitment toward the muscle when endothelial cells were present, compared to lung-derived fibroblast. These overall results showed that when cultivating endothelial cells with skeletal muscle cells, they acquire an organ-specific signature. In turn, this will recruit organ-specific fibroblasts.

This work really emphasized on co-cultures in a large extent. Lots of different co-cultures were investigated. Unfortunately, skeletal muscle maturation was not that studied. No alignment, nuclei behavior or forces generation were assessed. They didn't mention striations aspect of their muscle construct. Interestingly, as previously reported, the muscle construct contracted a lot and ended up with a 70 µm. But they however show a novelty: the organ-specific signature acquisition by endothelial cells, recruiting muscle-specific fibroblasts. This mechanism should be further investigated. Plus, their vascular network wasn't built in a controlled way, resulting in a random vascular network. Although they showed lumen-like structures, they didn't investigate whether they were perfusable of not.

Osaki *et al.* built a muscle construct with parallel vessel-like structures combined with optogenetic stimulation (Figure 57, [118]).

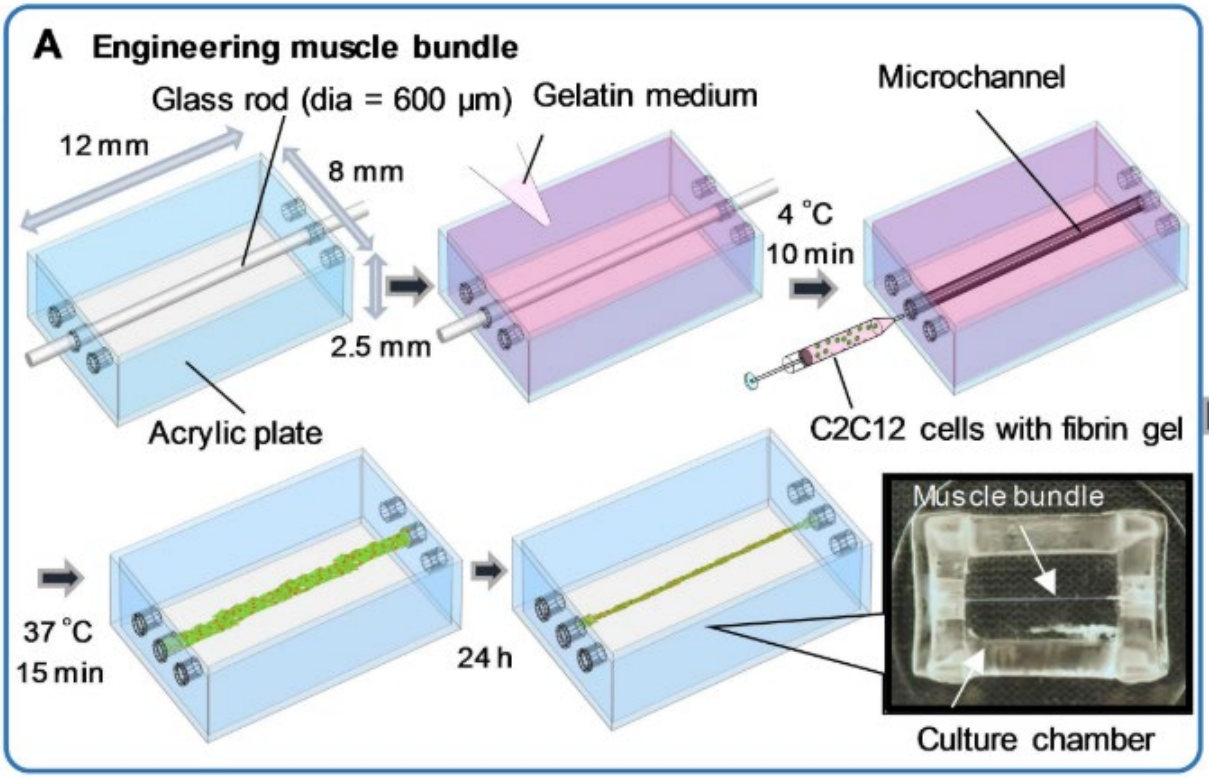

Figure 57: Schematic showing the formation of the muscle construct. From [118].

C2C12 myoblasts were genetically modified to express a light-sensitive ion channel, the Channelrhodopsine-2 (ChR2[H134R]). Thus, when exposed to a specific wavelength light, muscle construct can contract. Muscle construct was generated using a single glass rod (600 µm in diameter) inserted in the central hole. A gelatin solution at 5% was poured into the chamber around the rod. The glass rod was removed after gelation, and a mixture of genetically modified C2C12 myoblasts, fibrin, thrombin and Matrigel was injected inside the channel. The fibrin gel polymerized in 5 min at 37°C, while the gelatin melted, resulting in a free-standing muscle construct surrounded by growth medium (Figure 57, bottom right). To anchor the construct, droplets of fibrin containing C2C12 were deposited at the inlet and outlet of the channel. Muscle construct generation rate was much higher with these anchors. After 24 hours, growth medium was switch to differentiation medium for 7 days. Then, two rods were inserted into the lateral holes. The

differentiation medium was replaced with a collagen I (2.4 mg/ml) solution. After polymerization at 37 °C, both glass rod was carefully removed in PBS to avoid contamination. A cell suspension of HUVEC ($5 \times 10^6 cells/ml$) was injected in both lateral channels. Muscle construct local displacement was analyzed manually. Eight LED lights were aligned along the bottom of the chamber, to stimulate muscle construct contraction.

Their construct exhibited high aligned multinucleated myotubes expressing α-actinin striations. The local displacement of the muscle construct that reflects the generated force, was higher at day 7 with a 6-fold increase. The muscle construct also exhibited contraction upon light exposure. Lateral channels exhibited full endothelialization after 24 hours. A higher magnification in muscle sides of vessel-like structures showed that HUVEC sprouted preferentially toward the muscle construct, making a vascular network with larger sprouting area and length when the muscle tissue was present. VE-cadherin immunostaining showed a typical aspect of barrier-functionality of the vessel, that interestingly decreased when muscle tissue was present. Indeed, it can reflect the fenestrated endothelium when communicating with a nearby process, such as inflammation and regeneration. A novel approach of their work is the proof of a crosstalk between the muscle construct and the vessels by performing RT-qPCR assays. Angiopoetin-1, which is a, angiogenic factor secreted by muscle cells, is upregulated by the presence of EC. Neureglin-1, a myogenic factor secreted by endothelial cells was also upregulated in the presence of muscle cells, whereas VEGF expression did not change significantly. All genes related to muscle maturation (fast MyHC, slow MyHC, myogenin and myoD) were upregulated with the presence of EC co-culture. All these observations successfully demonstrated that muscles cells enhanced EC development, that in turn enhanced muscle development, in a circular cross talk.

This team is the same that successfully developed an innervated skeletal muscle on-a-chip we previously described [112]. Contrarily to Bersini *et al.,* vascularization is controlled and even allow neo angiogenesis to occur with sprouting. One point they could have shown is the perfusability of the vessel construct, they didn't investigate here. The way the device is fabricated also limits the fluidic connections. In my experience, having input and output on the side is not that convenient for connecting tubing. But they successfully achieved to build a vascularized skeletal muscle on a chip within a fully collagenic ECM. That is a critical point as molecules can diffuse through the ECM.

More recently, Urciuolo *et al.* developed a device made of poly acrylamide [119]. The main advantage of their technique is the material stiffness tunability. They created a scaffold with a stiffness of around 15 kPa, which has been reported to be the natural stiffness of skeletal muscle that has been reported [94]. Briefly, tense nylon threads of desired diameter were placed in the poly acrylamide solution. After curing and thread removal, they obtained various perfectly cylindrical channels, which were subsequently coated with laminin (Figure 58).

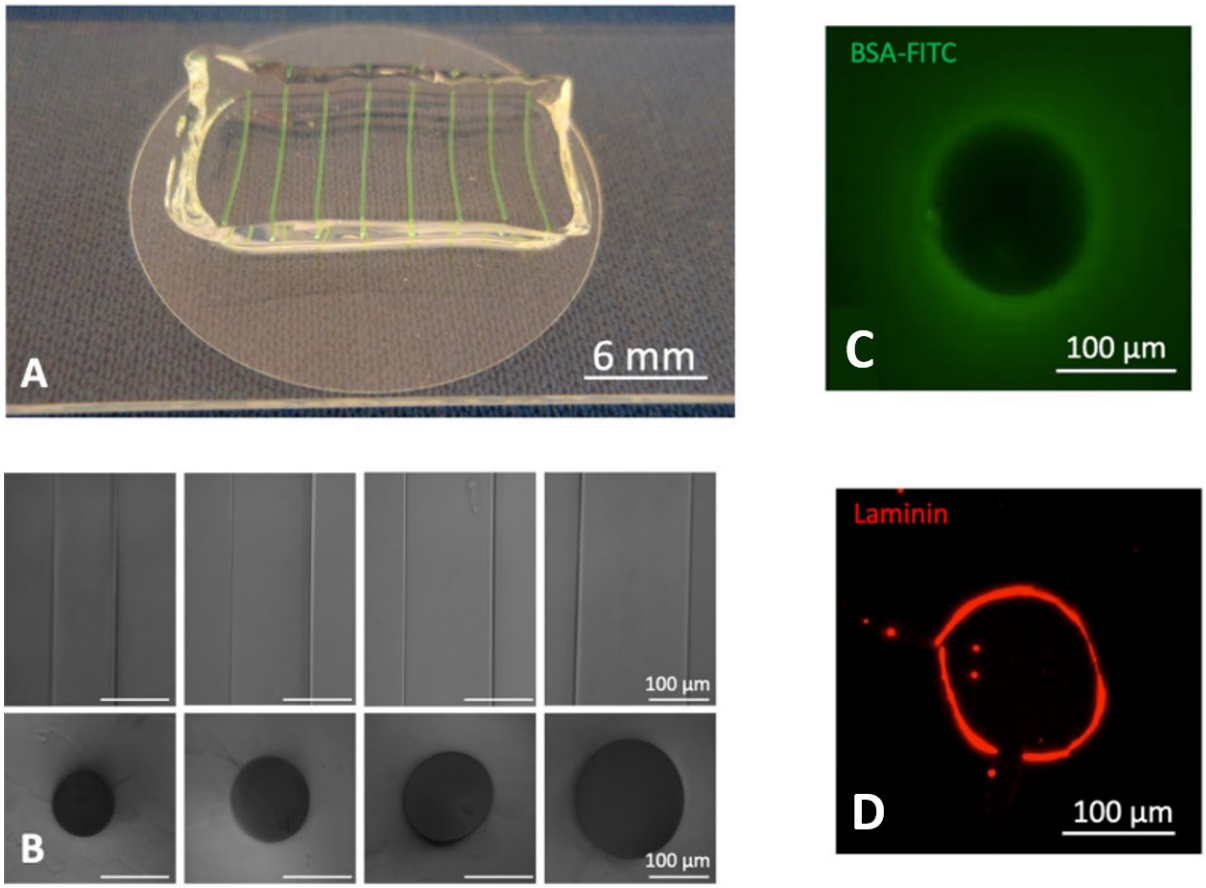

Figure 58: (A, B) Photography and phase contrast images of the 3d hydrogel with various hollow channel within it. (C) Cross-section of a 120 µm channel loaded with a solution of fluorescent BSA. (D) Cross section of a 120 µm channel coated with laminin. From [119].

A mixture of growth medium, C2C12 cells or human primary skeletal muscle cells with 25% Matrigel was seeded inside channels. The hydrogel structure was completely immersed in growth medium for 24h, then in differentiation medium until day 10. Their results showed that the optimal channel diameter was 120 µm. Muscle construct exhibited positive desmin and α-actinin staining after day 5, and positive myosin heavy chain as well as striations aspect at day 10.

The main drawback of their device is the lack of communication between each channel, hence resulting in no co-culture possible. Even though they have a physiologic stiffness of the material, it is still not biomimetic since it is polyacrylamide-based gel. No cells can be embedded within that gel. They device is also not compatible with any fluidic connection; hence no perfusion is possible either. An interesting point though is the 120 µm diameter selection as the optimal one to obtain homogeneous cell seeding. It is unfortunate they didn't show the results on the other diameter. Regrettably, there was no myotube diameter assessment nor forces measurement for further assess myotube maturation state.

4.3. **The MyoChip device**

In this first chapter, I tried to share with the readers a rather complete (if possible) view of the different existing models to develop in vitro muscle constructs. A majority of these approaches

relies on the tissue self-organization between anchors. One important contribution in the field, succeeded using geometrical cues on building a vascularized skeletal muscle on-a-chip, but without perfusion and permeability assays of the vessel structures.

- **The MyoChip device have therefore the potential to bring several key features for skeletal muscle on-chip engineering:**

- Biocompatible and biomimetic matrix capable of embedding other cell types for co-cultures with skeletal muscle cells
- Parallel multi tubes system, bringing independent yet connected compartments for different cell type culture
- Easy fluidic connection for microfluidics, allowing semi-automated cells seeding step
- The continuous perfusion of the co-cultured skeletal muscle tissue thanks to the the micro-vessel on chip

With these tools, we want to investigate the key elements required to build a skeletal muscle-on-a-chip. A strong emphasize should be underlined for co-cultures of skeletal muscles with fibroblasts and their crosstalk, since they are crucial for ECM remodeling.

In the next chapter, we will discuss about how the MyoChip device was fabricated and optimized, and how we cultivated cells within.

CHAPTER 2: MYOCHIP DEVICE OPTIMIZATION

In order to develop a skeletal muscle-on-chip, we first needed to determine the specifications regarding the geometry, the dimensions and the hydrogel that would best mimic the *in vivo* structure. The micro device should allow the culture several cell types in independent compartments, yet connected through a bio compatible hydrogel. As imaging will be one of the main output, the device should be compatible with high resolution microscopy. Finally, since engineering a micro-vessel on-chip is one of our objectives, connection of the device with microfluidic systems to perfuse the vessel should be easy and intuitive. We will therefore discuss these points in this chapter.

1. MyoChip micro device specifications

- **Cylindrical tubes**

To develop the MyoChip device that fulfills the requirements previously mentioned, we decided to design it as a multi tubular system embedded in biomimetic ECM. Indeed, as described in chapter I, *in vivo* muscle cells are encapsulated within arrays of aligned tubes surrounded by ECM. Another reason is that blood vessels also present a cylindrical shape. Even though we saw in chapter 1 that myofibers are vascularized by a dense network of micro capillaries, they all emerged from principal arteries that are cylindrical and parallel to myofibers. Compared to other 3D based on tissue self-organization of muscle cells between two anchors, working with a cylindrical hollow tube where we seed cells inside, allows an improved control of the geometrical cues imposed to cells. Knowing that cell alignment is a pre-requisite for further maturation, this configuration appeared to be an appropriate strategy. Last but not least, our lab had some know-how on the fabrication of such hollow structures. For all these reasons, the cylindrical geometry seemed to be the way to go for MyoChip project.

- **Hollow tubes dimensions**

As reported in chapter 1 (section 3.2.1), myofibers diameter is about tens of microns, and a fascicle's diameter is about hundreds of microns with a length of few millimeters. Regarding the vessel compartment and as reported in section 3.2.2, the average diameter of arterioles is hundreds of microns. Therefore, working at the muscle fascicle and the primary artery scale could be an appropriate combination both on the physiological side, and on the technological one. In my PhD, we thus aim at producing hollow tubes, which will be used to culture the different cell types, in the range of hundreds of microns in diameter, with a smaller diameter for blood vessel.
In vivo, the average distance between two fascicles is about few tens of microns. Since blood vessels can generate new vessels by neo angiogenesis, it is easier to consider the same inter distance between all the parallel tubes within our device.

The working dimensions to develop the MyoChip device are thus:

- Diameter of muscle tube: hundreds of μm.
- Diameter of blood vessel tubes: tens of microns.
- Few millimeters length for each tube.
- Inter tube distance of tens of microns.

- **Collagen I matrix**

In the MyoChip project, we aim at considering the culture of cells both within the tubes and in the surrounding ECM (fibroblasts, neurons), and thus decided to use collagen type I to mimic as much as possible *in vivo* conditions. Indeed, collagen I is the main component in skeletal muscle ECM. In addition, the stiffness of collagen gels can be easily tuned by changing the concentration as quantified by Verhulsel *et al* [120].

- **Imaging compatibility**

Among the possible experimental readouts of the MyoChip device, imaging and in particular confocal imaging has been considered as a 'must have'. Stacking all the focal planes from the bottom to the top of samples would allow a 3D reconstruction of the bioengineered scaffold. But considering this type of imaging technique, there is a crucial limitation: the depth of field that depends in particular on the numerical aperture (NA) of the objective (Figure 59).

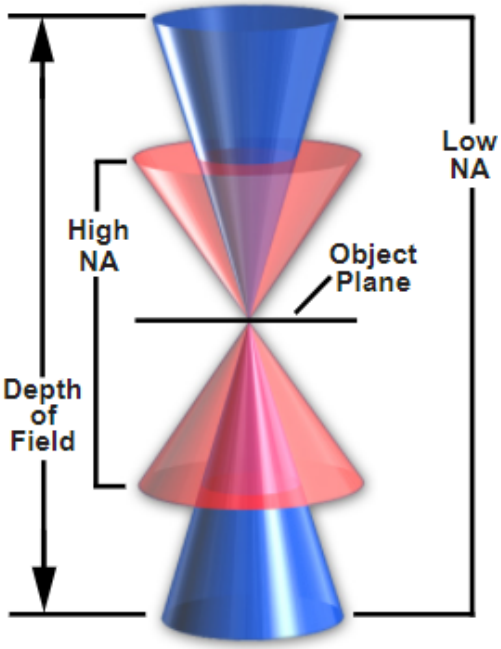

Figure 59: Schematics of depth of field depending on low (blue) and high (red) numerical aperture. From www.microscopyu.com.

A higher NA brings a better resolution, but on a small depth of field. High NA are usually found in high magnification objectives. The material through which light travels also impacts the image quality, even more in the presence of fluorescent dyes. The image quality will thus depend on technical limitations of the microscope. Therefore, the bottom part of the device and the positioning of the hollow tubes with respect to the objective should be minimal.

- **Fluidic connections**

In the MyoChip device, the cells (any cell type) will be in contact with medium through the

collagen gel. However, one single compartment of the MyoChip device, the endothelial one, requires a specific fluidic control. As we envision to perfuse the micro-vessel structures, inlets and outlets tubing are required. These connections should fit with standard microfluidics and should be easy to handle (*i.e.,* to connect and disconnect). Finally, each tube should be independent in a fluidic point of view, with their own inlet and outlet.

2. Development of the MyoChip micro device

Designing and micro-fabricating the chip was a long and tedious task in my PhD work with many iterations, but it was also a very interesting challenge. It was a circular process, from idea, to drawings, mold fabrication and chip testing. 3D printing by stereo-lithography was the main choice for mold prototyping, because it allowed fast prototyping compared to conventional photolithography process.

2.1. Design optimization

- **3D printed frames**

To generate micrometric hollow tubes in a collagen chamber, a frame with 3 holes on each side for the insertion of 3 parallel tubes was first 3D printed (Figure 60). This frame allowed the fabrication of 3 PDMS chips simultaneously.

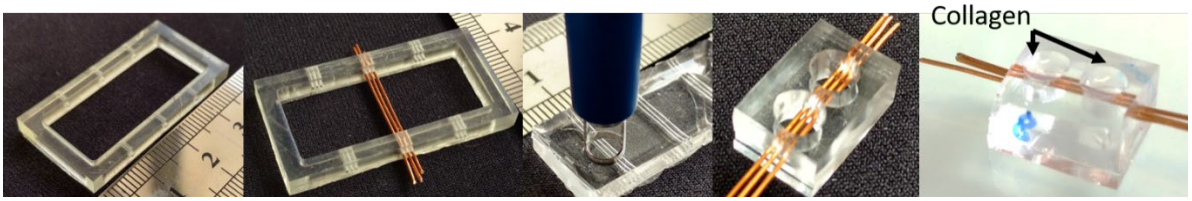

Figure 60: Photographs of 3D printed frames with 3 holes on each side for 3 parallel tubes. Each frame allowed the fabrication of 3 PDMS chips simultaneously. Copper wires were introduced, PDMS was casted. After PDMS curation, wire removal, unmolding, cutting and punching, the PDMS chip was plasma-bonded with a thin layer of PDMS at the bottom. Wires were then re-introduced again, in order to cast collagen around.

In the initial design, copper wires of 600 µm diameter were introduced before pouring PDMS. After PDMS curing, peeling, cutting and punching, the PDMS chip was plasma-bonded with a thin layer of PDMS at the bottom. Wires were then re-introduced again, in order to cast collagen around. This first generation presented several advantages along with some limitations. Thanks to this approach, the wires could be positioned precisely and the inter-tube distance could be tuned, as well as the bottom thickness of the device. However, at this stage, there were no fluidic connections and these wires are not easily removed after collagen polymerization (at 4, 6 and 8 mg/ml). Collagen stuck to the wires, thus removing them often resulted in completely deformed collagen channels. Finally, final tube diameter was still too large (around 600 µm).

- **3D printed molds**

A second generation design based on this initial concept was then developed. This mold was based on the previous frame concept that could be combined with another mold part, which perfectly fitted in the center of that frame (Figure 61).

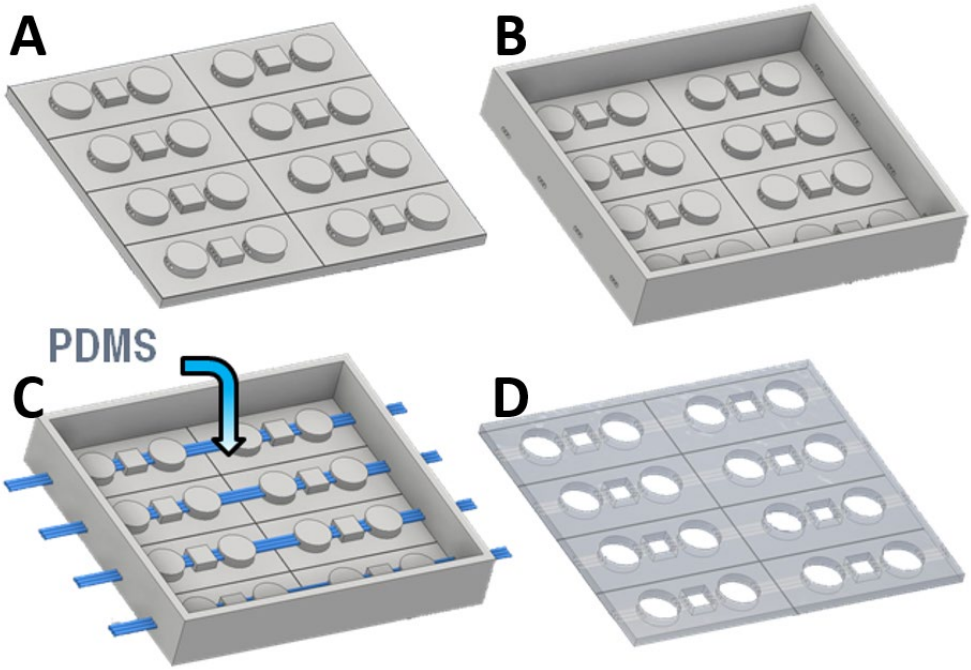

Figure 61: 3D designs of the two-parts mold. (A) The first part of the mold containing the central reservoir motif (square) and two lateral reservoirs for medium (round). (B) The second part of the mold: a frame containing side holes, fitting perfectly with the first part of the mold. (C). After inserting PEEK tubings (blue), PDMS is casted. After PDMS curing, PEEK tubing removal and unmolding, (D) an array of 8 PDMS chips is obtained.

Basically, the first part of the mold consisted of an array of 8 chips. The pattern for one chip was composed of a central reservoir for the collagen, and two lateral reservoirs for the culture medium (Figure 61A). The second part of the mold was a frame with side holes, which fitted with the first part of the mold (Figure 61B) and allowed the insertion of PEEK tubing (OD of 800 µm) through the side holes, through the patterns from end to end (Figure 61C). After PDMS casting and curing, PEEK tubing removal and unmolding, an array of 8 PDMS chips was obtained (Figure 61D). Short PEEK tubing of 5 mm length with OD of 800 µm could then be inserted back at each extremities of the PDMS channels (Figure 62A) to be used as connectors for further fluidic control. An acupuncture needle of 200 µm of diameter and 30 mm length was then inserted inside the PEEK tubing (ID of 250 µm), crossing the whole chip to generate the hollow tubes in collagen. The collagen pre-polymer solution was poured in the central reservoir. After 2 hours at 37°C, the collagen was polymerized around the needles (Figure 62B). After their removal, hollow collagen tubes were generated (Figure 62C).

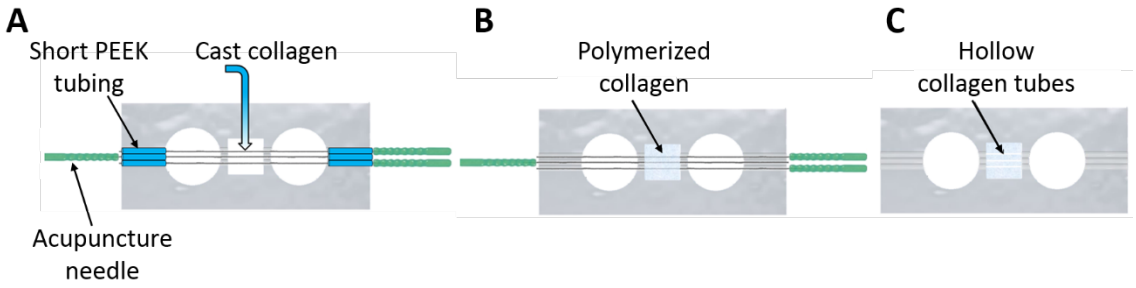

Figure 62: Collagen tubes generation with acupuncture needles. (A) Short PEEK tubing (blue) are inserted at each end of the newly generated PDMS channels. An acupuncture needle is then inserted inside the PEEK tubing, crossing the whole chip. Collagen is casted in the central reservoir, around the acupuncture needles. (B) After 37°C for 2 hours, the collagen is polymerized around the needles. (C) After needle removal, hollow collagen tubes are generated.

In these conditions, since tubes were generated with microfluidic standard PEEK tubing, it could be easily connected for fluid control. Using PEEK tubing to maintain acupuncture needles in place allowed much smaller collagen tube diameter compared to previous models (ranging from 120 µm to 200 µm). We also decided to seal the bottom part of the chip using a glass cover slip to improve imaging.

This new design presented several advantages but major drawbacks remained. In particular, fluidic connections were on the sides and were not easy to handle. The device bottom part remained too thick for an optimal confocal imaging. Because of PEEK tubing dimensions (OD 800 µm, ID of 250 µm), the inter-tube distance from center to center as well as the distance of the hollow tube from the bottom of the chip were similarly too large (Figure 63).

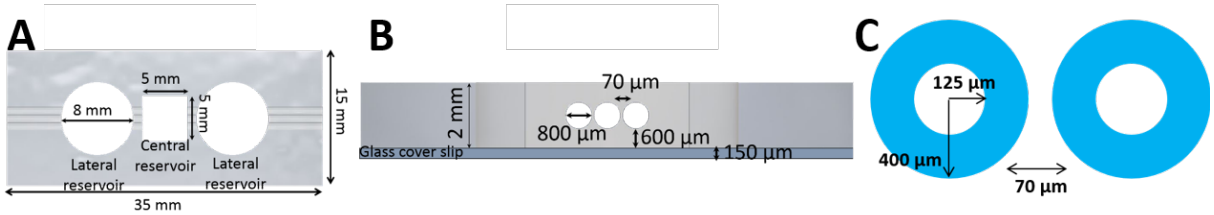

Figure 63: (A) Top view and (B) side view of the PDMS chip, depicting the dimensions. The central reservoir is a square of 5 x 5 mm. Lateral reservoirs for culture medium are 8 mm diameter. Bottom thickness of the chip is 750 µm, considering the glass cover slip (side view). (C) PEEK tubing schematic (in blue) with an inter-tube distance from center to center of 870 µm.

2.1. The final MyoChip design

To overcome these limitations, and in particular to further reduce the distance between tubes, we decided to directly use the acupuncture needles to shape PDMS channels instead of short PEEK tubing as it presents a smaller diameter. 3D printing laser parameters along with the nature of the 3D printed resist were optimized to properly print the structures that will maintain needles in place throughout the mold.

2.1.1. Resists and 3D printing optimization

DS3000 resin. First prototypes were made of DS3000 resist[i], which is a sold by DWS manufacturer as a biocompatible resist for dental applications. As explained previously, side micrometric holes were 3D printed directly onto the mold to position the short PEEK tubing and the needles. During the MyoChip development, we faced some difficulties related to the shrinkage of the 3D printed structures with an observed diameter reduction of about 30% compared to the expected one.

Our 3D printing strategies relied on stereo lithography which is a layer by layer approach. The moving plate is immersed into the photo polymerizable resist tank. The laser then sweeps the resist tank following the designed pattern. The plate is lifted with the polymerized resist layer and is immersed again. The process is repeated until completion of the. This process could explain the

[i] https://plastics.ulprospector.com/datasheet/e253455/digitalwax-ds-3000

reduced dimensions of the holes present on the frame of the mold.

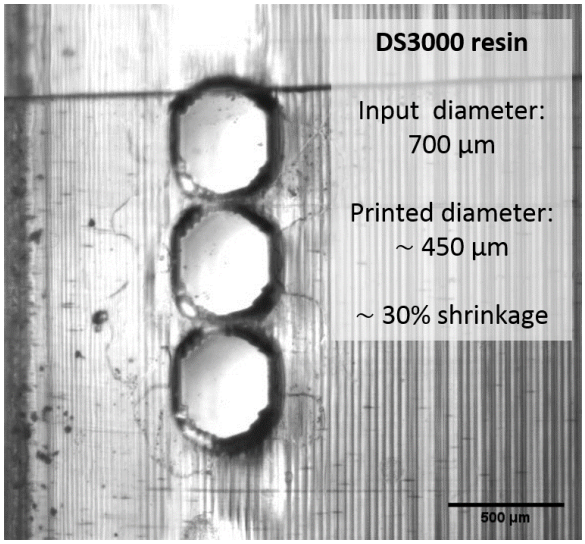

Figure 64: Light microscopy images of the side holes of a 3D printed mold using DS3000 resin. Hole's diameter is set to be 700 µm in the software, but a shrinkage of about 30% was observed resulted in about 450 µm hole diameter after 3D printing.

Indeed, 3D printed layers containing the holes pattern are going to be exposed several times. Layers that have been already exposed and lifted still have a thin layer of liquid resin on their surface. The repeated exposures will then reduce the holes diameter by photo-polymerizing these extra resist layers. This phenomenon is even more accentuated for holes in thicker walls, resulting in obstructed holes. Attempts have been made to tune the laser speed (hence the exposure time) and the number of times the laser would expose contours. But experimentally, the maximal wall thickness for which holes were not obstructed was 1 to 2 mm. Above that, mechanically drilling the mold was necessary.

To overcome this difficulty, we considered another resist: the Precisa DL260. This is a liquid non-transparent blue-grey resist containing nanometric silica particles[i]. It is sold as a resist that 'delivers extremely smooth surfaces and exceptionally precise and sharp details' according to DWS manufacturer. However, holes obstruction was still observed but for holes diameter less than 200 µm and wall thickness above 5 mm long, probably due to resin trapped inside. To print the final design mold, z-step was set at 100 µm for layers below and above layers containing the lateral holes. We then optimized the z-step for the holes 3D printing and we clearly observed that a small z-step increased over-exposure phenomenon leading to reduced or obstructed holes while a larger z-steps lead to enlarged holes, hence not maintaining the needles as desired. Finally, we observed that the optimal z-step for the layers containing the holes was at 30 µm.

2.1.2. PDMS curing inhibition by 3D printed resin mold

When using 3D printed mold for the PDMS chip fabrication, we faced specific issues related to curing inhibition, as we mostly obtained very sticky PDMS chips that were often impossible to

[i] https://www.dwssystems.com/en/configurator/X/15/precisa-dl260-en

unmold. Following the manufacturer's guidelines, newly 3D printed molds were washed in isopropanol along with ultrasound cleaning, then exposed in UV light for 30 min. However, at this stage it did not improve the chip quality.

Optimization of UV exposure and baking times were thus necessary. 3D printed molds in Precisa DL260 resin were submitted to different UV exposure times (30 min and 60 min) and to different baking time at 60°C (1 hour, 12 hours and 24 hours). We finally, achieved optimal conditions where molds were immersed in isopropanol and sonicated for 2 min. Isopropanol was then discarded and replaced with fresh isopropanol. After another 2 min of sonication, molds were flushed with air until dried, UV-exposed (13 mW/cm²) for 30 min and baked at 60°C for 24 hours.

PDMS curing inhibition due to 3D printed mold has recently been investigated by another team [121]. They compared PDMS curing inhibition for 16 commercial resists, depending on different post-printing treatments. The main conclusion of their work was that, to fully cure the PDMS, experimental UV exposure and baking times were finally always longer than the indications of the manufacturer guidelines. The optimal post-treatment for Precisa DL260 resin they found was either no UV exposure and baking at high temperature (120°C) for 2 hours, either UV exposure (14 mW/cm²) for 2 hours and baking at lower temperature (60°C) for 24 hours, which was similar to the optimal conditions we found.

2.1.3. Optimized MyoChip fabrication process

The final mold design is depicted in Figure 65A. Briefly, needles of 200 µm were inserted into the side holes of the mold through the hollow patterns (Figure 65A). PDMS is then casted on top, after PDMs curing, the needles are removed (Figure 65B and C). The central reservoir, the inlets and the outlets are then punched into the PDMS chip, before oxygen plasma-bonding a glass cover slip (Figure 65D, E). The device was sterilized in ozone-UVs for 5 min and is placed under sterile biological hood. Sterile needles of desired diameter were inserted back in the chip, and collagen was poured in the central reservoir, containing the suspended needles (Figure 65F).
Collagen preparation must be done very carefully to avoid bubbles trapping within the gel. Chips were then put inside the incubator at 37°C for 2 hours. After collagen polymerization, needles were carefully removed, generating hollow collagen tubes (Figure 65G, H). When collagen is polymerized, chips are all immersed in PBS and stored at 4°C for at least 12 hours. Working with needles of 200 µm, collagen tubes are spaced by 300 µm distance (Figure 65I). A small circular PDMS well is fixed with silicon glue on top of the central reservoir to reduce the use of cell culture medium when compared to fully immersing the chip (Figure 66).

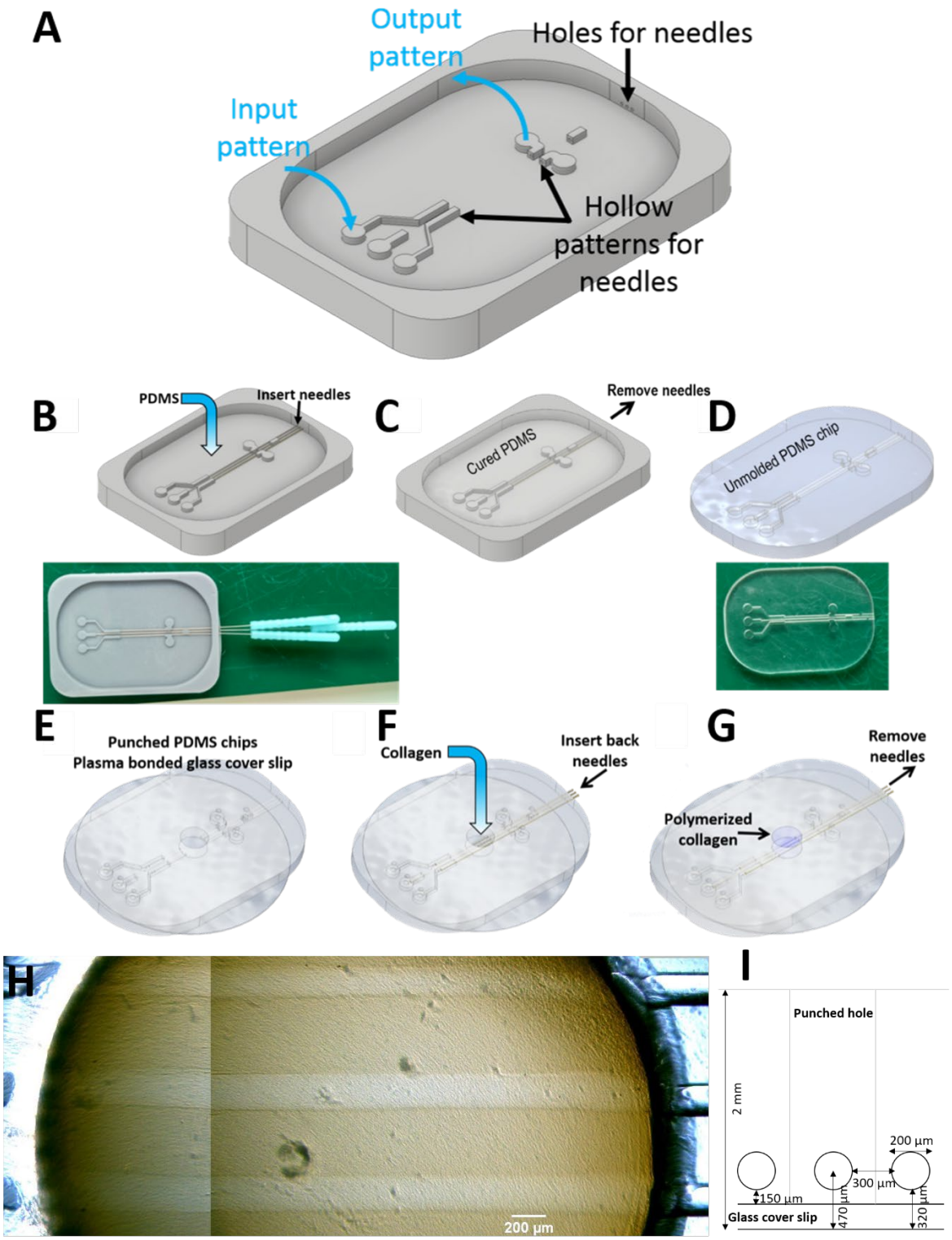

Figure 65: (A) Final mold design. Holes and hollow patterns to maintain needles are printed on the mold. Inputs and outputs patterns are also directly printed on the mold, so the fluidic tubing will be connected from the top. (B) Needles of 200 µm are inserted from the side holes of the mold, through the hollow patterns. PDMs is then casted on top. Actual picture of the mold below. (B) After PDMS curing, the needles are removed and (D) PDMS chip is unmolded. (E) The central reservoir, inputs and outputs are then punched into the PDMS chip. A glass cover slip is plasma-bonded underneath the chip. (F) Collagen is then casted in the central reservoir, surrounding the needles. Chips are then put inside the incubator at 37°c for 2 hours. (G) After collagen polymerization, needles are carefully removed to generate hollow collagen tubes. (H) Collagen hollow tubes obtained after needles removal. (I) Schematics of a cross-section view of collagen channels with dimensions within the PDMS chip.

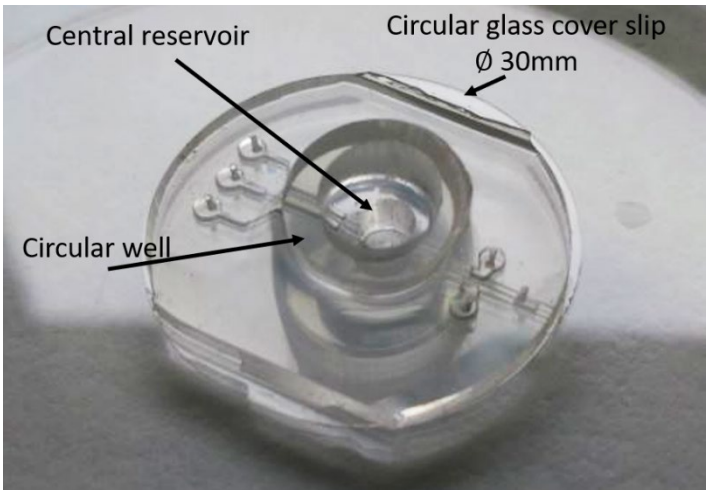

Figure 66: PDMS chip with the PDMS circular well on top of the central reservoir, to use less medium and immunostaining reagents.

Compared to previous versions, in this one, the fluidic connections are now at the top of the chip, making it easier to plug/unplug tubing. The mold directly maintains the needles in place, so distance between two tubes is decreased, as well as the bottom thickness (320 μm vs. 750 μm). Customizing the tube diameter is easily done by changing the needle diameter. A circular PDMS well placed on top of the central reservoir greatly reduced the volume of medium used as well as immunostaining reagents.

This design fulfilled our specifications. However, it is worth mentioning that despite being our final and favorite one, we also consider that there is still room for improvement. In particular, the mold is not designed for high throughput fabrication. Obviously, optimization is an infinite process and a design can always be further optimized. But considering all the improvements made and the fulfilled specifications, it was reasonable at this stage to start biological experiments with that one.

The optimized micro-fabrication process

- **1/ PDMS Chip fabrication**

Three stainless steel acupuncture needles of 200 μm diameter were inserted into the mold from the side holes. Then 1.7 μL of PDMS (1:10) was casted into the mold, surrounding the needles. Molds were degassed in vacuum for 1 hour and PDMS was cured at 75°C in the oven for 2 hours. Needles were removed and PDMS chip was unmolded. Each chip was cropped with a 30 mm diameter punch, in order to fit into a 6-wells plate. A 6 mm diameter punch was used to generate the central reservoir. A 0.75 mm diameter punch was used for inlets and outlets. The chips were cleaned in ethanol and air-dried. PDMS chips bottom part were sealed with a round glass cover slip by oxygen-plasma bonding, before heated at 75°c for 30 min. To use less medium and immunostaining reagent, a PDMS circular well was plasma-bonded on top of the central reservoir as shown in Figure 66. To make these circular wells, 90 g of PDMS (1:10) was poured in a 15 mm petri dish, and let on a flat surface for 12 hours, before heated at 75 °c for 2 hours. A 12 mm PDMS piece was first punched, then a hole of 8 mm diameter was punched inside this piece to make the circular well. Chips were then heated at 75 °C for 30 min.

- **2/ PDMS surface treatment by APTES and GA**

A 10% APTES solution (v/v) in absolute ethanol was injected with a glass syringe through each of the three inlets. Treating the inputs PDMS channels with APTES (without glutaraldehyde)

allows the surface to be hydrophilic to limit bubble nucleation. Then the APTES solution was added in the central reservoir until filled. After 30 min, chips were immersed in absolute ethanol, submitted to 2 min vacuum then to 30 min ultrasound at 60°C. The chips were then air-dried, before adding a solution of GA at 2.5 % only in the central reservoir until filled. After 30 min, the chips were immersed into milliQ water, submitted to 2 min vacuum, then to ultrasound for 30 min at room temperature. MilliQ water was discarded, and the chips were immersed for 12 hours in fresh milliQ water. After air-dried, the chips were sterilized with ozone UV for 10 min.

- **3/ Collagen preparation**

Under a sterile biological hood, needles of desired diameter, priorly treated by immersion in sterile PBS BSA 4% for at least 30 min, were inserted into the PDMS chips. Experimentally, the needles are usually stored immersed in sterile PBS-BSA 4% solution at 4°C for an indefinite period of time. To generate 200 µm collagen tubes, acupuncture needles were used. To generate smaller collagen hollow tubes, we used straight tungsten wires of 75 µm. Manipulation on ice is recommended for collagen. Stirring is carefully done with a micro spatula to avoid bubbles. If there are bubbles while preparing the collagen solution, a quick vortex can be done. Collagen at desired concentration was prepared following the manufacturer's instructions, and casted in the central reservoir until filled. A particular care must be placed for collagen casting so it goes beneath the needles. An extra caution must also be placed to avoid bubbles in collagen, monitored by phase contrast microscope. If there are bubbles in the collagen gel after casting onto the chip, placing the chip at 4°C for 30 min can help eliminating the bubbles. After collagen casting, the chips are let at room temperature for 10 min, before being placed the incubator at 37°C for 2 hours. After collagen polymerization, the chips are immersed in sterile PBS and stored at 4°C for 12 hours before cell seeding. Channel generation occurs when removing the needles. But that step is only done while seeding cells.

2.2. On-chip PDMS-collagen bonding

To withstand the forces applied by cells, the collagen has to be covalently grafted to PDMS. Several strategies have been reported in the literature. In our case, to covalently graft collagen, the PDMS surface was first silanized by (3-aminopropyl) triethoxysilane (APTES) and the collagen was covalently bound thanks to the use of a cross-linker such as glutaraldehyde (GA) [122], [123] (Figure 67). Table 1 gathers different surface treatment conditions based on APTES and GA used to graft different biomolecules to PDMS.

From this literature survey, we can conclude that reagents concentrations are usually at 10% (v/v) for APTES and 2.5% (v/v) for GA These concentrations were also optimal regarding collagen attachment for the MyoChip device.

However, GA is toxic for cells, and rinsing it did not seem to be emphasized in most of these papers (Table 1). Indeed, when optimizing surface treatment process with high GA concentrations, experiments failed because of cell death although collagen attachment to PDMS was satisfying. It appeared that rinsing GA for 12 hours in distilled water was not sufficient.

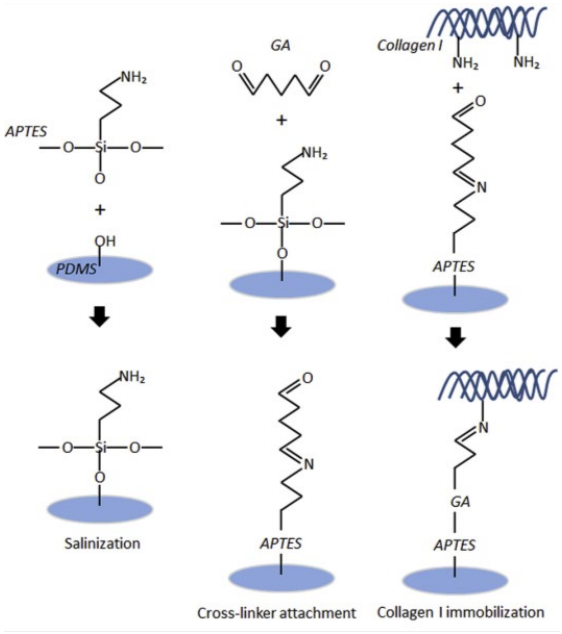

Figure 67: PDMS surface treatment using (3-aminopropyl) triethoxysilane (APTES) and glutaraldehyde (GA). The PDMS surface is oxidized with oxygen-plasma before being exposed to subsequently to APTES then GA. Deposited collagen will then covalently attach to the PDMS-treated surface.

Table 1: PDMS surface treatment conditions using (3-aminopropyl) triethoxysilane (APTES) and glutaraldehyde (GA) for biomolecules grafting.

Articles	APTES	Solvent	Time	Rinsing	GA	Time	Rinsing
Lab previous protocol	2%	PBS	30 min	PBS	0.5%	30 min	Distilled water 12h
W. Tan *et al.*, 2004 [123]	100% at 60°C	Vapor deposition	70 min	N/A	6%	20 min	Water
L. Yu *et al.*, 2005 [124]	10% at RT	Ethanol (absolute)	10 min	96% Ethanol Heat 80°C 2h	2.5%	60 min	Tris-HCl pH 8
P. Wipff *et al.*, 2009 [125]	10% at 60°C	Ethanol	60 min	PBS	3%	20 min	PBS
S. Kuddannaya *et al.*, 2013 [126]	10% at 50°C	N/A	60 min	Nuclease free water	2.5%	60 min	Nuclease free water
V. Pinto *et al.*, 2015 [127]	50% at RT	Ethanol (absolute)	10 min	Ethanol Heat 80°C 2h	2.5%	60 min	N/A
Y. Chuah *et. al*, 2015 [122]	10% at 54°C	N/A	120 min	Distilled water	2.5%	60 min	Distilled water
Z. Qian *et al.*, 2018 [128]	10%	Ethanol	120 min	Ethanol	2.5%	60 min	Deionized water

RT: room temperature.

The main difference between our configuration and the one reported in Table 1**Error! Reference source not found.**, is the opened flat surface configuration they are working with, making the rinsing step much easier. We thus optimized rinsing steps both for APTES and GA

grafting.

Previous APTES rinsing was performed by pipetting PBS onto the treated surface to wash it three times. However, APTES white depositions and aggregates formed when adding GA in water, frequently obstructing the chip PDMS channels. To avoid these depositions, two main rinsing methods were investigated (Table 2**Error! Reference source not found.**). The optimal APTES rinsing condition was to immerse the chips into absolute ethanol, to submit them to vacuum for 2 min, then to expose them to ultrasound for 30 min at 60°C.

GA rinsing conditions were the same as for APTES rinsing (Table 2). It appeared that the optimal condition for GA rinsing was the same as for APTES rinsing, except milliQ water was used for all steps instead of absolute ethanol. An extra step was needed after 30 min ultrasound exposure (at room temperature): immersion for 12 hours in fresh milliQ water. With this surface treatment rinsing protocol, cells survived inside collagen tubes.

Table 2: Investigated APTES rinsing methods.

Rinsing method			**APTES depositions**
Three washed wish absolute ethanol			++++
Chips immersed in absolute ethanol			
In a beaker with magnetic stirrer	RT	10 min	+++
		30 min	+++
	60°C	10 min	++
		30 min	+
In a beaker, exposed to ultrasound	RT	10 min	+
		30 min	+
	60°C	10 min	+
		30 min	+
In a beaker, under vacuum for 2 min at RT Then exposed to ultrasound	60°C	30 min	Rare

RT: room temperature.
Cross marks indicate very high (++++) or few (+) depositions of APTES.

2.3. Collagen hollow tubes characterization

To characterize our microfabrication method, the collagen tubes were first coated with, fluorescent BSA Alexa Fluor™ 488 (Figure 68A). We observed that collagen channel diameters were slightly decreased compared to theoretical value of 200 µm (Figure 68B). To further characterize the collagen tube diameter, 10 different z-stacks of several collagen tubes were analyzed using ImageJ software (Figure 69).

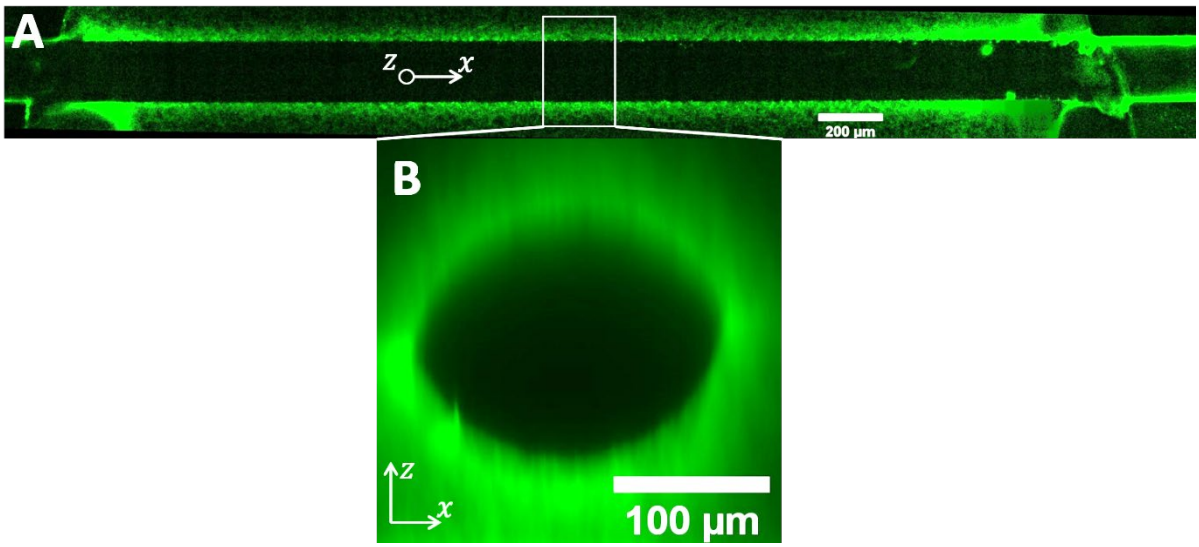

Figure 68: Collagen hollow tubes characterization in confocal microscopy after 200 µm needle removal and fluorescent BSA injection. (A) A longitudinal section of the collagen tube. (B) Cross-section of the collagen hollow tube, showing an elliptical-shaped tube.

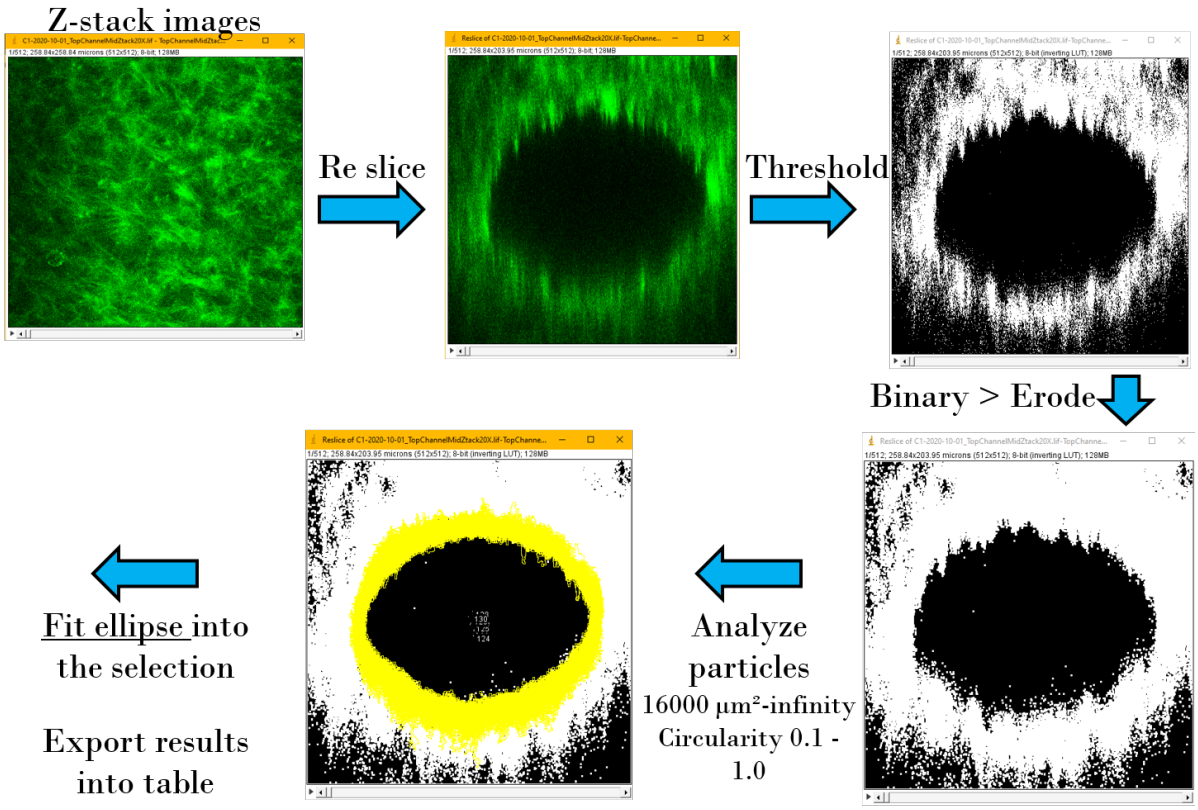

Figure 69: Collagen tubes diameter characterization using ImageJ software. Starting from a z-stack images, a cross-sectional re slice is performed. After thresholding, making the image binary and eroding, 'analyze particles' function is called. Particle's area was set to 16 000 µm² to infinity, and circularity was set to 0.1 - 1.0. An ellipse was then fit to the selections, and results were exported into a table.

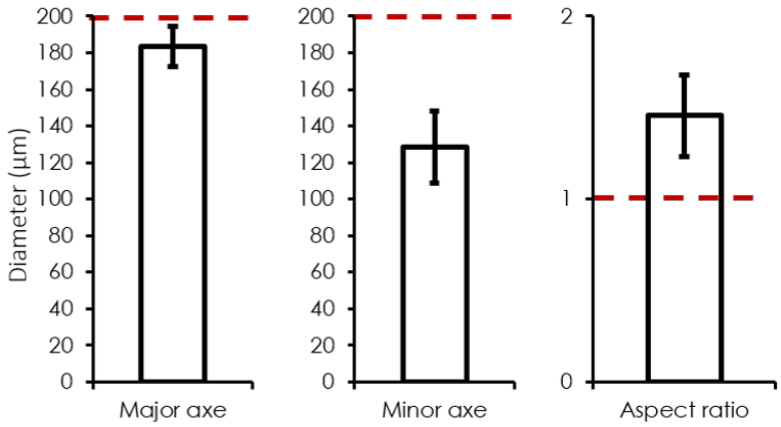

Figure 70: Collagen tube diameter characterization by analyzing z-stacks on ImageJ software. Generated collagen tubes are elliptical, with an average major axe of 184 ± 11 µm, an average minor axe 129 ± 20 µm leading to an average aspect ratio of 1.5 ± 0.2. The red dashed line is the theoretical value for a 200 µm diameter needle. n = 10.

Our results showed that these elliptical-shaped collagen tubes had an average major axe of 184 ± 11 µm and an average minor axe of 129 ± 20 µm. The aspect ratio was thus at 1.5 ± 0.2 on average (Figure 70). Such results were unexpected as the acupuncture needles present a cylindrical shape. However, collagen being a hydrogel can swell in liquid, the swelling rate depending on the hydrogel properties. Collagen is an extremely high swelling hydrogel, capable of increasing its weight up to 50-folds [129] compared to other frequently used hydrogels such as agarose, that can increase its weight only by 5 to 6-fold [130]. Hence, as the chip is completely immersed in PBS for 12 hours at least, collagen soak PBS and swells in an isotropic way. This swelling could explain the reduced diameter compared to expected values. And finally, generating an elliptic-shaped collagen tube was not seen to be an issue as in vivo myofibers are never perfectly cylindrical but have a more elliptic shape.

3. On-chip cells seeding

Seeding cells inside collagen tubes appeared to be a complex task, with several challenges. In the literature, cells seeding method is rarely mentioned or emphasized [116]–[118]. When mentioned, it was usually performed manually with a micropipette [104], or with a syringe [111]. However, preliminary experiments revealed the difficulty to achieve reproducible conditions with manual cells seeding, we thus investigated how to improve cells injection using a pressure pump controller.

To allow live monitoring of cells seeding, this step was performed on a phase contrast microscope. Different cell types have been used as it will be discussed in the next chapter, but our system has been optimized with C2C12 cells (5 to 10 $\times$ 10^6 cells/ml).

3.1. Manual cells seeding

Considering that one collagen tube dimension was 6 mm length and 200 µm of diameter, the volume of each collagen tube was thus about 0.75 µl. However, 'dead volumes' of PDMS channels

also have to be considered (Figure 71). Each PDMS channels 'dead volumes' has a volume of about 4.7 µl per channels for the inlets, and of about 5 µl per channels for the outlets. Therefore, a volume of about 1 µl of cells suspension is needed to fill the collagen tube, followed by a volume of 4.7 µl to push the cells through the PDMS channels dead volume (Figure 71).

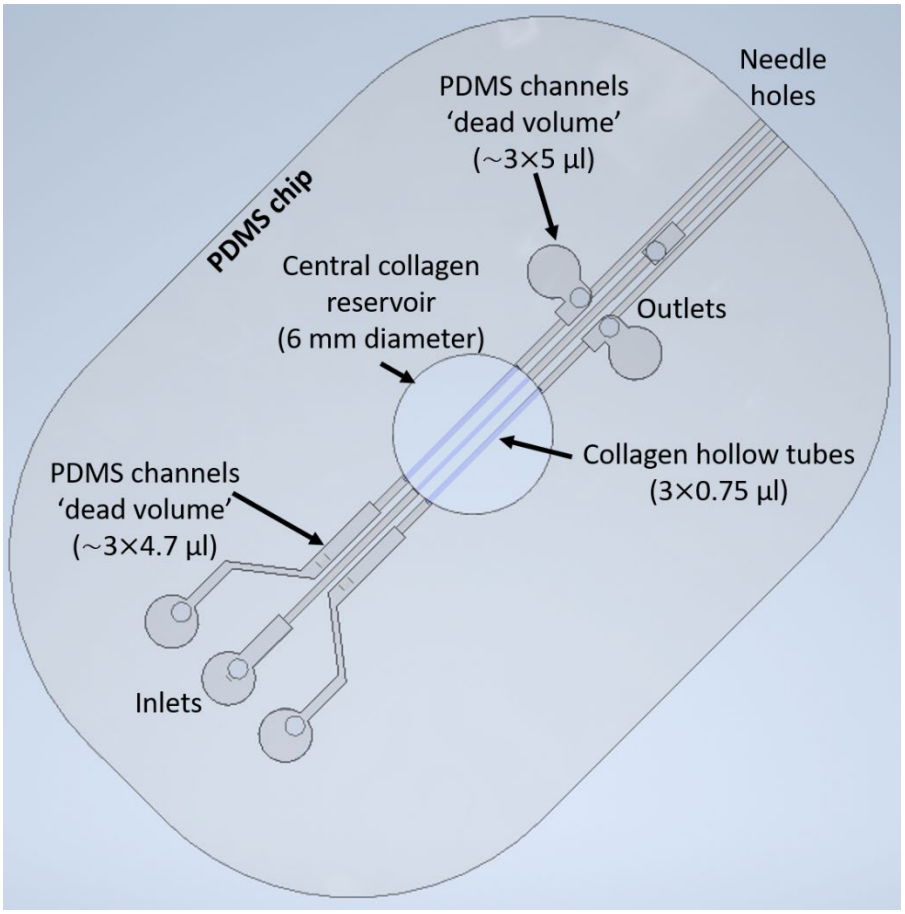

Figure 71: Schematics of the PDMS chip containing three hollow collagen tubes of 200 µm each. Collagen hollow tubes volume is about 0.75 µl per tubes. PDMS channels 'dead channels' volume is about 4.7 µl per channels for the inputs and about 5 µl per channels for the outputs. The resulting total PDMS channels dead volume is about 30 µl.

Micropipettes of 10 µl and 100 µl were used to seed the cells inside the device. Several issues were observed using this method. Seeding using micropipettes did not yield high cell density inside collagen tubes in a reproducible manner. Most of the time, collagen tubes were empty or filled with less than few tens of cells after the seeding (Figure 72).

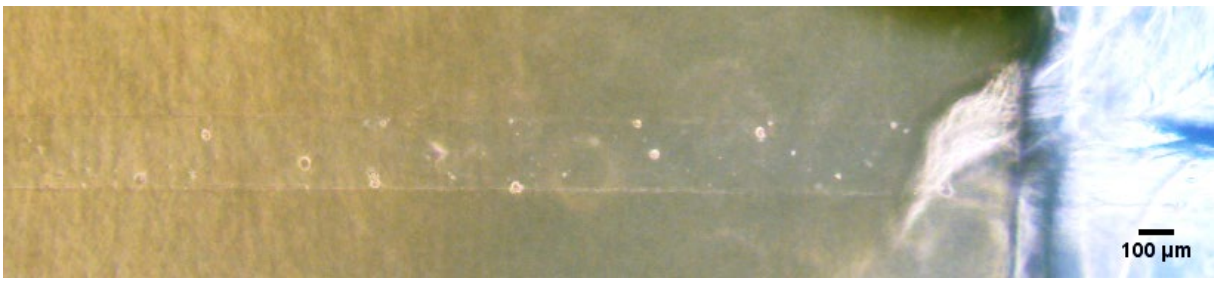

Figure 72: Collagen tube after seeding with micropipette. Note that cell density inside the tube is very low although the cells suspension concentration is 5-10 × 10^6 cells/ml.

Some hypothesis can explain this behavior. Cells tend to aggregate, hence resulting in an increased object mass. This leads to sedimentation. The PDMS channels-collagen tube transition

is sharp, worsening the sedimentation phenomena (Figure 73).

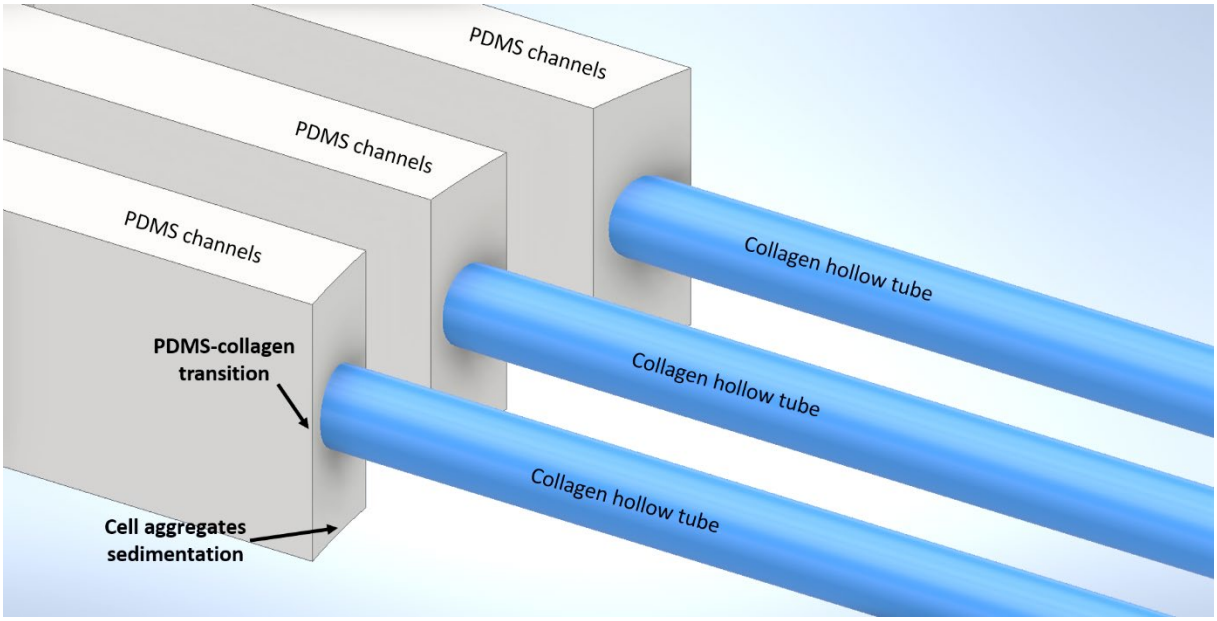

Figure 73: Schematics of the PDMS-collagen transition showing a very sharp junction, with a potential location for cells aggregate sedimentation at the bottom of the PDMS channel.

Another hypothesis is the collagen elastic deformation. Indeed, the over pressure continuously generated by pushing the cells suspension inside leads to collagen channel expansion since it is a deformable material. When this over pressure stops (end of seeding), there is a collagen relaxation that tend to return to its initial state, ejecting the additional volume with the cells outside the tubes (Figure 74). As we saw, the volume inside a collagen tube is less than 1 µl. This volume ejection due to collagen relaxation phenomenon is probably more complex if we consider the whole collagen bulk deformation and relaxation.

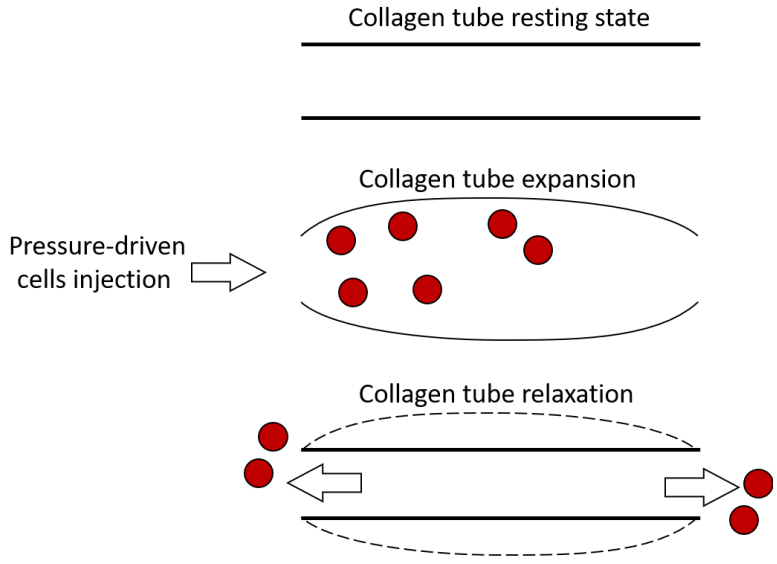

Figure 74: Schematics of the collagen tube elastic deformation hypothesis. (A) Collagen tube at resting state. (B) When cells suspension is injected inside the tube (red circles represent cells), an over pressure is generated inside, expanding the tube diameter. (C) When the seeding stops, the tube returns to its resting state due to collagen relaxation, ejecting the same amount of volume inside the tube, hence ejecting the cells.

It is also worth mentioning that micropipette seeding frequently introduced bubbles inside the system and once a bubble got trapped inside the system, it was near impossible to seed the chip

anymore (Figure 75).

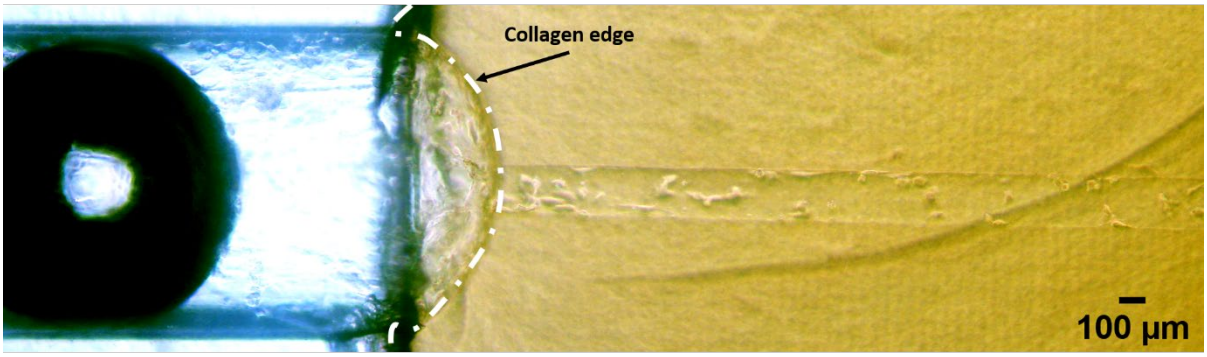

Figure 75: Collagen detachment from PDMS surface (white dashed line: collagen edge). Note the bubble in the PDMS channel on the left, which is frequent when seeding with a micropipette.

3.2. Using a semi-automated pressure controller

Based on these first observations, we considered in collaboration with Fluigent to perform cells seeding using a pressure pump controller that could pressurize an air-tight tube containing cells suspension. The suspension then flows inside a tubing that is connected to the MyoChip device (Figure 76).

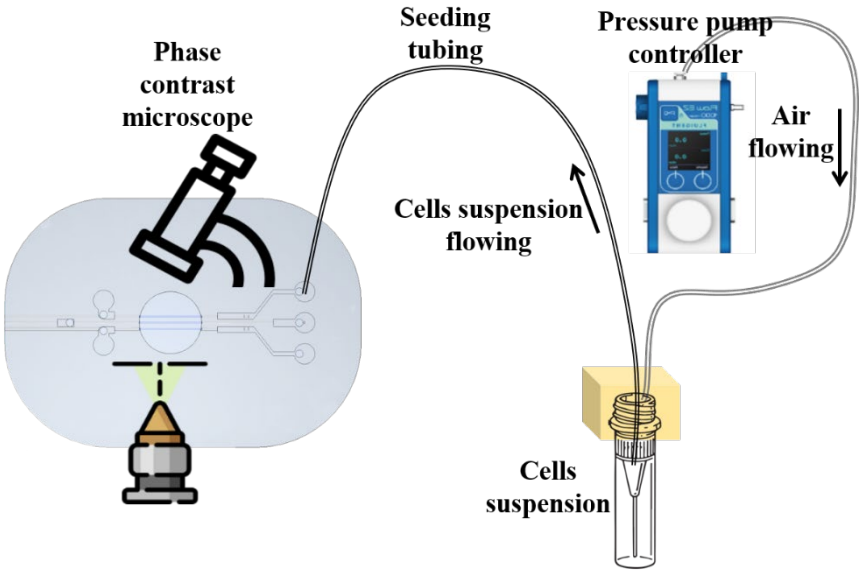

Figure 76: Schematics of the cells seeding set-up using a pressure pump controller. The pump pressurizes the cells suspension tube. The suspension then flows though the seeding tube, connected to the MyoChip device. The experiment is live-monitored under a phase contrast microscope.

Cells were prepared as discussed earlier, and suspended in a tube. Prior to seeding, the seeding tubing (PTFE tubing, inner diameter of 300 µm, length of about 25 cm) was rinsed with about 350 µl of growth medium. The injection pressure was set to 25-40 mbar for cell seeding to avoid applying high shear stress on cells. When the seeding of one collagen tube was performed, the seeding channel was disconnected and re connected to the second input of the device. While the pressure pump gave more control over the seeding, such as cells speed and stable pressures avoiding collagen detachment, some issues remained and other appeared. Unfortunately, as previously, after the seeding step the cell density in tube remained very low.

Experimentally, we showed that C2C12 cells adhere to the collagen in about 1 hour. Working at $\Delta P = 40$ mbar, the average flow rate within the tube is about 6.22×10^{-9} m^3s^{-1} corresponding to an average flow velocity of $v \approx 1.41$ ms^{-1}. Therefore, the residence time of the cell inside the collagen tube of 6 mm long is about 4.26 ms, which is way smaller than the adhesion time of the cells.

We could argue that by reducing the flow rate (by decreasing ΔP), cells could have time to adhere. However, it is experimentally difficult because of cells aggregation and sedimentation. To improve our seeding density and in particular cell residence time, we decided to vary the device hydrodynamic resistance. To do so, during collagen tube molding, the needles are removed but their tip remains at the collagen-PDMS junction to drastically increase the hydrodynamic resistance (Figure 77A, black arrow). Collagen being a porous medium, in these conditions cells seeding resulted in a higher cell density inside collagen tubes (Figure 77B) that will be further characterized in the next chapter.

Figure 77: (A) A PDMS chip showing (black arrow) the tip location of the needles after removal during collagen tube generation. Letting the needles tip at that location mimic the presence of a bubble, hence resulting in (B) higher cell density while seeding from the inputs (which are on the left side).

To avoid backflow when unplugging the tube after seeding, we implemented a very simple but efficient approach. The principle was to perform the seeding with a flexible PTFE tubing (inner diameter of 300 µm, external diameter of 760 µm) then, to directly cut the tubing with scissors while maintaining a pressure of 30 mbar, letting about 3 mm of tubing still connected to the inlet. In these conditions, we did not experienced any backflow and the cells remained to adhere in the tube after their seeding.

CHAPTER 3: DEVELOPING A SKELETAL MUSCLE-ON-CHIP

Based on the MyoChip technologies optimized in the chapter 2, here we will discuss about the different parameters that influenced on-chip cell growth and maturation. A cell line model (C2C12 myoblasts) was first used to investigate what the minimal conditions are to achieve a muscle on chip model with features close to *in vivo* conditions. Finally, we will see how moving toward more complex cell models, such as primary mouse myoblasts is not trivial, although the experimental conditions have been optimized for C2C12 cells.

1. Defining the minimal cues to generate a skeletal muscle tissue-on-chip

In 1977, in order to create a model of muscular dystrophies, Yaffe and Saxel designed an experiment to isolate myocytes and to cultivate them [131]. From two months-old dystrophic mice, thigh muscles were collected and dissected. The muscle tissue was digested in trypsin and collagenase. Cells were then plated, and suspended myocytes were selected after several passages on their attribute to adhere slower than other cell types. Two days prior to muscle tissue collection, thigh muscle injury resulted in higher myogenic cells. The same protocol was applied to two months-old healthy mice, as controls. From these latest, they obtained myogenic cells with high proliferative capacities and high maturation capabilities as they could fuse into myotubes and contract. Thus, their model became nowadays the C2C12 myoblasts cell line.

To develop our microdevice, using a simple cell model such as this one was the best option to optimize the whole system, before moving to more complex cell models.

1.1. Influence of initial cell seeding conditions on muscle cells organization in collagen tubes

As we discussed in chapter 1, *in vivo* fascicles average diameter reaches hundreds of µm. We thus decided to start by generating collagen tubes of 200 µm diameter, as well for biological relevance as for micro fabrication simplicity.

1.1.1. Regularly spaced cell aggregates

- **Seeding condition 1: seeding cells suspended in growth medium**

To investigate the ability of C2C12 cells to self-organize inside hollow collagen tubes, we prepare a cells suspension in growth medium, which we seeded inside the collagen tubes. After day 6 of culture (3 days in growth medium + 3 days in differentiation medium), we observed an unexpected behavior within 200 µm diameter collagen tubes. Indeed, aggregates of C2C12 were observed inside the tube. As shown in Figure 78 observed by phase contrast microscopy, muscle cells in between the aggregates seemed oriented along the main tube axis, while cells inside the aggregates appeared to orient more perpendicularly.

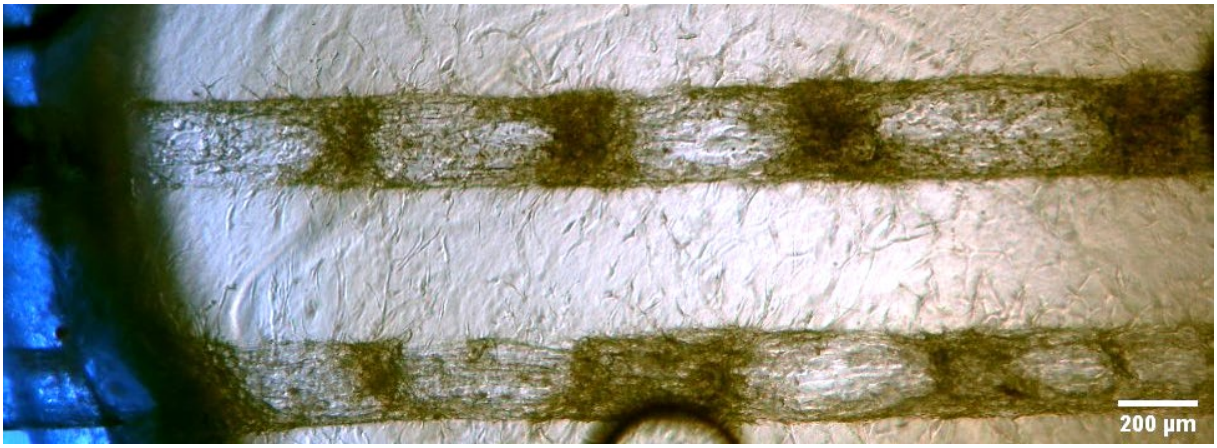

Figure 78: Phase contrast microscopy image of muscle tissue regularly spaced aggregates at day 6 of culture (3 days in growth medium, 3 days in differentiation medium), reflected in darker areas. Seeding conditions: cells without inter cellular matrix. The aggregates were stable from day 6 to day 10 of culture.

These aggregates were stable from day 6 to day 10 of culture. Within our team, we work with other cells in collagen tubes but such behavior was never observed (kidney cell lines such as MDCK or PCT, or with HUVEC endothelial cells for instance). The review of the literature did not yield much results about such cell behavior in tubes.

At midpoint between day 6 and day 10 of culture, live/dead assays centered on aggregates showed that cells mainly adhered and survived on the collagen surface (Figure 79).

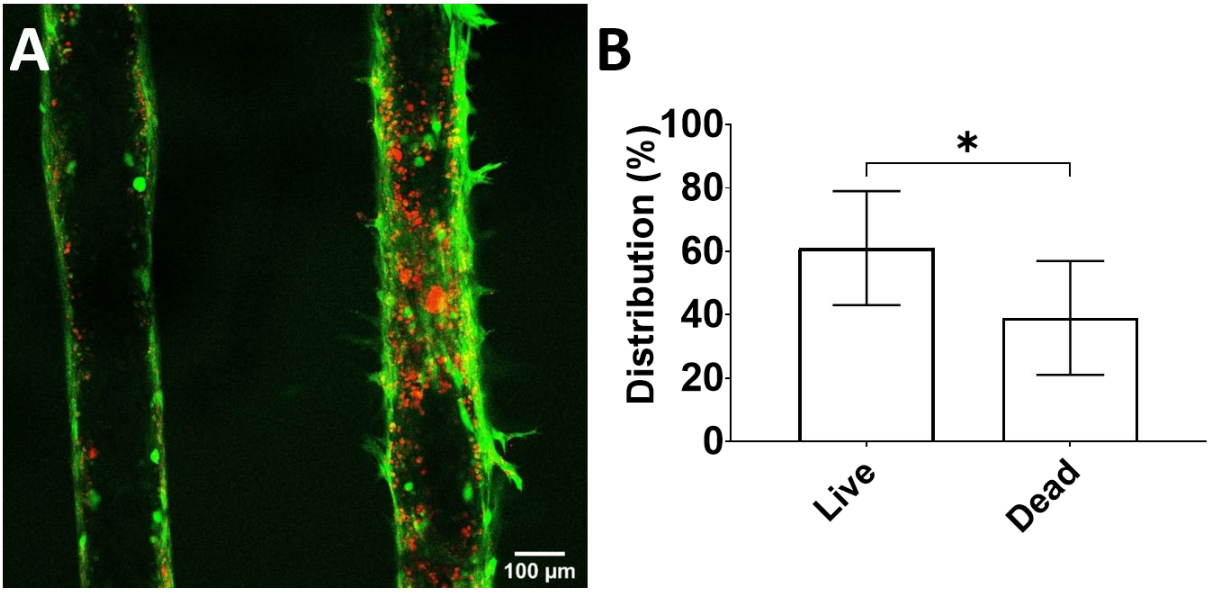

Figure 79: Live dead assays of C2C12 myoblasts cultivated in 200 µm collagen tube, at day 8 of culture. (A) Cells mainly adhered and survive on the collagen surface. (B) Estimated survival rate of C2C12 in tubes (n = 8, p = 0.0283).

This phenomenon could remind us the 'Rayleigh Plateau instability' well known in fluid mechanics. This phenomenon can be observed when slowly turning on the water tap: the water goes out as a cylinder of liquid but at a certain point, starts to break into droplets. This phenomenon is also seen when a fiber is coated with a liquid (spider web after rain), undergoes spatial thickness variations over time (Figure 80).

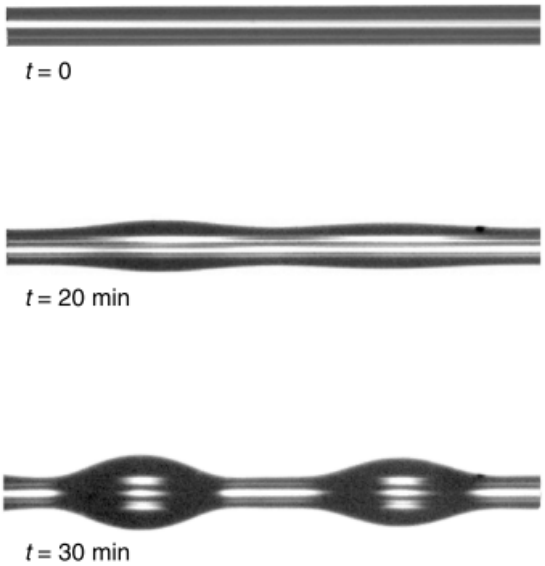

Figure 80: Optical micrographs illustrating the Rayleigh-Plateau instability of a liquid film on a glass fibre. Note the instability over time, where the liquid film separates into droplets. Image width is 560 µm. Images from

Briefly, free surfaces cost energy due to surface tension and nature tends to minimize surface area to minimize the energy cost [132]. Therefore, the liquid tends to minimize its surface area by breaking a cylinder into a series of regularly spaced droplets [133]. This instability can be controlled in different ways such as coating the fiber and changing the liquid properties [134]. Indeed, a way to stabilize the liquid film is to add polymers and to adjust their self-adhesiveness (varying salts concentration) or to vary the thickness of the liquid film, which can even completely suppress the Rayleigh-Plateau instability [134].

In a similar way, we therefore considered adding extracellular matrix mixed with the cells before seeding. Adding extracellular matrix should bring more adhesion molecules and thus, increase the adhesive surface available to cell volume ratio (S/V) compared to hollow collagen tubes where cell adhesion molecules are only present on the collagen surface.

- **Seeding condition 2: seeding cells mixed with extracellular matrix**

We thus suspended cells in growth medium containing collagen I (2 mg/ml) and 10% Matrigel before seeding them inside collagen tubes. According to the manufacturer, Matrigel is a preparation containing 60% laminin and 30% collagen IV and growth factors[k]. Hence, collagen would provide the hydrogel structure within the tube, while Matrigel would provide extracellular adhesion molecules such as laminin. Indeed, collagen fibrils has binding sites for laminin [32] and C2C12 cells have the specific integrin to bind laminin molecules [135].

[k] https://www.corning.com/catalog/cls/documents/faqs/CLS-DL-CC-026.pdf

As expected, seeding the cells adding ECM resulted in less aggregates (Figure 81). The average aggregates count normalized by the length of the muscle tissue significantly decreased in the presence of extracellular matrix (1.9 aggregates/mm of tissue vs. 0.4 aggregates/mm of tissue with extracellular matrix at day 6 of culture) (Figure 82A). As the mean aggregates count decreased in the presence of extracellular matrix, the distance between each aggregate significantly increased (415 µm vs. 1305 µm at day 6 of culture) (Figure 82B).

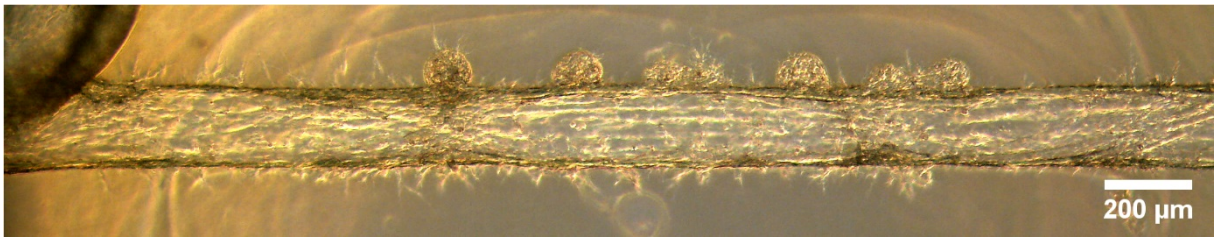

Figure 81: Phase contrast microscopy image of muscle tissue at day 10 of culture (3 days of growth medium, 6 days in differentiation medium). Note the presence of two aggregates-like structures. Seeding conditions: cells mixed with ECM containing collagen at 2 mg/ml and 10% Matrigel.

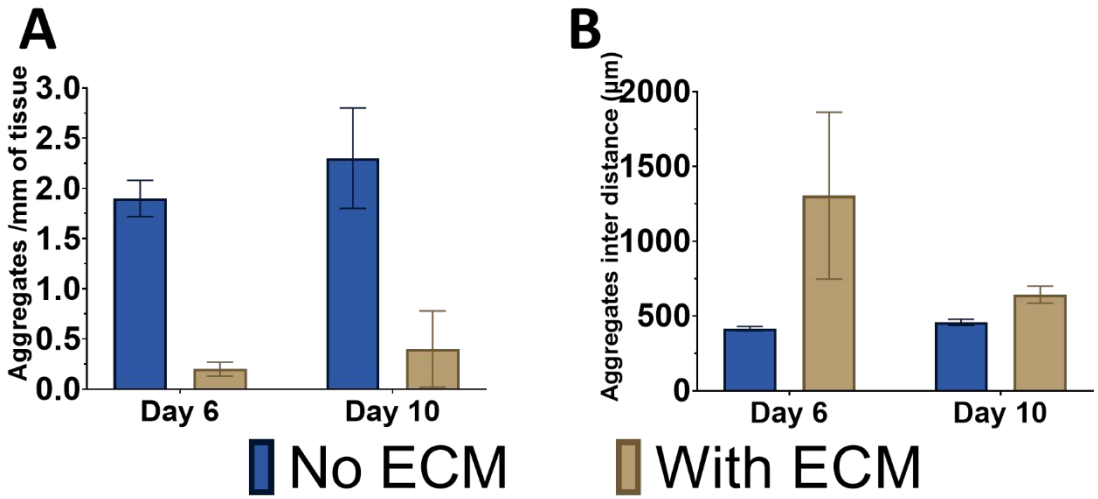

Figure 82: (A) Number of aggregates normalized by the muscle tissue length without or with the addition of extracellular matrix. Adding ECM significantly decreased the number of aggregates ('No ECM', n = 31 and 24 tubes for day 6 and day 10 respectively. 'With ECM', n = 15 and 15 tubes for day 6 and day 10 respectively). (B) Distance between aggregates. As there were less aggregates with the addition of ECM, the distance between each aggregate significantly increased ('No ECM', n = 25 and 2 tubes for day 6 and day 10 respectively. 'With ECM', n = 18 and 3 tubes for day 6 and day 10 respectively).

- **Discussion**

Why C2C12 myoblasts behave in such a way in collagen tubes compared to other cell types is still unclear. However, a higher adhesive surface to volume ratio (by adding ECM) drastically decreased this phenomenon. Considering the contractile nature of the C2C12, and the time point of that phenomenon (day 6 of culture, meaning 3 days in differentiation medium which enhances cell fusion and maturation), a complex interplay between contractile forces and adhesion forces might be involved.

While searching for explanations, some papers brought very interesting and insightful elements. Collagen type I is a complex yet well-ordered fibrillary hydrogel with many different binding sites for cells via integrins receptors or for other proteins such as laminin [32]. Integrins are cell-surface receptors that are involved in cell-cell or cell-matrix interactions. They are composed of two sub-

units α and β. Several isoforms of each subunit can combine into heterodimers. The main integrin heterodimers that have been reported to bind collagen type I are: $\alpha_1\beta_1$ and $\alpha_2\beta_1$ [136]. However, gelatin, which is a denatured form of collagen resulting in the exact same chemical composition yet in a disorganized network of fibrils, exhibits binding sites for other integrin heterodimers such as $\alpha_5\beta_1$ [137]. In the other hand, C2C12 cells mainly express integrin heterodimers $\alpha_5\beta_1$ and $\alpha_7\beta_1$ [138]. As a consequent assumption, C2C12 myoblasts should preferentially adhere to denatured collagen which exhibit binding sites for $\alpha_5\beta_1$ integrin. Collagen remodeling is mediated by proteins called matrix metalloproteinase (MMP). Gelatin is the degradation product of collagen, mainly from sources rich in type I collagen, by MMP *in vivo* [139], [140]. It has been reported that one MMP is abundantly expressed when C2C12 are cultivated in growth medium for 2 days, with virtually no MMP inhibitor [141]. However, when switching to differentiation medium, MMP inhibitor expression increases while MMP expression decreases. Interestingly, they reported that MMP and their inhibitor both reach a peak expression after 7 days of culture in differentiation medium.

Concerning our experiments, C2C12 myoblasts in growth medium for 3 days should be able to remodel the collagen surface, exposing binding sites. When switching to differentiation medium from day 3 to day 6, collagen remodeling should then be downregulated as MMP inhibitor expression starts to rise. During these three days exposure to differentiation medium, myoblasts fuse and differentiate, starting to exert contractile forces. These tensile forces, once in equilibrium with adhesion forces could maybe explain the formation of these aggregates.

Obviously, these potential explanations are partial and limited. Although this phenomenon is interesting in a biophysics point of view, *in vivo* mature skeletal muscles do not have such shape. Therefore, no further investigations were conducted regarding this phenomenon.

In these first series of experiments (seeding cells suspended in growth medium without adding ECM), the most striking results regarding C2C12 organization, is the observation of a hollow muscle structure with a lumen. Confocal images obtained after the fixation and staining (DAPI for the nuclei and phalloidin for actin) of the fixed on-chip skeletal muscle tissue indeed clearly showed a lumen structure in the tube longitudinal section as well as in cross-section as early as day 3 of culture (Figure 83). This lumen remained even at day 10 of culture.

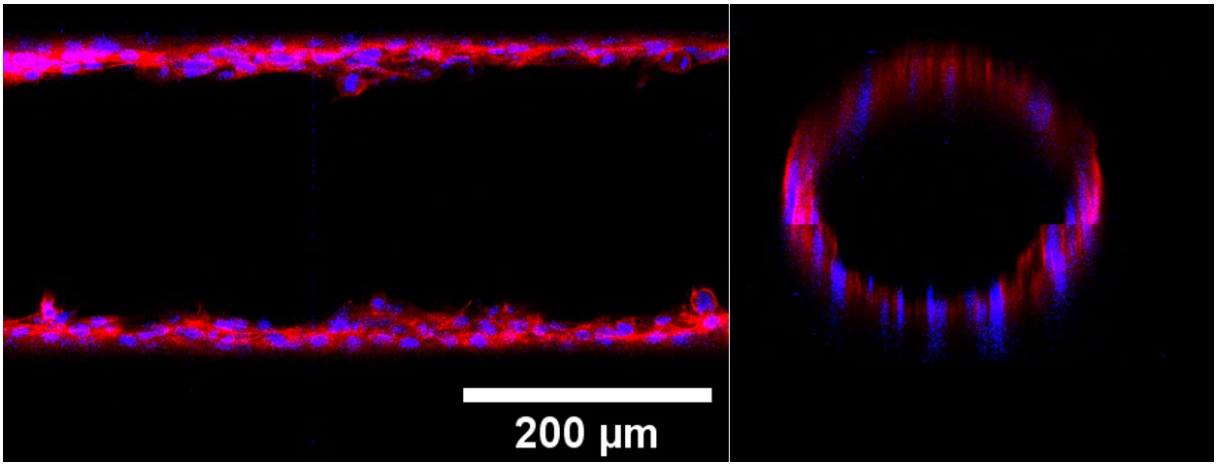

Figure 83: Confocal microscopy images of fixed on-chip skeletal muscle tissue, stained for nucleus (DAPI) and for actin (phalloidin) at day 3 of culture, showing a lumen in longitudinal section and cross-section.

Such behavior is expected for endothelial cells, however it is much more surprising for muscle cells that were expected to proliferate and fill the tube and then fuse.

We first hypothesized that the cell seeding density may be too low failing to fill the collagen tube entirely. To investigate if the seeding cell density could influence C2C12 cells organization within the collagen tube, we set up an assessment of in-tube cell density on phase contrast images using the ImageJ plugin 'PHANTAST'. The experiment time points of interest were right after the seeding, and at day 3 of culture when switching to differentiation medium.

1.1.2. Influence of initial seeding cell density on C2C12 organization

The PHANTAST plugin (PHAse coNTrAST segmentation toolbox) was developed as an automated tool for rapid estimation of cell confluency from phase contrast microscopy images [142]. Collagen tubes images were converted to 32 bits images then cropped so the entire image fits the collagen tube area (Figure 84A). The plugin then generated a mask corresponding to the cells (Figure 84B) and a binary image was created from that mask (Figure 84C). Computed in-tubes cell confluency was approximated as cell density, and was estimated as the ratio of cells area over the tube area (Figure 84D). Hence, 'cell density' here referred to the fraction of area occupied by the cells within the collagen tube. The advantage of this method was its very rapid estimation of the collagen tubes filling, hence giving an approximate estimation of cell density. Moreover, this method did not need to sacrifice a chip by fixing and counting stained nuclei. It allowed us to estimate that parameter on the same chip over time. Of course, the cell density estimations were assessed over 2D projected images, which was the main drawback. Overall, it was a good tool to start with and to do quick assessment.

To promote as much as possible fusion and differentiation within the collagen tube, we aimed at reaching a high cell density right after seeding. We arbitrarily defined a high cell density range inside collagen tube corresponding to cell density higher than 90% and evaluated for which initial seeding density this high cell density is achieved at day 3 (3 days in growth medium conditions). Our experiments showed that an initial seeding density of at least 60% should be reached to achieve the high cell density conditions at day 3 where the growth medium will be replaced by differentiation one (Figure 84D).

We therefore decided to work with an initial seeding density higher than 60%. To control on-chip cell seeding density, the microdevice optimization we discussed in chapter 2 was crucial. Indeed, the key point was letting needles at the collagen tube output, thus increasing the hydrodynamic resistance. Cells therefore accumulated in the collagen tubes during the seeding. The seeding time was consequently the main parameter to change the seeding cell density. However, whatever the initial cell density, our experiments showed that for a suspension of cells prepared in growth medium and for a collagen tube of 200 μm in diameter, we do not observed an expected muscles cells organization and that a lumen-structure remained independently of the initial cell seeding density.

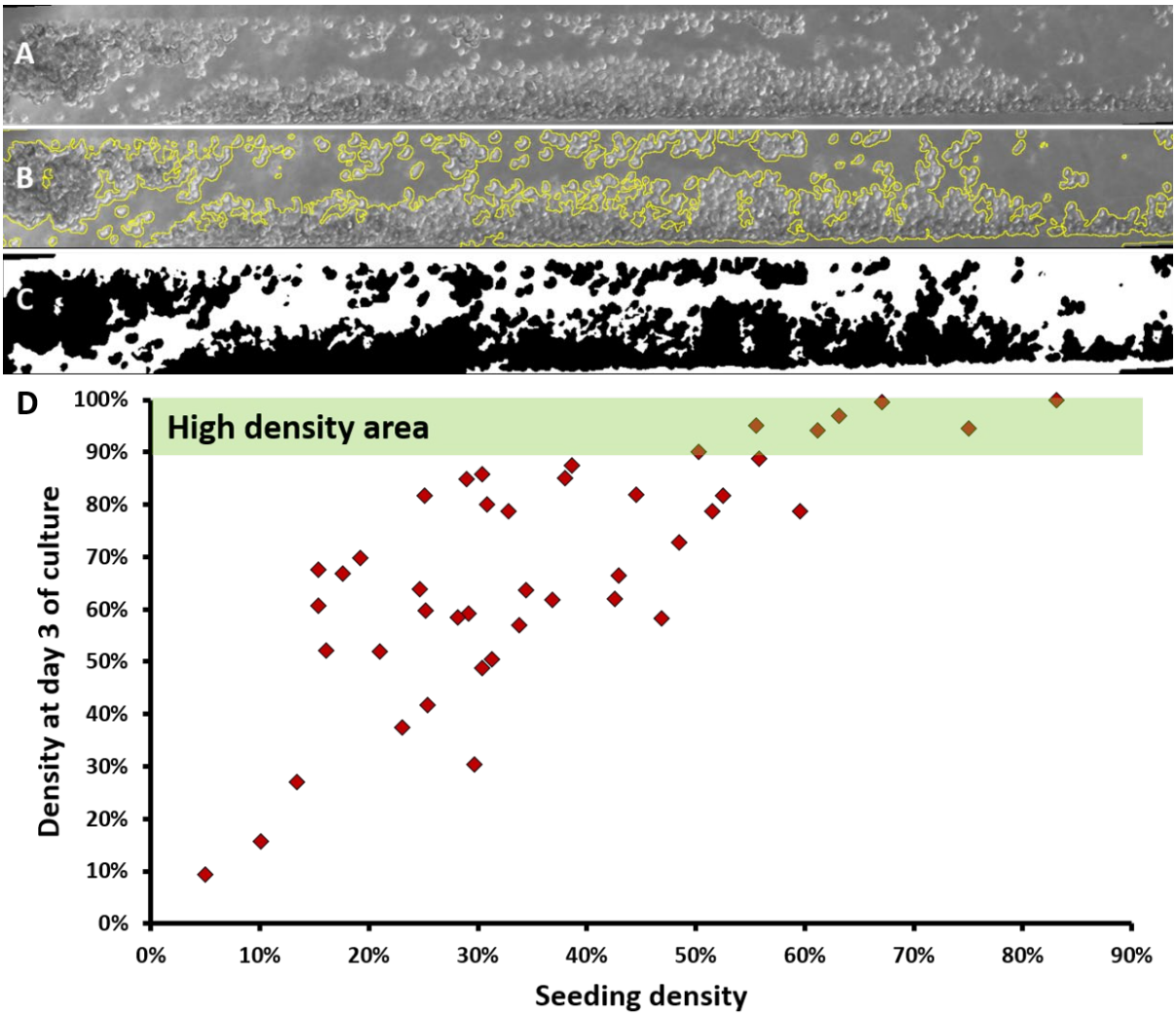

Figure 84: (A) Phase contrast microscopy 32 bits image of a collagen tube right after cell seeding. (B) Cell segmentation using PHANTAST plugin generating a mask. (C) Binary image extracted from the generated mask, allowing an estimation of the cell confluency, which was approximated as 'cell density' and was defined as the fraction of area occupied by the cells within the collagen tube. (D) Cell density at day 3 of culture depending on the seeding density. To have a very high density (> 90%) right before switching to differentiation medium at day 3, the initial seeding density must also be high (> 60%). Initial seeding density was controlled the seeding time: longer seeding time resulted in higher initial cell density.

1.1.3. Could the presence of in-tube extracellular matrix help to promote a proper muscle cells organization within collagen tubes?

Our previous experiments showed that the second seeding condition (cells suspended in growth medium, mixed with collagen I and Matrigel) prevented periodic aggregates formation. Following a similar reasoning, we investigated if the presence of ECM in the seeding suspension could improve muscle cells organization. This mostly relied on the assumption that the lumen-structure resulted from the lack of adhesion molecules in the center of the collagen tube. As previously described, C2C12 myoblasts were suspended in growth medium containing collagen at 2 mg/ml and 10% Matrigel. To avoid matrix polymerization during seeding, the seeding procedure was carried out on ice.

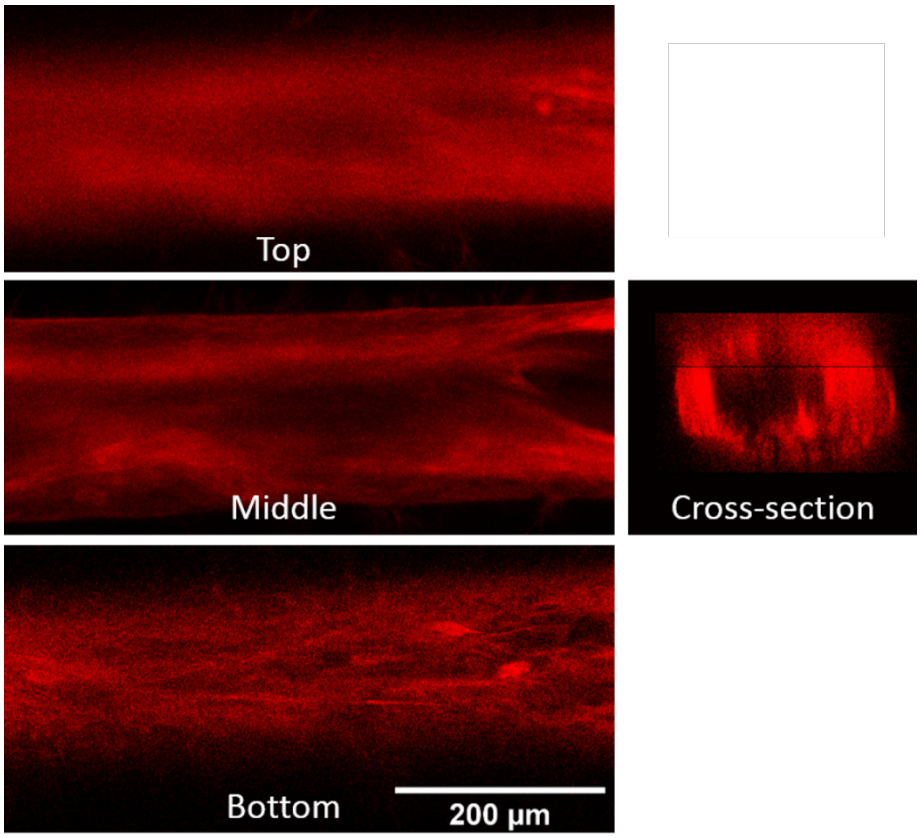

Figure 85: Confocal images of fixed on-chip skeletal muscle tissue within 200µm collagen tubes in the presence of inter cellular matrix (collagen 2 mg/ml and 1:10 Matrigel) at day 10 of culture. Longitudinal section on the left showing the bottom, the middle and the top part of the tube. The right image shows the cross section of the tube, showing a lumen-structure. Red: F-actin.

- **Seeding condition 3: seeding cells layer by layer (LbL)**

While searching for solutions to build a more physiological muscle-construct, one insight emerged from *Engler et al.* work, on seeding C2C12 myoblast sequentially [94]. As discussed in chapter 1, the authors investigated the possibility to perform a layer by layer C2C12 cell culture in order to provide cells with a relevant stiffness scaffold. More precisely, they plated a first layer of C2C12 myoblasts, then another one on top of it 2 days after. Their results showed that multiple layers of cells on top of each other influenced the orientation and the maturation of the tissue. The newly plated cell layer could realign following the bottom cell layer and develop significantly higher sarcomere striations [93]. Therefore, we consider the possibility to perform a similar approach within our tubes, first generating a lumen structure, and to sequentially fill it with cells.

The idea was therefore to first generate a layer of lumen-structure. Then, another layer of cells would be seeded inside the hollow structure repeatedly. The layer by layer (LbL) condition was only possible using cells suspended in growth medium. Indeed, for cells seeded in a suspension containing collagen and Matrigel, right after seeding the polymerization of the matrix will prevent the subsequent injection of a second layer of cells.
To investigate if a LbL seeding would improve muscle cells organization within the collagen tube, cells were seeded inside collagen tubes once every day during three successive days. After the third seeding, on-chip cells were incubated in growth medium for 5 hours before switching to

differentiation medium and pursuing the culture with the same time points as usual. Unfortunately, the lumen-structure still remained after ten days of culture although multi-layers of cells were clearly visible on the tube cross-section (Figure 86).

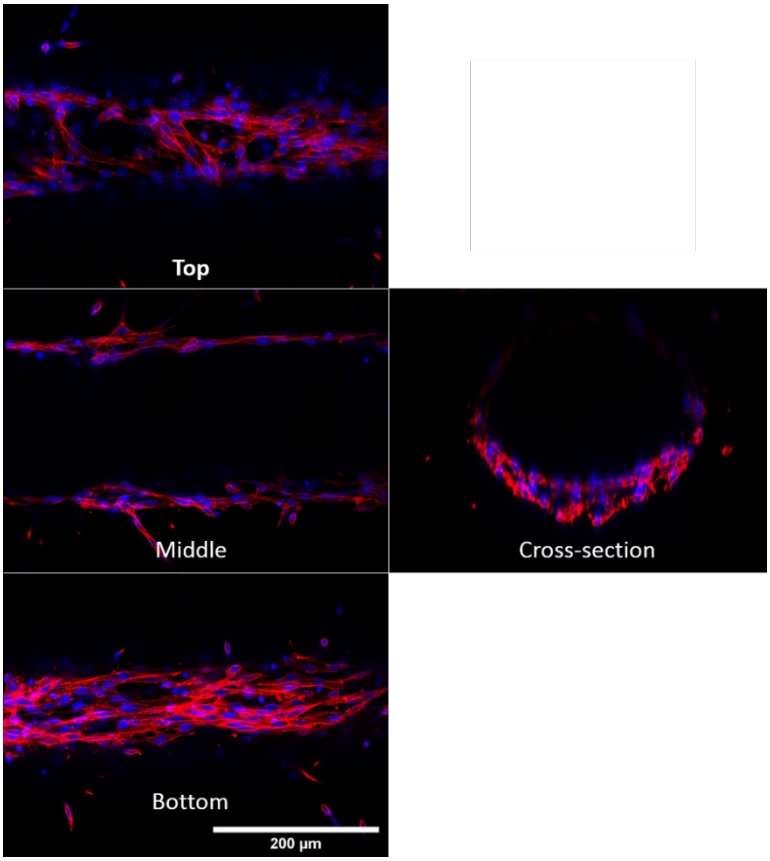

Figure 86: Confocal images of fixed on-chip skeletal muscle tissue within 200µm collagen tube without inter cellular matrix at day 10 of culture. Seeding conditions: layer by layer seeding involving cell seeding once a day for three successive days.

1.1.4. Myotubes alignment

Even though these three different seeding conditions (condition 1: cells suspended in growth medium; condition 2: cells suspended in an ECM mixture; condition 3: layer by layer) led to a lumen-structure skeletal muscle tissue, we also aimed at investigating if they could affect specifically muscle cells alignment. To quantify cells alignment, a 3D z-stack confocal acquisition for F-actin staining was performed combined with a z-projection. Such typical images are shown in Figure 87 , which were then processed with OrientationJ. Basically, a vector field was generated based on each pixel analysis. Since each vector is associated with an orientation, it resulted in a table of orientations distribution.

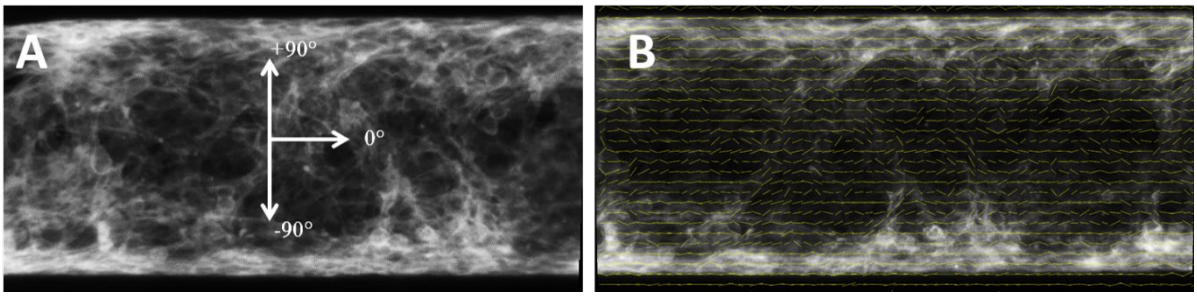

Figure 87: (A) Typical image of a Z-projection from a 3D Z-stack acquisition (F-actin staining) to be processed in OrientationJ (C2C12 seeded in 200 µm collagen tube without intercellular matrix at day 3 of culture). Note that the 0° orientation is parallel to the collagen tube long axis. (B) A vector field (small yellow lines) was generated based on each pixel analysis, resulting in a distribution of orientations. Here the vectors were scaled up for image clarity.

Focusing the analysis on [− 10°; +10°] allowed a more precise estimation of the myotubes alignment along the tube main axis (Figure 88, area highlighted by red dashed box). Therefore, myotubes oriented within that range were qualified as 'aligned myotubes'.

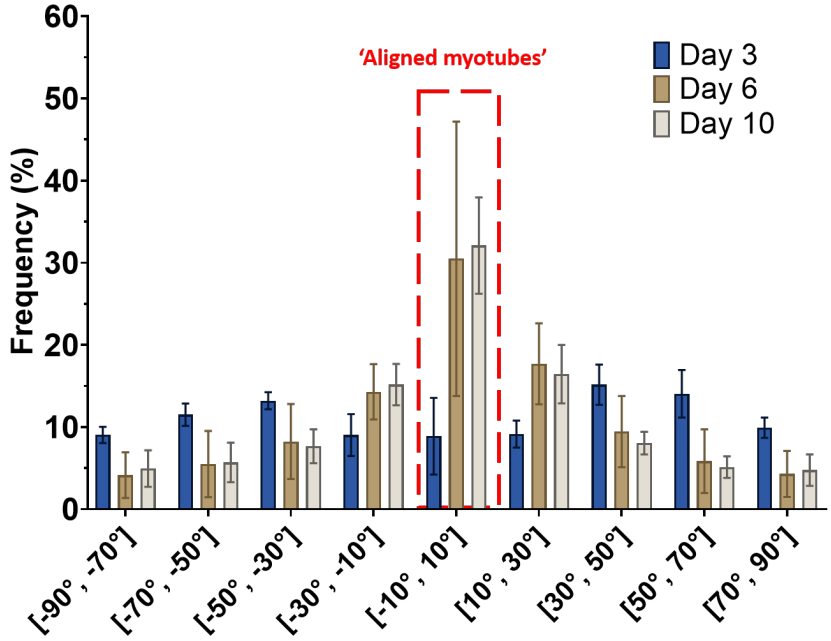

Figure 88: Myotubes F-actin orientations distribution over time for C2C12 myoblasts suspended in growth medium, and seeded in 200 µm collagen tubes (seeding condition 1). The collagen tube long axis is parallel to 0° orientation. To have a more precise assessment of myotubes alignment toward the tube long axis, analysis focusing on [-10°; 10°] were performed (red dashed box). n = 5, 10 and 8 for day 3, 6 and 10 respectively.

- **Cell alignment for seeding condition 1 (cells suspended in growth medium)**

When seeding C2C12 cells in 200 µm collagen tubes without extracellular matrix, aligned myotubes toward the tube long axis significantly increased over time (Figure 89). Indeed, aligned myotubes reached 9.7% ±5% after three days of culture compared to 32.9% ±17.7% and to 34.5% ±6.2% after day 6 and day 10 of culture respectively.

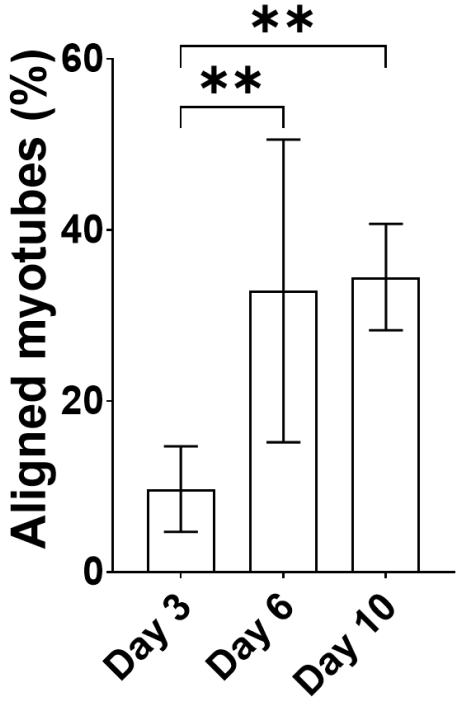

Figure 89: On–chip aligned myotubes toward the collagen tube long axis significantly increased from day 3 to day 6, but stabilized afterward (seeding condition 1: C2C12 suspended in growth medium). n = 6, 11 and 8 for day 3, 6 and 10 respectively.

These results were expected and many studies already reported the great impact of anisotropic geometrical guidance on cell alignment. For instance, *Sun et al.* cultivated human endothelial cells on substrates micro patterned with parallel half-cylinders and observed that cells preferentially aligned toward the long axis compared to non-pattern flat surface [143]. *Ahmed et al.* cultivated C2C12 myoblasts on substrates micro patterned with long parallel lines of fibronectin, and observed that cells also strongly align toward the long direction of the patterns compared to control non patterned surfaces [144].

Interestingly, there was no significant difference in aligned myotubes between late culture times (day 6 and day 10 of culture). These results suggest that myotubes organization mainly occurs in early differentiation phase (between day 3 and day 6) and tend to stabilize afterward. Indeed, myoblast proliferation rate is higher during the first three days as the medium is concentrated in serum with growth factors.

Although our system is by nature a 3D collagen tube, we saw that cells only colonize the surface. Thus, it resembles to a curved-2D anisotropic substrate at the cell scale. To investigate cell organization on a 2D substrate with a curvature radius of 200 μm, compared to a substrate with no curvature (essentially a flat substrate), experiments have also been conducted on 2D. Petri dishes were filled with collagen at 6 mg/ml, which was the same concentration as used for on-chip 3D collagen tube concentration. C2C12 myoblasts were plated at a density of 50 000 cells/cm² and cultivated in growth medium, allowing them to reach a high confluency of more than 90% at day 3 of culture before switching to differentiation medium. All 2D experiments subsequently followed the exact same procedures than on-chip experiment with the same time points. As expected, myoblasts cultivated on 2D dishes showed no preferential orientation (Figure 90) compared to on-chip 3D culture.

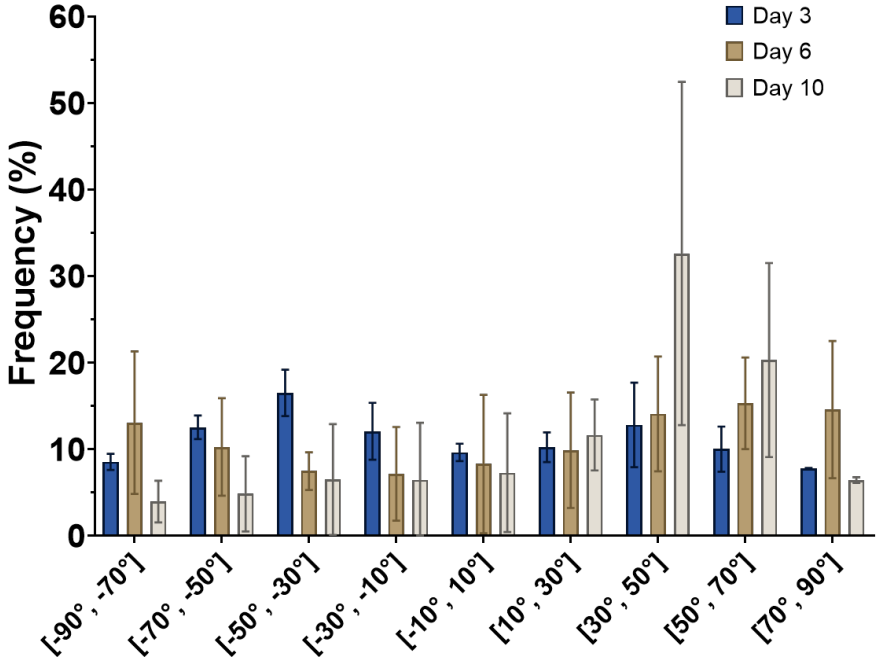

Figure 90: Myotubes F-actin orientations distribution for C2C12 myoblasts plated on 2D dishes coated with collagen at 6 mg/ml, over time. Horizontal axis is parallel to the 0°. Note that there is no preferential distribution over time on 2D dishes compared to 3D on-chip culture. For each time point, n = 2.

These results are in good agreement with *Engler et al.* publication showing that myoblasts alignment is transmitted to neighboring cells, but only over distances of 5 to 10 cells width (approximately 100 µm) [94]. Indeed, considering on-chip collagen tube surface, the maximum distance separating two cells is the diameter of the tube, hence 100 µm, whereas this distance is infinite on dish, at the cell scale. Our 3D micro device, by inducing geometrical guidance, allowed a better cell alignment toward a preferential direction compared to 2D dishes, which is a pre requisite for myoblasts fusion and myotubes fusion and differentiation.

- **C2C12 alignment as a function of cell seeding conditions**

Between the three seeding conditions, the one that resulted in a significantly higher aligned myotubes at day 10 of culture was the LbL seeding (Figure 91). Aligned myotubes reached 34.5% ±6.2%, 27.3% ±12.6 and 44.1% ±8.6% for cells suspended in growth medium, mixed with ECM and LbL seeding conditions respectively.

Seeding the cells mixed with ECM was supposed to provide cell-matrix adhesion sites for cells to colonize the center of the collagen tube. The ECM used in this condition contained collagen type I (2 mg/ml) for cell-matrix adhesion, and 10% Matrigel to bring growth factors and laminins to further promote cell-matrix adhesion within the whole section of the tube. That experimental condition was closer to a real 3D environment at the cell scale since myotubes are totally surrounded by matrix even toward the center of the collagen tube. Cells thus are supposed to have adhesion cues to explore and colonize the entire volume (Figure 85, cross-section). However, it also meant that the added ECM would limit the geometrical guidance, breaking locally the anisotropy by providing cell-matrix adhesion sites in all directions. It is reflected in a slightly lower aligned myotubes at day 10 of culture (though not statistically significant) when comparing these two experimental conditions (Figure 91).

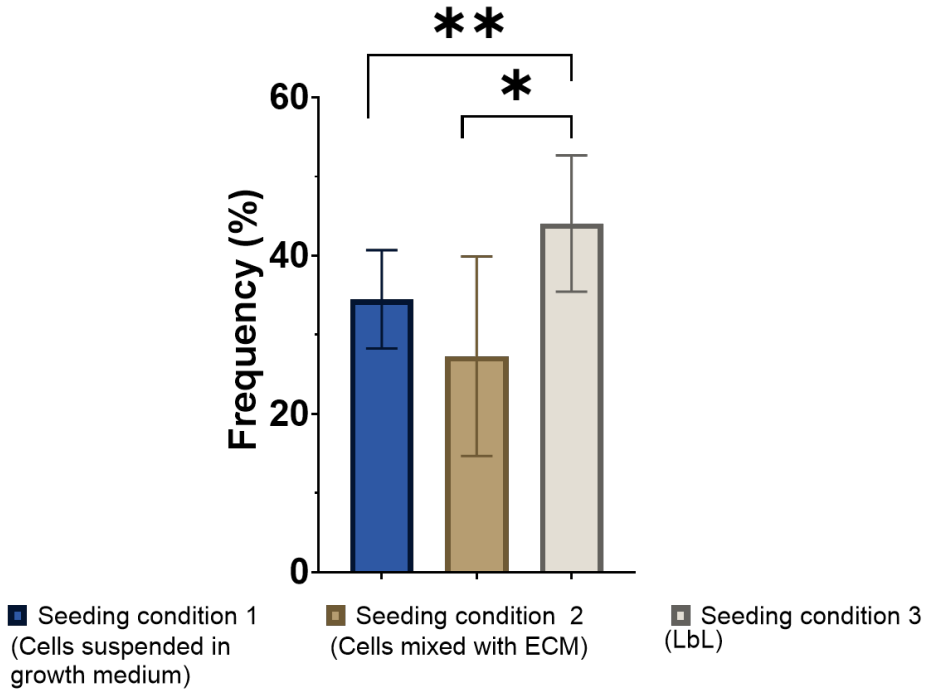

Figure 91: Aligned myotubes toward the 200 µm diameter collagen tube axis at day 10 of culture as a function of the initial seeding condition. Note that the LbL seeding condition resulted in a significantly higher aligned myotubes. n = 8, 5 and 10 for cells suspended in growth medium, mixed with ECM and LbL seeding conditions respectively.

The LbL seeding condition, where myoblasts were repetitively seeded inside the muscle-lumen each day within the proliferation phase obviously exposed cells to repeated shear stress. It resulted in a significantly higher aligned myotubes at day 10 of culture compared to the two previous experimental conditions (Figure 91). Higher aligned myotubes can also be explained by re orientation of the newly seeded myoblasts toward the long tube axis. Indeed, previous work already showed that newly deposited muscle-construct sheets re orient toward the preexisting muscle-construct sheet [93].

To further characterize myoblasts alignement as function of the different seeding conditions, we quantified, thanks to the same ImageJ plugin, the alignment coherency. The coherency reflects whether fibers are predominantly aligned to each other or not independently of the orientations (Figure 92). A high coherency (value of 1) means that fibers tend to align parallel to each other, whereas a low coherency (value of 0) translates in fibers with a wide distribution of orientations.

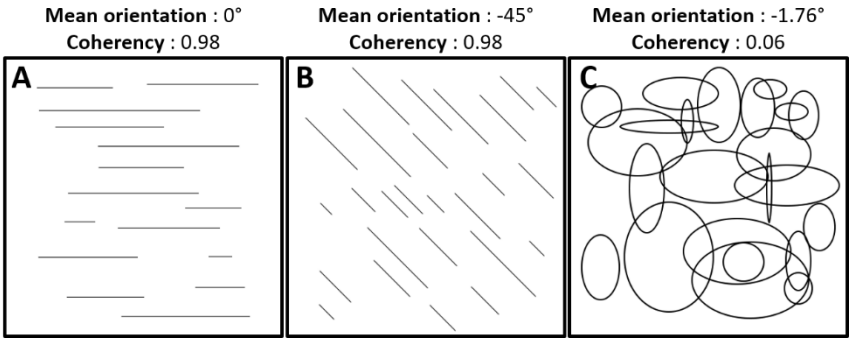

Figure 92: An illustration of OrientationJ coherency with test images. (A) and (B) have the same coherency value although structures are aligned in different directions. (C) Structures do not have any dominant direction hence resulting in a very low coherency.

It is another way to quantify the myotubes alignment. Myoblasts seeded in 200 µm collagen tubes resulted in a coherency value of 0.21 ±0.12, 0.35 ±0.18 and 0.28 ±0.08 for seeding conditions 1, 2 and 3 respectively (Figure 93A).

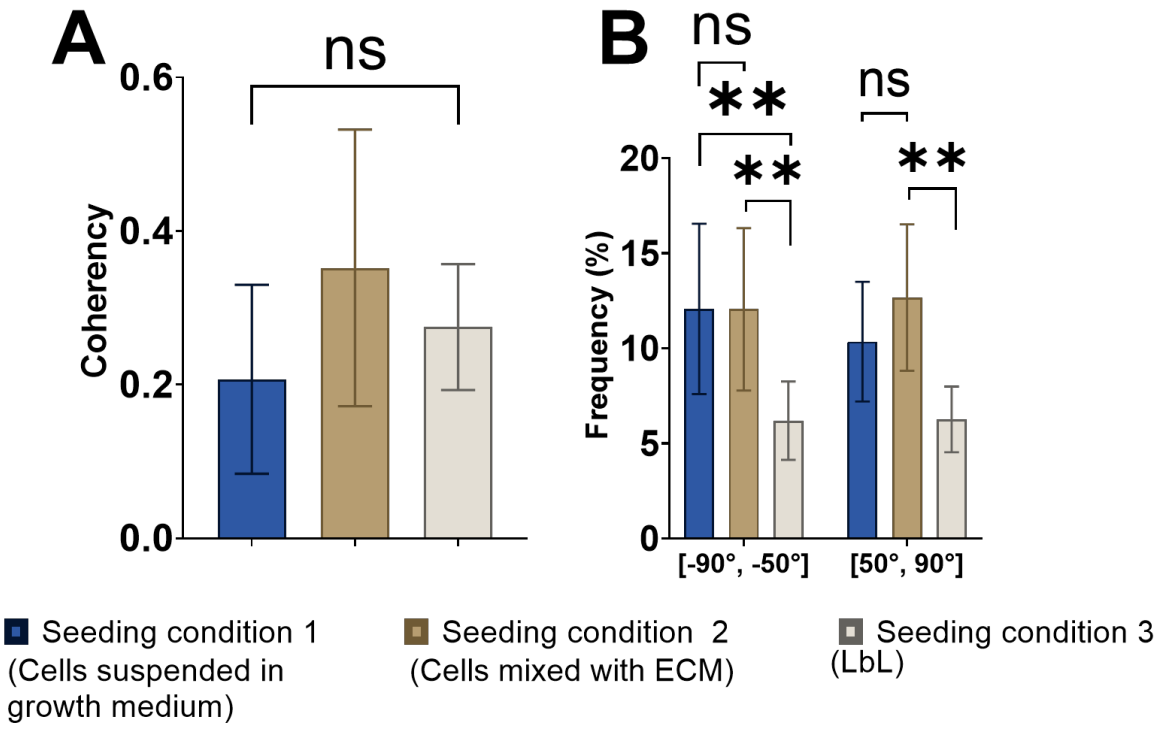

Figure 93: (A) Coherency values for myotubes in 200 µm collagen tubes at day 10 of culture between all experimental conditions. Note that the coherency does not significantly differ between the conditions. (B) Distributions of myotubes 'perpendicular' to the long axis, meaning oriented within [− 90°; 50°] or [50°; 90°] with respect to the long axis. The higher frequency of perpendicular myotubes in seeding conditions 1 and 2 compared to the seeding condition 3 can explain that coherency values were not significantly different although more aligned myotubes are present with LbL conditions.

Surprisingly, the coherency did not significantly differ between conditions for 200 µm collagen tubes although the layer by layer resulted in higher aligned myotubes. A possible assumption could be that as coherency measures the isotropy of local structures independently of orientations, myotubes can also be aligned together perpendicular to the collagen tube axis in a coherent way as it has been observed in confocal microscopy (Figure 94).

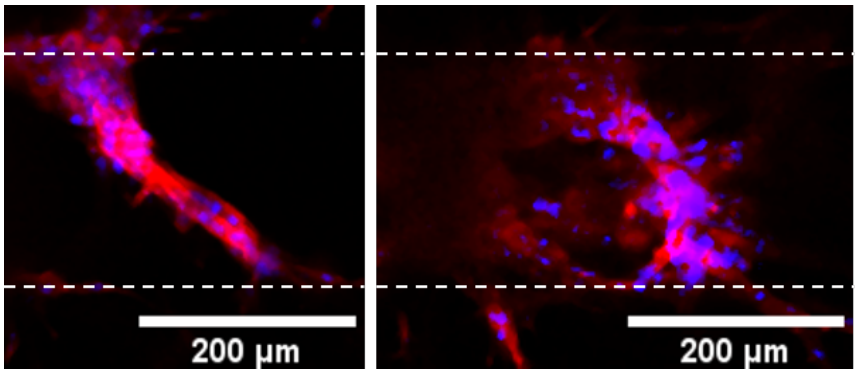

Figure 94: Confocal images of muscle-construct at day 10 of culture for myoblasts seeded without intercellular matrix, showing myotubes oriented perpendicular to the long axis of the tube. White dashed lines are the tube boundaries.

Indeed, when investigating the myotubes oriented within [− 90°; 50°] or [50°; 90°] with respect to the long axis, we found differences between experimental conditions. At this stage, these myotubes

were qualified as 'perpendicular myotubes'. Perpendicular myotubes were significantly in higher proportion in seeding condition 1 (12.1% ±4.5%), and seeding condition 2 (12.1% ±4.3%) compared to seeding condition 3 (6.2% ±2.1%) (Figure 93B). Therefore, we can reasonably claim that the coherency value was mainly driven by myotubes aligned with the main tube axis in the LbL seeding condition whereas perpendicular myotubes had a strong weight in the coherency value for the two other seeding conditions.

1.1.5. Discussion

Our results evidenced that seeding myoblasts inside 200 µm collagen tubes did not allow to reproduce faithfully on-chip the muscle tissue organization, as it resulted in a muscle-lumen construct even at day 10 of culture and independently of the experimental seeding conditions. The collagen tube dimensions were initially selected regarding *in vivo* parameters and ease of microfabrication. To improve the myoblasts organization in collagen tube, we further explored how the cell seeding conditions could affect their in-tube organization. We first demonstrated that working at high or low initial cell density did not improve their in-tube organization. We then investigated if seeding myoblasts seeded in presence of extracellular matrix could allow muscle cells to explore the volume inside the tube. Unfortunately, it did not, as the lumen still remained. Finally, a last seeding conditions was set up consisting in a layer by layer seeding. As for previous seeding conditions, this LbL seeding that was supposed to provide an adequate stiffness for cells did not induce neither a proper muscle cells organization.
Next, we investigated how these different seeding conditions influenced C2C12 alignment. In particular, our results showed that a seeding without or with ECM resulted in a higher proportion of perpendicular myotubes whereas LbL seeding resulted in a higher proportion of aligned myotubes, probably due to repeated shear stress during each seeding. Unfortunately, at this stage, none of those experimental conditions resulted in sarcomeric striations, suggesting the presence of immature myotubes.

These results suggest that, our initial device configuration only partially provided to cells the cues necessary to form a muscle tissue within the collagen tubes.

There are, growing evidences showing that substrates curvature could guide the spatiotemporal cell and tissue organization. Several studies on epithelial cells, but also on mesenchymal cells such as neurons, osteoblasts, muscles cells or fibroblasts, have reported the impact of geometrical guidance cues. For instance, neurons cultivated on cylindrical substrates emitted neurites that stronger aligned with minimal curvature (meaning toward the long axis) as the substrate size approached the size of an axon [145]. The authors also showed a direct negative correlation between the distribution of aligned neurites toward the long axis of the cylinder substrate and its diameter (Figure 95).

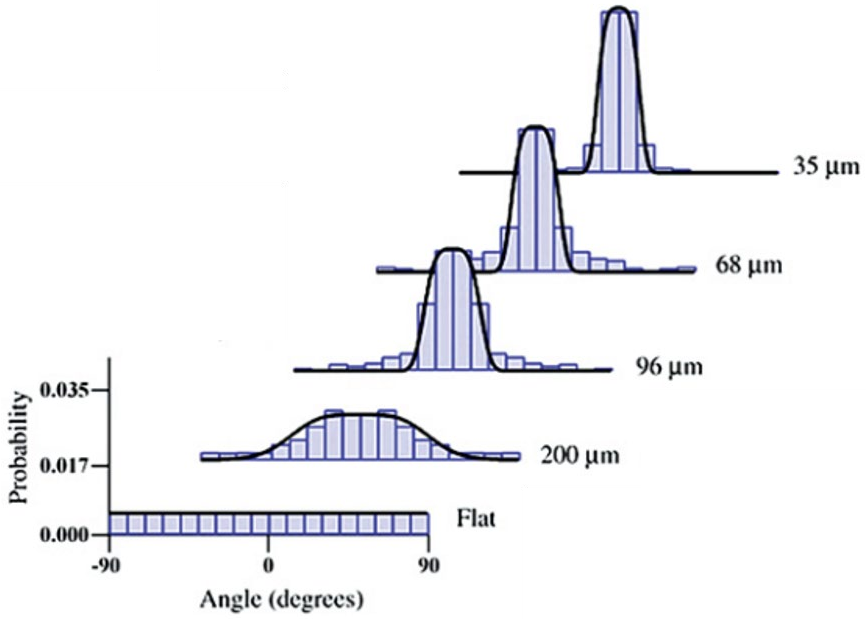

Figure 95: Modified figure from [145] **showing the orientation distribution of neurites from neurons cultivated on cylindrical substrate with different diameter. The long axis is represented by 0°. Note that aligned neurites toward the long axis is stronger with small diameter (200 µm vs. 68 µm). The black line is the fitted curve from their theoretical model.**

A quite complete review on the interplay between substrate curvature and cell growth describes fibroblasts and muscle cells seeded on cylindrical substrates [146]. It has been shown that these cells preferentially align their elongated bodies and cytoskeletal structure along the cylinder long axis. By doing so, they avoid curvature by aligning along the direction of zero curvature. In a similar manner, cultivated osteoblasts inside non-cylindrical channels resulted in preferential tissue growth starting in corners with high curvature with no tissue formed on flat sides [147]. As the tissue kept growing, it rounded the sharped corners and lead to the formation of a cylindrical central opening (Figure 96A-D).

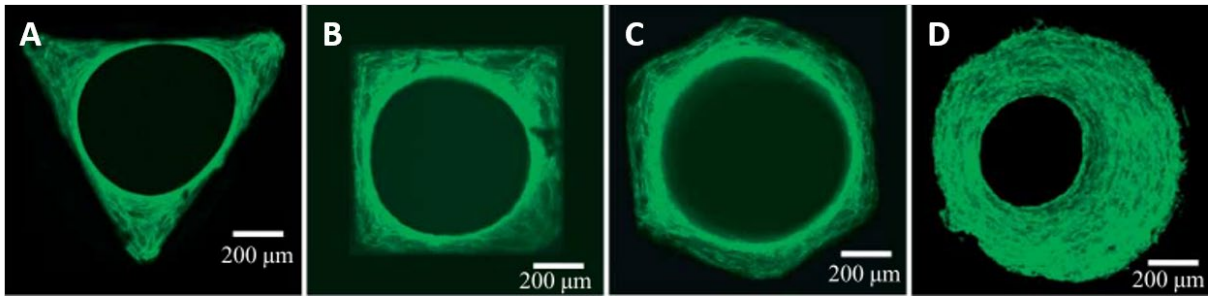

Figure 96: Cultivated osteoblasts inside non-cylindrical channels (A, B, C) and cylindrical tube (D) after 21 days of culture with F-actin staining in green [147]**. For non-cylindrical channels, tissue preferentially grew starting at the corners of high curvatures (A, B, C). As the tissue kept growing, it rounded the corners and lead to a cylindrical central opening. Seeding the osteoblasts inside cylindrical tubes lead to a more homogeneous growth inward the tube with larger tissue thickness (D).**

Interestingly, seeding the cells inside cylindrical tubes lead to a more homogeneous growth inward the tube with larger tissue thickness (Figure 96D). Therefore, it appeared that osteoblasts tend to grow preferentially in substrates with higher curvature, colonizing a higher fraction of the tube section. With that insight, we hypothesized that increasing the substrate curvature (hence decreasing the tube diameter) could improve the muscle cells self-organization within the collagen tube, thus generating a more biomimetic skeletal muscle construct.

1.2. Influence of substrate curvature on muscle cells organization in collagen tubes

1.2.1. Seeding condition 1 (C2C12 suspended in growth medium)

We first investigated how C2C12 cells self-organized in a collagen tube with increased curvature. To do so, we compared C2C12 organization in cylinder of 200 µm, 120µm and 75 µm in diameter. Our experiments evidenced that cells colonized the whole collagen volume at day 3 of culture, only when seeding them within 75 µm diameter collagen tube, meaning for the highest curvature ($\kappa = 1.3\times 10^{-2}$ µm^{-1}), as shown in Figure 97 (cross-sections). This organization remained stable in differentiation medium until day 10 of culture.

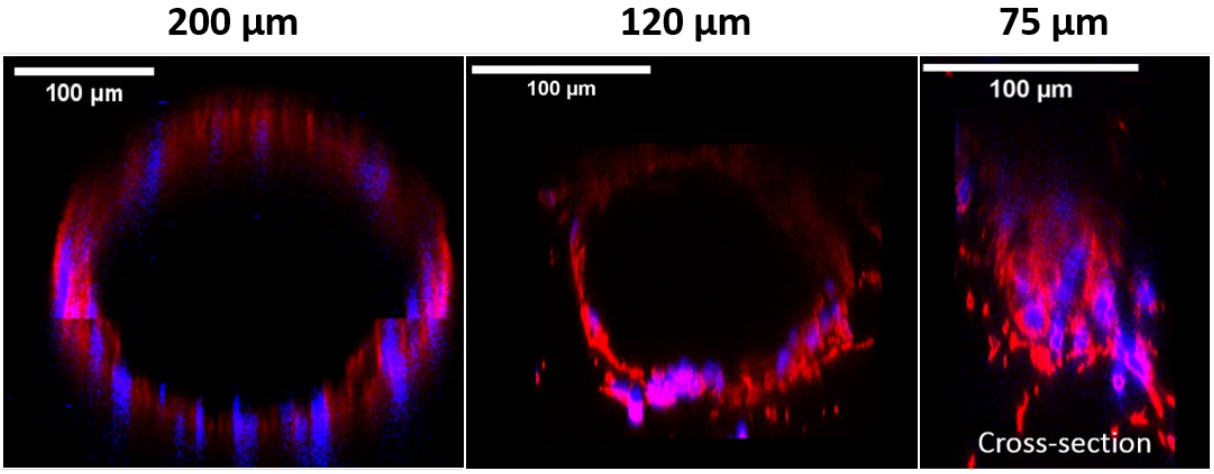

Figure 97: Confocal images, showing cross-sections of muscle-constructs generated within 200 µm, 120 µm and 75 µm collagen tubes, at day 3 of culture. Note that a lumen-structure was observed when seeding C2C12 within 200 µm and 120 µm collagen tubes.

Here by decreasing the collagen tube diameter from 200 µm to 75 µm, the curvature increased by almost 3-folds. These results could suggest a threshold curvature that induces a proper tissue organization. Interestingly, this diameter threshold has already been reported in other studies. Kidney cell line (MDCK) seeded inside fibronectin-coated PDMS tubes of various diameter showed different migration behavior with a clear threshold at 75-100 µm [148]. The authors also observed that actin stress fibers aligned more parallel toward the tube axis for small diameter such as 75 µm compared to larger tubes, meaning more than 100 µm. For example, cells exhibited a significantly decreased velocity by from 100 µm tube to 75 µm tube, while increasing their average height. The authors used epithelial cells and intriguingly observed multilayered epithelial structures filling the tube inward with a loss of cell polarity for smaller tubes diameter.

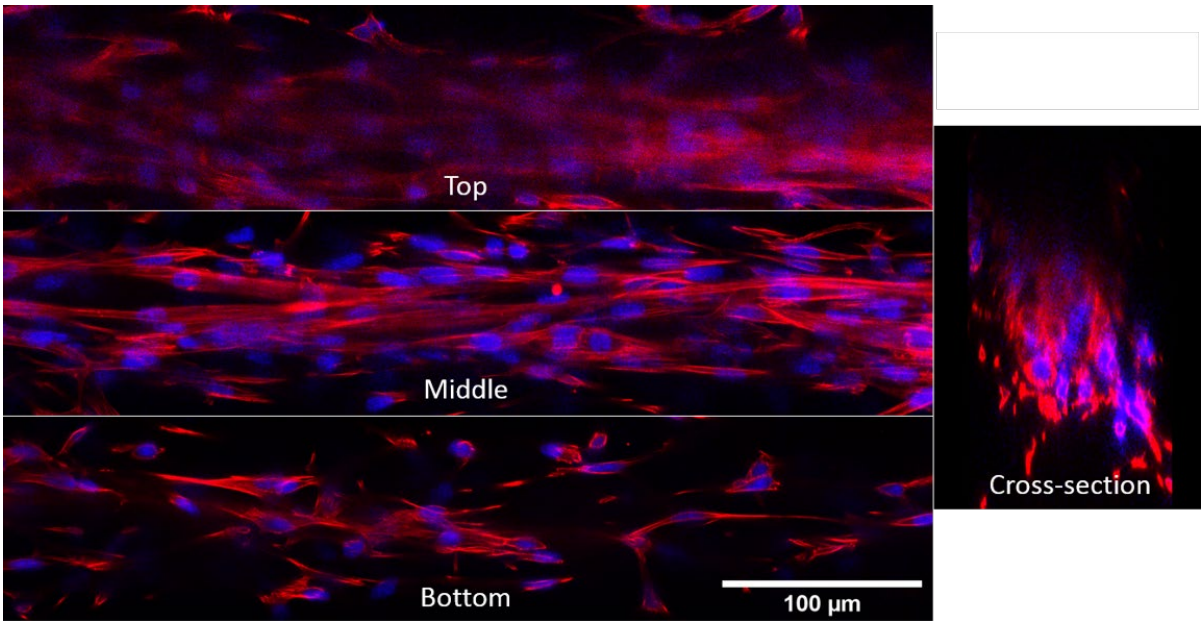

Figure 98: Confocal images of fixed on-chip skeletal muscle tissue generated with seeding condition 1 (cells suspended in growth medium) in 75 µm collagen tubes at day 3 of culture.

Another study focused on C2C12 myoblasts alignment depending on the substrate curvature [149]. They cultivated cells on top of concave semi-cylindrical substrates, with different diameters. They observed a stronger alignment toward the long axis for smaller diameter (180 µm) compared to larger ones (500 µm). However, they also observed an impact of even small curvatures (500 µm) compared to flat surface on cell alignment. These observations are in good agreement with our results. In addition to the substrate curvature, the adhesion surface over cell volume ratio (S/V) is almost 3-fold increased when working within 75 µm collagen tubes compared to 200 µm, bringing more adhesion cues to the cells. Reducing the tube diameter also constrained the cells, decreasing the maximum distance between two myoblasts, as we discussed earlier cell alignment transmitted to adjacent cells is within a range of approximately 100 µm.

We previously showed for 200 µm collagen tubes, that initial seeding conditions influenced myoblast alignment, although the lumen-structure remained. Then we managed to better organize myoblasts by decreasing the tube diameter to 75 µm. We therefore wanted to investigate whether the initial seeding conditions still have an impact on myoblast alignment, or if the geometrical aspect of the system dominates the myoblasts organization. To do so, we investigated additional seeding conditions.

1.2.2. Seeding condition 2 (C2C12 mixed with ECM)

Since hydrodynamic resistance greatly increases with diameter decrease, we observed collagen tube deformations (diameter: 75 µm) when seeding myoblasts mixed with ECM (collagen type I + Matrigel). To keep the tube integrity, we thus decided to investigate the effect of ECM during the seeding step by splitting into two different sub-conditions. The seeding condition 2.1 involved seeding of myoblasts mixed with collagen type I at 2 mg/ml. As Matrigel was supposed to bring basal membrane adhesion molecules such as laminin, the seeding condition 2.2 involved seeding

myoblasts mixed with laminin at 100 µg/ml.

Our results showed that, independently of the seeding conditions, seeding C2C12 myoblasts in collagen tubes with a higher curvature (diameter of 75 µm) repeatedly resulted in muscle cells colonizing the whole volume available of the collagen tube section, leading to a better muscle tissue organization (Figure 99).

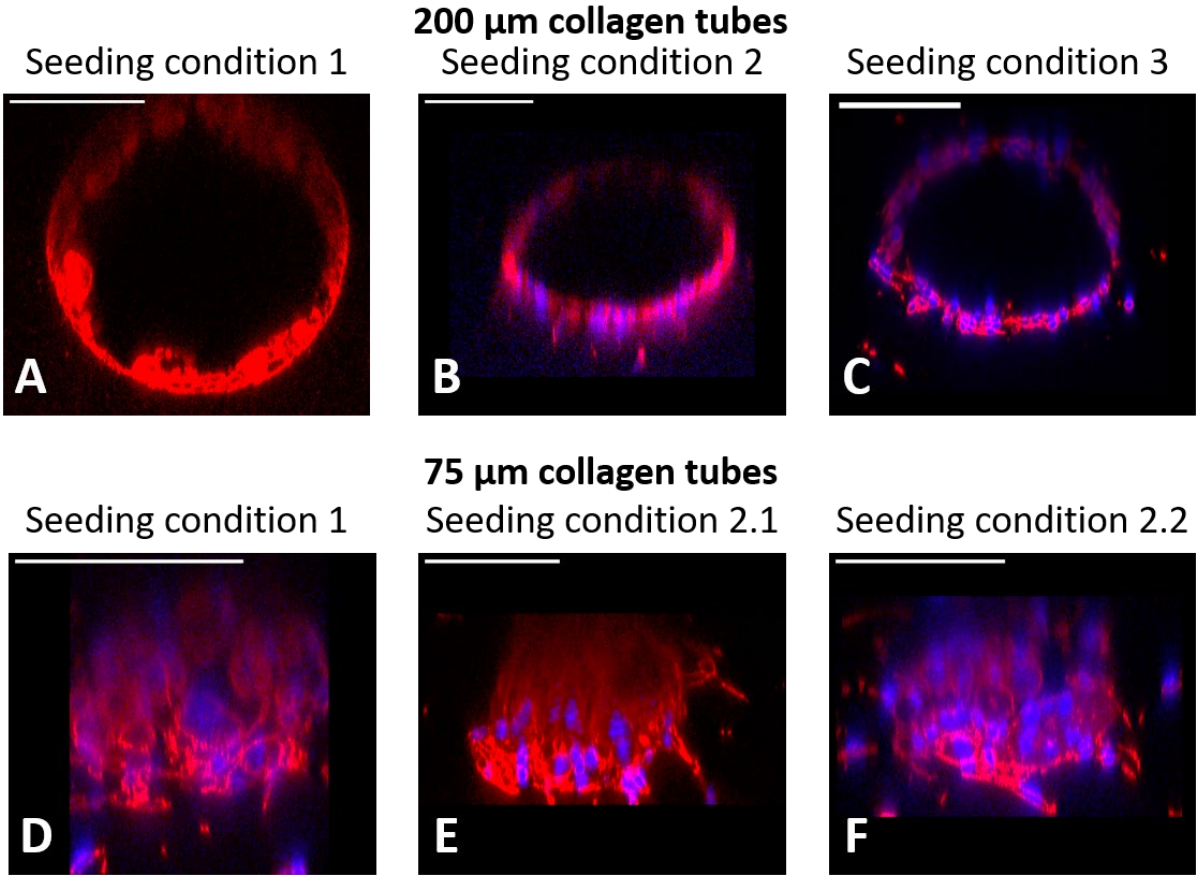

Figure 99: Confocal images of muscle-construct generated in collagen tubes of 200 µm (A, B, C) and 75 µm (C, D, E) diameter at day 10 of culture. C2C12 myoblasts seeded suspended in growth medium (Condition 1: A, D), mixed with ECM (Conditions 2: B, E, F) and seeded layer by layer (Condition 3: C). Scale bars: 100 µm.

Overall, our results suggest that the substrate curvature takes over the seeding conditions for myoblasts organization in our system.

Interestingly, we observed the presence of striated myotubes as early as day 6, generated in collagen tubes of 75 µm diameter, in seeding condition 1 (Figure 100). As we previously discussed, these sarcomeric striations reflect the intracellular organization of the contractile apparatus, which is a maturation marker of myotubes. The presence of sarcomeric striations therefore sets a further milestone in myotubes maturation on-chip.

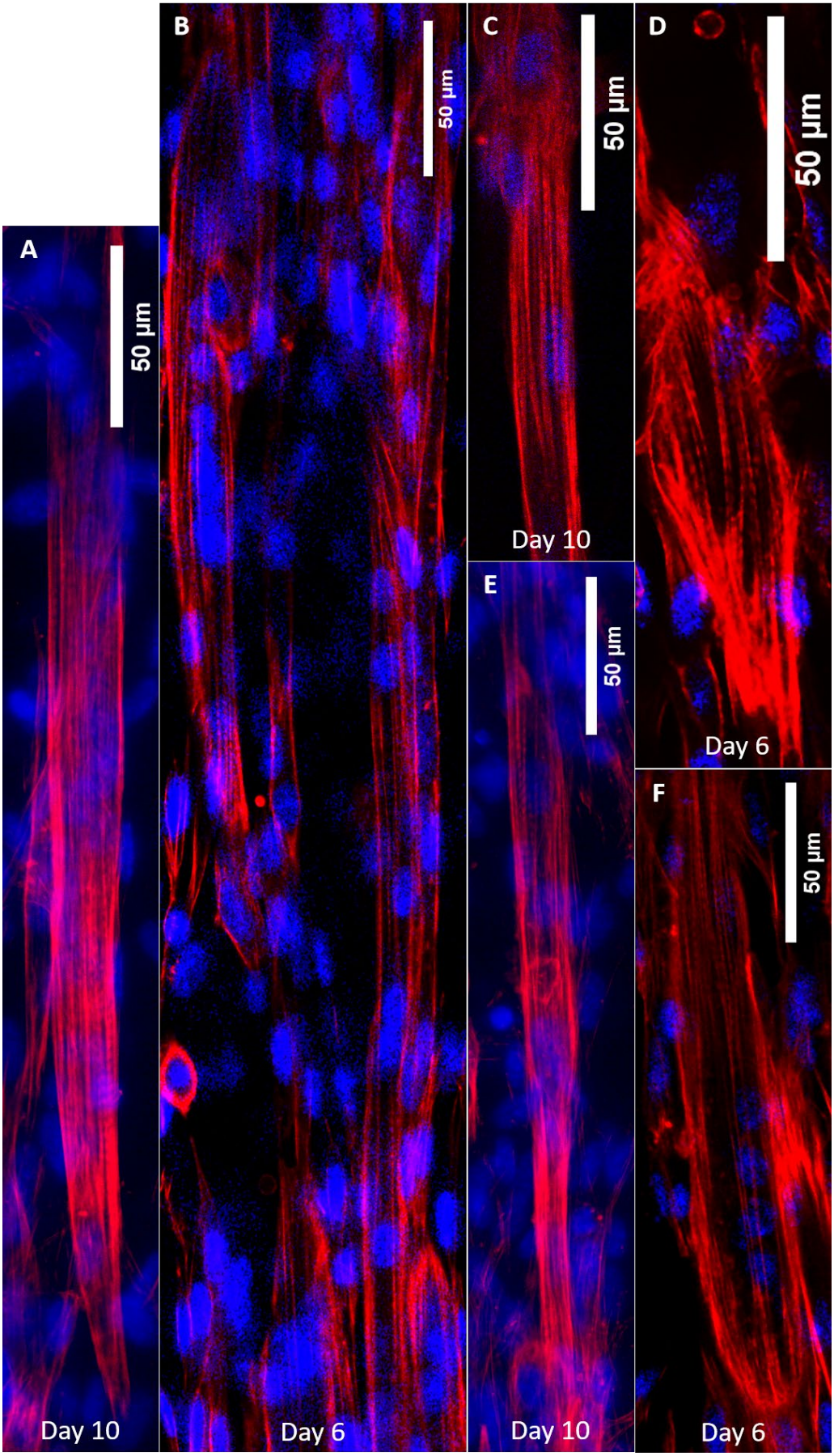

Figure 100: Confocal images of sarcomeric striations (red: F-actin. Blue: nucleus) at day 6 (B, F and D) and day 10 (A, C, and E) of culture. Seeding condition 1 in 75 µm collagen tubes.

1.3. **Probing myotubes maturation by quantifying sarcomeric striations**

As sarcomeres produce the force necessary for contraction, we quantified their presence in the different conditions as a marker of myotubes maturation.

Sarcomeric quantification method

To understand the way we quantified it, we have to explain how the experiments were designed. For each experimental condition, several sets of experiments were performed. One set of experiments involved several chips developed using the same batch of prepared collagen, and seeding C2C12 cells coming from the same culture flask. Hence, there is a variability between two sets of experiments even for the same experimental condition. For more simplicity, 'a set of experiments' will be defined as 'an experiment'.

Sarcomeric striations were quantified by the count of experiments containing at least one chip with striated myotubes, over the total count of experiments for the same experimental condition. For example, one experiment contains 6 chips, seeded with C2C12 myoblasts with seeding condition 1. For each time point (day 3, day 6 and day 10), 2 chips are fixed with PFA. Let's assume we found one chip containing striated myotubes, at day 6. Now if we perform 3 experiments with the same protocol, the proportion of experiment with striated myotubes will be 0%, 33% and 0% for day 3, day 6 and day 10 of culture respectively, for seeding condition 1.

In contrary to tubes of 200 and 120 µm, myoblasts seeded in 75 µm collagen tubes with the seeding condition 1 exhibited sarcomeric striations, as discussed earlier (Figure 100). Our experiments also showed that, as expected, sarcomeric striations increased over time although not reaching 100%. More precisely, no sarcomeric striations were visible at day 3 (3 days of culture in proliferation medium), while they were observed in 33% and 50% of experiments for day 6 and day 10 of culture in differentiation medium, respectively (Figure 101).

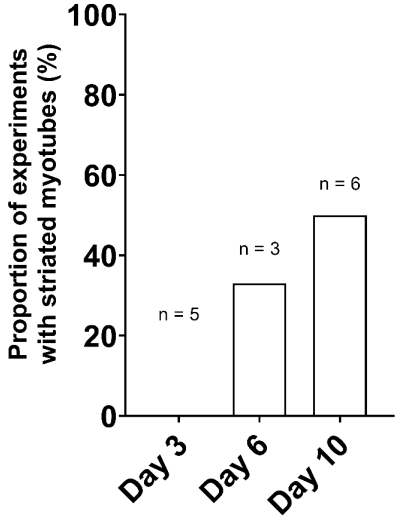

Figure 101: Proportion of experiments resulting in sarcomeric striations for 75 µm diameter collagen tubes without intercellular matrix, over time.

Sarcomeric striations reflect a further myotube maturation because it is the sign of the functional organization of the muscle-construct. It is interesting though to notice that our system does not

reach 100% proportion of experiments resulting in striated myotubes, at day 10 of culture. Since there is an increase over time, one hypothesis would be to run longer experiments.
Indeed, by cultivating polymerized C2C12-laden fibrin gel inside sacrificial gelatin tubes, then replacing gelatin ECM with collagen I, several works reported striated myotubes at day 8 of culture [118], at day 10 [116]. On 2D microgrooves substrates, Hosseini *et al.* reported striated myotubes at 8 days of culture only after 48 h of electrical stimulation [90]. None of them reported quantification on striated myotubes, except for one study that reported over 45 % of total myotubes exhibiting sarcomeric striations at 4 weeks of culture, for C2C12 cultivated on 2D poly acrylamide substrate with a stiffness of 11 kPa stiffness [94]. Unfortunately, our results on striated myotubes quantification do not match any comparable studies.

Interestingly, seeding conditions with added ECM did not result in sarcomeric striations, whether we used collagen type I (seeding condition 2.1) nor laminin (seeding condition 2.2). Adding ECM modifies several parameters for cells environment. It modifies the overall stiffness that cells sense and it increases the local adhesion molecules concentration. Therefore, we were interested on how the substrate stiffness can influence the presence of sarcomeric striations, witness of myotubes maturation.

1.4. **Influence of stiffness on myotubes maturation**

Several papers reported the influence of substrate stiffness on myoblasts differentiation. C2C12 myoblasts have been cultivated on poly-caprolactone substrate with tunable stiffness, coated with collagen I (1 mg/ml) [150]. They observed that myoblasts differentiated earlier on substrates with an elastic modulus of ~ 1 MPa compared to stiffer ones (~ 50 MPa – 130 MPa). However, they did not assess sarcomeric striations.
Another study reported an optimum gel stiffness at 12 – 15 kPa where around 45% of myotubes had striations after 4 weeks, using poly acrylamide (PA) gels with micro arrays of collagen I (1 mg/ml) (Figure 102) [94].

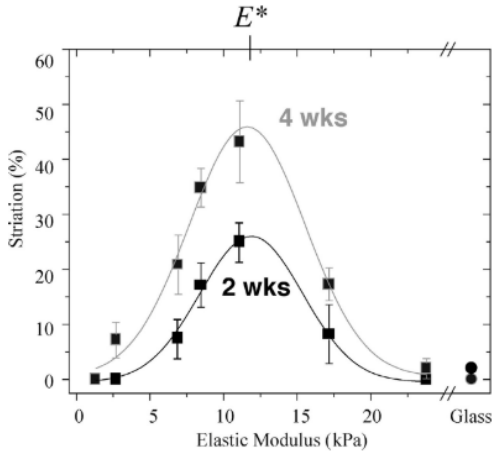

Figure 102: Proportion of striated myotubes plotted against the stiffness of the substrate [88]. The stiffness E* that resulted in the higher proportion of striation ranged between 10 – 15 kPa.

Unexpectedly, when these myoblasts were seeded on another 2 days-old myoblasts layer, up to 80% of myotubes were striated at 4 weeks. From previous studies, the authors reported that the

first myoblasts layer had a stiffness of 12 – 15 kPa, which they concluded was comparable to the optimal stiffness for striated myotubes generation they found on PA substrate. To evaluate the relevance of these values, they measured the elastic modulus of dissected skeletal muscles from mice and found comparable values (12 – 18 kPa). On the contrary, they observed that myoblasts cultivated on a glass substrate (elastic modulus of a glass cover slide according to Thorlabs® manufacturer ~ 700 GPa[l]) patterned with arrays of collagen I did not exhibit sarcomeric striations, but a lot of actin stress fibers. Another team reported higher proportion of myotubes on gels made of poly-lactic acid/poly-lactic co glycolic acid with an elastic modulus of 200 kPa compared to stiffer substrate (280 kPa) of softer ones (60 kPa) [151]. Again, they did not quantified sarcomeric striations.

Our system was composed of tubes made from commercially available Corning® rat tail derived-collagen I at 6 mg/ml. On the manufacturer's website, the elastic modulus of collagen I has been measured by a shear rheology apparatus[m] (Figure 103A).

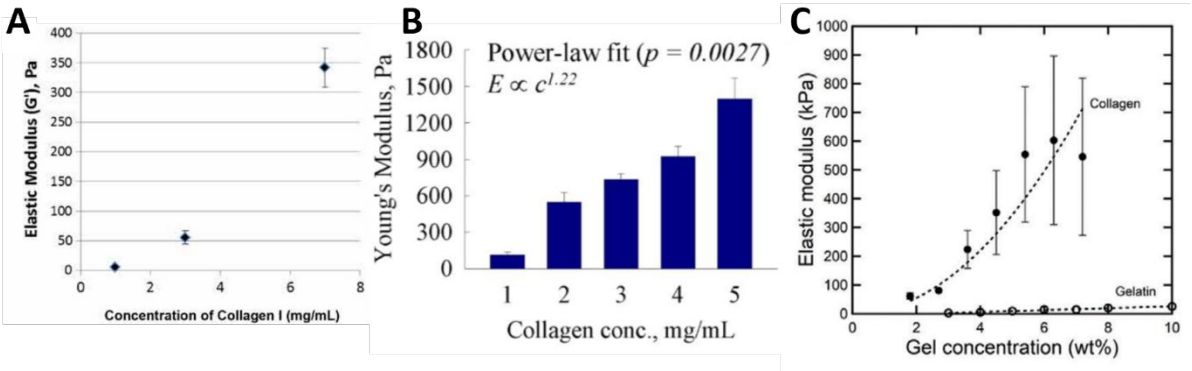

Figure 103: (A) Elastic modulus of Corning® rat-tail derived-collagen I gel measured by the manufacturer using shear rheology. (B) Exact same commercial collagen I elastic modulus measured by AFM [152]**. (C) Elastic modulus measured by traction tests of collagen I extracted from rat-tails** [153]**, where 2 mg/ml and 6 mg/ml are equivalent to 0.24 wt% and 1.32 wt% respectively.**

An exponential fit curve from their value yielded an elastic modulus at ~ 0.2 kPa for 6 mg/ml. Using the exact same commercial collagen I, different values were reported (Figure 103B) [152]. Their results allowed them to fit a power-law curve, that would yield a value of ~ 2 kPa for 6 mg/ml, an order of magnitude higher than the manufacturer's measurements.
One point is noteworthy throughout all these studies: stiffness measurement were measured using different methods each time, either by a rheological measurements (with different configurations) or by AFM.

Quite recently, a team we collaborate with (Sciences et Ingénierie de la Matière Molle, ESPCI, Paris. Team of Alba Marcellan) published studies on the mechanical properties of collagen I extracted from rat-rails [153]. Using a commercial tensile test apparatus and different concentrations of collagen I, they obtained higher values than the previous one mentioned (Figure 103C). Their exponential fit curve estimates the elastic moduli for 2 mg/ml (0.24 wt%) and 6 mg/ml (1.32 wt%) collagen I at about 30 kPa and 60 kPa respectively.

[l] https://www.thorlabs.com/newgrouppage9.cfm?objectgroup_id=9704
[m] https://www.corning.com/catalog/cls/documents/application-notes/CLS-AC-AN-449.pdf

Facing these discrepancies, we decided to test the Corning® collagen I from our own stock. Three rectangular samples (10 mm × 20 mm × 2 mm height) were prepared at different days in a PDMS mold. Samples were then mounted on the tensile apparatus (Instron™ machine with a force cell of 10 N. Collagen samples were in immersed in DMEM glutamax at room temperature, and attached between two gripping jaws with a tightening tork of 5N to prevent slipping. The traction speed was set at 102.8 mm/min). In these conditions, stress-strain curves can be achieved as illustrated on Figure 104.

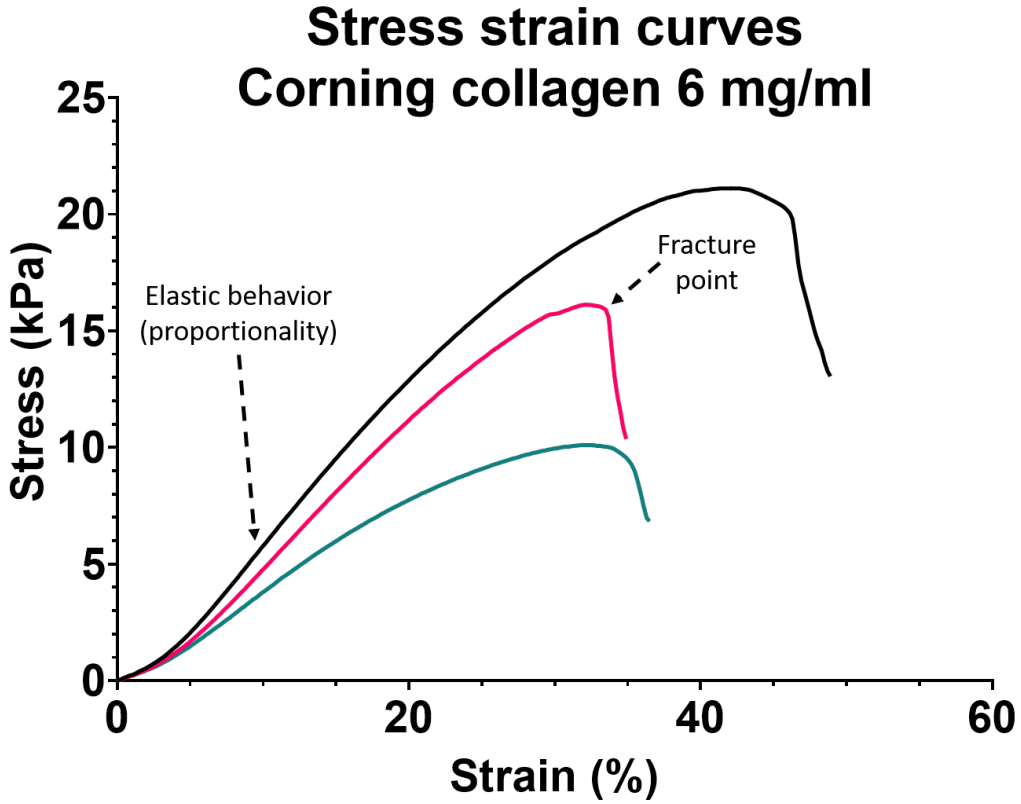

Figure 104: Stress strain curves for our stock Corning® 6 mg/ml collagen measured in traction test (n = 3). By exerting increasing stress on the sample, it deforms at a certain point compared to its initial state (strain).

For each curve, there is an initial elastic state where the stress and the strain are proportional. Within this range of proportionality, the elastic modulus can be extracted from the slope of the linear fit (it also called Young's modulus). The average measured elastic modulus was 54.8 ±14.7 kPa. Obviously, these mechanical properties experiments are preliminary results and have to be repeated. However, the value we found seems consistent with what our colleagues from ESPCI found with collagen I extracted from rat tail [153].

To further investigate the influence of stiffness on the presence of sarcomeric striations within our 3D tubular system, we generated 75 µm collagen I tubes of 2 and 8 mg/ml and performed a seeding condition 1. When seeding C2C12 myoblasts into 2 mg/ml collagen tubes, the collagen matrix first detached from one side of the PDMS at day 3 of culture, then detached from the other side at day 6 of culture (Figure 105A). At day 10 of culture, there were no striated myotubes (Figure 105B).

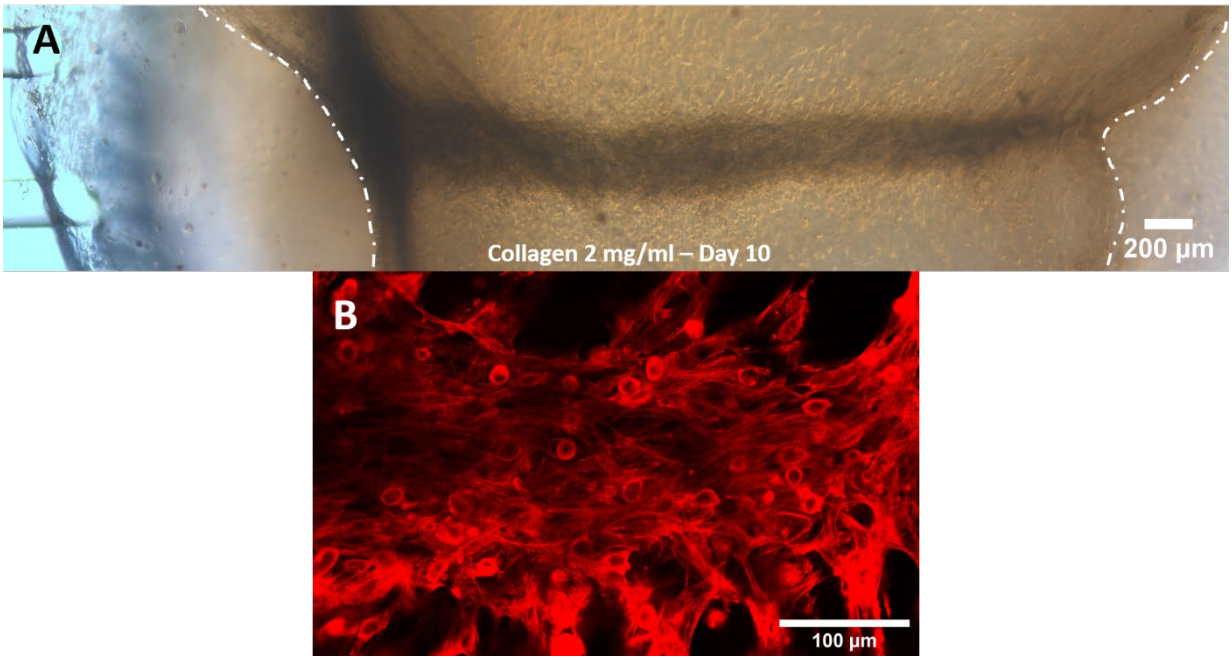

Figure 105: (A) Phase contrast image of muscle-construct in 2 mg/ml collagen tube, at day 10 of culture. White dashed lines are the collagen matrix interface that detached from the PDMS. (B) Confocal images of the same muscle-construct stained for F-actin, showing no striated myotubes.

On the other hand, 8 mg/ml collagen did not detach from the PDMS. However, there were no striated myotubes either at day 10 of cultures (Figure 106).

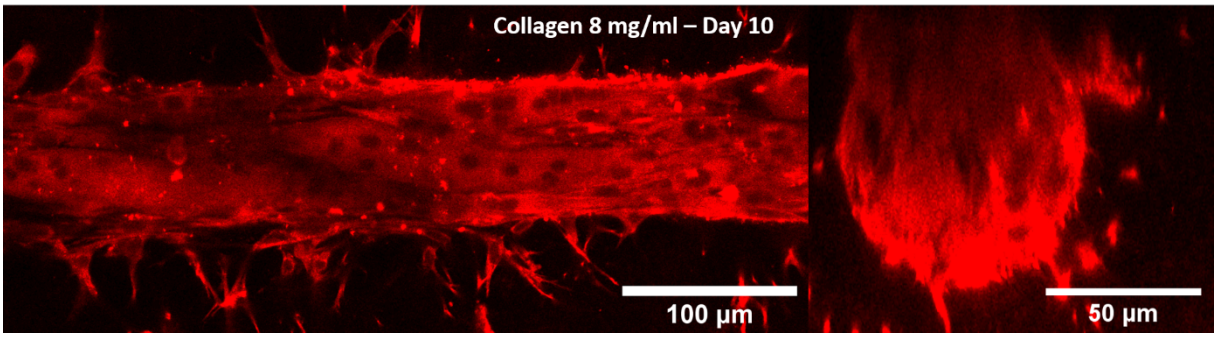

Figure 106: Confocal images of muscle-construct in 8 mg/ml collagen tubes, at day 10 of culture, stained for F-actin.

We performed 2D cultures on 24-wells dishes with the same conditions to evaluate how the substrate stiffness influenced the sarcomeric striations formation, independantly of the substrate curvature. Cells were seeded on collagen I, at 2, 4 or 6 mg/ml. As expected, our results showed that C2C12 myoblasts cultivated on collagne I-coated dish did not show any striated myotubes at any time point, independantly of the collagen I concentration (Figure 107).

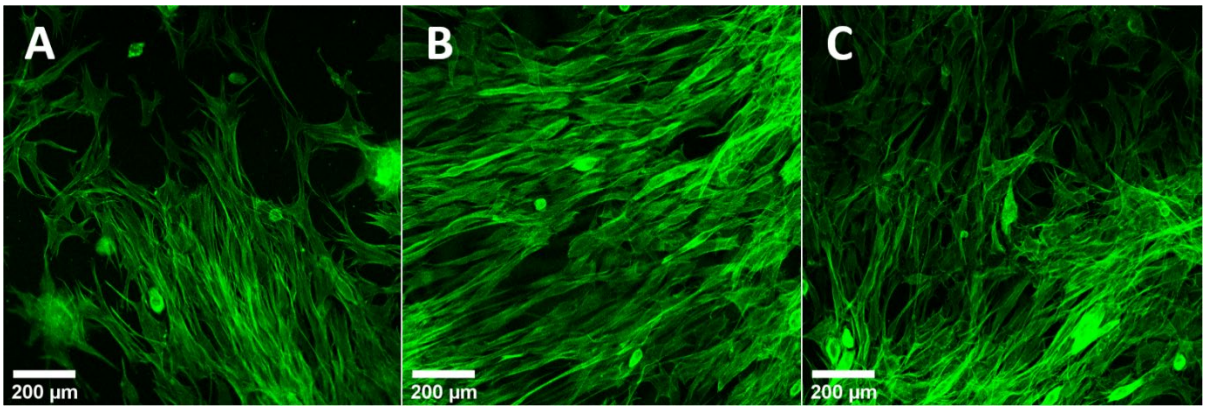

Figure 107: Confocal images of C2C12 cultivated on collagen I coated dished, at (A) 2 mg/ml, (B) 4 mg/ml or (C) 6 mg/ml at day 6 of culture. F-actin were stained with phalloidin.

Here when analyzing cells alignment, we observed an isotropic orientation of the cells (Figure 108). Since myoblasts anisotropic alignment is a pre requisite for cells fusion and myotubes formation, it is thus expected that myotubes within that configuration will not mature well.

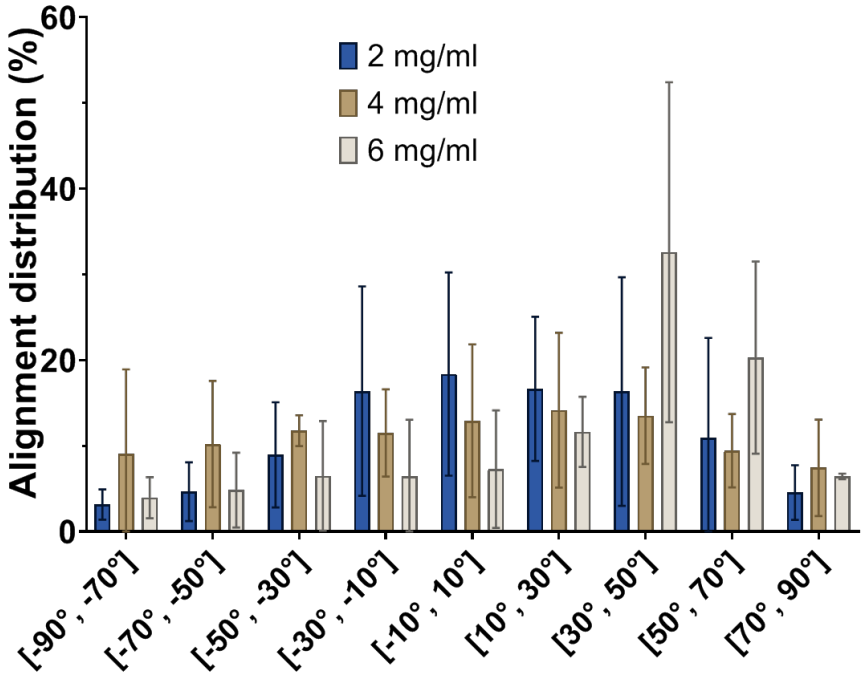

Figure 108: Cell orientation for C2C12 cultures on collagen I coated 2D dishes with different initial concentrations.

Without doubt, cultivating C2C12 in a 3D tubular system allowed the muscle tissue to mature more compared to 2D dishes. Then, substrate stiffness seems to affect myogenesis in our 3D tubular system. However, we saw that myotubes still developed on substrates with a very wide range of stiffness values. It suggests that other parameters may influence cells fate.

1.5. Influence of laminin coating on muscle cells differentiation in collagen tubes

1.5.1. Seeding condition 3 (Laminin coating prior to C2C12 seeding)

Another working hypothesis emerged from these insights. Laminin is one of the major components of the basal membrane and enhances cell adhesion to ECM [31], [33]. Hence to improve cell adhesion to the collagen tube we investigated another seeding condition (seeding condition 3): a laminin-coating of the collagen tubes inner surface was performed, prior to myoblasts seeding suspended in growth medium. Briefly, laminin was mixed in PBS (100 µg/ml) and injected inside collagen tubes at a pressure of 30 mbar for 2 min. Chips were then incubated at 37°C for 30 min. Myoblasts were subsequently seeded suspended in growth medium. When coating the collagen tubes inner surface with laminin, striated myotubes only formed at day 10 of culture (Figure 109).

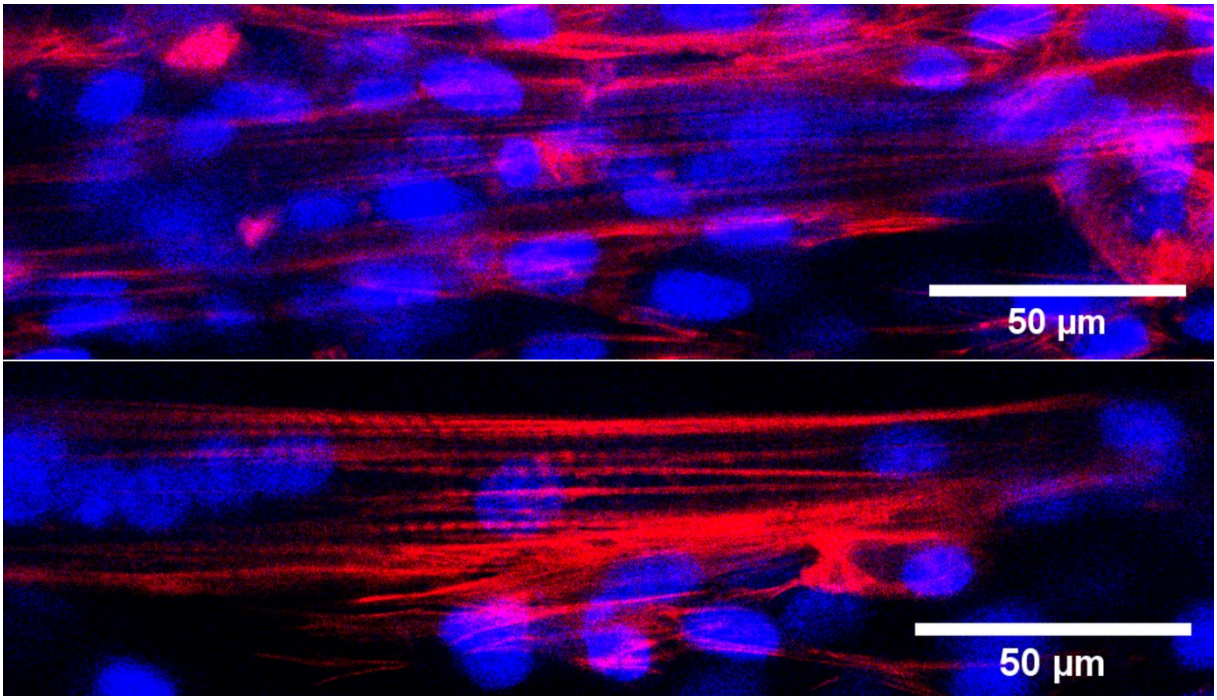

Figure 109: Confocal images of striated myotubes at day 10 of culture, for seeding condition 3.

However, these results are preliminary as we only have n= 1 for each time point. Although we cannot have a strong conclusion yet, these results could suggest that striated myotubes formed when coating the collagen tube surface with laminin, whereas there were none when using laminin mixed with cells during the seeding.

We also performed 2D cultures on collagen I with laminin coated dishes, with the same experimental condition as on 3D collagen tubes. As previously, none of the C2C12 myoblasts on dishes resulted in striated myotubes at any time point. The muscle construct usually detached from the substrate either at day 6 or at day 10 of culture.

Altogether, these first results suggest that the formation of striated muscle construct mostly relies on geometrical cues and that the presence of ECM component during the seeding step could impede or slow down myotubes maturation. Our results also suggest that in this cylindrical

configuration, hydrogel stiffness strongly affects myotubes maturation with an optimum for collagen at 6 mg/ml. To further compare how these different parameters affect the muscle-on chip generation, deeper myotubes characterization has been performed.

1.6. On-chip muscle construct characterization

To further evaluate the effect of the different culture/seeding conditions, we focused on different characterization parameters such as myotubes alignment, diameter and length and cell fusion indicator. Myotubes dimensions were compared to *ex vivo* samples. We also analyzed the nuclei 3D alignment toward the collagen tube axis, the nuclei inter distance globally and specifically within myotubes. Finally, we quantified the myoblast differentiation genes expression by RT-qPCR assays.

1.6.1. Myotubes alignment

- **Myotubes orientation**

When seeding C2C12 suspended in growth medium without adding ECM, the percentage of aligned myotubes (*i.e.,* oriented within [-10°;10°] toward the tube long axis) in 75 µm collagen tubes reached 43.5 ±9.3 % compared to 200 µm collagen tubes (34.5 ±6.2 %) (Figure 110). These results showed as expected that increasing the cell scaffold curvature increased myotubes alignment.

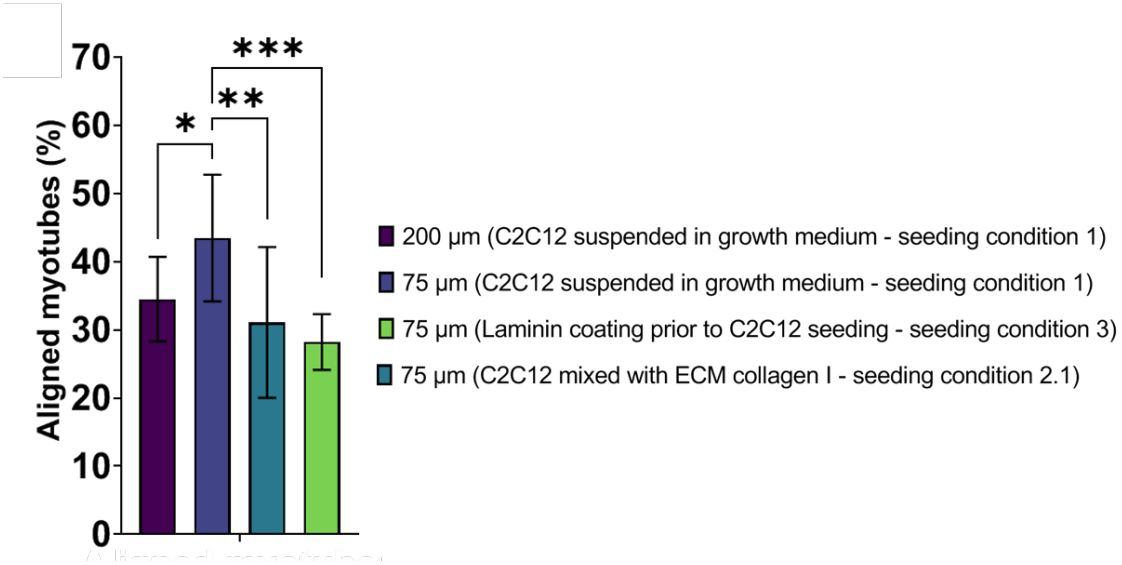

Figure 110: Distribution of aligned myotubes (within [-10°;10°]) in 200 µm collagen tubes compared to 75 µm collagen tubes. n = 8, 17, 9 and 9 for 200 µm and 75 µm seeding condition 1, 75 µm seeding conditions 3 and 2.1 respectively.

On the other hand, for the 75 µm diameter condition, seeding with ECM components or performing a laminin coating prior to cell seeding significantly decreased percentage of aligned myotubes (31.1 ±11.1 % and 28.2 ±4.1 % respectively). These results are in good agreement with our previous observations regarding the absence of striated myotubes with added ECM.

- **Orientation coherency**

Myotubes within 75 µm collagen tubes had a higher orientation coherency when no ECM was

added during seeding (0.43 ±0.09) compared to myotubes generated with added ECM during seeding (0.31 ±0.11) or with a laminin-coating (0.28 ±0.04) (Figure 111).

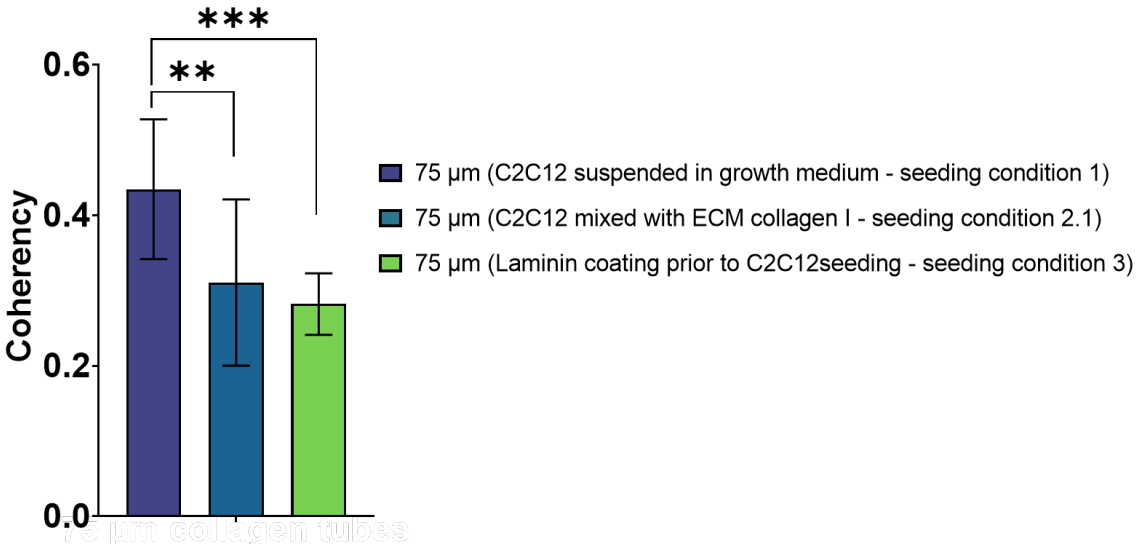

Figure 111: Coherency values for myotubes in 75 µm collagen tubes, at day 10 of culture depending on experimental conditions. Orientation coherency is significantly higher when no ECM was added during seeding compared to all other experimental conditions. n = 17, 9 and 9 for seeding condition 1, 2.1 and 3 respectively.

Combined with the results on myotubes alignment, it means that myotubes within 75 µm collagen tubes were more oriented toward the collagen tube long axis, but also were more aligned with respect to other myotubes in the absence of intercellular matrix. When ECM was added during the seeding, we even observed very heterogeneous and branched myotubes (Figure 112).

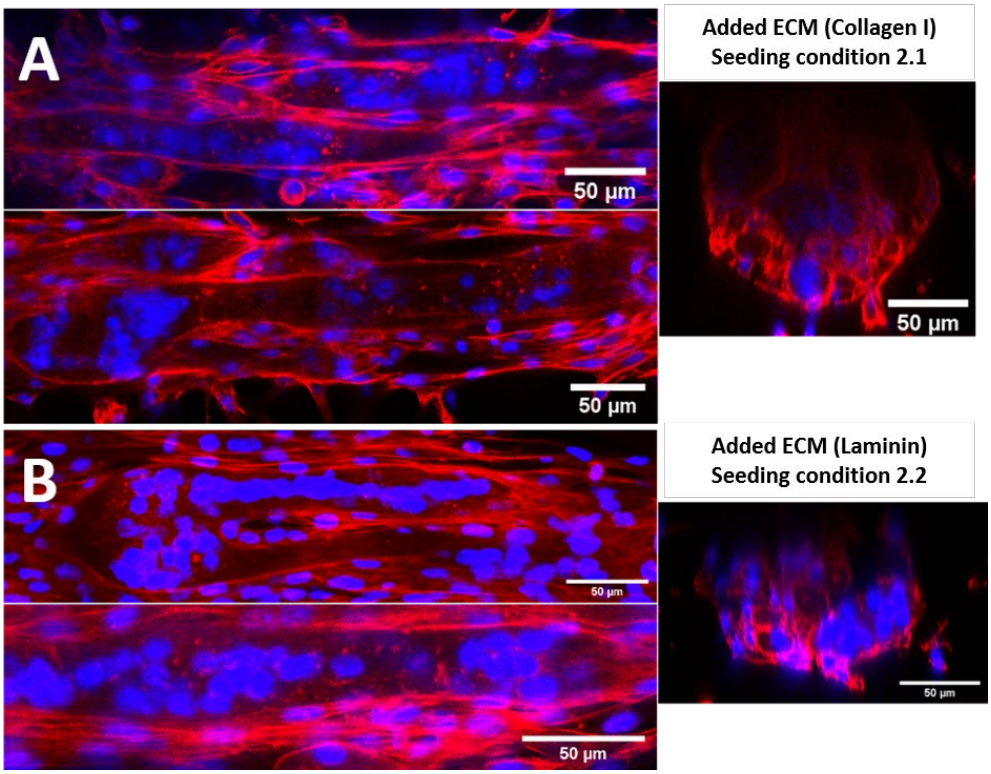

Figure 112: Confocal images of fixed on-chip muscle-constructs within 75 µm collagen tubes, when adding ECM during seeding, for (A) seeding condition 2.1 and (B) seeding condition 2.2.

Heterogeneous myotubes with large syncytia and the absence of sarcomeric development could suggest that added ECM potentially hinder normal myogenesis. This situation is actually comparable to abnormal secretion of ECM proteins, called fibrosis, which is also described in muscular dystrophies or other inflammatory myopathies and result in aberrant skeletal muscle repair [41]. Indeed, pathological regeneration leads to muscle fibrosis, heterogeneity in cell size and an increased in extracellular collagen deposition. The skeletal muscle physiologic regeneration goes through several steps. It involves transient ECM secretion which satellite cells use as a scaffold to proliferate, differentiate and fuse. Immune cells, mainly macrophages, invade the tissue under regeneration and participate to the regulation of the inflammatory process. They finally clear myofiber debris and degrade the transient ECM. The inflammatory process in skeletal muscle regeneration is actually complex, involving different kind of macrophages and several other cell types [41]. An increase in collagen deposition has been reported in skeletal muscle of obese and type 2 diabetic mice and humans [154]. The absence of striated myotubes for cells seeded with ECM component could therefore be attributed to an abnormal muscle environment, similar to fibrotic and pathological one.

1.6.2. Myotubes dimensions

In vivo myotubes are generally described to have an elliptic cross section, which was also the case within our collagen tubes. One chip containing 3 collagen tubes, each chip has therefore 1 to 3 muscle-constructs. For each muscle-construct, we isolated myotubes and measured at its largest cross-section area, the minor and major axis (Figure 113).

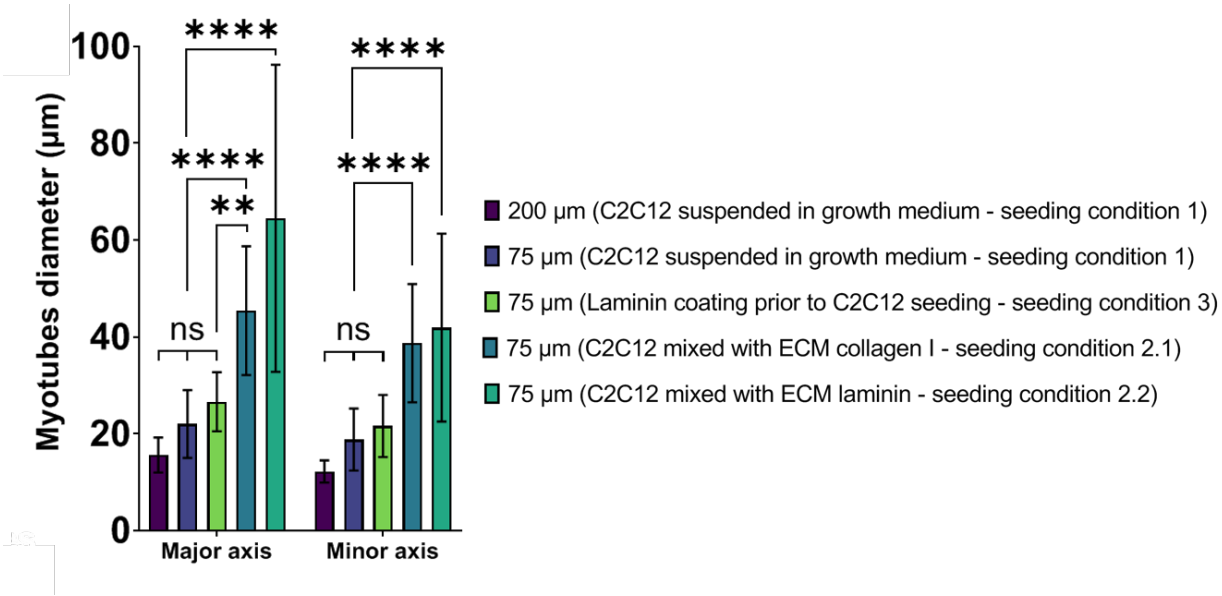

Figure 113: Myotubes diameter (major and minor axis) depending on the experimental conditions, measured at their largest cross-section. n = 17, 20, 9, 4 and 9 for 200 µm and 75 µm seeding condition 1, 75 µm seeding condition 3, 2.1 and 2.2 respectively.

In the seeding condition 1 without added ECM, myotubes in 200 µm collagen tubes exhibited a maximum major axis of 15.6 ±3.6 µm and a maximum minor axis of 12.2 ±2.3 µm, which was comparable to the myotubes in 75 µm tubes with or without laminin coating (Figure 113, seeding conditions 1, and 3). On the other hand, adding ECM during seeding (seeding conditions 2.1 and 2.2) seemed to affect myotubes dimension. Indeed, myotubes exhibited a major axis of 45.4 ±13.3

µm and a minor axis of 38.7 ±12.2 µm (seeding condition 2.1), and a major axis of 64.5 ±31.7 µm and a minor axis of 41.9 ±19.4 µm (seeding condition 2.2). If we look back at cross section the Figure 112, we clearly see that some myotubes are very large, almost filling the whole section of the tube.

Next, we measured myotubes length as a function of the different seeding conditions. We showed that the myotubes in 200 µm collagen tubes were significantly shorter than in the 75 µm ones, with average lengths of 152 ±69 µm and 357 ±85 µm respectively (Figure 114). In contrast, the length of the myotubes in the 75 µm collagen tubes did not differ significantly under any of the seeding conditions.

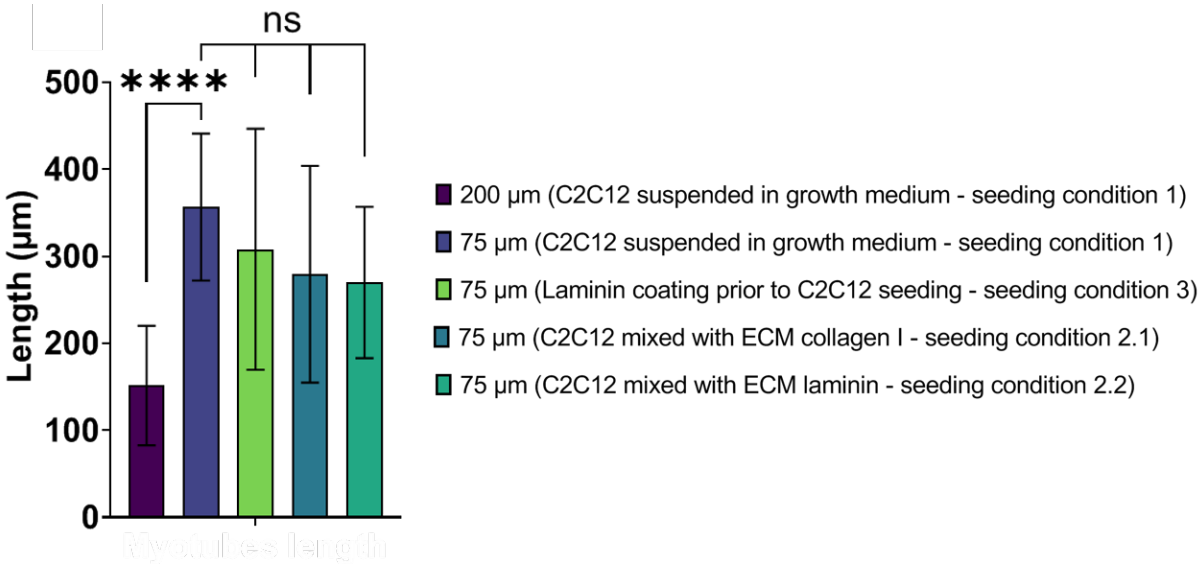

Figure 114: Myotubes length as a function of the seeding conditions. n = 17, 20, 9, 5 and 8 for 200 µm and 75 µm seeding condition 1, 75 µm seeding condition 3, 2.1 and 2.2 respectively.

We thus wanted to know if the myotubes we generated in our on-chip system were comparable to *in vivo* conditions. We thus dissected mice quadriceps and processed them for immuno-histological analysis.

1.6.3. Comparison with ex vivo samples

As discussed in the chapter 1, *ex-vivo* skeletal muscle exhibits striated myotubes, and elongated nuclei that are positioned toward the periphery under the plasma membrane. *Ex vivo* samples we processed shared the same characteristics (Figure 115).

Myotube diameter was estimated with the same method used previously for our on-chip experiments: fitting an ellipse to myotubes surrounded by an F-actin ring, on cross-section images. However, due to the intrinsic limitations of the microtome cutting method, slices thickness was less than 50 µm. Therefore, images usually displayed uncomplete myotubes. This obviously results in underestimating the myotubes diameter.

Ex vivo myotubes extracted from dissected quadriceps exhibited a major axis of 40.4 ±11.4 µm and a minor axis of 29.0 ±4.5 µm (Figure 116), rather similar to the myotubes generated within 75 µm collagen tubes with ECM components (seeding condition 2.1).

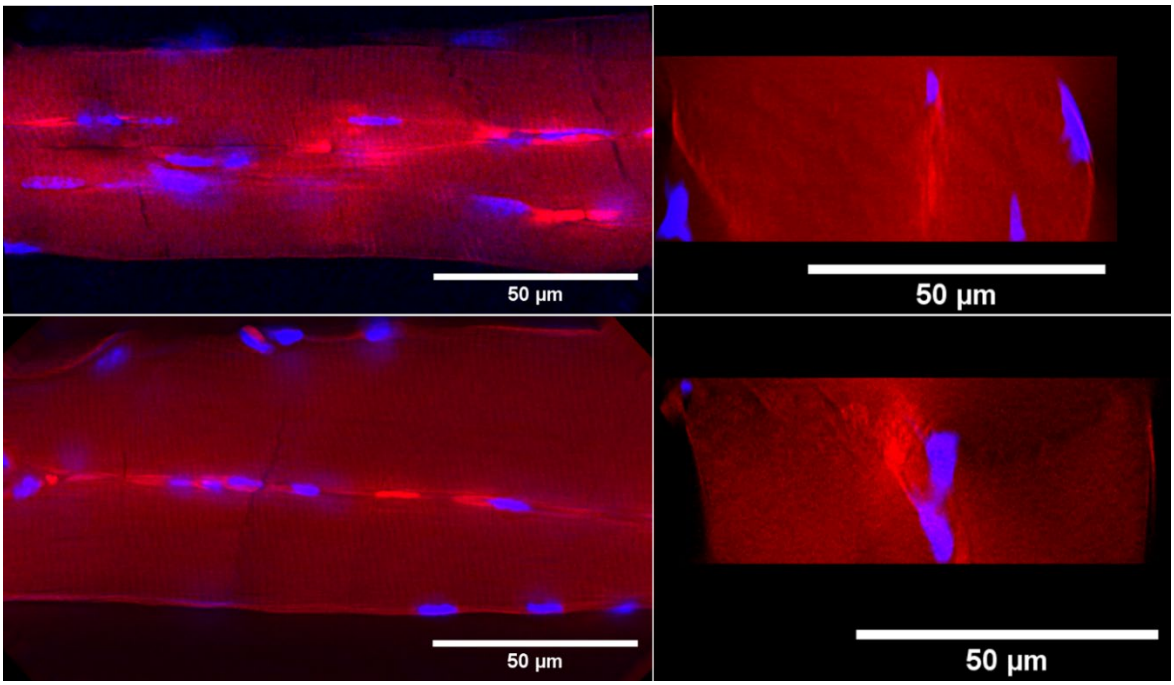

Figure 115: Confocal images of fixed immuno-stained dissected mice quadriceps, cut using a microtome. Red staining is F-actin, blue is DAPI for nucleus. Left: longitudinal sections. Right: cross-section.

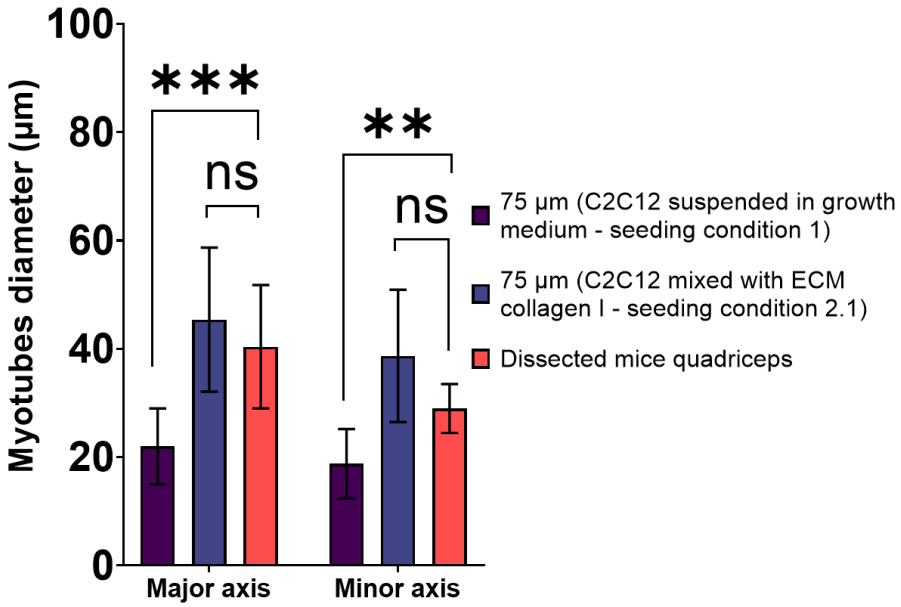

Figure 116: *Ex-vivo* skeletal muscle myotubes diameter from dissected mice quadriceps, compared to the myotubes diameter from our system at day 10 of culture.

These results thus suggest that the presence of ECM components during seeding might result in a more physiologic myotubes in terms of size. As previously mentioned, longer experiments have to be performed to verify if they might end in striated myotubes with nuclei spreading and dispersion.

1.6.4. Cell fusion indicator

The fusion indicator referred to the average number of nuclei per myotube. Since each nucleus

obviously originated from one single myoblast, it was considered as a good parameter to measure cell fusion (Figure 117).

Our results showed that for cells seeded with growth medium (seeding conditions 1), the myotubes in 200 µm collagen tubes had a significantly lower fusion indicator (3.39 ±1.78) than those in 75 µm collagen tubes (9.90 ±4.22), which was in agreement with the myotubes dimensions previously mentioned. The fusion indicator was not significantly affected by the presence of a laminin-coating (seeding condition 3; 13.11 ±9.06).
On the other hand, adding ECM during seeding resulted in a significantly higher fusion indicator. Indeed, the fusion indicator were 18.1 ±6.7 and 28.0 ±15.3 for myotubes in 75 µm collagen tubes for seeding conditions 2.1 (ECM collagen I) and 2.2 (ECM laminin) respectively. We can distinguish two distinct: cells seeded with no added ECM and lower fusion indicator, cells seeded with added ECM and higher fusion indicator.

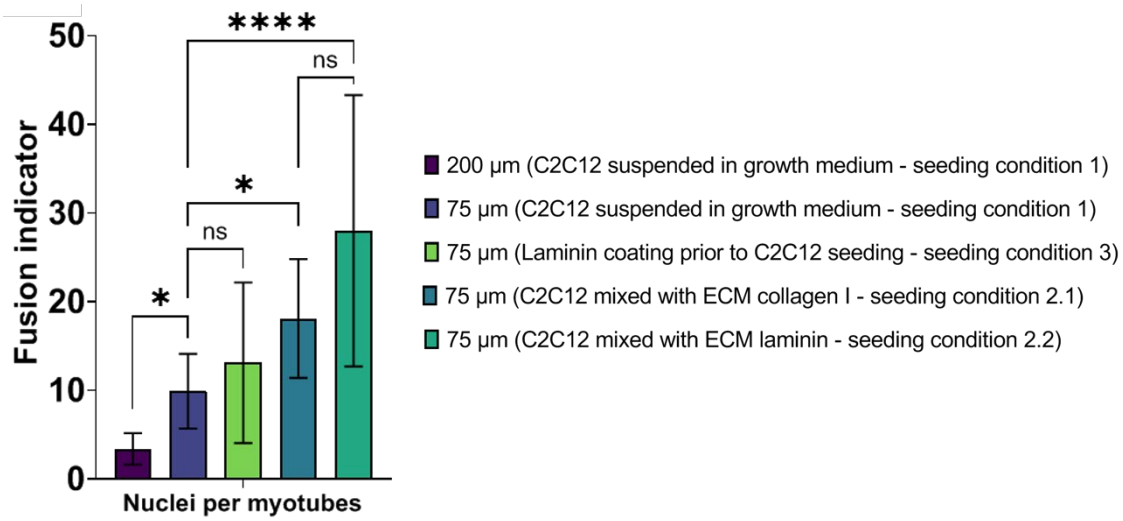

Figure 117: Fusion indicator, referring to the average number of nuclei per myotubes. Since each nucleus obviously originated from one single myoblast, it was considered as a good parameter to measure cell fusion. n = 18, 20, 9, 5 and 9 for 200 µm and 75 µm seeding condition 1, 75 µm seeding condition 3, 2.1 and 2.2 respectively.

Our results suggest that the fusion indicator is correlated with myotube diameter in agreement with the fact that, the higher the fusion indicator, the larger the myotube diameter. The presence of ECM component during seeding resulted in a larger muscle syncytium with heterogeneous (larger standard deviations) and branched myotubes (Figure 112) whereas, myotubes were morphologically more aligned and had no branching when seeded in absence of ECM (Figure 98 and Figure 100). As previously discussed, such large branched heterogeneous myotubes are also observed in several myopathies and in muscle fibrosis, defined as an excess of ECM in the skeletal muscle.

Another hypothesis could also bring further explanation to these results. For conditions with added ECM, we observe that nuclei tend to aggregate in the center of the newly formed myotube (Figure 112). Myoblast fusion is actually followed by nuclei movements that are finely regulated [59]. At least, four different nuclear movements have been reported to occur in myofiber formation: nuclear centration, spreading, dispersion and clustering (Figure 118).

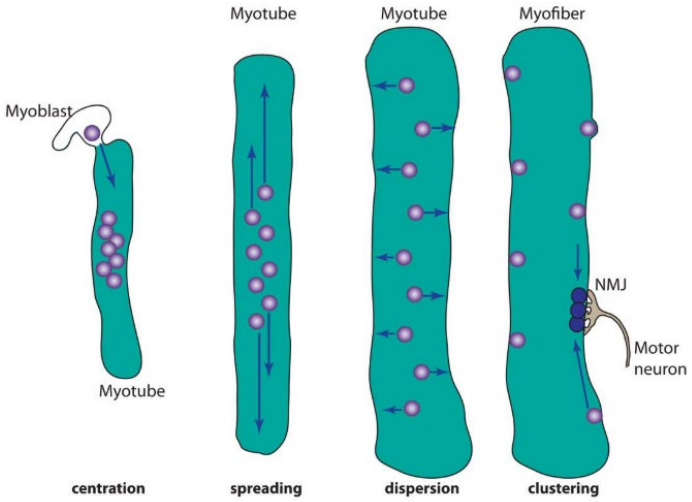

Figure 118: Nuclear movements during muscle formation, from [59]**. After cell fusion, nuclei gather toward the center (centration). Then they spread and become evenly spaced (spreading). During myotube maturation, nuclei move to the periphery close to the plasma membrane (dispersion). Finally, some nuclei make cluster under NMJ (clustering).**

Rapidly after cell fusion, nuclei aggregate toward the center of the myotube (nuclear centration). Nuclei then start to spread and become evenly spaced (nuclear spreading). During myotube maturation, nuclei migrate to the periphery, close to the plasma membrane (nuclei dispersion). Finally, some nuclei gather under the NMJ (nuclear clustering). These movements are regulated by microtubules network and their associated proteins. Therefore, the increased fusion indicator and myotubes diameter could mean that myogenesis is undergoing, but is still at an early stage. The absence of striated myotubes could thus simply result from myotubes still under maturation, being at the stage of nuclear centration or spreading (Figure 118). A way to confirm this hypothesis would be to maintain these on-chip myotubes in culture longer.

In 75 µm collagen tubes, cells seeded without ECM component exhibited striated myotubes, but lower fusion indicator and diameter compared to cells seeded in presence of ECM component. These contradictory observations could mean that the conditions of muscle cells seeding with ECM component hold a higher biomimetic potential, however experiment on extended culture time should be further investigated to confirm this assumption.

Finally, whatever the seeding conditions, in 75 µm tube, we observed cell fusion resulting in multinucleated muscle cells. *In vivo* nuclei organization is very specific in mature muscle cells: they are elongated, oriented parallel to the myotube axis, and are regularly distributed along the myotube length. Therefore, the quantification of nuclei parameters can bring us supplementary information about myotubes maturation.

1.6.5. Nuclei analysis

At this stage, the experimental condition that resulted in the most mature myotubes was the seeding of myoblasts in 75 µm collagen tubes (presence of striations), suspended in growth medium (seeding condition 1). We will therefore focus on the nuclei analysis for this optimal experimental condition.

- **3D segmentation process with ImageJ**

Nuclei analysis was processed using an algorithm to clean and segment nuclei of a 3D z-stack of images. Few remarks must be discussed herein. As we already saw on confocal images, myotubes in our system were packed together. Hence, nuclei sometimes were very close together, making them very challenging to segment. This behavior usually resulted in unreasonably large nuclei volume. In other hand, background noise resulted in unreasonably small nuclei volume.

We reported in chapter 1 that mature myotubes nuclei have an average nuclei diameter of 10 µm, with a long axis reaching 18 µm. If we approximate the nucleus as a sphere, we obtained volumes ranging from ~ 520 μm^3 up to 4000 μm^3. We therefore decided to apply size thresholding in our 3D segmentation, only analyzing counted objects within that volume range. The output we obtained was a 3D segmented nuclei image as represented in Figure 119.

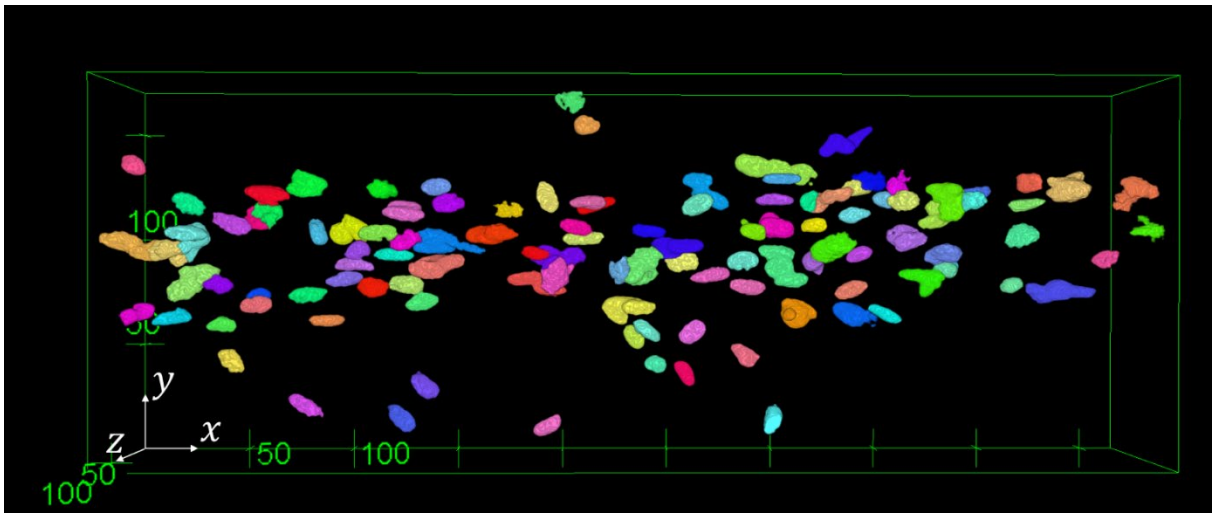

Figure 119: 3D segmented nuclei representation in the XY plan view with scalebar, processed in ImageJ, from Z-stack confocal images of nuclei within muscle-construct generated with seeding condition 1 in 75 µm diameter collagen tubes.

The process fitted an ellipsoid to each nucleus, and computed the volume, the sphericity, the center of mass in 3D, the radii and the 3D orientations. We focused here on nuclei from myotubes generated within 75 µm collagen tubes with seeding condition 1.

- **Nuclei dimensions**

Myotubes nuclei had an average volume of 1206 ±228 μm^3, with a major axis of 11.2 ±0.8 µm and a minor axis of 5.5 ±1.9 µm. Nuclei were therefore elongated toward the long axis of the collagen tube, similarly to myotubes orientation.

- **Nuclei alignment**

To better understand the orientation in 3D, let's pay attention to the definitions first. 3D orientations are defined by the Euler angles (Figure 120). Considering an object in a 3D space, the first angle is the 'azimuth' that defines the orientation between the x unit vector (0°) toward the object in the XY plan. Then the other angle to consider is the 'elevation' that defines the orientation between the XY plan (0°) and the object, toward the z unit vector. Finally, the 'twist' angle defines the rotation of the object around the axis that passes through the coordinate's origin and the long axis of the object.

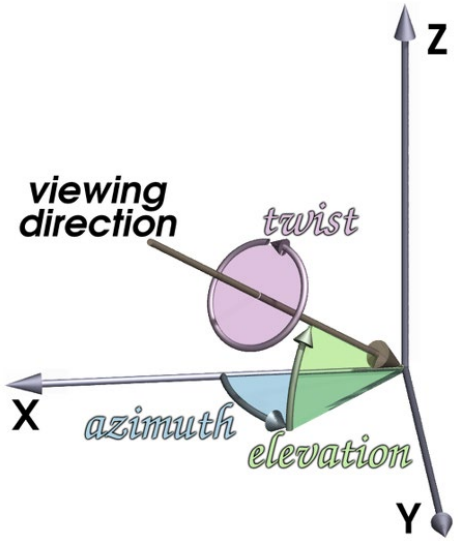

Figure 120: Euler angles defining the 3D orientations in space using cartesian coordinates. The "azimuth" angle determines the orientation between the *x* unit vector (0°) and the considered point, on the XY plan. Then, the "elevation" angle determines the orientation between the XY plan (0°) and the z unit vector. Finally, the "twist" angle determines the rotation around the axis that passes through the coordinate's origin and the long axis of the considered object.

With this insight in mind, we can now focus on nuclei alignment. The muscle-construct long axis being mostly oriented toward the *x* axis, we only considered the 'azimuth' angle of the nucleus, which is the one projected into the XY plan, independently of the 'elevation' and the 'twist' orientations. The nuclei 'azimuth' angles therefore have the same frame of reference as myotubes orientation we previously analyzed (Figure 121). We will now refer to 'azimuth' angle as 'nuclei orientation'.

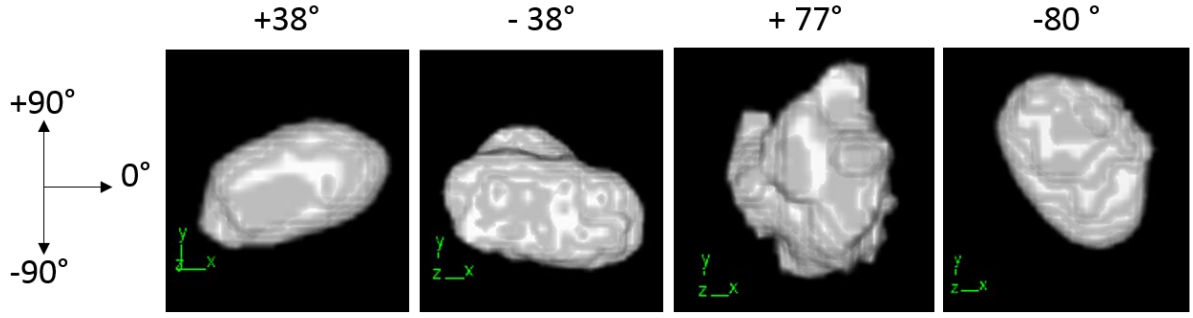

Figure 121: Selected nuclei illustrating the azimuth angles extracted from the analysis.

Nuclei orientations were extracted from 8 muscle-constructs, generated in 75 µm collagen tubes as day 10 of culture. In a similar way to 'aligned myotubes' mostly oriented within [-10°, 10°] toward the long axis of the collagen tube, nuclei aligned in the same direction with about 50 of the nuclei oriented in the [-10°, 10°] interval (Figure 122).

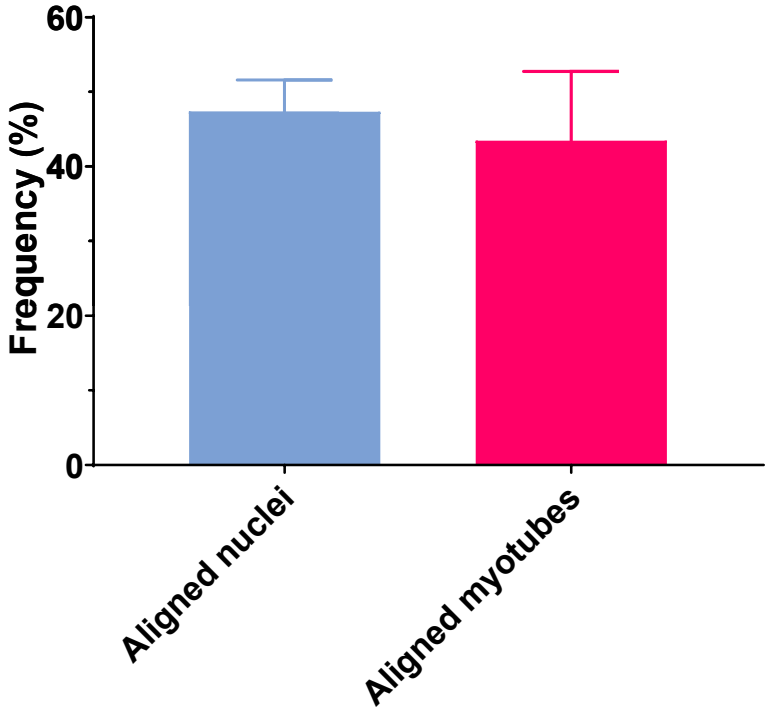

Figure 122: 3D Nuclei orientation distribution, within myotubes in 75 µm collagen tubes in seeding condition 1, at day 10 of culture. In the similar way to 'aligned myotubes' previously discussed, 'aligned nuclei' are the myotubes nulei oriented within [-10°, 10°] toward the collagen tube. n = 8.

As described in chapter 1, *in vivo* mature skeletal muscles nuclei are aligned parallel to myotubes long axis. When compared to the proportion of 'aligned myotubes' (43.5 ±9.3 %), the 'aligned nuclei' (47.4 ±4.2 %) were within the same range of values.

- **Inter nuclei distances**

In a 3D space, the minimum distance d between two points $M_1(x_1, y_1, z_1)$ and $M_2(x_2, y_2, z_2)$ is computed as $d = \sqrt{(x_2 - x_1)^2 + (y_2 - y_1)^2 + (z_2 - z_1)^2}$. All nuclei were fitted with an ellipsoid having a center of mass, located with its (x_i, y_i, z_i) coordinates. For each nucleus, the inter distance between all the other nuclei was computed. We then only kept the minimal value, which was the distance between the nearest nucleus. Finally, these minimal nuclei inter distances were averaged on all the different experiments.

In these conditions, we obtained an average nuclei inter distance was 19.3 ±2.3 µm. However, when we focused our analysis on nuclei positioned within a single myotube, we observed that the average nucleus inter distance was significantly higher (25.7 ±7.7 µm) (Figure 123).

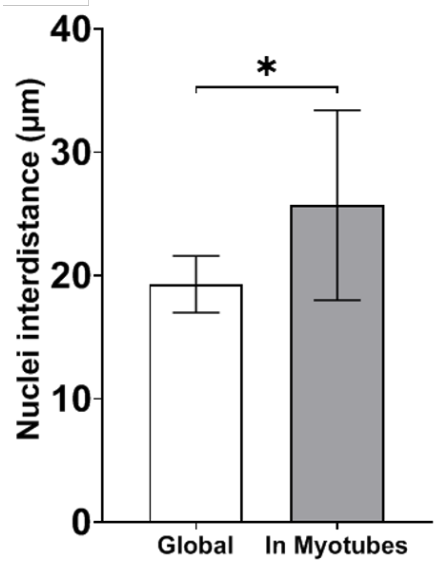

Figure 123: Nuclei inter distance between nuclei analyzed globally within the whole muscle-construct (white) compared to nuclei specifically analyzed within myotubes (grey). n = 8 and 5 for 'global' and 'in myotubes' respectively.

Table 3: Nuclei parameters extracted from myotubes generated in 75 µm collagen tubes with seeding condition 1, compared to *in vivo*.

	Alignment [-10°, 10°]	**Volume**	**Major axis**	**Minor axis**	**Nuclei inter distance**
In vivo [61]	Parallel to myofibers	~1885 µm^3	18 ±2 µm	5 ±1 µm	30-32 µm
MyoChip device	43.46 ±4.24%	1205.57 ±228.33 µm^3	11.19 ±0.80 µm	5.49 ±1.95 µm	19. ±2.3 µm 25.37 ±7.7 µm†

† Inter distance for nuclei within the same myotubes.

- **Discussion**

Nuclei analysis results extracted from myotubes generated in 75 µm collagen tubes with seeding condition 1 are summarized in Table 3. We previously discussed (chapter 1) some of the nuclei key features in mature skeletal muscle cells [61]. In a similar manner to *in vivo*, nuclei within our microdevice mostly oriented parallel to myotubes as well, but had a smaller long axis and were closer to each other. Interestingly, the nuclei inter distance was higher when specifically analyzing nuclei within the same myotube. As it has been reported, nuclei movements undergo several steps as the myotube mature through time, before spreading further hence increasing the nuclei inter distance [59]. One conclusion is that the muscle-construct within our microdevice has myotubes in different state of maturation, with some myotubes reaching a further maturation state.

Beside morphological analysis, myotubes maturation is also reflected through molecular modifications with variation in genes expression, allowing the cell to synthesize several proteins such as transcription factors to initiate myogenesis and different myosin isoforms to set the contractile apparatus.

1.6.6. Gene expression

To characterize the molecular maturation of on-chip myotubes, we performed gene expression quantification by RT-qPCR assays for comparing C2C12 myoblasts cultivated on dish and on-chip. For each on-chip time point, since the cells count per chip was low (about 2000 cells), at least 3 different experiments were pooled together to perform the RT-qPCR assay. Each gene expression was normalized by the GAPDH housekeeping gene. Results were then expressed as a relative quantification (RQ) of the expression at the considered time point, normalized by the basal state (cells on flask at day 0 before seeding) using the $2^{-\Delta\Delta Ct}$ method.

To select the genes of interest, two excellent reviews have are particularly interesting: one discussing about the function of the myogenic regulatory factors (MRF) [155], and the other describing the skeletal muscle fiber types in mammals [156] have been selected. Four main MRF have been reported to induce myogenic differentiation: Myogenic Factor 5 (*Myf5*), Myogenic Differentiation 1 (*MyoD1*), Myogenic Regulatory Factor 4 (*MRF4*) and Myogenin (*MyoG*). Myogenin is a transcription factor, which activates the myogenic differentiation program and drives the cells to undergo myogenic differentiation, resulting in myoblasts exiting the cell cycle and fusing into multinucleated myofibres. Interestingly, knocked-out mice for the other MRF still resulted in viable mice, whereas knocked-out mice for myogenin lead mice death at birth. Myogenin is therefore indispensable for myogenic differentiation and its gene expression was therefore an appropriate way to evaluate cell commitment to myogenic differentiation. In mammals, such as mouse, skeletal muscles are still immature at birth. Major changes take place during the early postnatal development. Embryonic and neonatal myosin heavy chain (MyHC) isoform progressively disappear. In parallel, there is an upregulation of MyHC 2A, MyHC 2X and MyHC 2B in fast-twitch fibers sub population, by days 2 to 5 after birth in rat limbs. Finally, there is a progressive switching of MyHC 2A to MyHC 1 in slow-twitch muscles.

Our results showed that C2C12 myoblasts cultivated on dish exhibited a 20-fold increased expression of myogenin compared to the basal state, reflecting their commitment to the myogenic differentiation (Figure 124A). However, cells did not express any of the myosin heavy chain (MyHC) genes over time. Our results suggest that even though myoblasts are committed to the myogenic differentiation, they did not succeed in setting up the contractile unit, hence failed to differentiate properly.

On the other hand, cells grown on-chip exhibited a different profile of gene expression compared to cells cultivated on dish. They not only expressed myogenin at higher levels, but also MyHC genes with an expression peak after 3 days in differentiation medium (day 6 of culture) (Figure 124B). These results suggest that cultivating C2C12 myoblasts in our system allowed myotubes to better mature compared to 2D conditions in agreement with previous observations (alignment, striations).

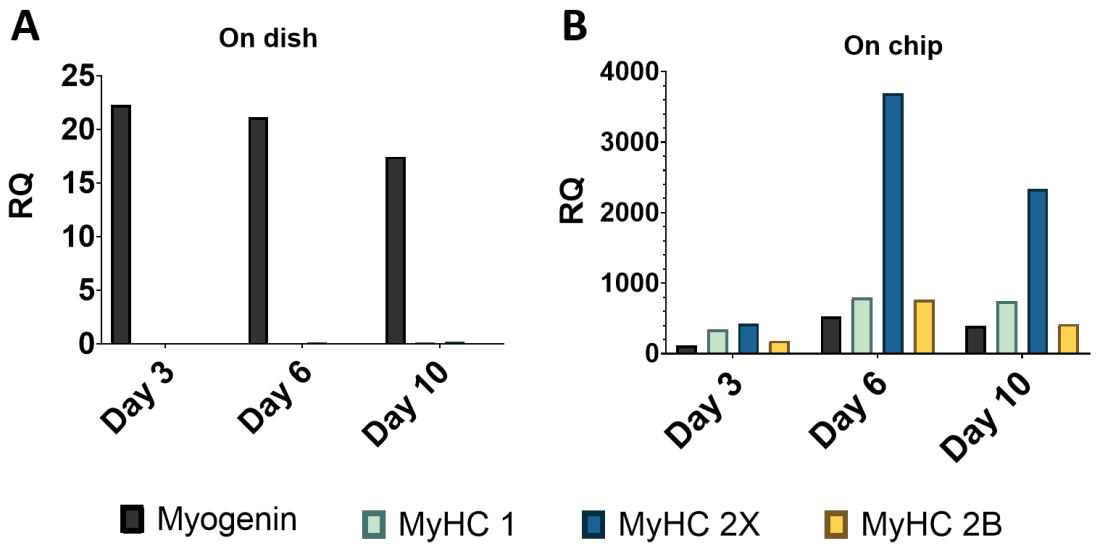

Figure 124: Myoblast differentiation genes expression (myogenin, myosin heavy chain fast isoforms (fMHC1, fMHC2) and slow isoform (sMHC) for C2C12 cultivated on dish or on chip, each time point expressed in relative quantification (RQ), normalized by GAPDH gene and compared to the basal state (cells on flask at day 0 before seeding). For each on-chip time point, since the cells count per chip was low (about 2000 cells), at least 3 different experiments were pooled together to perform the RT-qPCR assay.

Our results also showed that, in the contrary to dish cultures, cells cultivated on-chip upregulated the expression of MyHC 1, MyHC 2X and MyHC 2B genes, which are genes expressed in mouse during the early postnatal development.

1.6.7. Conclusion

To conclude on experiments using C2C12 myoblasts as a model, let's review the key parameters that resulted in the optimal condition for skeletal muscle-on-chip generation.

- Firstly, seeding myoblasts without adding ECM at high density was critical to maintain that same high cell density at day 3 of culture, when the growth medium is replaced by the differentiation medium.

- Secondly, the muscle-construct exhibited a lumen in 200 µm collagen tube whereas it entirely filled the collagen tube when decreasing the diameter to 75 µm, hence being more physiological.

- The alignment of myotubes along the collagen tube long axis increased through time, and was higher within 75 µm collagen tubes for cells seeding in absence of ECM component. This experimental condition was also the only one exhibiting striated myotubes.

- Adding ECM component during cells seeding increased the fusion indicator and the myotubes diameter but did not result in striated myotubes.

- Tube collagen stiffness seemed to influence the myofibrillogenesis. Too soft (2 mg/ml)

or too stiff (8 mg/ml) collagen did not result in striated myotubes. The optimal tube collagen concentration appeared to be around 6 mg/ml, yielding an elastic modulus of 54.8 ±14.7 kPa.

- Nuclei of myotubes generated within 75 µm collagen tubes without ECM component were mostly aligned parallel to the myotubes. Nuclei dimensions on-chip were in the same order of magnitude than *in vivo*. Their inter distance showed myotubes in different state of maturation, with some myotubes reaching further maturation state.

- Gene expression analysis showed that on-chip muscle constructs exhibited higher levels of myogenin, reflecting their commitment to the myogenic differentiation, as well as an upregulation of MyHC genes expression, which are physiologically expressed in mouse *in vivo* early postnatal development.

In conclusion, thanks to the MyoChip design, we first evidenced how important are the geometrical cues to properly organize muscle cells on-chip, we also showed that seeding conditions could strongly affect the muscle construct organization and maturation. Finally, we succeed in developing an on-chip 3D muscle-constructs exhibiting several key features of mature skeletal muscle cells, by cultivating C2C12 myoblasts in our microfluidic device.

1.7. Perspectives: increasing the relevance of the muscle cell type

1.7.1. Mouse primary myoblasts

Working with C2C12 myoblasts allowed us to greatly develop the MyoChip device. The next step is naturally to use more physiological cell types. Mouse primary myoblasts are cells directly extracted from dissected newborn mice muscles (hindlimb muscles, tibialis anterior, extensor digitorum longus, gastrocnemius and quadriceps). After dissection, myoblasts were isolated and frozen.

Within the MyoChip consortium, our collaborators from the Instituto de Medicina Molecular (Lisboa, Portugal) have the expertise and the knowledge in muscle cell biology. We therefore relied on their precious help for mouse primary myoblasts harvesting. Indeed, the most straightforward way to cultivate primary myoblasts extracted from mice would be to dissect, isolate and plate the cells immediately. In that way, the survival rate is much higher. However, we had to ask our collaborator to ship the frozen vials to Paris. Upon arrival, the first step was to assess if primary myoblasts in frozen vials could be stored for long term, thaw and cultivated on dish without losing its differentiation potential.

Following our collaborator's instructions, we coated 35 mm dishes with 500 µl of Matrigel diluted in 1:100 cold medium (IMDM + Glutamax) for one hour at room temperature. We subsequently washed the Matrigel-coated dish with PBS. Primary myoblasts were thaw and plated at a density of 200 000 cells per dish. Primary myoblasts were cultivated in growth medium for 3 days (IMDM

Glutamax, 20% FBS, 1% home-made chicken embryo extract, 1% PS) before switching to differentiation medium (IMDM Glutamax, 2% HS, 1% PS) until day 10 of culture. Cells were fixed and stained for nucleus (DAPI) and F-actin (phalloidin) for confocal imaging.
Mouse primary myoblasts cultivated on Matrigel-coated dishes exhibited striated myotubes at day 6 of culture (Figure 125) compared to none when plating C2C12 on dishes.

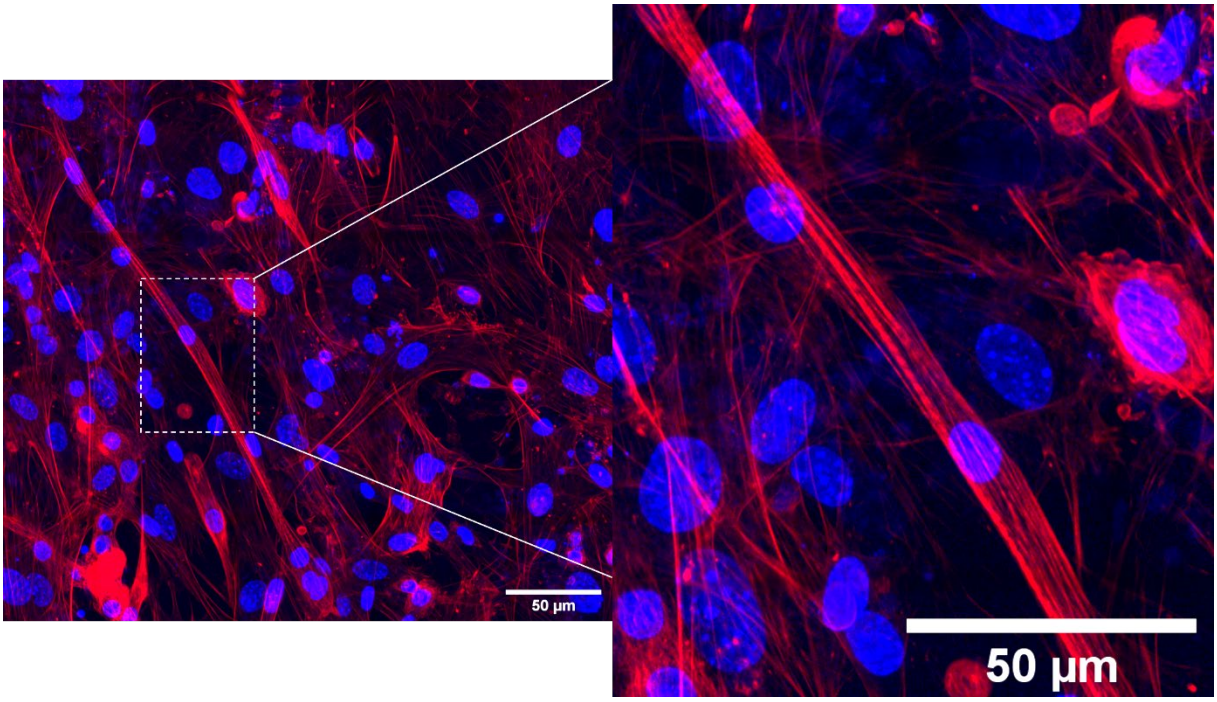

Figure 125: Confocal images of fixed mouse primary myoblasts at day 6 of culture on Matrigel-coated petri dish, stained for nucleus (DAPI, blue) and F-actin (phalloidin, red). Striated myotubes were observed with primary myoblasts (image on the right) where none was observed on dish with C2C12 myoblasts.

Interestingly primary myotubes exhibited spontaneous contractions at day 6 and day 10 of culture on phase contrast imaging, although being irregular. These results gave us evidence that frozen mouse primary myoblasts kept their differentiation potential.

The next step was to seed primary myoblasts inside collagen tubes within our system, using the optimized conditions discussed earlier thanks to the C2C12 myoblasts cell line. Handling primary myoblasts required more carefulness. Indeed, these are more fragile and sensitive cells than C2C12 cell line. We saw that the optimal experimental conditions were to seed myoblasts within 75 µm collagen tubes, without intercellular matrix. Therefore, two vials of primary myoblasts were thaw and pooled together in their growth medium, resulting in a concentration of 1.0×10^6 cells/ml. Cells were subsequently seeded inside 75 µm collagen tubes and cultivated for 3 days in growth medium (Figure 126). Controls were performed by plating primary myoblasts on matrigel-coated dish as previously described.

Concerning the seeding procedures, we usually had a lot more C2C12 to work with compared to primary myocytes, because it is intrinsically easier to cultivate C2C12 cell line. Another point is the cell diameter. Although not measured for the primary myoblasts, these cells seemed slightly smaller than C2C12 cells. Since the volume varies as $\sim r^3$, it grealty decreased the cell volume. Therefore, it usually took more time to entirely fill the collagen tube (Figure 126B).

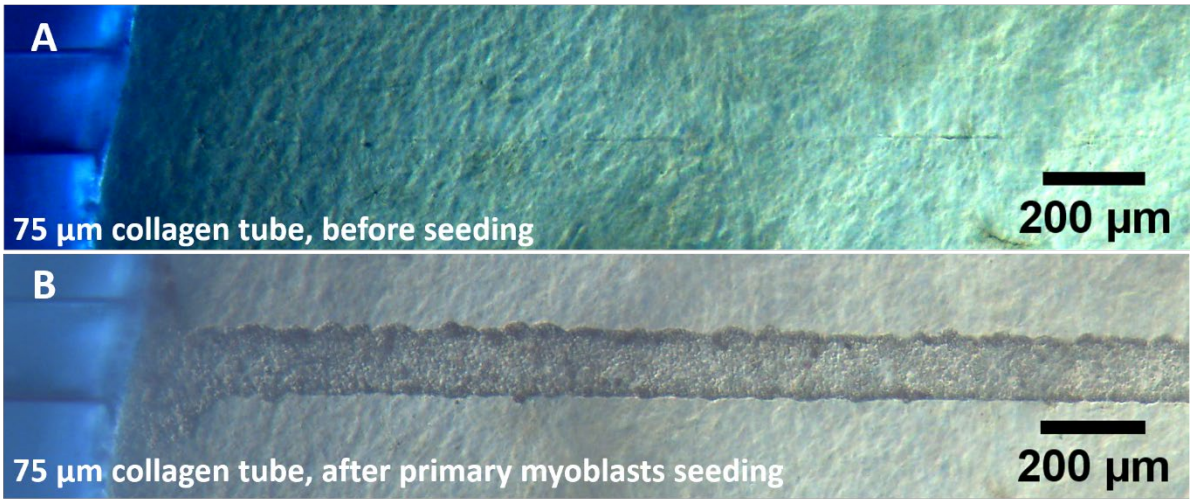

Figure 126: (A) 75 µm collagen tubes before seeding and (B) right after seeding with primary myoblasts, suspended in growth medium without intercellular matrix.

Nevertheless, the outcome was different compared to C2C12. Indeed, at day 3 of culture, primary myocytes still have not proliferated well on dish (

Figure 127).

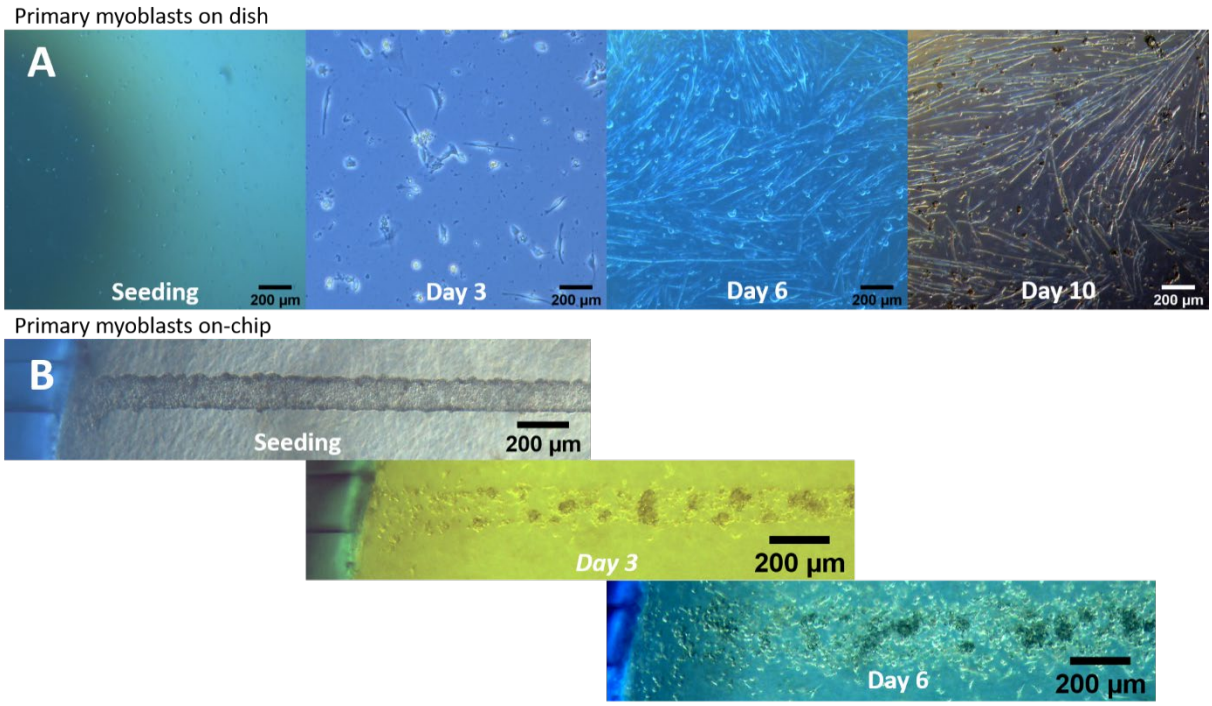

Figure 127: Primary myocytes cultivated (A) on Matrigel-coated dish and (B) on-chip without intercellular matrix, at day 3, day 6 (on-chip) and day 10 of culture.

On-chip, primary myocytes did not colonize the collagen tube. At day 6 (3 days in differentiation medium), cells proliferated and started to differentiate into myotubes on dish with visible spontaneous contractions, whereas primary myocytes had a spherical shape that probably reflected cell death. At day 10 of culture, primary myocytes still maintained spontaneous contraction, although we started to observe some cell blebs reflecting apoptosis and cel death.

These results can be explained by several hypothesis. Firstly, dishes where coated with Matrigel, giving cells extra adhesive molecules and growth factors. As we discussed, the optimal experimental condition was a seeding condition without ECM component. However, since primary myoblasts are obviously of different nature than C2C12 myoblasts, Matrigel is probably needed for their survival. Inded, primary myoblasts plated on non-coated dish did not survive (data not shown). Another options to be tested would be to coat collagen tubes with laminin, therefore partially mimicking adhesive molecules Matrigel brings.

The second hypothesis would be that primary myocytes cannot be stored for long term. At this point, I think it is important to highlight the particular context where those experiments on primary myoblasts were performed within. As we all know, there was a Covid-19 pandemic with several lock downs and restrictions for sanitary reasons. As a MD resident, I was helping in a covid19 unit at hospital for 3 months. Thus, primary myocytes were kept in -150°C for more than 6 months before fully re starting experiments. The delay between frozen vials arrival and experiments might be too long. Our collaborator also told us that there is no warranty about primary myocytes integrity after several months of storage. As a consequence of the Covid-19 pandemic, many manufacturers could not ship products. There was an important shortage of Matrigel that still remain right now (in February 2022).

That being said, next experiments we would like to do with primary myocytes are numerous. As discussed, suspending cells with Matrigel prior to seeding within collagen tubes should be considered. Different concentration of Matrigel should be assessed: 10% or 20 % v/v. Coating the inner surface of collagen tubes with laminin is also very interesting to investigate as an alternative to Matrigel-derived adhesive molecules, avoiding in-tube Matrigel polymerization, clogging and tube deformation.

There is also another point to consider when using primary myocytes. In previous experiments, cells were thaw and immediately seeded inside collagen tubes. We saw that cells did not proliferate well after 3 days of culture in growth medium, on dish (
Figure 127A). This behavior was also reflected in-tube with cells not colonizing the collagen tube. Therefore, plating the cells on Matrigel-coated dish first, as we do with flask and C2C12 cell line, would be an alternative. We would wait for a confluency of about 80% before detaching the cells with trypsin and seeding them inside collagen tubes without intercellular matrix.

In conclusion, primary myocytes were successfully cultivated after being frozen, stored for short term and thawed on Matrigel-coated dish. Cultures on-chip were only preliminary and need to be repeated as several experimental conditions have to be investigated.

1.7.2. Human induced pluripotent stem cells

I will only say a few words about human induced pluripotent stem cells (hiPSC) since our collaborators from Lisboa shipped us some vials, but we did not yet have the opportunity to

cultivate them. Indeed, they developed a protocol to differentiate hiPSC into myogenic progenitors, based on a previous work [157]. As we already discussed in the chapter 1, some other microdevices used human iPSC to successfully generate muscle-constructs.

Obviously, using human iPSC from healthy patients and from patients having myopathies will greatly improve the biomedical relevance of *in vitro* 3D skeletal muscle models. Being able to cultivate cells directly harvested from patients, within an *in vitro* relevant and controlled 3D microenvironment that recapitulates the functional unit of the organ, is the ultimate goal of organ-on-chip technologies. It will bring more potential to personalized medicine and to targeted therapies. Therefore, one major step of this project will be to work with these human iPSC.

CHAPTER 4: MUSCLE ON-CHIP CO CULTURES

Until now, we have focused on developing a skeletal muscle-on-chip using muscle cells exclusively. However, we have already mentioned that about many other cell types that regulate the skeletal muscle homeostasis: macrophages and fibroblasts during muscle regeneration, vessels that allow the inflammatory response to recruit leukocytes, motor neurons that send signals to the muscle. If we aim at recapitulating a skeletal muscle that is as much biomimetic as possible, we must consider this level of complexity in our system. Indeed, this has to be tackled methodically. We chose to focus on skeletal muscle on-chip co-cultures with two other cell types: endothelial cells and fibroblasts.

1. Skeletal muscle and blood vessels

1.1. Optimization of vessels-on-chip

1.1.1. Context

We collaborated with **Maria Carla Parrini**'s team, and especially with **Christine Lansche** (Institut Curie, U830 Cancer, Heterogeneity, Instability and Plasticity) to build a blood vessel on-chip, using our technology. Gene expression analysis were performed with the valuable support of Fabrice Soncin (CNRS UMI 2820 LIMMS/IIS). Briefly, our common work mainly focuses on cancer and the interplay between blood vessels, cancer cells, immune cells and fibroblasts. To develop such a vascularized tumor on-chip with Christine, we team-up first for the development of a blood vessel on-chip that will be compatible with our previously designed muscle on-chip platform. In that process, I also partnered with **Giacomo Gropplero** from our team. Finally, this device will also be used to study the lung cancer response to treatments and is therefore one of their interests. It really was a synergistic work, since my role was to engineer and micro fabricate the device for her to cultivate and characterize the vessel-on-chip. Then, that functional vessel-on-chip was transferred back for skeletal muscle co-cultures on-chip.

1.1.2. Cell models used

To mimic the lung micro environment, human primary microvascular endothelial cells from lung (HMVEC-L) were purchased from Lonza. On-chip vessels were generated using HMVEC-L with a maximum passage of 5. Cells were maintained on flask with endothelial cell growth medium at 37°C and 5% CO_2.

Optimizations of on-chip endothelial cells culture were performed using these microvascular cells. The optimal experimental conditions were then translated to co-cultures with skeletal muscle cells. For muscle on-chip co-cultures, human umbilical vascular endothelial cells (HUVEC) were used with a maximum passage of 5. These cells were maintained on flask with EGM2 medium.

1.1.3. Vessel-on-chip generation

Along with organ-on-chip technologies development these past decades, recapitulating vasculature on microfluidic chips has been attempted. Michna *et al.* reported a microfluidic platform to mimic the tumor microenvironment, using a 22G (700 µm) needles to generate collagen hollow tubes (Figure 128, [158]).

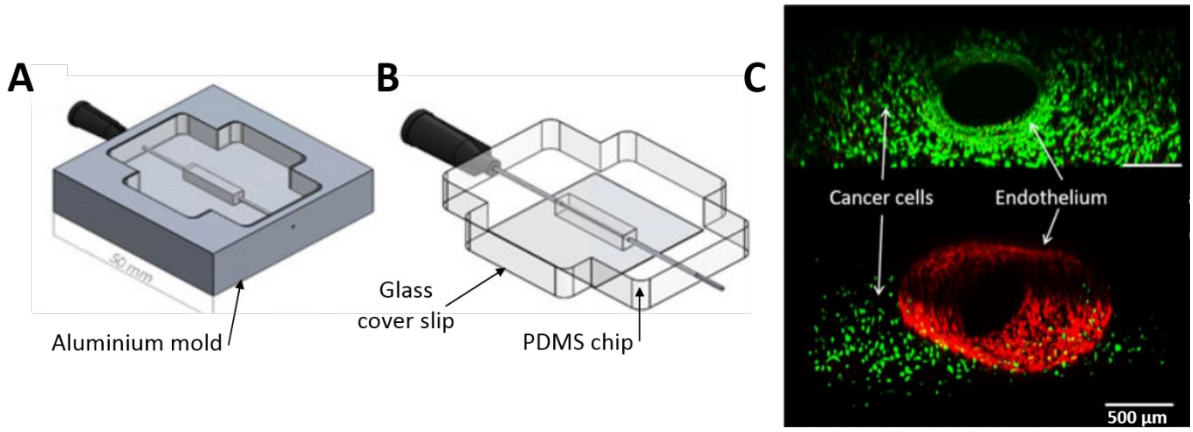

Figure 128: (A) Aluminum mold allowing the generation of (B) a PDMS chip for vessel-on-chip culture with a 22G (700 µm in diameter) needle. (C) co-culture of cancer cells with endothelial cells that organized in a lumen (red). From [158].

Using that device, they co-cultivated endothelial cell which had a lumen organization, with a breast cancer cell line. Generating a hollow tube made of a biocompatible hydrogel using needles have been used by other groups to develop vessel-on-chip [118], [159].
Photolithography has also been used for vessel-on-chip generation. Zervantonakis *et al.* developed a microfluidic chip with 2 lateral channels (cross-section: 500 µm × 120 µm), one seeded with endothelial cells and the other with cancer cells, the two channels communicating through a middle channel containing biocompatible hydrogel (Figure 129, [160]).

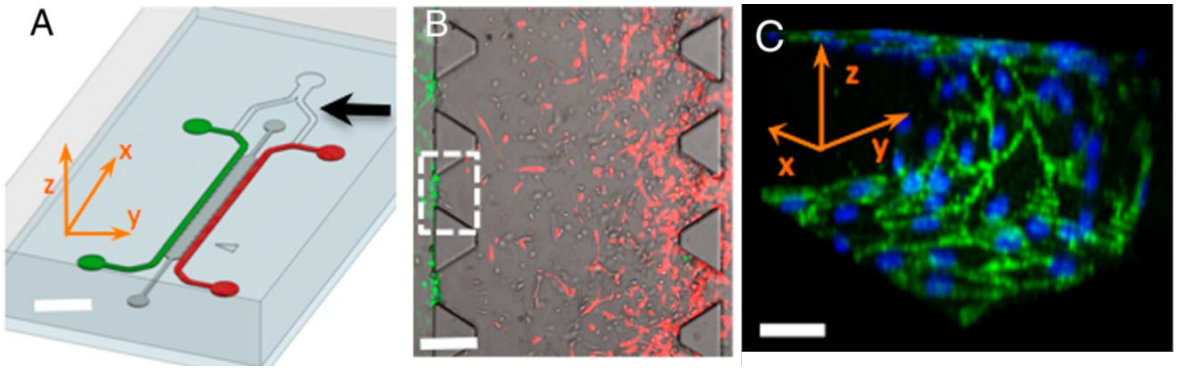

Figure 129: (A) Schematic of the PDMS chip, with a channel for endothelial cells (red) and another for cancer cells (green), communicating through (B) a middle channel containing a biocompatible hydrogel, thanks to PDMS pillars. (C) VE-cadherin and nuclei staining in the vessel channel. Note that endothelial cells sprout toward cancer cells (B). Scale bars are 2 mm for (A), 300 µm for (B) and 30 µm for (C).

Several other systems were developed using photolithography [161], [162] or 3D printing [163].

Pollet *et al.* published a recent review discussing about the different techniques used for *in vitro* vessel generation [164].

In our case, combining the MyoChip project requirements with our collaborator's one resulted in a common agreement on the device parameters: the geometry should be cylindrical hollow tubes, made of collagen I; the diameter should be 200 µm; the device should be easily connected to fluidic tubing, as well as imaged on microscope (particularly with the confocal microscope).

- **Vessel-on-chip micro fabrication**

The chip design used to set-up this next generation of vessel on chip progressively differed from the original MyoChip final design, the main difference being a completely sealed collagen chamber compared to the originally open one, and one unique collagen hollow tube (Figure 130). Briefly, a 200 µm diameter needle was inserted then 'sliding walls' were also inserted to isolate the central chamber, where 6.5 mg/ml type I collagen was injected through the collagen port. After collagen polymerization, the needles and the sliding walls were removed, generating 200 µm collagen hollow tubes. An inner surface coating of the collagen tubes with 10 µg/ml of human fibronectin in PBS was performed followed by 30 min of incubation at 37°C to promote endothelial cells adhesion. Collagen tubes were then washed several times with cell culture medium. After needles complete removal from the side holes, a drop of pre-polymerized PDMS was deposited to close these remaining holes. Hence, the fibronectin-coated collagen tube remained connected to only one input and one output.

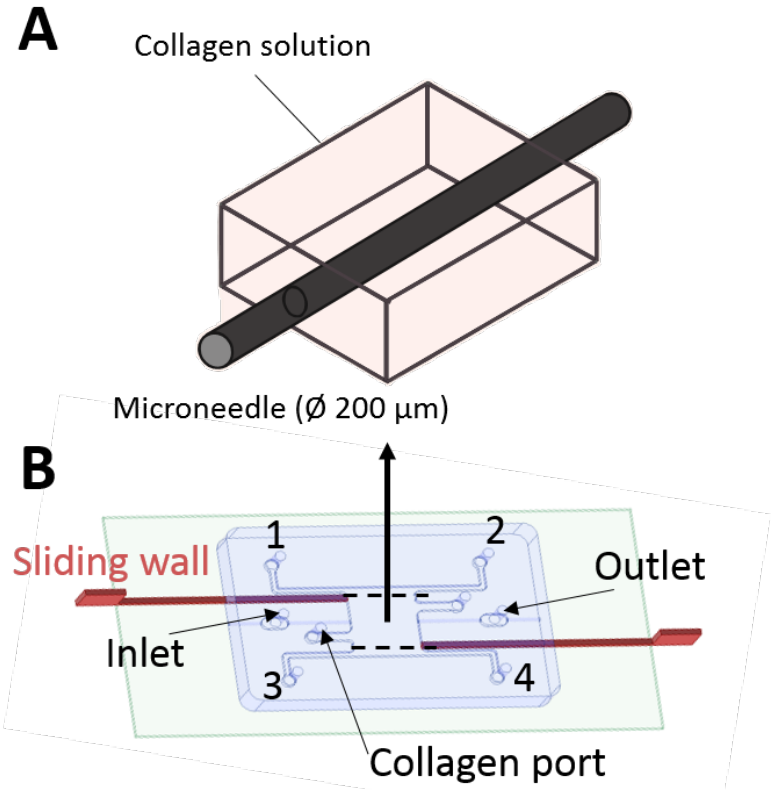

Figure 130: (A) Schematic of the collagen hollow tube generated using microneedles, zoomed from (B) the schematic of the PDMS chip. Sliding walls are inserted, then microneedle is inserted and collagen is injected through the collagen port. Once the collagen has polymerized, the microneedle and the sliding walls are removed. Ports 1 to 4 serve to inject solutions and generate a gradient across the collagen width.

- **Endothelial cells seeding**

HMVEC-L on flask were detached using trypsin, and suspended at a concentration of 10 × 10^6 cells/ml, in growth medium containing 70 kDa dextran at 4% (w/v). For cell seeding, Christine decided to use the micropipette. Indeed, microfluidics equipment and setup were not available in her laboratory at that moment. A total of about 40000 endothelial cells (25 µl of cells suspension) were seeded inside the collagen tube. Microdevices were then incubated up-side for 20 min, then down-side for another 20 min. This ensured cell adhesion to both top and bottom inner surface of the tube. Non-adherent cells were then carefully manually washed away with fresh medium. After an overnight incubation, a confluent cell monolayer formed at the inner surface of the collagen tube. Live/dead assay at day 2 of culture showed a monolayer of living cells with a lumen, forming a vessel construct (Figure 131).

- **Immunostaining**

One key feature of *in-vivo* endothelial cells is the presence of adherent junctions and tight-junctions with specifically associated proteins such as VE-cadherin or ZO-1. Their presence was therefore a good marker to assess the *in vitro* vessels morphology. Immunostaining were performed for VE-cadherin and nuclei. Images were captured using a confocal laser scanning microscope, mounted with a 40× water immersion objective or a 10× air objective VE-cadherin was localized as expected at the cell-cell junctions, bringing the evidence of a confluent endothelium (Figure 132).

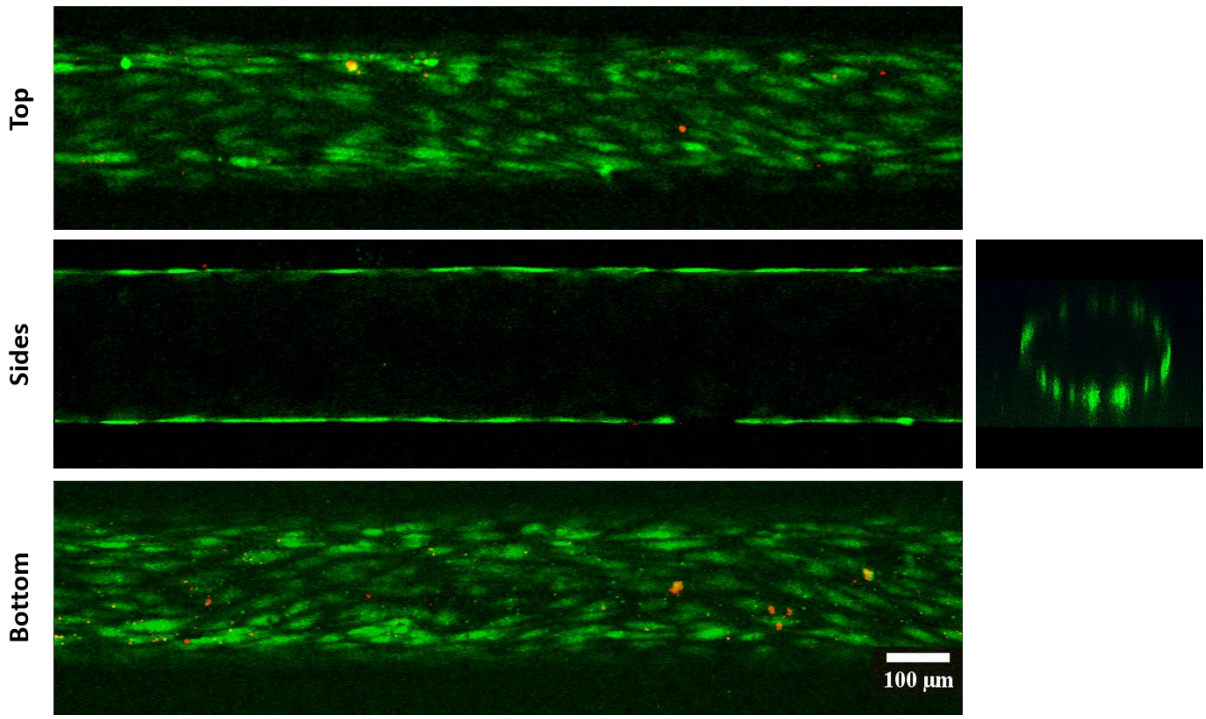

Figure 131: Live/Dead assay of the vessel-construct at day 2 of cultures, using HMVEC-L, showing mostly living cells in a confluent monolayer at the inner surface of the 200µm collagen tubes, with the cross-section image on the right.

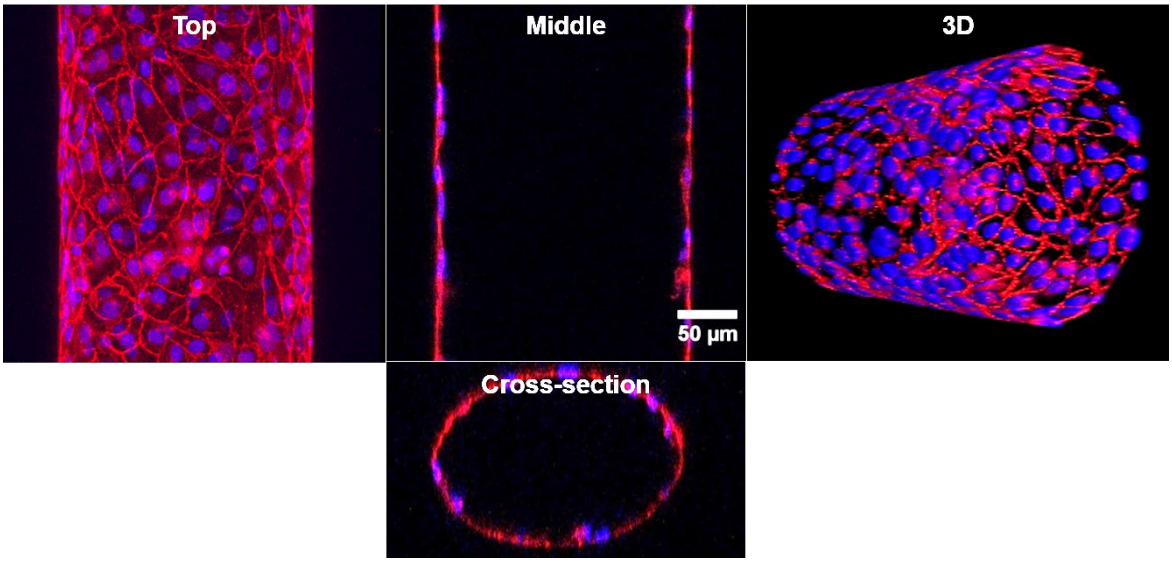

Figure 132: Confocal images of fixed on-chip vessel-construct at day 2 of culture, immuno-stained for adherent junction protein VE-cadherin (red) and for nuclei (blue). Note the confluent monolayer of cells covering the whole inner surface of the collagen tube.

1.1.4. Functionality assays

- **Permeability assay**

A key feature of a vessel is its barrier function, compartmentalizing vasculature and tissues. The barrier function of the vessel on-chip was assessed with permeability assays, which were performed by flowing FITC-Dextran 70 kDa inside the vessel-construct, after 2 days of culture.

The microdevice was mounted on an inverted wide-field fluorescence video microscope within a built-in incubation chamber at 37°C with 5% CO_2. Fluid controls were implemented using a pressure controller connected to a flow-rate sensor.

The flow rate was chosen according the wall shear stress τ_{wss} exerted on the surface of the endothelium. τ_{wss} is the frictional force arising from blood flow, parallel to the vessel lumen surface, in comparison to the blood pressure which is a perpendicular force.

Indeed, τ_{wss} depends on the vasculature diameter, but typical has been reported to be 0.4 Pa on average for the microvasculature, and can be lower in a tumoral microvascular environment [165], [166]. The wall shear stress in a cylindrical channel is described by the equation (1) [165]:

$$\tau_{wss} = \frac{4\mu Q}{\pi r^3} \quad (1)$$

μ is the fluid viscosity, Q is the flow rate and r is the radius of the channel. Therefore, a wall shear stress of 0.1 Pa has been chosen to mimic tumoral environment, resulting in a flow rate of 6.7 µL/min.

The permeability coefficient describes the ability of a solute to escape uniformly from the vascular lumen [167]. Vessel-on-chip apparent permeability P_{app} was measured as previously described in the literature [165], [167] based on the equation (2) below:

$$P_{app} = \frac{1}{I_1 - I_b}\left(\frac{dI}{dt}\right)\frac{r}{2} \quad (2)$$

I_b is the average background fluorescence intensity prior to FITC-dextran perfusion, I_1 is the average fluorescence intensity within the selected area of measurement, encompassing the whole collagen bulk with the vessel-construct, after flowing FITC-dextran at the end of the experiment. As the FITC-dextran flowed through the system, the average fluorescence intensity increased and reached a plateau after 5 min. Therefore, the variation of the fluorescence intensity through time $\frac{dI}{dt}$ was the slope of the linear fitting during those initial 5 min.

Compared to an acellular collagen tube, we not only observed that the barrier function was indeed functional in the presence of endothelial cells (Figure 133A, B and D), but was enhanced under continuous flow condition (Figure 133C and D). Indeed, mean permeability values were at 1.4×10^{-5}, 4.5×10^{-6} and 1.1×10^{-6} cm/s at day 2 of culture for acellular collagen tube, vessel-construct under static and continuous flow conditions respectively. Values were similar for day 6 of culture for acellular collagen tube and vessel-construct under static condition.

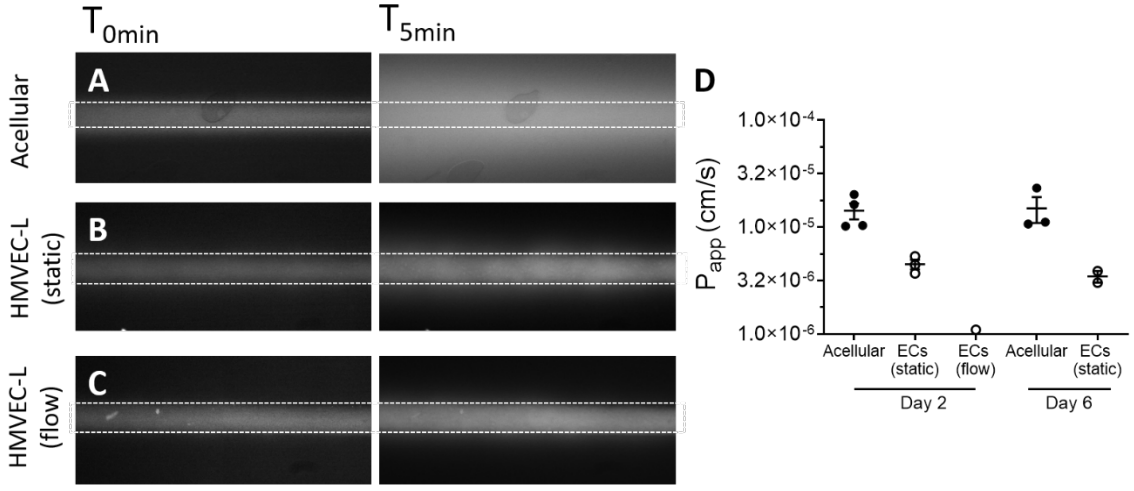

Figure 133: Vessel-on-chip fluorescent images after injecting 70kDa FITC-Dextran at 0 min (left) and at 5 min (right) (A) without cells (B) with HMVEC-L under static condition and (C) under continuous flowing condition at 6.7 µL/min (D). Measured apparent permeability for each condition at day 2 and day 6 of culture, showing a barrier function when cells are present, that is enhanced under continuous flowing condition.

In the literature, permeability in acellular collagen tube has been reported to be around 5.0×10^{-5} to 1.5×10^{-5} cm/s in collagen tubes for 20 kDa and 150 kDa dextran respectively [168]. When seeding HUVEC inside collagen tubes, enhanced barrier function has been reported, with lower permeability values ranging from 1.5×10^{-6} to 6×10^{-6} cm/s at day 2 of culture. Several studies have reported an enhanced vascular barrier with the presence of cells, under continuous flow with permeability values around 1.0×10^{-6} cm/s [169], [170].

Although our permeability values were similar, it is worth noticing that the way of implementing flow can differ. Some authors used a rocker plate that generated flow in alternative direction [168], [169] while others used a syringe pump [159]. Interestingly, applying unidirectional flow via the syringe pump promoted better cell alignment and higher stress fiber count, resulting in a better vascular barrier function compared to the rocker [159]. Indeed, back and forth flow generates alternative wall shear stress and has been reported to be part of endothelial cells dysfunction [171]. In our case, using a pressure pump controller allowed us to generate a unidirectional flow with a tunable wall shear stress. Moreover, this method will allow us to implement pulsatile flow

afterwards by oscillating the pressure, albeit not having investigated it yet.

Several articles and excellent reviews on the impact of flow and shear stress on vascular endothelium pathophysiology leaned towards the same direction: disturbed flow and low or alternative shear stress are associated with endothelium dysfunction whereas laminar flow and high shear stress are protective [171]–[173]. Without going into details, *in vitro* studies showed that cultured endothelial cells exposed to disturbed flow and low and alternative shear stress exhibited very different behavior in terms of molecular signaling, gene expression, structure and function compared to laminar flow with relatively higher shear stress (~20 folds) [171]. These results, which were in good agreement with *in vivo* studies and observations, conclude that alternative flow and low shear stress lead to inflammation and endothelium activation, resulting in higher white blood cells adhesion.

- **Endothelium activation**

Physiologically, the endothelium at a resting state should not promote white blood cell adhesion. However, the endothelium should get activated in response to inflammatory cues such as TNF-α or IL-8 secreted whenever there are lesions such as wounds or infections. Activated endothelium exhibits an upregulation in adhesion molecules such as ICAM-1, VCAM-1 and E-selectin that mediate the recruitment of white blood cells on the endothelium surface [172].
To investigate the capacity of our vessel-on-chip to be activated upon inflammatory cues, treatment with TNF-α at 100 ng/ml for 4 hours were performed and fluorescently labeled Jurkat T-cells as white blood cells model were injected inside at a concentration of 1.0×10^6 cells/ml. The injection flow rate was set at 6.7 µl/min resulting in a τ_{WSS} of 0.1 Pa.

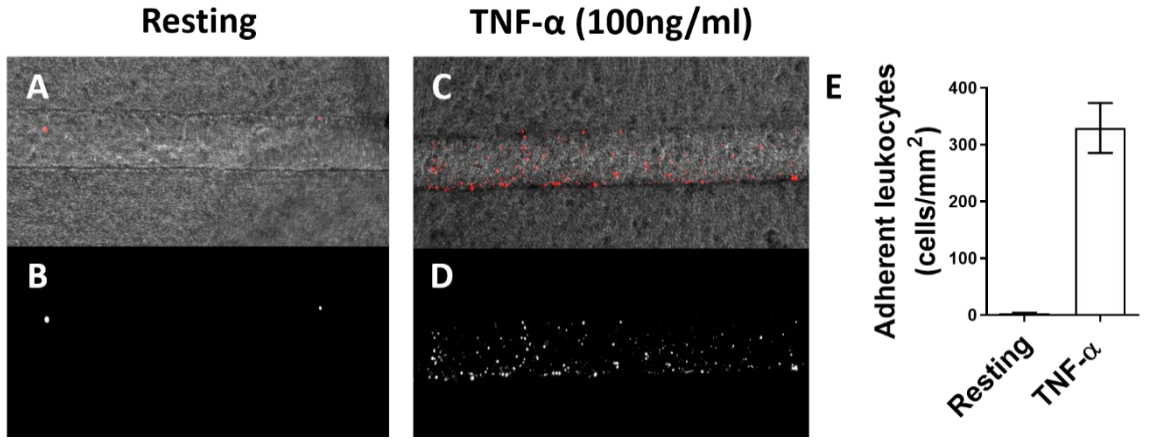

Figure 134: Leukocytes adhesion assay on resting (A, B) or TNF-α treated (C, D) vessel-constructs. (A) and (C) shows video microscopy images with the vessel-construct overlaid with fluorescently labelled leukocytes. (B) and (D) only shows fluorescently labeled leukocytes. (E) Leukocytes adhesion count.

Compared with resting vessel-constructs (Figure 134A and B), TNF-α treated ones exhibited higher leukocytes adhesion (Figure 134C and D). Indeed, the presence of inflammatory cue resulted in significantly higher adherent leukocytes (373 ±285 /mm²) compared to the resting state (4 ±1 /mm²) (Figure 134E).

Finally, to assess the vessel-construct activation, we extracted endothelial cells from the system and performed a RT-qPCR to analyze the expression of genes coding for inflammatory-dependent

adhesive molecule (ICAM-1, VCAM-1 and E-selectin). Gene expression was normalized by β2-microglobulin housekeeping gene, then compared to the condition without TNF-α, using the $2^{-\Delta\Delta Ct}$ method. This process resulted in a relative quantification (RQ). Upon inflammatory cue mimicked by the TNF-α treatment, the significant upregulation of those genes brought evidences of endothelium activation (Figure 135). An upregulation of 7.87 ±3, 18.65 ±10 and 133.99 ±77 fold was observed for ICAM-1, VCAM-1 and E-selectin.

- **Conclusion**

Using a similar device and approach than the one developed for muscle-on-chip, we managed to build a 200µm diameter perfusable vessel-on-chip that exhibited an efficient barrier function, and the ability to activate itself upon inflammatory cues, recruiting leukocytes at the surface of the lumen. This vessel-on-chip building block achievement brought us closer to the multi-cellular skeletal muscle-on-chip we wanted to build.

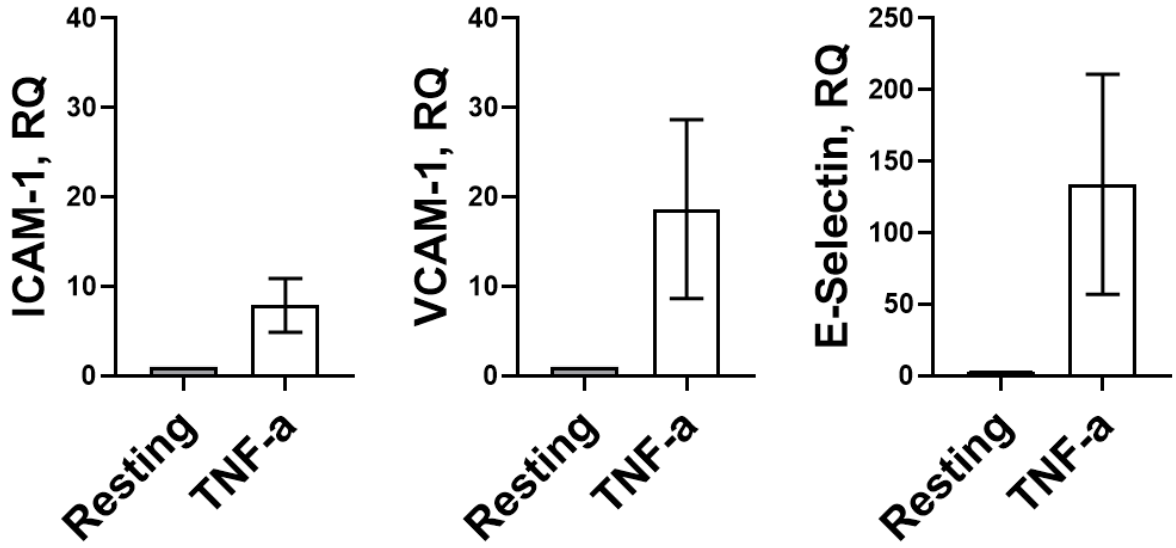

Figure 135: RT-qPCR results for ICAM-1, VCAM-1 and E-selectin obtained on endothelial cells extracted from the microdevice. The results are displayed in relative quantification (RQ), normalized to β-2 microglobulin.

1.2. On-chip co-culture of skeletal muscle cells with endothelial cells

- **Experimental conditions**

To perform the on-chip co-culture of endothelial and muscle cells, we decided to use HUVEC to vascularize our skeletal muscle-on-chip model, as it is an easier to manipulate. Microdevices with three parallel collagen tubes of 75 µm each were generated with tungsten wires, to match the skeletal muscle optimal experimental conditions. First, C2C12 myoblasts were seeded in the lateral collagen tubes as previously described. They were cultivated for 3 days in proliferation medium, then in differentiation medium for only one day until day 4 of culture. The central collagen tube was then coated with fibronectin prior to HUVEC seeding (C = 5×10^6 cells/ml). The co culture system of skeletal muscle cells and endothelial cells was kept in EGM-2 medium only. Considering that EGM-2 is a low-serum culture medium, using it as a myoblast differentiation medium seemed relevant. Culture medium was changed every 2 days until day 10 of culture, where time points

matched day 10 and day 6 of culture for C2C12 myoblasts and HUVEC respectively. Live/dead assays were performed at the midpoint of the experiment (day 5 of culture). On-chip co cultures were then fixed with 4% PFA for confocal imaging at day 10 of culture.

- **Live dead assessment**

The vessel-construct located in the central collagen tube, co-cultivated with two muscle-constructs on each of the lateral collagen tubes, exhibited a lumen and an estimated survival rate of 57 ±18% at day 5 of culture (Figure 136). When looking at the muscle-construct side, we observed a low survival rate at 25 ±13% for myoblasts in the co-culture set-up (Figure 137).

The actual relatively high cell death in the vessel-construct can be explained by the high mortality in the muscle-construct compartment. Indeed, one hypothesis is that myoblasts did not grow well in EGM-2 endothelial cells medium.

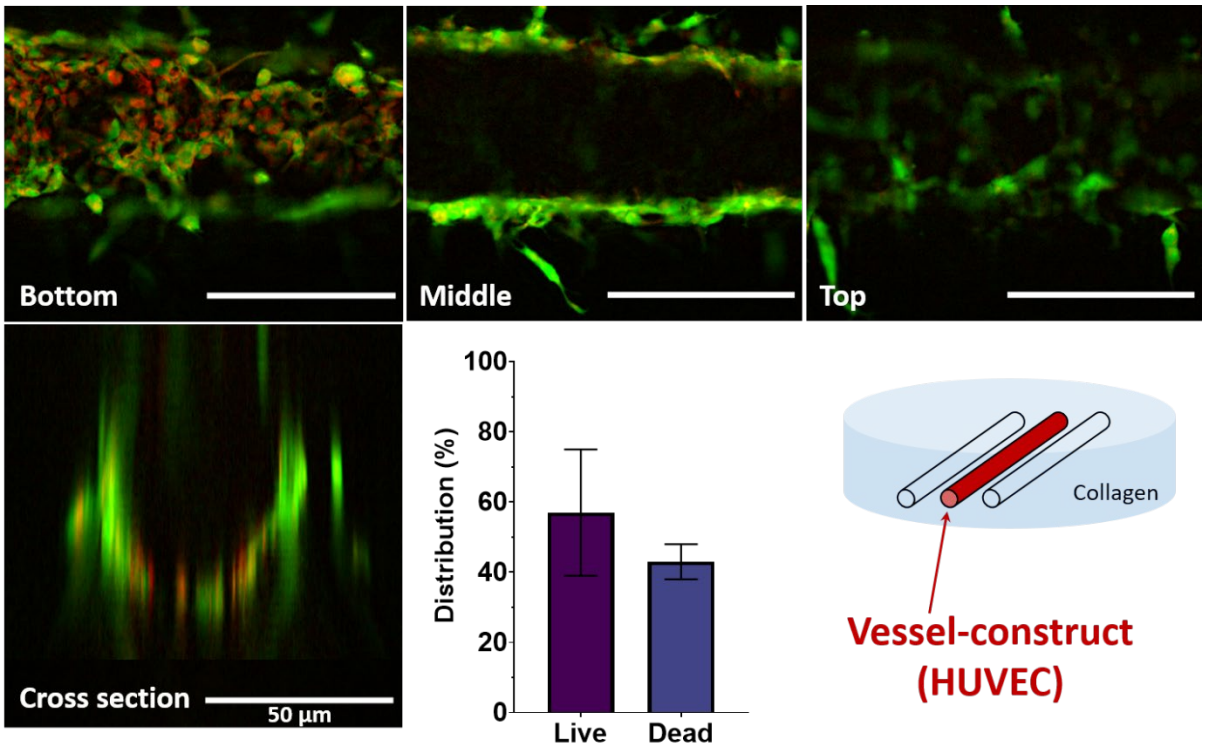

Figure 136: Live/dead assays for the vessel-construct using HUVEC located in the central collagen tube, in a C2C12-HUVEC co-culture set-up, at day 5 of culture. Scale bars are 50 µm.

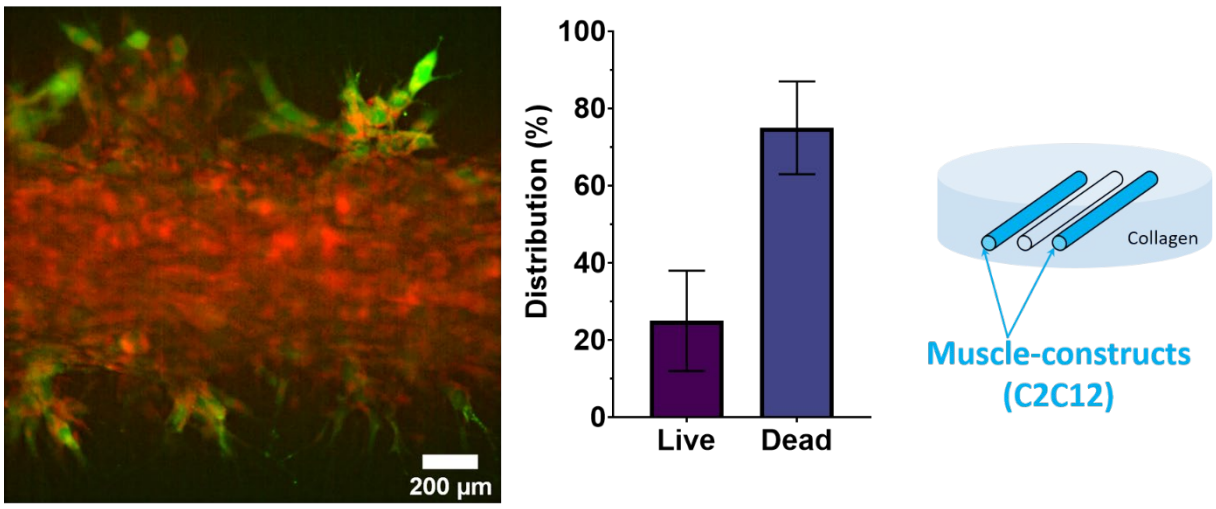

Figure 137: Live/dead assay for the muscle-constructs located in the lateral collagen tubes, in a C2C12-HUVEC co-culture set up, at day 5 of culture.

Myoblasts may therefore undergo cell death by necrosis, releasing their cytoplasmic content in the medium that will negatively act on endothelial cells. Confocal imaging of F-actin staining from muscle-constructs at day 10 of culture brought more evidences toward this hypothesis. Indeed, compared to a muscle-construct generated previously in myoblast differentiation medium, the muscle-construct here exhibited a very different morphology (Figure 138A and B).

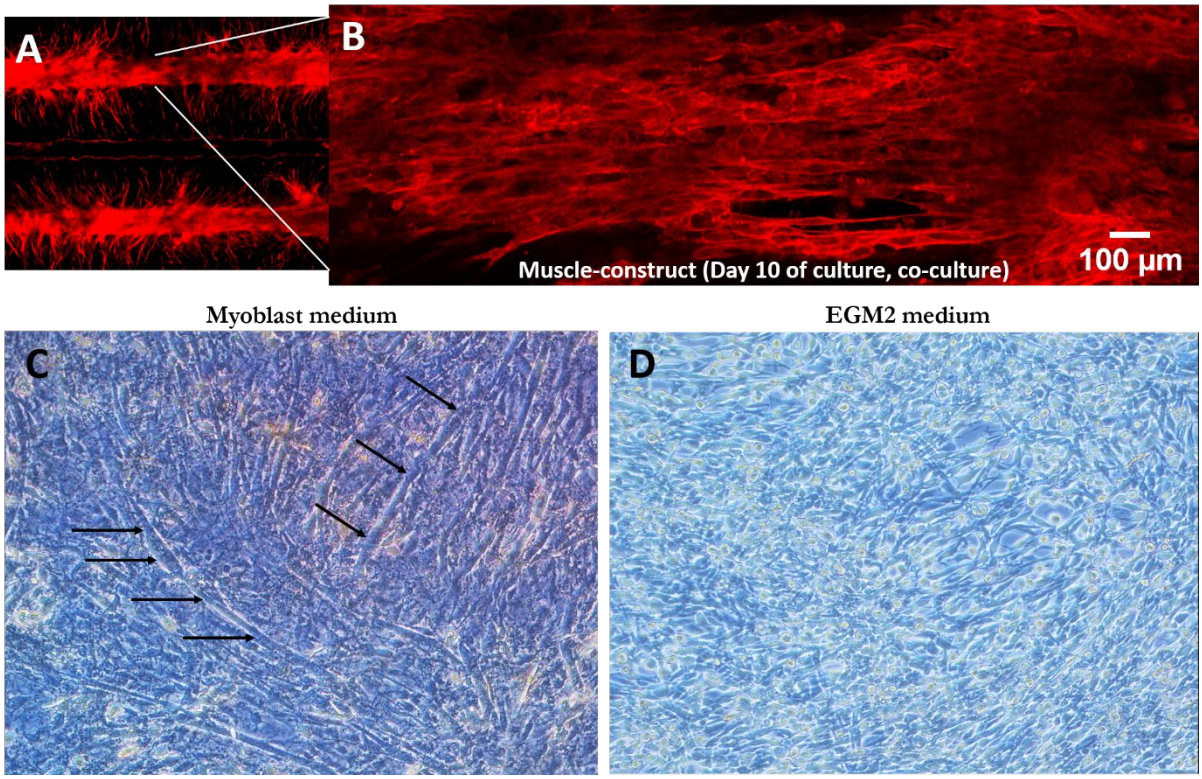

Figure 138: (A) Confocal images of the muscle-construct in the C2C12-HUVEC co-culture set-up for F-actin staining at day 10 of culture. (B) Close-up view of the muscle-construct. C2C12 myoblasts cultivated, from confluency, in (C) myoblast differentiation medium or in (D) EGM2 medium for 7 days. C2C12 in myoblast differentiation medium resulted in clearly visible and more myotubes (dark arrows) compared to EGM2 medium.

- **Media incompatibility**

To investigate this hypothesis, C2C12 myoblasts were cultivated on dishes with proliferation medium until confluency, then the cell culture was split in two: one with myoblast differentiation medium and one with EGM2 medium. Cells were cultivated for 7 days. Compared to EGM2 medium, C2C12 cultivated in myoblast differentiation medium resulted in clearly visible myotubes (Figure 138C and D).

A less efficient growth of skeletal muscle cells in endothelial medium has indeed been reported. Human myoblasts cultivated on dish in EGM2 medium contained significantly lower number of nuclei per myotubes, along with a decrease of diameter compared to the skeletal muscle specific medium [174]. However, the authors reported a success to obtain aligned myotubes, although not describing any sarcomeric striation nor myosin heavy chain expression.
On-chip co-cultures of C2C12 and HUVEC that has been reported from Kamm's team also mentioned this medium incompatibility [118]. To overcome this, they first differentiated the muscle-construct in myoblast differentiation medium for 7 days, before generating the vessel-construct and switching to EGM2 medium, until day 14 of culture.

Within the MyoChip consortium, our collaborators from Gomes's lab (IMM, Lisboa) and especially **Katharina Hennig**, also investigated this issue of co-culture media incompatibility. Different ratios of mixed media were assessed (Endothelium medium/Myoblast medium at ratios 1:0, 1:1, 1:2, 1:3, and 1:4) on monocultures and on co-cultures. While the results were not binary, they observed interesting results. Mixing both media at 1:1 ratio resulted in non-functional myotubes as assessed with calcium signaling assays (data not shown). HUVEC cultivated in whatever media ratios resulted in a significantly lower mean migration speed compared to endothelial medium only. In contrast, primary mouse myoblasts cultivated in a ratio of 1:4 did not differ in mean migration speed, and exhibited contractile myotubes. Hence, the optimal ratio for HUVEC and primary mouse myoblasts for co-culture appeared to be 1 volume of endothelial medium for 4 volumes of muscle medium. Further experiments with such conditions have to be performed to improve the endothelial cells/myoblasts co-culture on-chip.

- **Vessel-construct immunostaining**

Finally, to assess how confluent was this vessel-on-chip in co-culture conditions, ZO-1 immunostaining of tight junctions was performed at day 10 of culture. We observed that ZO-1 staining was present (Figure 139A) but its location was diffuse and irregular (Figure 139B and C). These results are in good agreement with the relatively low survival rate of the endothelial cells observed in co-culture conditions.

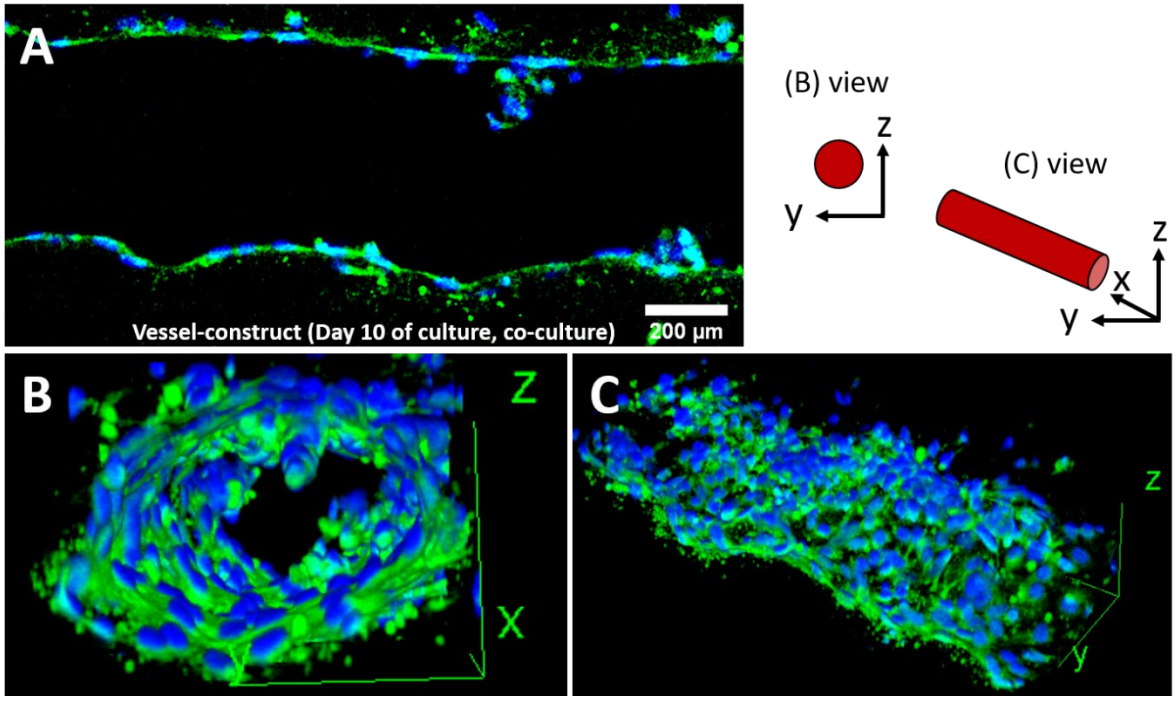

Figure 139: Confocal images of the vessel-construct in the C2C12-HUVEC co-culture set up, for ZO-1 immunostaining (green) and nuclei (blue) at day 10 of culture. (A) A Longitudinal section of the vessel showing the lumen. (B) and (C) are 3D views of the vessel-construct, showing a diffuse and irregular ZO-1 staining.

Conclusion. Obviously, on-chip co-cultures experiments have to be repeated since the co-culture uncovered many other challenges to tackle. Different seeding approaches should also be investigated. As previously seen, first differentiating the muscle-construct toward an advanced state prior to generating the vessel-construct could be an option if we do not mix the different media. With the capacity to perfuse the system, an alternative could be to immerse the microdevice in muscle medium while perfusing endothelial medium within the vessel-construct. As we previously mentioned, this method will not only allow the endothelium to mature further under flow, but also to be cultivated with the right medium.

2. On-chip skeletal muscle and fibroblasts co-culture

The other cell type we focused on for muscle co-cultures was the fibroblasts. Indeed, fibroblasts regulate skeletal muscle homeostasis, by remodeling the ECM and bringing the proper scaffold for muscle growth and regeneration.

2.1. Embedding fibroblasts into the collagen matrix

As we discussed in the chapter 1, *in vivo* fibroblasts are located in the ECM and are important for skeletal muscle homeostasis. For myoblast-fibroblast co cultures, we generated 6 mg/ml collagen tubes wherein NIH 3T3 fibroblasts were encapsulated at different concentrations. Data on *in vivo* fibroblasts concentration in healthy skeletal muscle is scarce. One study reported a fibroblast density of 26 cells/mm² of muscle tissue from human biopsies [175]. On the biopsy sections, it clearly appears that myofibers occupies the vast majority of the area (about 87 % of the total surface, Figure 140).

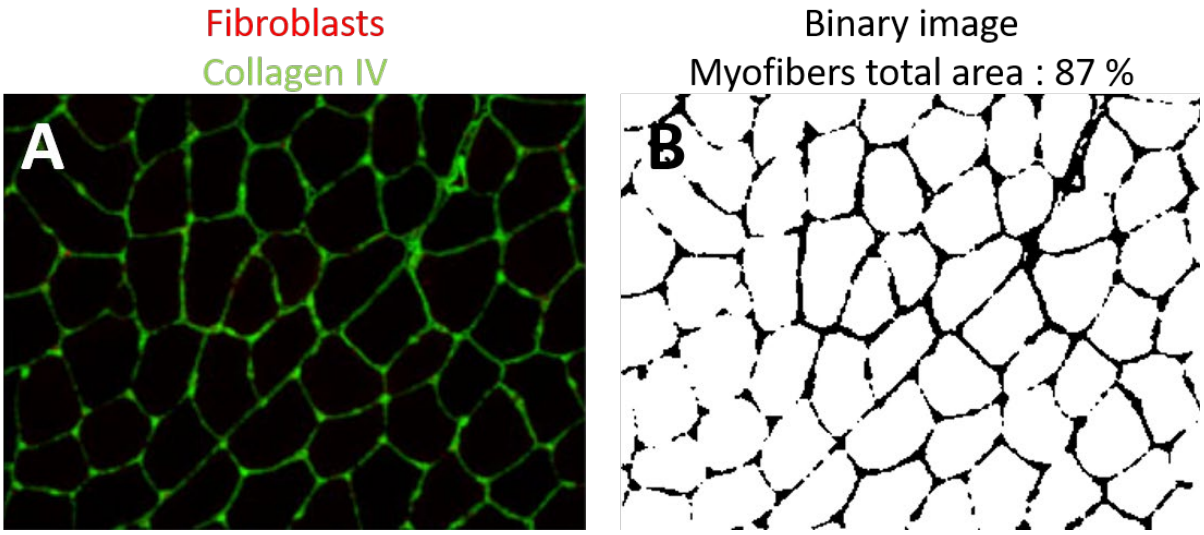

Figure 140: (A) Human skeletal muscle biopsy cross section stained for collagen IV in green and fibroblast in red. Fibroblasts are exclusively located in the ECM. (B) Same image in binary mode, showing myofibers (white areas) occupying 87% of the total area. Adapted from [175].

However, in the skeletal muscle section, fibroblasts are only localized in the ECM. Therefore, as fibroblasts density is 26 cells/mm² of muscle total section and the ECM occupies 13% of this section area, fibroblasts density should be estimated at 200 fibroblasts/mm² of ECM. The authors reported a section width of 10 µm, resulting in an estimated fibroblasts concentration of 20×10^6 cells/ml of ECM.

Therefore, we encapsulated fibroblasts within the collagen by investigating a wide range of initial concentrations: 30×10^6 cells/ml, 7.5×10^5 cells/ml and 3.0×10^5 cells/ml. Compared to high or low concentrations, an encapsulation concentration of 7.5×10^5 cells/ml resulted in a higher cell survival rate through time (Figure 141). For high and low concentrations, fibroblasts death rate was high (data not shown).

Confocal images of on-chip PFA fixed co-culture stained for nucleus and F-actin also showed that fibroblasts spread within the whole collagen volume in 3D with no cell sedimentation (Figure 142).

Subsequent myoblasts and fibroblasts co-cultures were thus performed by encapsulating fibroblasts into 6 mg/ml collagen at 7.5×10^5 cells/ml.

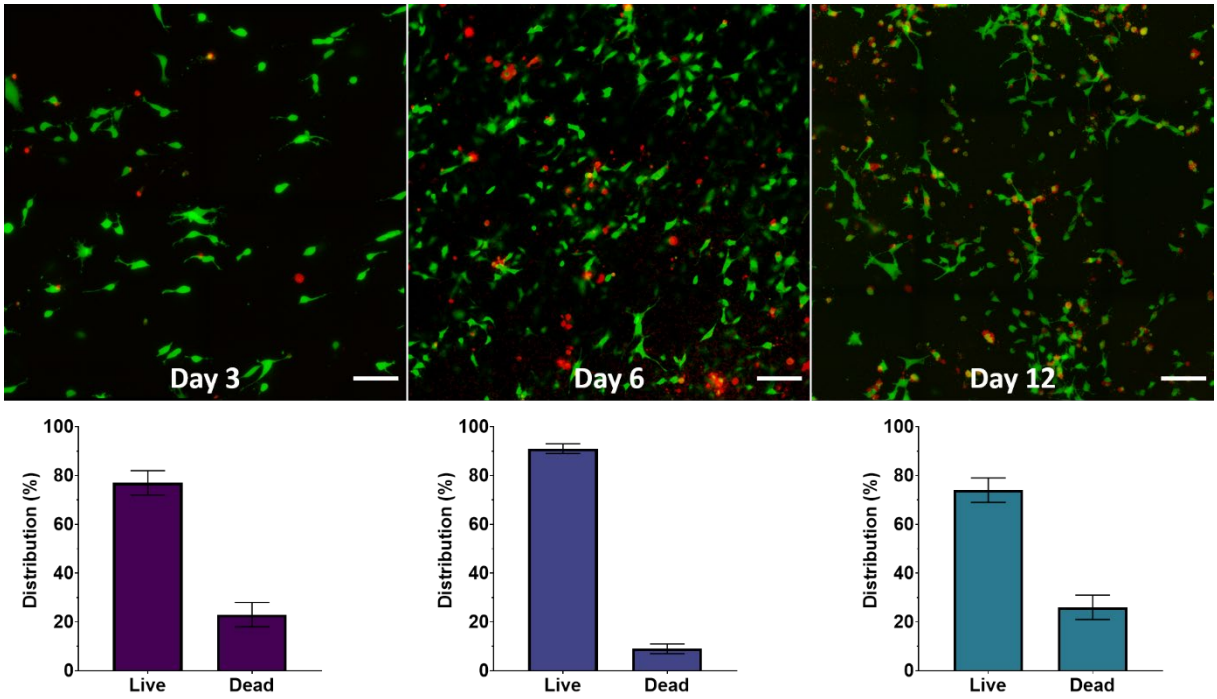

Figure 141: Live/dead assay for NIH 3T3 fibroblasts at a concentration of 7.5×10^5 cells/ml encapsulated in the 6 mg/ml collagen prior to generating collagen tubes, at different days of culture (n = 8 for each time point). Scale bar: 100 µm.

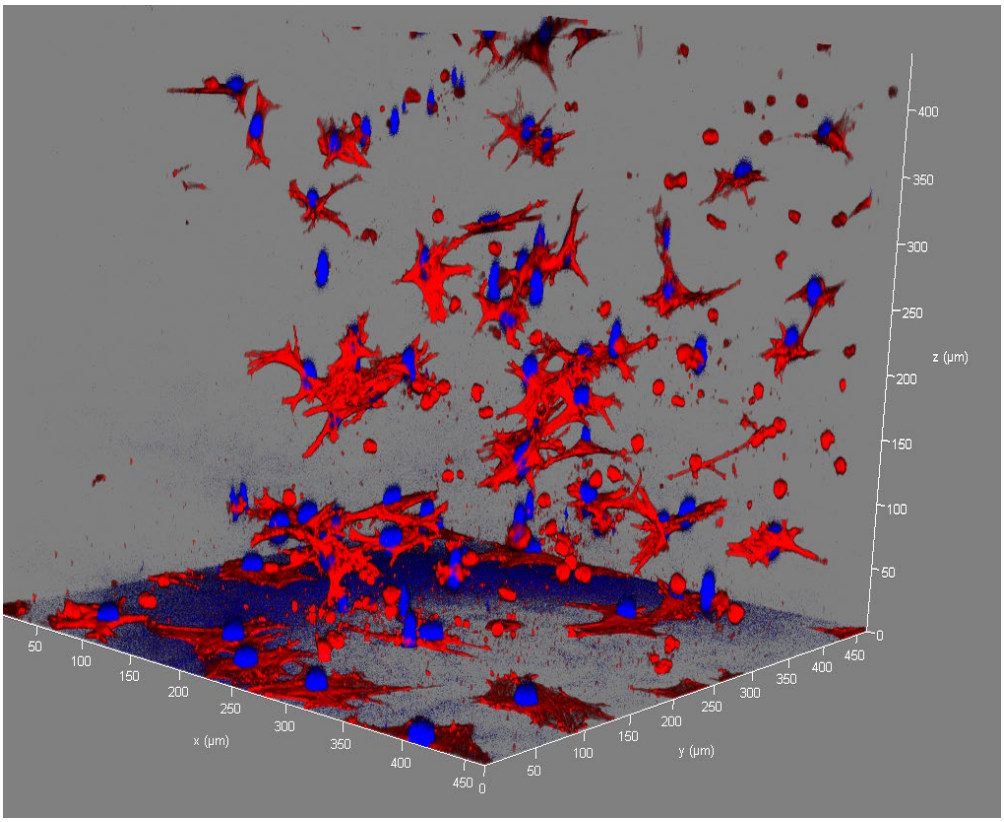

Figure 142: Confocal images of NIH 3T3 fibroblasts encapsulated in 6 mg/ml collagen stained for F-actin (red) and nucleus (blue), co-cultivated on-chip with C2C12 myoblasts at day 10 of culture. At z=0 µm, the cells spread on the glass cover slip sealing the bottom of the microdevice.

2.1. Crosstalk between muscles cells and fibroblasts

2.1.1. Myotubes maturation analysis in myoblasts/fibroblasts co-culture condition

Fibroblasts were cultivated within passages P7 and P10 for our experiments in the same growth medium as for the myoblasts. The different time points of this co-culture experiment were as follow: fibroblasts encapsulation at day 0, myoblasts seeding at day 3 of culture, switching to differentiation medium at day 6 until day 10 of culture.

At the end of the experiment (day 10), fibroblasts were cultivated for 10 days (3 days in growth medium, 7 days in differentiation medium) whereas myoblasts were cultivated for 6 days (3 days in growth medium and 3 days in differentiation medium. On-chip co-cultures were fixed at day 6 and day 10 of culture, then imaged on confocal microscope.

In these co-culture conditions, aligned myotubes, which we defined as myotubes oriented within [-10°, 10°] toward the collagen tube axis, significantly increased over time in parallel with the orientation coherency, which reflects at which degree the myotubes are aligned together (Figure 143A and C). In the same time, perpendicular myotubes, defined as myotubes oriented within [-90°, -50°] and [50°, 90°] with respect to the collagen tube axis, decreased with time, as observed previously for mono-culture experiments (Figure 143B). Myotubes diameter, length and fusion indicator did not differ through time (Figure 143D-F). At day 10, the nuclei inter distance reached an average of 18.6 ±0.6 µm globally, and was significantly higher when specifically analyzing nuclei within myotubes with an average value of 27.1 ±11.6 µm.

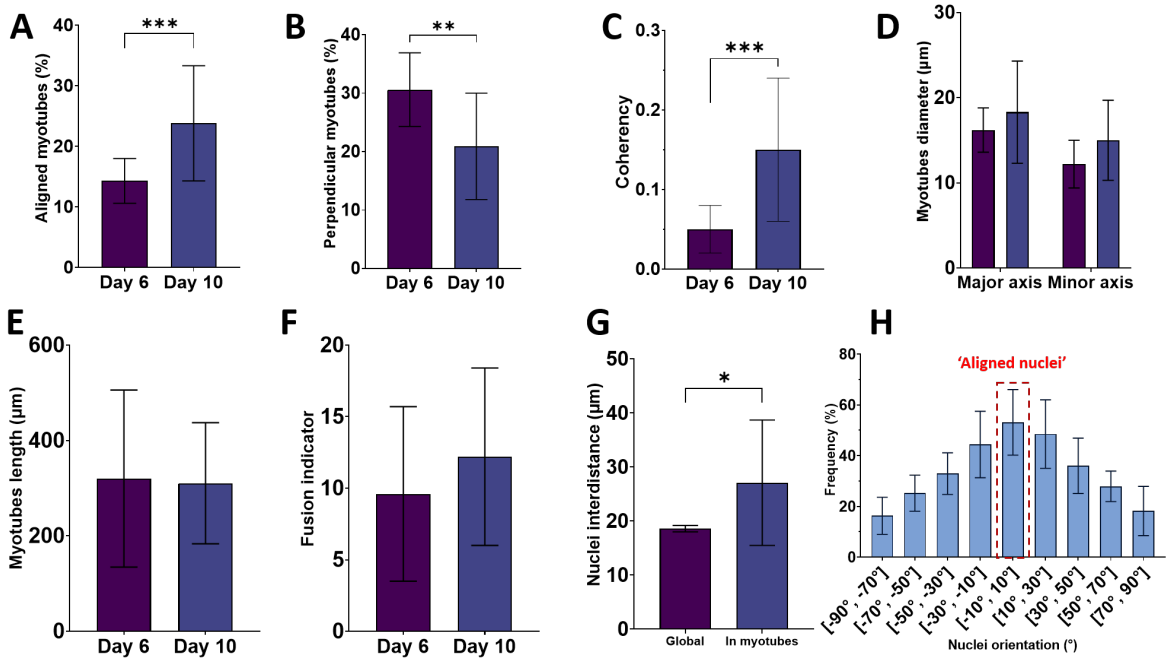

Figure 143: Myotubes analysis in fibroblast-myoblasts co-culture set-up. (A) Aligned myotubes oriented within [-10°, 10°] toward the long axis of the collagen tube. (B) Perpendicular myotubes oriented [-90°, -50°] and [50°, 90°] with respect to the collagen tube axis. (C) Myotubes orientation coherency. Myotubes diameter (D), length (E) and fusion indicator (F). (G) 3D nuclei inter distance when analyzing all the nuclei globally within the muscle-construct, or by specifically analyzing the nuclei within myotubes. (H) 3D nuclei orientation distribution, with the highlighted 'aligned nuclei' defined as the nuclei oriented parallel to the aligned myotubes. For (A), (B) and (C), n = 17 and 14 for day 6 and day 10 respectively. For (D) to (F), n = 10 and 16 for day 6 and day 10 respectively. For (G) and (H), n = 11 'global' nuclei analysis, and n = 8 for 'in myotubes' specific analysis.

Compared to myotubes in mono-culture using the previously optimized conditions (75 µm collagen tubes, seeding C2C12 without ECM components), aligned myotubes and orientation coherency were significantly lower in the co-culture set up at day 10 of culture (Figure 144A-B). Interestingly, myotubes (*i.e.* diameter, length, fusion indicator, aligned nuclei globally and within myotubes) in a co-culture set-up did not differ in any of the other maturation parameter compared to myotubes generated in a mono culture set-up (Figure 144C-G).

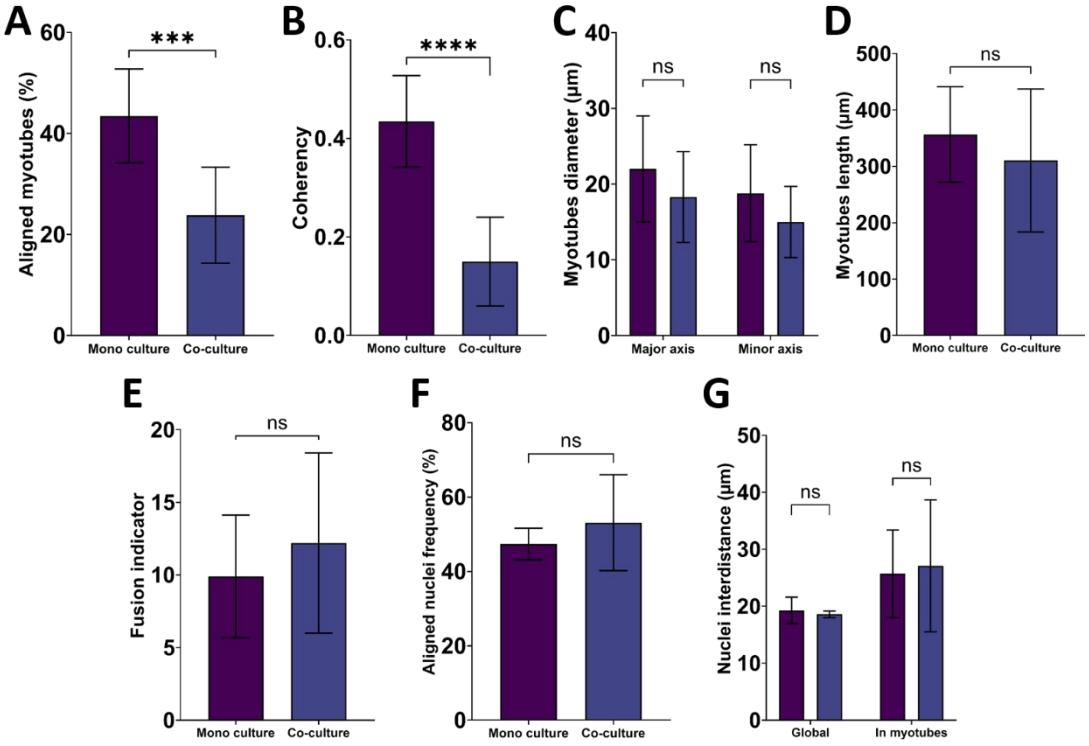

Figure 144: Myotubes comparison between myoblasts mono culture and fibroblast-myoblasts co-culture. (A) Proportion of aligned myotubes and its (B) orientation coherency. Myotubes (C) diameter, (D) length and (E) fusion indicator. (E) Proportion of aligned nuclei oriented parallel to aligned myotubes. (F) Nuclei inter distance analyzed globally in the muscle-construct or analyzed specifically in myotubes. Day 10 of culture. N = 17 and 14 for mono culture or co-culture set up respectively.

Confocal images of on-chip myotubes generated in this co-culture set-up showed striated myotubes at day 10 of culture, corresponding to day 6 of culture for the myoblasts (Figure 145). When we look at the proportion of the experiments exhibiting striated myotubes, we observed that at day 10 of co-culture, 50% of the experiments resulted in striated myotubes (n=2). Considering a day 10 of co-culture actually matches a day 6 of mono culture for myoblasts, it suggests that fibroblasts have an influence on myotubes maturation, helping them to mature earlier.

Fibroblasts have been reported to regulate skeletal muscle differentiation through paracrine actions of secreted factors [176]. Among these different secreted factors, interleukin-6 (IL-6) is a cytokine produced by several cell types, mainly by activated monocytes/macrophages, vascular endothelial cells and fibroblasts, but also by skeletal muscle cells upon various stimuli [176]–[178]. A paper reported that C2C12 myoblasts co-cultivated with human dermal fibroblasts generated myotubes in a higher state of maturation compared to myoblasts in mono culture, assessed by the myotubes count per unit area and the myoblasts fusion [176].

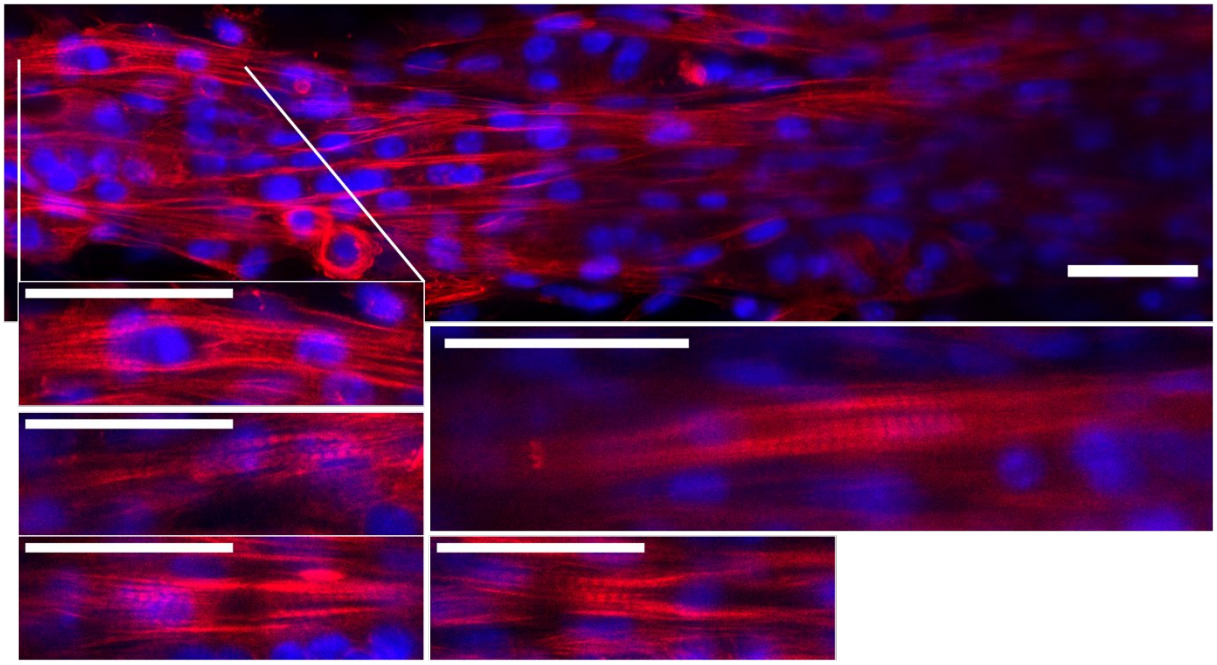

Figure 145: Confocal images of PFA fixed on-chip myotubes generated in fibroblast-myoblasts co-culture set up, at day 10 of culture, showing the overall morphology and striated myotubes. Scale bars: 50 µm.

They also showed that fibroblasts expressed a 10-fold increase in IL-6 secretion when co-cultivated with myoblasts. It is worth mentioning that the ELISA kit they used only detected human IL-6 secreted by human cells, therefore not detecting mouse IL-6 secreted by C2C12 myoblasts.

They observed a decreased myoblast differentiation when blocking IL-6 activity with neutralizing antibodies in the co-cultures. On the other hand, adding IL-6 neutralizing antibodies in myoblasts mono culture did not change their differentiation, highlighting the importance of IL-6 secreted by fibroblasts. Another study reported an enhanced myoblasts differentiation, assessed by the upregulation of specific muscle gene expression, when adding exogenous mouse recombinant IL-6 to C2C12 myoblasts cultures on collagen I-coated dish [178].

We therefore investigated more in detail the impact of fibroblasts on myoblasts differentiation in the on-chip co-culture set-up. The experimental time points were adjusted to better match on-chip myoblasts mono culture. At day 0, fibroblasts were encapsulated within collagen and cultivated for 3 days in growth medium. At day 3, myoblasts were seeded and cultivated for 3 days in growth medium. At day 6, we switched for differentiation medium. Medium was changed every 2 days until day 13. By doing so, the co-cultured myoblasts were similarly exposed to 3 days of growth medium, then 7 days of differentiation medium as mono cultured myoblasts. Thus, 'Day 0' will be defined as the day of myoblasts seeding for all experiments. For each condition and time points, several chips were pooled together ($n \geq 2$) to perform RT-qPCR. Gene expression was normalized to GAPDH housekeeping gene. Then, multiple comparison was performed. Results were expressed in relative quantification (RQ), using the $2^{-\Delta\Delta ct}$ method.

In parallel, the exact same volume of 6mg/ml collagen type I, containing encapsulated fibroblasts at 7.5×10^5 cells/ml was deposited in the center of 24 wells-plate, and submitted to the same experimental conditions. These were the fibroblasts mono culture controls. At each time

point, collagen was digested by collagenase and cells were retrieved for RT-qPCR assays.

2.1.2. Upregulation of IL-6 expression in co-cultures

Compared to the basal state (*i.e.,* in flask at the day of collagen encapsulation for 3T3 fibroblasts or of the seeding for C2C12 myoblasts), IL-6 expression globally increased over time for every experimental condition (Figure 146A). The expression was higher at any time point for C2C12 mono cultures on-chip compared to dish culture (Figure 146B). However, IL-6 expression was significantly higher in the co-culture set-up at day 10 than either on-chip C2C12 monoculture of 3T3 monoculture (Figure 146C, D)

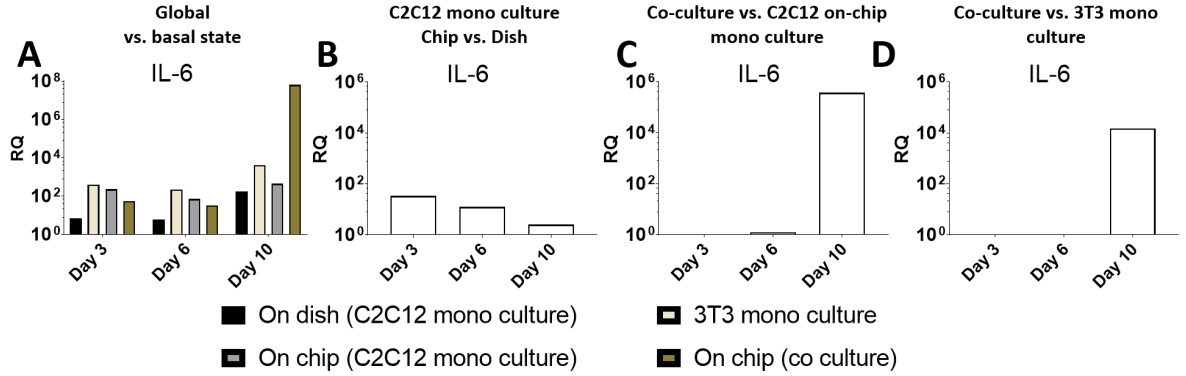

Figure 146: IL-6 gene expression normalized by GAPDH housekeeping gene. (A) Global IL-6 expression over time for every experimental condition, compared to the basal state (*i.e.,* in flask at the day of collagen encapsulation for 3T3 fibroblasts or of the seeding for C2C12 myoblasts). (B) Comparison of C2C12 mono cultures, on-chip vs. dish. (C) Comparison of co-culture vs. on-chip C2C12 mono culture. (D) Comparison of co-culture vs. 3T3 mono culture.

It is interesting to note that IL-6 is secreted both by myoblasts and fibroblasts in mono culture, but its expression is much higher in co-culture than only the sum of two separately. Therefore, the upregulation of IL-6 expression in co-culture is not only the effect of adding the expression of both mono cultures, but is the results of a crosstalk between myoblasts and fibroblasts.
As we already mentioned in chapter 3 when performing RT-qPCR assays for on-chip mono-cultures, several chips were pooled (from 3 to 4) for each condition to perform one RT-qPCR assay because of low cells count for on-chip cell culture. But these co-culture and gene expression assays must be repeated to have more representative data.

However, based on the preliminary results, it seems that the presence of fibroblasts upregulates IL-6 expression in C2C12 in on-chip co-cultures compared to on-chip mono-culture. To further investigate if this upregulation lead to a better myotube maturation, we performed RT-qPCR assays on myoblast differentiation genes.

- **Upregulation of myoblast differentiation genes expression**

We previously mentioned in chapter 3 that several genes, such as myogenin, MyHC 1, MyHC 2X and MyHC 2B were markers of myogenic differentiation. As previously, gene expression was normalized by GAPDH housekeeping gene. Then, on-chip C2C12 co-cultures with fibroblasts expression was compared to on-chip C2C12 mono-cultures at day 10 of culture.

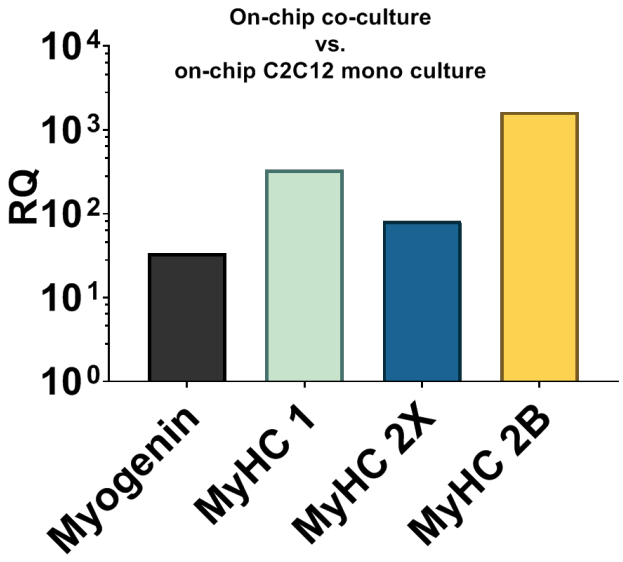

Figure 147: Myoblast differentiation genes expression relative quantification (RQ) in on-chip co-cultures compared to on-chip C2C12 myoblasts mono culture at day 10.

Co-cultures lead to the upregulation of all the myogenic differentiation genes compared to C2C12 on-chip mono cultures (Figure 147). Interestingly, results on morphological analysis (Figure 144) showed no significant difference between myotubes generated in C2C12 on-chip mono cultures compared to the ones generated in co-cultures condition. However, results here evidenced that myotubes have a better maturation on a molecular point of view when generated in a co-culture condition.

2.1.3. Co-culture leads to a myofibroblast phenotype

As we discussed in chapter 1, fibroblasts are supporting cells and secrete the ECM, but can also be activated into myofibroblasts expressing αSMA. Interestingly, the fibroblasts we used exhibited higher expression of αSMA than Col 1α (collagen 1α gene) compared to the basal state (Figure 148A). Co-cultivated with C2C12 myoblasts, it appeared that fibroblasts upregulated αSMA expression at day 10 compared to fibroblasts mono cultures (Figure 148B). On the other hand, Col 1α expression was stable in both mono and co-culture conditions.

Myofibroblasts are defined as ECM-producing (such as collagen I) and contractile cells that stain positively for αSMA [33]. An increase number of collagen I producing cells in mice fibrotic skeletal muscles has been reported [33], and that Col 1α gene upregulation was correlated with fibrosis severity [179]. In our system, Col 1α expression was stable both in mono and co-cultures conditions, over time. The αSMA has not been reported to be a marker of fibrosis in skeletal muscles either [179]. These results suggest that our device does not mimic the pathogenic muscle fibrosis in the co-culture condition.

On the other hand, fibroblasts activation into myofibroblasts expressing higher level of αSMA has been reported to play a major role in tissue repair [180], [181].

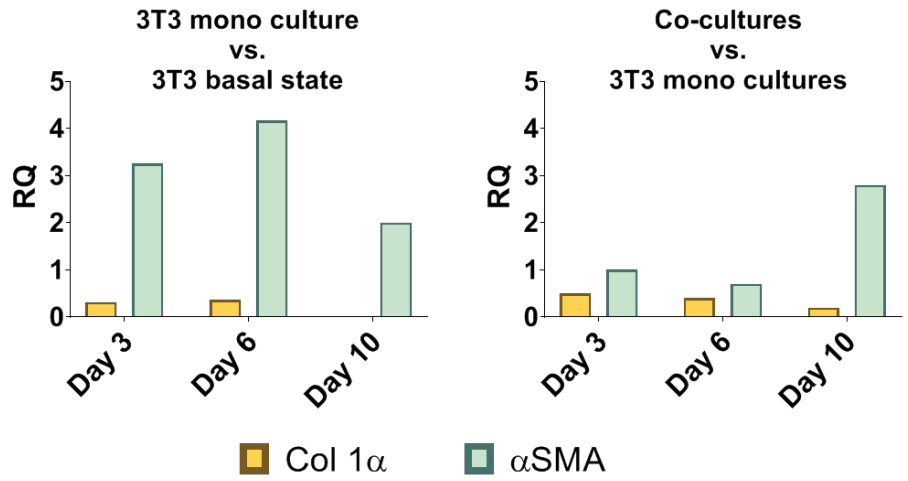

Figure 148: 3T3 fibroblasts Col α and αSMA expression in relative quantification (RQ). (A) Comparison of 3T3 mono culture vs. 3T3 basal state. (B) Comparison of 3T3 co-cultures vs. 3T3 mono culture for each time point.

Our results showing an upregulation at day 10 of the αSMA in co-cultures compared to fibroblasts mono-cultures suggest that our system may lead the co-cultivated muscle tissue toward a regenerating muscle rather than a fibrotic one, which is encouraging.
Here again, we pooled several chips for each condition to perform one RT-qPCR assay. Skeletal muscle and fibroblasts co-cultures have to be repeated to confirm these preliminary data.

The *in vivo* skeletal muscle is inherently a multicellular system. It is thus expected that cultivating together different relevant cells in an *in vitro* system should bring more relevance. More and more studies are bringing evidences toward that paradigm and our work followed the same path [117], [118], [182], [183].

Regarding enhancing myoblasts differentiation and maturation using fibroblasts, other factors are worth investigating. For instance, a transcription factor named p65 has been reported to induced IL-6 transcription via NF-κB signaling pathway [178]. Myoblasts transfected with silencing RNA blocking p65 translation resulted in a downregulation of IL-6 expression and a reduced myoblasts differentiation. It has also been reported that submitting fibroblasts to mechanical stretching could change their gene expression, with a higher IL-6 secretion [176]. Skeletal muscles are obviously designed to support loads and mechanical deformations. Implementing mechanical stretching within our microdevice would be relevant and very interesting as well as more physiologic. Finally, using other fibroblasts type could also be worth investigating. Cultivating primary fibroblasts from mice skeletal muscles would bring even more relevance to our model.

2.1.4. Conclusion

To conclude on C2C12 myoblasts co-cultures with other cell types, let's review the main achievements we made.

- We evidenced the versatility of our MyoChip device as we successfully developed a vessel-on-chip of 200 μm diameter.

- Morphological, functional and gene expression analysis showed the integrity of this vessel-on-chip.

- First myoblasts co-cultures with endothelial cells evidenced the cell culture medium incompatibility challenge and highlight the necessity to optimize co-cultures media.

- We also showed that the MyoChip device also successfully allows stromal cells to be embedded in the collagen type I matrix.

- First myoblasts co-cultures with fibroblasts evidenced an interplay between these two cell types, first helping the myotubes to maturate as shown by gene expression analysis, then leads fibroblast toward a myofibroblast phenotype.

- Preliminary myoblasts co-cultures with hiPSC-derived motor neurons have been conducted but did not result in satisfactory results. More optimization experiments will have to be performed.

In conclusion, the MyoChip design evidenced the possibility to co-cultivate different cell types on the device and importance of an optimized co-culture medium. Finally, on-chip myoblasts co-cultures with fibroblasts showed muscle-constructs exhibiting a further state of maturation, and a crosstalk between these two cell types.

CONCLUSION AND PERSPECTIVES

1. Developing a skeletal muscle-on-chip

1.1. MyoChip device: achievements

I started my PhD when the MyoChip European project was launched in January 2019, aiming at developing a microfluidic platform for the generation of a 3D biomimetic skeletal muscle-on-chip. For that purpose, I developed an original microfluidic device that contains tubes embedded in a collagen I matrix.

I first showed that seeding C2C12 cells in growth medium did not faithfully recapitulate the skeletal muscle architecture, as cells organized into a lumen structure when working with collagen tubes of 200 µm diameter. To modify muscle cells self-organization, I investigated the effect of cell seeding conditions with the presence of ECM components in cell suspension, allowing cells to adhere through the whole collagen tube section, as well as a layer by layer seeding approach (LbL) giving cells an appropriate substrate stiffness. Unfortunately, in these 200 µm tubes, the lumen organization remained whatever the seeding conditions.

I then evidenced a strong influence of the substrate curvature on cells organization on-chip, as working with a substrate with 3-folds higher curvature (tubes of 75 µm) resulted in muscle cells colonizing the whole available volume of the collagen tube. My results showed that seeding cells suspended in growth medium resulted in a better cell organization with higher aligned myotubes toward the long axis, a better nuclei alignment parallel to the myotubes, the formation of striated myotubes, and an upregulation of myogenic differentiation genes. On the other hand, cells mixed with ECM generated branched and heterogeneous myotubes, with larger diameter and higher fusion indicator, similarly to what is observed in some myopathies.

In parallel and in order to provide a muscle on-chip that recapitulates the different cell types present *in vivo*, I demonstrated the versatility of our MyoChip device as vessel-on-chip of 200 µm diameter using human primary endothelial cells, can be easily generated in this platform. Investigations by immunostaining of adherent junction (VE-cadherin), vascular permeability, leukocytes adhesion and gene expression analysis showed the morphological and functional integrity of this vessel-on-chip. However, the first results of co-culture with C2C12 cells evidenced cell culture medium incompatibility, leading to a high cell death. I also performed co-cultures of C2C12 with NIH 3T3 fibroblasts, allowing the generation of myotubes with the same morphological maturation as the one generated previously in monoculture within 75 µm collagen tubes. However, our results suggest that this co-culture allowed a better myotubes maturation on a molecular point of view, with an upregulation of the muscle differentiation genes.

To conclude, this MyoChip device is quite promising in terms of biomimicry and versatility. Future perspectives include cultivating primary cells or induced pluripotent stem cells. This would allow us to create diseases models and to study the impact of perfused drugs through the vessel, on the muscle-construct.

1.2. Skeletal muscle-on-chip perspectives

- **Optimizing the MyoChip design**

System optimization is an infinite process as no system can be a perfect mimic of *in vivo* complexity. Although the device we work with allowed us to achieve the main goals we aimed for, several parameters can still be optimized.

First, regarding device microfabrication, the surface treatment using APTES and GA to covalently attach the collagen to the PDMS is a tedious and very long step with several potential drawbacks if the protocol is not well performed. In particular, APTES could make aggregates if it is not well rinsed, and GA is toxic for cells leading to long rinsing steps. Park *et al.* reported another surface treatment involving poly-dopamine (PDA) to attach collagen to PDMS [184]. Cultures of cells-laden collagen I on PDA-treated PDMS substrate not only allowed the hydrogel to remain stable over time whatever the initial substrate shape, but also allowed the cells to grow. Recently in the team, we successfully reproduced this protocol, and cultivated a human pancreatic cancer cell line (PANC-1) I collagen I. It has been reported that PDA surface coating harnessed great interests recently in material science, biology and biomedical fields [185]. Using PDA to attach collagen to PDMS would bring several advantages. First, it has been reported to be biocompatible with negligible cytotoxicity on cultivated human embryonic kidney cells and in rats when injected as PDA-nanoparticles [185]. Then, compared to APTES and GA, it is drastically easier to manipulate since there are no long and tedious rinsing steps which last 2 days as we discussed in chapter 2. It means that PDMS chips can be micro fabricated on the day of the experiment, with subsequent cells seeding.

There is another parameter which we can optimize within the MyoChip device: implementing anchors at each of the extremities of the muscle-construct. Indeed, as one aspect is to cultivate muscle cells on-chip for longer culture time to enhance myotubes maturation, the forces generated by the tissue will also increase. This can potentially lead to collagen deformation and the muscle-construct to collapse if there are no anchors to maintain it. Indeed as we mentioned in chapter 1, this anchoring approach has been widely used for developing skeletal muscle-on-chip, but lacked the geometry for vessel-on-chip. By combining both approaches, we can bring together the advantages of each system.

- **Toward more cell complexity**

The ultimate goal of the MyoChip project is to cultivate human myoblasts derived from induced pluripotent stem cells, with human endothelial cells, fibroblasts and motor neurons. For that purpose, our collaborators from IMM (Lisbon) have already started to develop and optimize protocols to de differentiate human cells from dermal biopsies, and to differentiate them into myoblasts.

During my PhD, I also had the opportunity to work in collaboration with **Stéphane Nédelec**'s team from Institut du fer à Moulin (Paris), on cultivating hiPSC-derived motor neurons. I did some preliminary investigations teaming up with **Terence Saunier** (engineer in my team) using these motor neurons (optimizing the collagen type I concentration for motor neurons encapsulation with live/dead assays, cultivating motor neurons in collagen tubes). However, as those cells were obviously not as abundant as a cell lines, and that the protocol to differentiate them was tedious, I did not perform enough experiments to have satisfactory data. To develop this part, additional workforce will be needed.
Finally, cultivating patients' cells on-chip would be an ultimate goal as it would allow us to develop diseases models and to test potential drugs by perfusing the solution through the vessel-on-chip. Several diseases involving not only the skeletal muscle, but also motor neurons or vessels would be modeled using that device. The micro fabrication being affordable, although requiring few specific equipment, the technology is easily transferable to other laboratories and as such, participate to the diffusion of organ-on-chip technologies.

- **Enhancing myotubes maturation**

In vivo, postnatal development of skeletal muscle involves thyroid hormones [156], [186]. In mouse, it has been reported that hypothyroidism delayed the formation of adult fast MyHC, whereas hyperthyroidism or direct injection of thyroid hormones accelerated it [156]. It could therefore be interesting to investigate if adding more thyroid hormones in the medium could further maturate on-chip myotubes, as FBS already contains it.

Another way to promote the muscle maturation would be to mimic muscle exercise. As we discussed in chapter 1, several teams successfully implemented electrical stimulations to enhance myotubes maturation. Electrical stimulations leads to muscle contraction, mimicking the motor neuron efferent message. Implementing it in our team won't be so difficult, as all we need is to have a conductive cell culture medium and electrodes connected to a tension generator.
In our team, a mechanical stretcher mounted on an inverted epifluorescence microscope has been recently upgraded from a previous project for gut-on-chip technologies. The objective is to finely tune the stretching rate over time, and to track the structures on microscopy in an automated manner. The chip we developed for skeletal muscles can totally be adjusted to fit this mechanical stretcher, allowing us to apply mechanical forces on the muscle-construct.

Moreover, **Claire Wilhelm** who recently joined our team, works on the use of magnetic nanoparticles internalized by living cells for different purposes, one of them being a mean to manipulate/engineer living cells. During my PhD I was able to collaborate with her and **Noam Demri**, currently being a PhD student, to produce magnetic C2C12 myoblasts which act as tiny magnets once in contact with an external magnetic field. Several experiments that involved culturing magnetized myoblasts on a collagen I substrate, and to align them using external magnets have been performed with encouraging results. Spheroids of C2C12 myoblasts have also been produced thanks to their magnetic properties. This project will be continued thanks to Noam's PhD and in a next future we can imagine a muscle bio construct stimulated by a magnetic field.

2. Versatility of the MyoChip micro device – Side project

During my PhD I also had the opportunity to supervise Master's degree interns, **Ellyn Redheuil** and **Georgina Balkoska.** With Ellyn, we investigated the influence of adding ECM during seeding on C2C12 organization in 200 µm diameter collagen tubes. Georgina did her internship between our team, and **Isabelle Sermet-Gaudelus**'s team from Institut Necker Enfants Malades (INEM, Paris) which is focused on the cystic fibrosis disease. Taking benefit of the MyoChip device versatility, we started a collaboration with them in order to develop 3D bronchi-on-chip to study the disease.

- **Bronchial epidermal cells culture on-chip**

Briefly, cystic fibrosis (CF) is a recessive genetic disorder caused by mutations in the cystic fibrosis membrane conductance regulator (*CTFR*) gene, encoding a transmembrane chloride channel [187]. Patients with CF disease have a cilia dysfunction which leads to chronic bronchial infections and chronic inflammation along with other CF-related disorders such as pancreatic insufficiency, resulting in high morbidity and mortality. Several groups have published some interesting microfluidic systems to recapitulate the disease. Ingber's group has reported a human lung airway-on-chip [188]. They cultivated bronchial epithelial cells from patients with CF, separated to a vascular compartment by a porous PDMS membrane. Shik Mun *et al.* reported a model of pancreas-on-chip, cultivating pancreatic cells from patients with CF [189].

In collaboration with INEM, we took profit of the device we developed for the MyoChip project and cultivated human bronchial epidermal cells (16HBE), which is a cell line, in 200 µm collagen tubes. We successfully showed that cells survived in collagen tubes, organizing in a lumen structure.

Without going too much into details, we also showed that they organized in a confluent cell monolayer (by tight junction ZO-1 staining) and had the typical cobblestone morphology of bronchial cells (data not shown). The next step will be to investigate if they develop cilia, which is a marker of further maturation. To mimic the *in vivo* environment, an air-liquid interface has also to be implemented. These are obviously preliminary experiments, but it is clearly one of the perspectives of the MyoChip device, even aside from the MyoChip project.

MATERIAL AND METHODS

1. Development of the MyoChip micro device

- **3D printing by stereo lithography**

The molds from which we fabricated the chips were designed on Autodesk Inventor® and were created using the stereo lithography 3d printer Digitalwax 028J Plus® from DWS Company, (Italy). We used DS3000 resist and Precisa DL260 resist from DWS Company. Chips were made of PDMS from Dow Corning Company (Sylgard 184 Silicone Elastomer Kit). PEEK tubing (1/32" × 0.25mm, JR-T-5610) were bought from Cluzeau company (France). Round glass cover (#1.5, 30 mm in diameter) slips to seal the bottom part of the chip were purchased from VWR (USA). A plasma machine (Femto, Diener Electronic GmbH & Co KG, Germany) was used for surface activation.

- **Collagen tubes**

To generate the collagen tubes, we used acupuncture needles (SEIRIN Type J) from 3B Scientific Company (Germany) with 200, 120 and 100 µm of diameter. We also used tungsten wires of 75 µm (W 005305) from Goodfellow Company (UK). Needle or tungsten wire were coated with 1% BSA in PBS (w/v) (Sigma, USA). Rat tail collagen type I was purchased from Corning Company (USA).. For collagen attachment to PDMS, 3-Aminopropyltriethoxysilane 99% (APTES, ACROS Organics™) and glutaraldehyde solution (50%/Certified/BioReagent), Fisher BioReagents) were purchased from Fisher Scientific (USA). Collagen tubes were characterize using fluorescently labelled BSA Alexa Fluor™ 488 (ThermoFisher Scientific, USA).

2. On-chip cells seeding

2.1. Experimental set up preparation

As discussed earlier, the microfabricated chips with collagen are stored immersed in PBS at 4°C. During cells seeding, needles are removed to generate hollow collagen tubes. This seeding step is done on a phase contrast microscope for live monitoring. Since it is not under a sterile biological hood, extreme care must be placed on cleanliness of the environment surround the microscope. All the tools are sterilized before by generously spraying 70% ethanol and dried under the sterile biological hood. The microscope and all the apparatus used for cells seeding are also sterilized first with a detergent (Surfanios), then with 70% ethanol. Priorly, cells solution is prepared under a sterile biological hood. At any time of the experiment, gloves should be regularly cleaned with 70% ethanol or changed if soiled.

Cells suspension is prepared under the sterile biological hood. Different cell types have been

used as it will be discussed in the next chapter. But to optimize our system, starting with a simple cell line (C2C12) was a good option. Cells were used from passage 2 to passage 15. They were cultured in a T150 flask until 80% of confluency before using them for experiments or for next passages.

For experiments, supernatant medium was discarded, and cells were rinsed with PBS before detaching with trypsin. Cells were counted using a KOVA™ Glasstic Slide counting grid (Fisher Scientific, USA) according to the manufacturer's instructions. Then, cells were suspended in 1 ml of growth medium with seeding concentrations always within the same order of magnitude (5 to 10×10^6 cells/ml).

For cell seeding, we used a pressure pump controller (FlowEZ, 345 mbar) purchased from Fluigent Company (France)

2.1. Seeding procedure

- **Preparations**

Under a sterile biological hood, all the tools are sterilized with ethanol and let dry: 14 cm surgical scissors (Reference: S08090 from Fisher Scientific, USA), two sets of tweeters with flat squared ends (Reference: 136-9749 from RS components, France), a 40 ml glass crystallizing dish, a 15 cm petri dish and a single edge razor blade. The phase contrast microscope and the working space around it are carefully disinfected with first Surfanios, then with ethanol. About 25 cm of PTFE tubing (Reference: 11919445, Fisher Scientific) is cut with the razor blade to have a clean cut so it is easy to insert into microfluidic connections.

- **Cells preparation**

Device optimization was performed using a mouse cell line called C2C12 myoblasts (References: CRL-1772, ATCC, USA). Cells are washed with PBS and detached with trypsin. KOVA™ Glasstic™ slides (References: 22-270141, Fisher Scientific, USA) are used to count cells. Cultivating C2C12 myoblasts on a T150 flask at 80% confluency leads to approximately around 5 to 10×10^6 cells in total. Cells are centrifuged and are suspended in 1 ml of growth medium. The resulting seeding cell concentration is thus 5 to 10×10^6 cells/ml. According to the seeding technique discussed earlier with letting the needle tip in the PDMS channel, cells accumulate inside the collagen tube, independently of the initial cell concentration in the micro tube. Our aim is to fill the collagen tube with cells. The more concentrated the initial cell suspension is, the faster the collagen tube will get filled.

A microtube containing 1 ml of growth medium is connected to the system, then a pressure of 30 mbar is set to rinse the seeding tubing. Usually, one third of the micro tube is enough to properly rinse the seeding tubing. This step can be performed while preparing the above steps. An infrared heating lamp is mounted above the microscope plate, at approximately 15 cm.

- **Cell seeding**

2D controls are made by plating 500 000 cells on a 34 mm dish. The immersed 3D microdevices

are brought inside the sterile hood. Each microdevices are picked with a tweezer, which we will be referring as the 'sterile tweezer', and positioned on the 15 cm dish lid. The lid is then moved toward the phase contrast microscope. Another tweezer, which we will refer to as the 'seeding tweezers', will be manipulated at the microscope working place.

Under microscope live monitoring, needles are carefully and partially removed with the seeding tweezers, letting the needle tip in the PDMS channel. The seeding tubing (Adtech Polymer Engineering™ PTFE Microtubing 0.3 x 0.76 mm), which is still connected to the growth medium micro tube, is then connected to one input of the microdevice. Monitoring the system behavior is crucial. It allows to detect any anomaly that can possibly occur, such as collagen detachment, collagen tube deformation, bubbles presence or leakage due to micro fabrication errors.

The pressure is then set to 0, and the growth medium micro tube is replaced with the cell suspension microtube. The pressure is set back to 30 mbar while continuously monitoring the system behavior under microscope. When the collagen tube is entirely filled with cells, the seeding tubing is cut with the surgical scissors. The seeding process is repeated for the two other collagen tubes.

When the microdevice is seeded, the pressure is then lowered to 15 mbar to continuously have flow so it avoids cells aggregation and seeding tubing clogging. The microdevice is then brought back under the hood and placed into a sterile 10 cm dish. The remaining PBS that is on top of the collagen, inside the circular well of the microdevice is discarded and 400 µl of warmed growth medium is added. The dish is then placed inside the incubator at 37°C and 5% of CO_2. With the sterile tweezer, another microdevice is selected and placed onto the 15 cm dish lid mounted on the microscope. The whole seeding process is then repeated.

Letting the seeded microdevices in the incubator for 30 min is enough for the cells to adhere. Under the sterile hood, needles are carefully removed from each seeded microdevices, which are then placed into 6-well plates. A volume of 5 ml of growth medium is added to each well. The seeded microdevices are placed back to the incubator.

3. On-chip skeletal muscle cells

- **Culture conditions**

Cells-on-chip were incubated for a total of 10 days. The experimental time points were: day 3, day 6 and day 10. During the proliferation phase (seeding day to day 3), cells were cultivated with growth medium (DMEM Glutamax, 10% of FBS and 1% of PS). During the differentiation phase (day 3 to day 10), the medium was then replaced by differentiation medium (DMEM Glutamax, 1% of HS and 1% of PS) every 3 days until day 10 of culture.

- **Experiment time-points**

At each time point (day 3, day 6, day 10), pictures were taken and some microdevices were fixed in paraformaldehyde (PFA) at 4%, while the others remain on culture. For fixing, the

microdevice was transferred to a single 35 mm dish and washed three times with PBS. A volume of 5 ml of PFA at 4% was added, and let incubated for 1 hour. The microdevice was then washed three times in PBS, before immersed in PBS and stored in 4°C before immunostaining.

- **Immunostaining**

The PBS was discarded and 3 ml of a blocking solution (BSA at 4% W/V in PBS, Triton X100 at 0.5%) was added and let incubated for 1 hour. Blocking solution that was in the circular well on top of the collagen was discarded and the 500 µl of the primary antibody solution (S1) was added inside the circular well, at 4°C overnight. The S1 solution was discarded and the microdevice was washed by immersing 10 min in PBS, followed with two quick rinsing in PBS. A volume of 2 ml of the blocking solution was added around the chip, but not inside the circular well. Then, a volume of 500 µl of the second antibody solution (S2, dilution 1/1000) was added inside the circular well on top of the collagen chamber, for 2 hours at room temperature or overnight at 4°C. The S2 was discarded and the chips were washed by immersing in PBS in the same way then previously. A volume of 2 ml of a DAPI and filamentous actin staining (phalloidin) solution was then added and let incubated at room temperature for at least 2 hours. The last staining solution was discarded and the chip was rinsed with PBS following the same previous steps.

- **Storage**

Stained and fixed chips are stored within 6-wells plate, immersed in PBS and stored at 4°C in the fridge until imaging.

4. Dissected mice skeletal muscles

Mice were sacrificed in our lab by a colleague for another purpose. Right after, we dissected the quadriceps of two different mice, resulting in four quadriceps that were sent to Institut Curie pathology laboratory (Laboratoire de pathologie expérimentale) for processing. We also sent them the desired immunostaining for tissues (DAPI for nucleus, phalloidin for F-actin, primary and secondary antibodies for sarcomeric α-actinin).

5. Analysis methods

5.1. Confocal imaging

Chips are imaged with a Leica DMi8 inverted confocal microscope. Since the bottom of the microdevice is a glass cover slip, the chip is directly positioned onto the microscope stage. Objective magnification of 10x is used for a broad view, and a magnification of 25x with water immersion is used for higher resolution and better details. When 25x magnification is used, the X resolution (along the tube axis) was set to 2048 pixels whereas the Y resolution (perpendicular to the tube axis) ranged from 700 pixels to 2048 pixels depending on the tube diameter to gain in time

acquisition. The Z-steps were auto-optimized by Leica software to be the smallest possible, thus maximizing the information gathered in the z direction. The resulting Z-step was therefore usually a 568 nm step. The final acquired image had a voxel size of $0.2272 \times 0.2272 \times 0.5684\ \mu m^3$.

Each chip has three collagen tubes. Depending on the experiment, the number of tubes filled with muscle tissue varied. The acquisition focused on three main parts of the muscle tissue tube: the two extremities and the middle. The beginning of the Z-stack was set to be the most bottom part of the muscle tube, and the end was set to be the most upper part of the muscle tube. Due to the thickness of the chip, that collagen and the muscle tissue absorb part of the laser intensity and that the 25X objective has a limited working distance, imaging the upper part of the muscle tube was difficult.

5.2. Myotubes alignment

All alignment assessments were performed using image analysis software 'ImageJ'.

- **Alignment extraction**

The 3D acquired Z-stack underwent a Z-projection (sum images) resulting in a 2D image. To assess cell alignment, intra cytoplasmic filamentous actin were stained and its alignment was quantified using 'OrientationJ' plugin. Since actin fibers orient along the long axis of the myotube, it was considered as a good estimation of the myotube alignment itself. This plugin was developed by the Biomedical Image Group of EPFL (Switzerland) as a tool to characterize the orientation and isotropy properties of region of interests in an image, based on a mathematical model. Description and theoretical background of the algorithm are accessible on their website[n]. Alignment analysis was performed for each experimental condition and averaged for day 3, day 6 and day 10. Sarcomeric striations were also observed on stained filamentous actin confocal images.

- **Alignment distribution**

First, a distribution of orientation frequencies was generated with angles spanning from -90° (counter clockwise) to +90° (clockwise), where 0° is the long axis of the collagen tube. To have a more precise assessment on myotube alignment toward the tube long axis, orientations analysis focusing on $[-10°; +10°]$ surrounding the long axis were performed.

- **Coherency**

The coherency indicates if the local structures have a dominant orientation (coherency = 1) or if the image is essentially isotropic in the local neighborhood (coherency = 0).

5.3. Nuclei analysis

Nuclei analysis was assessed using 'MorphoLibJ' plugin[o], based on a 'Neubias nuclei

[n] http://bigwww.epfl.ch/demo/orientation/
[o] https://imagej.net/plugins/morpholibj

segmentaion workflow'[p]. The ImageJ macro is accessible in the supplementary data. Nuclei inter distances were computed using Mathlab.

5.4. Myotubes diameter

Myotubes diameter was manually assessed on ImageJ using filamentous actin staining z-stack images in a cross-sectional view. The maximum diameter of myotubes were hand-selected. They appeared as hollow circles of stained filamentous actin. An ellipse was fit to the hand-selection, and measurements were performed on that ellipse.

5.5. Other maturation markers

During the immunostaining step, S1 solution was composed of goat anti-mouse polyclonal antibodies targeting myosin heavy chain (1/1000 dilution), of goat anti-mouse polyclonal anti-pericentrin antibodies (1/2000 dilution) or of goat anti-mouse monoclonal anti-sarcomeric alpha actinin antibodies (1/1000 dilution).

5.6. Retro transcription and quantitative PCR (RT-qPCR)

RT-qPCR assays were mainly performed by **Fahima De Federico** from Institut Curie, who helped me a lot.

- **Cells harvesting**

Gene expression were assessed by retro transcription quantitative polymerase chain reaction (RT-qPCR). At each time point, the chips were rinsed in PBS and gently cut with a scalpel to release the muscle tubes-laden collagen part. This collagen part was subsequently incubated in PBS with collagenase at 1 mg/ml for 45 min in the incubator at 37°C. Cells cultivated on dish were simply detached with trypsin. After cell counting and centrifugation at 1500 rpm for 3 min, the supernatant was discarded and the cells were frozen at -80°C until qPCR processing.

- **Cells lysis and phase separation**

Frozen cells were slowly thawed in ice. A volume of 1 ml of Trizol was added to the tube and the cells pellet was homogenized and incubated at room temperature for 5 min. A volume of 200 µl of chloroform was then added for 2 min 30 sec at room temperature, before putting back the tube in ice for centrifugation at 4°C at 11000g for 15 min. After centrifugation, the tube contained a red phenol-chloroform phase that was discarded.

- **RNA precipitation and harvesting**

A volume of 500 µL of isopropanol was gently added to the tube and let incubated for 10 min at room temperature, before centrifugation at 11000g, 4°C for 10 min. Supernatant was discarded and 1ml of 75% ethanol was added before centrifugation at 11000g, 4°C for 5 min. Supernatant

[p] https://biii.eu/nuclei-segmentation-3d-dt-watershed-imagej

was then discarded. White precipitates, that corresponds to RNA, were let dried for 10 min at room temperature under the hood. RNA molecules are then re suspended in a buffer (10mM Tris pH 7, 0.1 mM EDTA, RNAse free) and incubated at 55°c for 10 min.

- **RNA quantification and verification**

A volume of 2 µl of the RNA solution was diluted in 600 µl RNAse free water, and quantified in with a Nanodrop machine. A satisfying yield corresponded to 15 µg of RNA per 10^6 cells. A mass of 1 µg of RNA was transferred to a RNAse free tube before adding 5 µl of RNAse free water and 1 µl of charging buffer.

- **Retro transcription and qPCR**

The High-Capacity cDNA Reverse Transcription Kit was used (Reference: 4368813, ThermoFisher, USA). Components were thawed in ice. The 2X RT master mix was prepared on ice as shown in Table 4.

A volume of 10 µl of 2X RT master mix was added in a tube with 2 µg of RNA. The total volume for the reaction was 20 µl. The tubes were briefly centrifuged and placed in to the thermocycler. Thermal cycling conditions used are shown in Table 5. All the primers used are listed on

Table 4: RT-qPCR 2X master mix preparation.

Component	Volume	
	With RNase Inhibitor	Without RNase Inhibitor
10X RT Buffer	2.0 µL	2.0 µL
25X dNTP Mix (100 mM)	0.8 µL	0.8 µL
10X RT Random Primers	2.0 µL	2.0 µL
MultiScribe™ Reverse Transcriptase	1.0 µL	1.0 µL
RNase Inhibitor	1.0 µL	—
Nuclease-free H_2O	3.2 µL	4.2 µL
Total per reaction	10.0 µL	10.0 µL

Table 5: Retro transcription thermal cycling conditions.

Settings	Step 1	Step 2	Step 3	Step 4
Temp.	25°C	37°C	85°C	4°C
Time	10 minutes	120 minutes	5 minutes	∞

Table 6: Primers sequences for RT-qPCR in C2C12 myoblasts and NIH 3T3 fibroblasts.

Gene name	Forward primer sequence (5' – 3')	Reverse primer sequence (5' – 3')
C2C12 myoblasts		
Myogenin1	TCCCAACCCAGGAGATCATT	AGTTGGGCATGGTTTCGTCT
Myogenin2	CAGGAGATCATTTGCTCG	GGGCATGGTTTCGTCTGG
Slow Myosin Heavy Chain (sMHC)	GAGCAGCAGGTGGATGATCT	GCTTGGCTCGCTCTAGGTC
Fast Myosin Heavy Chain 2X	TCGCTGGCTTTGAGATCTTT	CGAACATGTGGTGGTTGAAG
Fast Myosin Heavy Chain 2B	GTCACCAAAGGCCAGACG	ACATCTTCTCATACATGGACTTGG
GAPDH1	ATGTTTGTGATGGGTGTGAA	ATGCCAAAGTTGTCATGGAT
GAPDH2	ATCACCATCTTCCAGGAGCG	CCTG CTTCACCACCTTCTTG
Actb	TCCTGACCCTGAAGTACCCCAT	CTCGGTGAGCAGCACAGGGT
Desmin	TCTCCCGTGTTCCCT	ATACGAGCTAGAGTGGCA
IL6	GAGACTTCCATCCAGTTGCC	CTGATTATATCCAGTTTGGTAGCATC
NIH 3T3 fibroblasts		
Paxillin α	AACAAGCAGAAGTCAGCAGAGCC	CTAGCTTGTTCAGGTCGGAC
Paxillin β	AACAAGCAGAAGTCAGCAGAGCC	CTCTCCATCCACTCTCTGTT
GAPDH	TGTGTCCGTCGTGGATCTGA	CCTGCTTCACCACCTTCTTGA
αSMA	GACGTACAACTGGTATTGTG	TCAGGATCTTCATGAGGTAG
Col1α	GCTCCTCTTAGGGGCCACT	CCACGTCTCACCATTGGGG

5.7. Data analysis

Data extracted from orientations and RT-qPCR were analyzed using and GraphPad Prism 8. Statistical analysis was performed using built-in functions in GraphPad Prism 8. Mean and standard deviation values were compared using t-test when comparing two samples, or ANOVA test when comparing three or more samples.

6. Muscle on-chip co-cultures

6.1. Vessel-on-chip

For vessel-on-chip optimization, we used human primary microvascular endothelial cells from lung (HMVEC-L) were purchased from Lonza (References: CC-2527, Cologne, Germany) cultivated in their specific culture medium (endothelial cell growth medium (EGM-2 MV, reference: C-22022, PromoCell, Germany). Human umbilical vein endothelial cells (HUVEC) cells we used were a kind gift of **Sylvie Coscoy** from Institut Curie. We cultivated HUVEC in their specific culture medium (EGM2 medium, references: C-22011, PromoCell, Germany). To coat the inner surface of the collagen tubes, we used human fibronectin (References: F2006, Sigma-Aldrich, USA). Permeability assays were performed using 70 kDa dextran (References: 44886, Sigma Aldrich, USA). Immunostaining of vessel-on-chip were performed for VE-cadherin (References: Abcam ab33168, UK. Diluted at 1:100 in blocking solution), nuclei (References: Hoechst 33342, Invitrogen, USA. Concentration of 10 µM) on a confocal laser scanning microscope (References: LSM780, Carl Zeiss) with a 40× water immersion objective (References: Plan-Apochromat 40X/1.0 NA W) or a 10× objective (References: EC Plan-Neofluar 10X/0.3 NA).

6.2. Skeletal muscle and fibroblasts on-chip co-cultures

For skeletal muscle co culture with fibroblasts, we used a fibroblast cell line from mouse, called NIH 3T3 (References: CRL-1658, ATCC, USA). Fibroblasts were cultivated in 6 mg/ml collagen for 3 days in myoblast growth medium. Collagen tubes were then generated by removing the needles, and myoblasts were subsequently seeded into the tubes. Therefore, the new time point right after myoblasts seeding was considered to be 'Day 0' for the experiment. Next time points were the same as previously described for myoblast monoculture. Controls were performed by cultivating fibroblasts without myoblasts.

7. Bronchi-on-chip

Human bronchial epithelial cell line (16HBE) we used were from our collaborator in INEM. The fused silica tubing (References: TSP200350) for air-liquid interface implementation was purchased from Cluzeau Company (France)

SUPPLEMENTARY DATA

- **Muscle-construct periodic aggregates in 200 μm collagen tubes**

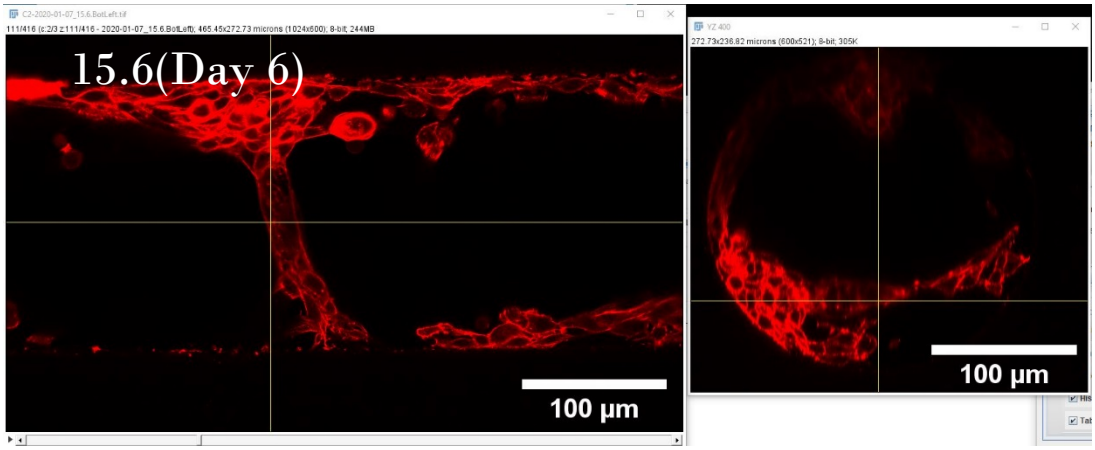

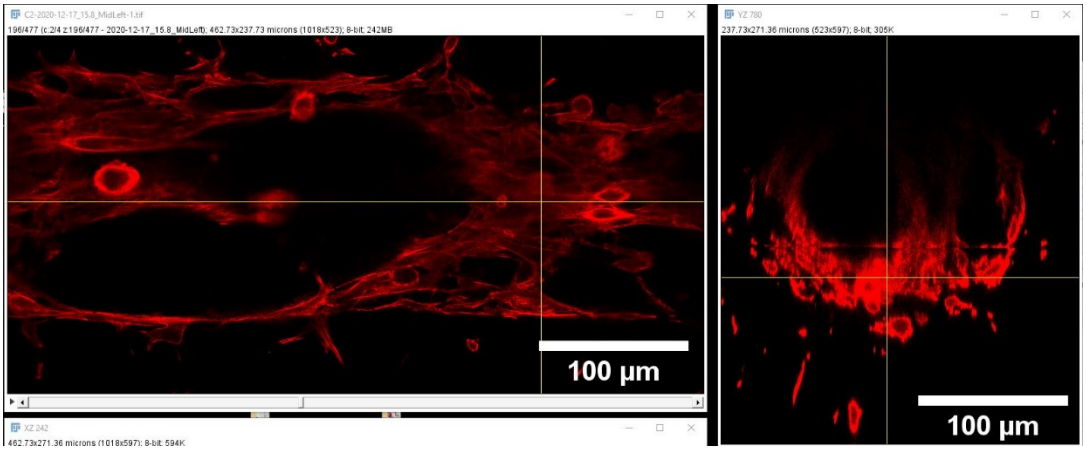

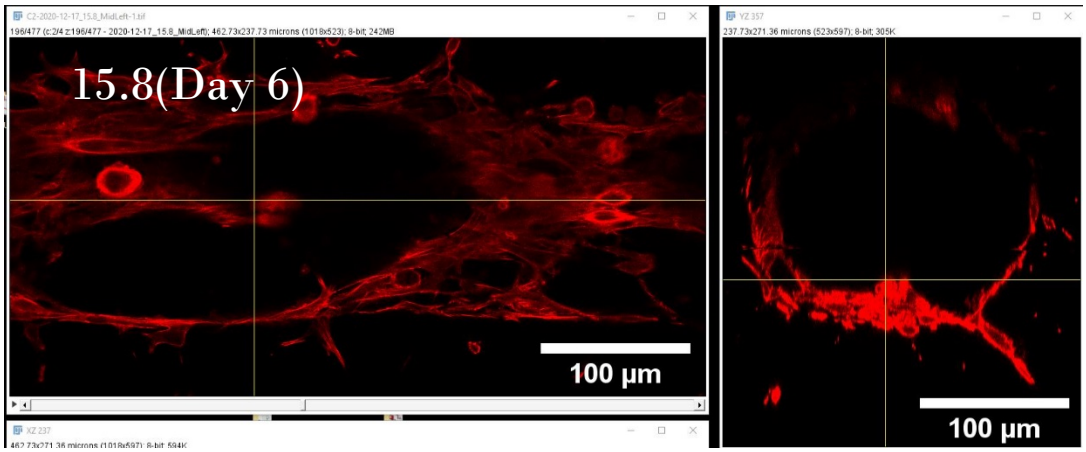

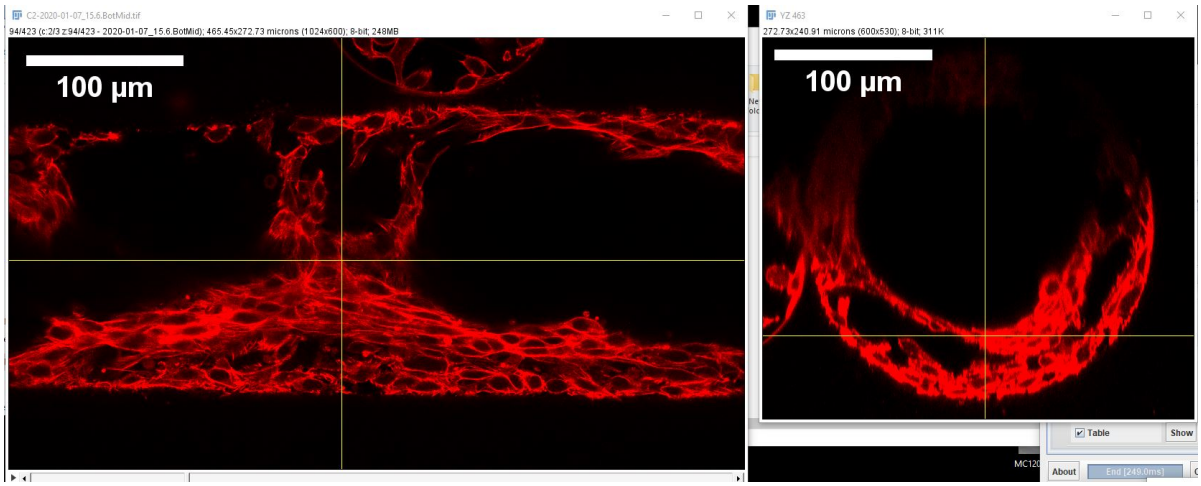

These are confocal images of muscle-construct in 200 µm collagen tubes, at day 6 of culture, stained for F-actin with phalloidin. Images focused on the aggregates.

- **Nuclei analysis ImageJ macro**

```
run("Duplicate...", "duplicate");
run("Despeckle", "stack");
run("Remove Outliers...", "radius=2 threshold=50 which=Bright stack");
run("Remove Outliers...", "radius=2 threshold=50 which=Dark stack");
run("Gaussian Blur 3D...", "x=2 y=2 z=2");

setAutoThreshold("Default dark");
//run("Threshold...");

setOption("BlackBackground", false);
run("Convert to Mask", "method=Default background=Dark calculate black");

run("3D Fill Holes");
run("Distance Transform Watershed 3D", "distances=[Borgefors (3,4,5)] output=[16 bits]
      normalize dynamic=2 connectivity=6");

run("Connected Components Labeling", "connectivity=6 type=[16 bits]");
run("Label Size Filtering", "operation=Greater_Than size=17000");
run("Label Size Filtering", "operation=Lower_Than size=130000");
run("Kill Borders");

run("Analyze Regions 3D", "voxel_count volume surface_area sphericity bounding_box centroid
      equivalent_ellipsoid ellipsoid_elongations max._inscribed surface_area_method=[Crofton
      (13 dirs.)] euler_connectivity=6");
run("Close All");
```

GLOSSARY

αSMA: Alpha smooth muscle actin.
AFM: Atomic force microscopy.
BSA: Bovine serum albumin.
FBS: Fetal bovine serum.
FITC: Fluorescein isothiocyanate
H&E: Hematoxyln and eosin staining
hiPSC : Human induced pluripotent stem cells.
HS: Horse serum.
HUVEC: Human umbilical vein endothelial cells.
ID: inner diameter.
IL-1β : Interleukin 1 beta.
IL-8: Interleukin 8
OD: outer diameter.
PEEK: poly ether ether ketone.
PS: Penicillin and streptomycin antibiotics.
Pt: platinum.
TGF-β : Tumor growth factor beta.
TNF-α: Tumor necrosis factor alpha
VE-cadherin : Vascular endothelium cadherin
ZO-1 : Zonula occludens 1

BIBLIOGRAPHY

[1] J. Chal and O. Pourquié, "Making muscle: Skeletal myogenesis in vivo and in vitro," *Dev.*, vol. 144, no. 12, pp. 2104–2122, 2017.

[2] P. R. H. Steinmetz *et al.*, "Independent evolution of striated muscles in cnidarians and bilaterians," *Nature*, vol. 487, no. 7406, pp. 231–234, 2012.

[3] W. R. Frontera and J. Ochala, "Skeletal Muscle: A Brief Review of Structure and Function," *Behavior Genetics*, vol. 45, no. 2. 2015.

[4] L. A. Rowland, N. C. Bal, and M. Periasamy, "The role of skeletal-muscle-based thermogenic mechanisms in vertebrate endothermy," *Biol. Rev.*, vol. 90, no. 4, pp. 1279–1297, 2015.

[5] K. Mukund and S. Subramaniam, "Skeletal muscle: A review of molecular structure and function, in health and disease," *Wiley Interdiscip. Rev. Syst. Biol. Med.*, vol. 12, no. 1, pp. 1–46, 2020.

[6] M. Widmann, A. M. Nieß, and B. Munz, "Physical Exercise and Epigenetic Modifications in Skeletal Muscle," *Sport. Med.*, vol. 49, no. 4, pp. 509–523, 2019.

[7] S. P. F. Bonny, G. E. Gardner, D. W. Pethick, and J. F. Hocquette, "What is artificial meat and what does it mean for the future of the meat industry?," *J. Integr. Agric.*, vol. 14, no. 2, pp. 255–263, 2015.

[8] M. J. Post, "Cultured meat from stem cells: Challenges and prospects," *Meat Sci.*, vol. 92, no. 3, pp. 297–301, 2012.

[9] J. N. Goodwin and C. W. Shoulders, "The future of meat: A qualitative analysis of cultured meat media coverage," *Meat Sci.*, vol. 95, no. 3, pp. 445–450, 2013.

[10] J. F. Hocquette, "Is in vitro meat the solution for the future?," *Meat Sci.*, vol. 120, pp. 167–176, 2016.

[11] H. L. Tuomisto and M. J. Teixeira De Mattos, "Environmental impacts of cultured meat production," *Environ. Sci. Technol.*, 2011.

[12] J. Lynch and R. Pierrehumbert, "Climate Impacts of Cultured Meat and Beef Cattle," *Front. Sustain. Food Syst.*, vol. 3, no. February, pp. 1–11, 2019.

[13] Y. Morimoto, H. Onoe, and S. Takeuchi, "Biohybrid robot powered by an antagonistic pair of skeletal muscle tissues," *Sci. Robot.*, vol. 3, no. 18, pp. 1–11, 2018.

[14] J. H. Lee, H. Kim, J. H. Kim, and S. H. Lee, "Soft implantable microelectrodes for future medicine: Prosthetics, neural signal recording and neuromodulation," *Lab Chip*, vol. 16, no. 6, pp. 959–976, 2016.

[15] T. Foltynie and M. I. Hariz, "Surgical management of Parkinson's disease," *http://dx.doi.org/10.1586/ern.10.68*, vol. 10, no. 6, pp. 903–914, Jun. 2014.

[16] Z. A. Puthucheary *et al.*, "Acute skeletal muscle wasting in critical illness," *JAMA - J. Am. Med. Assoc.*, vol. 310, no. 15, pp. 1591–1600, 2013.

[17] M. Quittan, "Aspects of physical medicine and rehabilitation in the treatment of deconditioned patients in the acute care setting: the role of skeletal muscle," *Wiener Medizinische Wochenschrift*, vol. 166, no. 1–2, pp. 28–38, 2016.

[18] S. Cohen, J. A. Nathan, and A. L. Goldberg, "Muscle wasting in disease: Molecular mechanisms and promising therapies," *Nat. Rev. Drug Discov.*, vol. 14, no. 1, pp. 58–74, 2014.

[19] C. Beaudart, R. Rizzoli, O. Bruyère, J.-Y. Reginster, and E. Biver, "Sarcopenia: burden and challenges for public health," *Arch. Public Heal. 2014 721*, vol. 72, no. 1, pp. 1–8, Dec. 2014.

[20] S. Crisafulli *et al.*, "Global epidemiology of Duchenne muscular dystrophy: An updated systematic review and meta-analysis," *Orphanet J. Rare Dis.*, vol. 15, no. 1, 2020.

[21] E. Mercuri, C. G. Bönnemann, and F. Muntoni, "Muscular dystrophies," *Lancet*, vol. 394, no. 10213, pp. 2025–2038, 2019.
[22] J. Larkindale *et al.*, "Cost of illness for neuromuscular diseases in the United States," *Muscle and Nerve*, vol. 49, no. 3, pp. 431–438, 2014.
[23] M. Cavazza *et al.*, "Social/economic costs and health-related quality of life in patients with Duchenne muscular dystrophy in Europe," *Eur. J. Heal. Econ.*, vol. 17, pp. 19–29, 2016.
[24] G. Nicholson, S. R. Gandra, R. J. Halbert, A. Richhariya, and R. J. Nordyke, "Patient-level costs of major cardiovascular conditions: A review of the international literature," *Clin. Outcomes Res.*, vol. 8, pp. 495–506, 2016.
[25] J. Morgan and T. Partridge, "Skeletal muscle in health and disease," *DMM Dis. Model. Mech.*, vol. 13, no. 2, 2020.
[26] M. van Putten, E. M. Lloyd, J. C. de Greef, V. Raz, R. Willmann, and M. D. Grounds, "Mouse models for muscular dystrophies: an overview," *Dis. Model. Mech.*, vol. 13, no. 2, 2020.
[27] S. Perrin, "Make mouse studies work," *Nature*, vol. 507, no. 7493. pp. 423–425, 2014.
[28] C. G. Begley and L. M. Ellis, "Drug development: Raise standards for preclinical cancer research," *Nature*, vol. 483, no. 7391, pp. 531–533, Mar. 2012.
[29] J. N. Kornegay, C. F. Spurney, P. P. Nghiem, C. L. Brinkmeyer-Langford, E. P. Hoffman, and K. Nagaraju, "Pharmacologic Management of Duchenne Muscular Dystrophy: Target Identification and Preclinical Trials," *ILAR J.*, vol. 55, no. 1, pp. 119–149, Jan. 2014.
[30] A. C. Ludolph *et al.*, "Guidelines for preclinical animal research in ALS/MND: A consensus meeting," *https://doi.org/10.3109/17482960903545334*, vol. 11, no. 1–2, pp. 38–45, 2010.
[31] A. R. Gillies and R. L. Lieber, "Structure and function of the skeletal muscle extracellular matrix," *Muscle Nerve*, no. September, p. n/a-n/a, 2011.
[32] M. Kjær, "Role of Extracellular Matrix in Adaptation of Tendon and Skeletal Muscle to Mechanical Loading," *Physiol. Rev.*, vol. 84, no. 2, pp. 649–698, 2004.
[33] M. A. Chapman, R. Meza, and R. L. Lieber, "Skeletal muscle fibroblasts in health and disease," *Differentiation*, vol. 92, no. 3, pp. 108–115, 2016.
[34] S. Hinds, W. Bian, R. G. Dennis, and N. Bursac, "The role of extracellular matrix composition in structure and function of bioengineered skeletal muscle," *Biomaterials*, vol. 32, no. 14, pp. 3575–3583, 2011.
[35] S. Kherif *et al.*, "Expression of matrix metalloproteinases 2 and 9 in regenerating skeletal muscle: A study in experimentally injured and mdx muscles," *Dev. Biol.*, vol. 205, no. 1, pp. 158–170, 1999.
[36] A. Singh, Z. L. Nelson-Moon, G. J. Thomas, N. P. Hunt, and M. P. Lewis, "Identification of matrix metalloproteinases and their tissue inhibitors type 1 and 2 in human masseter muscle," *Arch. Oral Biol.*, vol. 45, no. 6, pp. 431–440, 2000.
[37] A. R. Gillies and R. L. Lieber, "Structure and function of the skeletal muscle extracellular matrix," *Muscle and Nerve*, vol. 44, no. 3, pp. 318–331, 2011.
[38] U. Kühl, R. Timpl, and K. von der Mark, "Synthesis of type IV collagen and laminin in cultures of skeletal muscle cells and their assembly on the surface of myotubes," *Dev. Biol.*, vol. 93, no. 2, pp. 344–354, Oct. 1982.
[39] S. Hinds, W. Bian, R. G. Dennis, and N. Bursac, "The role of extracellular matrix composition in structure and function of bioengineered skeletal muscle," *Biomaterials*, vol. 32, no. 14, pp. 3575–3583, 2011.
[40] S. J. Mathew *et al.*, "Connective tissue fibroblasts and Tcf4 regulate myogenesis," *Development*, vol. 138, no. 2, pp. 371–384, 2011.
[41] C. J. Mann *et al.*, "Aberrant repair and fibrosis development in skeletal muscle," *Skelet. Muscle*, vol. 1, no. 1, pp. 1–20, 2011.
[42] J. Baum and H. S. Duffy, "Fibroblasts and myofibroblasts: What are we talking about?," *J. Cardiovasc. Pharmacol.*, vol. 57, no. 4, pp. 376–379, 2011.

[43] A. Uezumi *et al.*, "Fibrosis and adipogenesis originate from a common mesenchymal progenitor in skeletal muscle," *J. Cell Sci.*, vol. 124, no. 21, pp. 3654–3664, Nov. 2011.
[44] A. W. B. Joe *et al.*, "Muscle injury activates resident fibro/adipogenic progenitors that facilitate myogenesis," *Nat. Cell Biol.*, vol. 12, no. 2, pp. 153–163, 2010.
[45] B. Biferali, D. Proietti, C. Mozzetta, and L. Madaro, "Fibro–Adipogenic Progenitors Cross-Talk in Skeletal Muscle: The Social Network," *Front. Physiol.*, vol. 10, no. August, pp. 1–10, 2019.
[46] N. A. Dumont, C. F. Bentzinger, M. C. Sincennes, and M. A. Rudnicki, "Satellite cells and skeletal muscle regeneration," *Compr. Physiol.*, vol. 5, no. 3, pp. 1027–1059, 2015.
[47] J. E. Morgan and T. A. Partridge, "Muscle satellite cells," *Int. J. Biochem. Cell Biol.*, vol. 35, no. 8, pp. 1151–1156, 2003.
[48] L. Boldrin, P. S. Zammit, and J. E. Morgan, "Satellite cells from dystrophic muscle retain regenerative capacity," *Stem Cell Res.*, vol. 14, no. 1, pp. 20–29, 2015.
[49] L. E. Gosselin, C. Adams, T. A. Cotter, R. J. Mccormick, and D. P. Thomas, "Effect of exercise training on passive stiffness in locomotor skeletal muscle: Role of extracellular matrix," *J. Appl. Physiol.*, vol. 85, no. 3, pp. 1011–1016, 1998.
[50] S. E. Brashear, R. P. Wohlgemuth, G. Gonzalez, and L. R. Smith, "Passive stiffness of fibrotic skeletal muscle in mdx mice relates to collagen architecture," *J. Physiol.*, vol. 599, no. 3, pp. 943–962, 2021.
[51] A. M. Collinsworth, S. Zhang, W. E. Kraus, and G. A. Truskey, "Apparent elastic modulus and hysteresis of skeletal muscle cells throughout differentiation," *Am. J. Physiol. - Cell Physiol.*, vol. 283, no. 4 52-4, pp. 1219–1227, 2002.
[52] W. E. Reyna, R. Pichika, D. Ludvig, and E. J. Perreault, "Efficiency of skeletal muscle decellularization methods and their effects on the extracellular matrix," *J. Biomech.*, vol. 110, p. 109961, 2020.
[53] B. A. Valentine, "Skeletal Muscle," in *Pathologic Basis of Veterinary Disease*, no. January, Elsevier, 2017, pp. 908-953.e1.
[54] J. Walters and A. Baborie, "Muscle biopsy: What and why and when?," *Pract. Neurol.*, vol. 20, no. 5, pp. 385–395, 2020.
[55] D. E. Stevens, C. B. Smith, B. Harwood, and C. L. Rice, "In vivo measurement of fascicle length and pennation of the human anconeus muscle at several elbow joint angles," *J. Anat.*, vol. 225, no. 5, pp. 502–509, 2014.
[56] D. A. Sleboda, K. K. Stover, and T. J. Roberts, "Diversity of extracellular matrix morphology in vertebrate skeletal muscle," *J. Morphol.*, vol. 281, no. 2, pp. 160–169, 2020.
[57] B. L. Gaspar, R. K. Vasishta, and B. D. Radotra, "Introduction to Normal Skeletal Muscle: Anatomy, Physiology, Histology, and Ultrastructure," in *Myopathology*, Singapore: Springer Singapore, 2019, pp. 1–10.
[58] W. Roman and E. R. Gomes, "Nuclear positioning in skeletal muscle," *Semin. Cell Dev. Biol.*, vol. 82, pp. 51–56, 2018.
[59] B. Cadot, V. Gache, and E. R. Gomes, "Moving and positioning the nucleus in skeletal muscle-one step at a time," *Nucleus*, vol. 6, no. 5, pp. 373–381, 2015.
[60] T. Metzger *et al.*, "MAP and kinesin-dependent nuclear positioning is required for skeletal muscle function," *Nature*, vol. 484, no. 7392, pp. 120–124, 2012.
[61] J. C. Bruusgaard, K. Liestøl, M. Ekmark, K. Kollstad, and K. Gundersen, "Number and spatial distribution of nuclei in the muscle fibres of normal mice studied in vivo," *J. Physiol.*, vol. 551, no. 2, pp. 467–478, 2003.
[62] A. Espigat-Georger, V. Dyachuk, C. Chemin, L. Emorine, and A. Merdes, "Nuclear alignment in myotubes requires centrosome proteins recruited by nesprin-1," *J. Cell Sci.*, vol. 129, no. 22, pp. 4227–4237, 2016.
[63] B. W. Infantolino, M. J. Ellis, and J. H. Challis, "Individual Sarcomere Lengths in Whole Muscle Fibers and Optimal Fiber Length Computation," *Anat. Rec.*, vol. 293, no. 11, pp.

1913–1919, 2010.
[64] J. M. Squire, "Muscle contraction: Sliding filament history, sarcomere dynamics and the two Huxleys," *Glob. Cardiol. Sci. Pract.*, vol. 2016, no. 2, 2016.
[65] W. R. Frontera and J. Ochala, "Skeletal Muscle : A Brief Review of Structure and Function," pp. 183–195, 2015.
[66] C. N. Maganaris, "Force-length characteristics of in vivo human skeletal muscle," *Acta Physiol. Scand.*, vol. 172, no. 4, pp. 279–285, 2001.
[67] D. S. Gokhin, S. R. Ward, S. N. Bremner, and R. L. Lieber, "Quantitative analysis of neonatal skeletal muscle functional improvement in the mouse," *J. Exp. Biol.*, vol. 211, no. 6, pp. 837–843, 2008.
[68] L. A. Lesniewski, T. A. Miller, and R. B. Armstrong, "Mechanisms of force loss in diabetic mouse skeletal muscle," *Muscle and Nerve*, vol. 28, no. 4, pp. 493–500, 2003.
[69] A. Bonetto, D. C. Andersson, and D. L. Waning, "Assessment of muscle mass and strength in mice," *Bonekey Rep.*, vol. 4, no. February, pp. 1–10, 2015.
[70] P. Hendrickse and H. Degens, "The role of the microcirculation in muscle function and plasticity," *J. Muscle Res. Cell Motil.*, vol. 40, no. 2, pp. 127–140, 2019.
[71] A. Krogh, "The number and distribution of capillaries in muscles with calculations of the oxygen pressure head necessary for supplying the tissue," *J. Physiol.*, vol. 52, no. 6, pp. 409–415, May 1919.
[72] S. S. Segal, "Regulation of blood flow in the microcirculation," *Microcirculation*, vol. 12, no. 1. pp. 33–45, 2005.
[73] E. Boulpaep *et al.*, "Medical Physiology a Cellular and Molecular Approach," *Signal Transduct*, 2009.
[74] M. P. WIEDEMANN, "Lengths and diameters of peripheral arterial vessels in the living animal.," *Circ. Res.*, vol. 10, pp. 686–690, 1962.
[75] M. P. WIEDEMAN, "Dimensions of blood vessels from distributing artery to collecting vein.," *Circ. Res.*, vol. 12, pp. 375–378, 1963.
[76] J. Shansky, J. Chromiak, M. Del Tatto, and H. Vandenburgh, "A simplified method for tissue engineering skeletal muscle organoids in vitro," *Vitr. Cell. Dev. Biol. - Anim.*, vol. 33, no. 9, pp. 659–661, Sep. 1997.
[77] D. L. Felten, M. K. O'Banion, and M. S. Maida, "Motor Systems," *Netter's Atlas Neurosci.*, pp. 391–420, 2016.
[78] M. A. Fox, "Development of the vertebrate neuromuscular junction," in *The Sticky Synapse: Cell Adhesion Molecules and Their Role in Synapse Formation and Maintenance*, New York, NY: Springer New York, 2009, pp. 39–84.
[79] J. L. Salzer, "Schwann cell myelination," *Cold Spring Harb. Perspect. Biol.*, vol. 7, no. 8, 2015.
[80] R. A. Jones *et al.*, "Cellular and Molecular Anatomy of the Human Neuromuscular Junction Cellular and Molecular Anatomy of the Human Neuromuscular Junction," *CellReports*, vol. 21, no. 9, pp. 2348–2356, 2017.
[81] H. Vandenburgh *et al.*, "Tissue-Engineered Skeletal Muscle Organoids for Reversible Gene Therapy," *Hum. Gene Ther.*, vol. 7, no. 17, pp. 2195–2200, Nov. 1996.
[82] T. Okano, S. Satoh, T. Oka, and T. Matsuda, "Tissue engineering of skeletal muscle. Highly dense, highly oriented hybrid muscular tissues biomimicking native tissues," *ASAIO J.*, vol. 43, no. 5, pp. M749-53, 1997.
[83] J. Shansky, M. Del Tatto, J. Chromiak, and H. Vandenburgh, "A simplified method for tissue engineering skeletal muscle organoids in vitro.," *In Vitro Cell. Dev. Biol. Anim.*, vol. 33, no. 9, pp. 659–661, 1997.
[84] D. J. R. Evans, S. Britland, and P. M. Wigmore, "Differential response of fetal and neonatal myoblasts to topographical guidance cues in vitro," *Dev. Genes Evol.*, vol. 209, no. 7, pp. 438–442, 1999.
[85] P. Clark, D. Coles, and M. Peckham, "Preferential adhesion to and survival on patterned

laminin organizes myogenesis in vitro," *Exp. Cell Res.*, vol. 230, no. 2, pp. 275–283, 1997.
[86] P. Clark, G. A. Dunn, A. Knibbs, and M. Peckham, "Alignment of myoblasts on ultrafine gratings inhibits fusion in vitro," *Int. J. Biochem. Cell Biol.*, vol. 34, no. 7, pp. 816–825, 2002.
[87] P. Clark, P. Connolly, A. S. Curtis, J. A. Dow, and C. D. Wilkinson, "Topographical control of cell behaviour: II. Multiple grooved substrata," *Development*, vol. 108, no. 4, pp. 635–644, Apr. 1990.
[88] M. T. Lam, S. Sim, X. Zhu, and S. Takayama, "The effect of continuous wavy micropatterns on silicone substrates on the alignment of skeletal muscle myoblasts and myotubes," *Biomaterials*, vol. 27, no. 24, pp. 4340–4347, 2006.
[89] K. Shimizu, H. Fujita, and E. Nagamori, "Micropatterning of single myotubes on a thermoresponsive culture surface using elastic stencil membranes for single-cell analysis," *J. Biosci. Bioeng.*, vol. 109, no. 2, pp. 174–178, 2010.
[90] V. Hosseini *et al.*, "Engineered contractile skeletal muscle tissue on a microgrooved methacrylated gelatin substrate," *Tissue Eng. - Part A*, vol. 18, no. 23–24, pp. 2453–2465, 2012.
[91] A. Grosberg, A. P. Nesmith, J. A. Goss, M. D. Brigham, M. L. Mccain, and K. K. Parker, "Journal of Pharmacological and Toxicological Methods Muscle on a chip : In vitro contractility assays for smooth and striated muscle," *J. Pharmacol. Toxicol. Methods*, vol. 65, no. 3, pp. 126–135, 2012.
[92] A. P. Nesmith *et al.*, "A human in vitro model of Duchenne muscular dystrophy muscle formation and contractility," *J. Cell Biol.*, vol. 215, no. 1, pp. 47–56, 2016.
[93] H. Takahashi, T. Shimizu, M. Nakayama, M. Yamato, and T. Okano, "The use of anisotropic cell sheets to control orientation during the self-organization of 3D muscle tissue," *Biomaterials*, vol. 34, no. 30, pp. 7372–7380, 2013.
[94] A. J. Engler, M. A. Griffin, S. Sen, C. G. Bönnemann, H. L. Sweeney, and D. E. Discher, "Myotubes differentiate optimally on substrates with tissue-like stiffness: Pathological implications for soft or stiff microenvironments," *J. Cell Biol.*, vol. 166, no. 6, pp. 877–887, 2004.
[95] T. Sasagawa *et al.*, "Design of prevascularized three-dimensional cell-dense tissues using a cell sheet stacking manipulation technology," *Biomaterials*, vol. 31, no. 7, pp. 1646–1654, 2010.
[96] D. Huh, Y. Torisawa, G. A. Hamilton, J. Kim, and D. E. Ingber, "Lab on a Chip Microengineered physiological biomimicry : Organs-on-Chips {," pp. 2156–2164, 2012.
[97] T. Osaki, V. Sivathanu, and R. D. Kamm, "Vascularized microfluidic organ-chips for drug screening, disease models and tissue engineering," *Curr. Opin. Biotechnol.*, vol. 52, pp. 116–123, 2018.
[98] B. Zhang and M. Radisic, "Organ-on-A-chip devices advance to market," *Lab Chip*, vol. 17, no. 14, pp. 2395–2420, 2017.
[99] C. Oleaga *et al.*, "Multi-Organ toxicity demonstration in a functional human in vitro system composed of four organs," *Nat. Publ. Gr.*, no. August 2015, pp. 1–17, 2016.
[100] S. N. Bhatia and D. E. Ingber, "Microfluidic organs-on-chips," *Nat. Biotechnol.*, vol. 32, no. 8, pp. 760–772, 2014.
[101] K. Yue *et al.*, "Synthesis, properties, and biomedical applications of gelatin methacryloyl (GelMA) hydrogels," *Biomaterials*, vol. 73, no. 3, pp. 254–271, 2016.
[102] H. Aubin *et al.*, "Directed 3D cell alignment and elongation in microengineered hydrogels," *Biomaterials*, vol. 31, no. 27, pp. 6941–6951, 2010.
[103] S. Ostrovidov *et al.*, "Three-dimensional co-culture of C2C12/PC12 cells improves skeletal muscle tissue formation and function," *J. Tissue Eng. Regen. Med.*, vol. 11, no. 2, pp. 582–595, 2017.
[104] K. Shimizu, H. Araki, K. Sakata, W. Tonomura, M. Hashida, and S. Konishi, "Microfluidic devices for construction of contractile skeletal muscle microtissues," *Journal of Bioscience and*

Bioengineering, vol. 119, no. 2. pp. 212–216, 2015.
[105] M. Costantini *et al.*, "Engineering muscle networks in 3d gelatin methacryloyl hydrogels: Influence of mechanical stiffness and geometrical confinement," *Front. Bioeng. Biotechnol.*, vol. 5, no. APR, pp. 1–8, 2017.
[106] Y.-C. Huang, R. G. Dennis, L. Larkin, and K. Baar, "Rapid formation of functional muscle in vitro using fibrin gels," *J. Appl. Physiol.*, vol. 98, no. 2, pp. 706–713, 2005.
[107] C. Hernández-Sánchez *et al.*, "Differential regulation of insulin-like growth factor-I (IGF-I) receptor gene expression by IGF-I and basic fibroblastic growth factor," *J. Biol. Chem.*, vol. 272, no. 8, pp. 4663–4670, 1997.
[108] M. T. Lam, Y. C. Huang, R. K. Birla, and S. Takayama, "Microfeature guided skeletal muscle tissue engineering for highly organized 3-dimensional free-standing constructs," *Biomaterials*, vol. 30, no. 6, pp. 1150–1155, 2009.
[109] C. A. Powell, B. L. Smiley, J. Mills, and H. H. Vandenburgh, "Mechanical stimulation improves tissue-engineered human skeletal muscle," *https://doi.org/10.1152/ajpcell.00595.2001*, vol. 283, no. 5, pp. C1557–C1565, 2002.
[110] L. Madden, M. Juhas, W. E. Kraus, G. A. Truskey, and N. Bursac, "Bioengineered human myobundles mimic clinical responses of skeletal muscle to drugs," *Elife*, vol. 2015, no. 4, 2015.
[111] G. Agrawal, A. Aung, and S. Varghese, "Skeletal muscle-on-a-chip: An in vitro model to evaluate tissue formation and injury," *Lab Chip*, vol. 17, no. 20, pp. 3447–3461, 2017.
[112] T. Osaki, S. G. M. Uzel, and R. D. Kamm, "Microphysiological 3D model of amyotrophic lateral sclerosis (ALS) from human iPS-derived muscle cells and optogenetic motor neurons," *Sci. Adv.*, vol. 4, no. 10, p. eaat5847, 2018.
[113] T. Neumann, S. D. Hauschka, and J. E. Sanders, "Tissue Engineering of Skeletal Muscle Using Polymer Fiber Arrays," *Tissue Eng.*, vol. 9, no. 5, pp. 995–1003, 2003.
[114] H. G. Yevick, G. Duclos, I. Bonnet, and P. Silberzan, "Architecture and migration of an epithelium on a cylindrical wire," *Proc. Natl. Acad. Sci. U. S. A.*, vol. 112, no. 19, pp. 5944–5949, 2015.
[115] F. A. Maechler, C. Allier, A. Roux, and C. Tomba, "Curvature-dependent constraints drive remodeling of epithelia," *J. Cell Sci.*, vol. 132, no. 4, pp. 1–12, 2019.
[116] D. Neal, M. S. Sakar, L. L. S. Ong, and H. Harry Asada, "Formation of elongated fascicle-inspired 3D tissues consisting of high-density, aligned cells using sacrificial outer molding," *Lab Chip*, vol. 14, no. 11, pp. 1907–1916, 2014.
[117] G. Talò *et al.*, "Engineering an Environment for the Study of Fibrosis: A 3D Human Muscle Model with Endothelium Specificity and Endomysium," *Cell Rep.*, vol. 25, no. 13, pp. 3858-3868.e4, 2018.
[118] T. Osaki, V. Sivathanu, and R. D. Kamm, "Crosstalk between developing vasculature and optogenetically engineered skeletal muscle improves muscle contraction and angiogenesis," *Biomaterials*, vol. 156, pp. 65–76, 2018.
[119] A. Urciuolo *et al.*, "Engineering a 3D in vitro model of human skeletal muscle at the single fiber scale," *PLoS One*, vol. 15, no. 5, pp. 1–17, 2020.
[120] M. Verhulsel, M. E. Shivokhin, A. Simon, S. Descroix, C. Frétigny, and L. Talini, "High bandwidth noninvasive measurements of the linear viscoelasticity of collagen gels," *J. Rheol. (N. Y. N. Y).*, vol. 60, no. 6, pp. 1269–1278, 2016.
[121] B. Venzac *et al.*, "PDMS Curing Inhibition on 3D-Printed Molds: Why? Also, How to Avoid It?," *Anal. Chem.*, vol. 93, no. 19, pp. 7180–7187, 2021.
[122] Y. J. Chuah, S. Kuddannaya, M. H. A. Lee, Y. Zhang, and Y. Kang, "The effects of poly(dimethylsiloxane) surface silanization on the mesenchymal stem cell fate," *Biomater. Sci.*, vol. 3, no. 2, pp. 383–390, 2015.
[123] W. Tan and T. A. Desai, "Layer-by-layer microfluidics for biomimetic three- dimensional structures," vol. 25, pp. 1355–1364, 2004.

[124] L. Yu, C. M. Li, and Q. Zhou, "Efficient probe immobilization on poly (dimethylsiloxane) for sensitive detection of proteins," pp. 2848–2855, 2005.
[125] P. J. Wipff, H. Majd, C. Acharya, L. Buscemi, J. J. Meister, and B. Hinz, "The covalent attachment of adhesion molecules to silicone membranes for cell stretching applications," *Biomaterials*, vol. 30, no. 9, pp. 1781–1789, 2009.
[126] S. Kuddannaya *et al.*, "Surface Chemical Modi fi cation of Poly (dimethylsiloxane) for the Enhanced Adhesion and Proliferation of Mesenchymal Stem Cells," 2013.
[127] V. C. Pinto, G. Minas, and M. Correia-Neves, "PDMS biofunctionalization study for the development of a microfluidic device: Application to salivary cortisol," *Proc. - 2015 IEEE 4th Port. Meet. Bioeng. ENBENG 2015*, 2015.
[128] Z. Qian, D. Ross, W. Jia, Q. Xing, and F. Zhao, "Bioactive polydimethylsiloxane surface for optimal human mesenchymal stem cell sheet culture," *Bioact. Mater.*, vol. 3, no. 2, pp. 167–173, 2018.
[129] A. Gokaltun, M. L. Yarmush, A. Asatekin, and O. B. Usta, "Recent advances in nonbiofouling PDMS surface modification strategies applicable to microfluidic technology," *Technology*, vol. 05, no. 01, pp. 1–12, 2017.
[130] X. Bao, K. Hayashi, Y. Li, A. Teramoto, and K. Abe, "Novel agarose and agar fibers: Fabrication and characterization," *Mater. Lett.*, vol. 64, no. 22, pp. 2435–2437, Nov. 2010.
[131] N. Vol, "Serial passaging and differentiation of myogenic cells isolated from dystrophic mouse muscle," vol. 270, no. December, pp. 725–727, 1977.
[132] P.-G. De Gennes, F. Brochard-Wyart, and D. Quéré, *Capillarity and wetting phenomena: drops, bubbles, pearls, waves*. Springer Science & Business Media, 2013.
[133] S. Haefner *et al.*, "Influence of slip on the Plateau-Rayleigh instability on a fibre," *Nat. Commun.*, vol. 6, no. March, 2015.
[134] F. Boulogne, M. A. Fardin, S. Lerouge, L. Pauchard, and F. Giorgiutti-Dauphiné, "Suppression of the Rayleigh-Plateau instability on a vertical fibre coated with wormlike micelle solutions," *Soft Matter*, vol. 9, no. 32, pp. 7787–7796, 2013.
[135] A. Zolkiewska, W. C. Thompson, and J. Moss, "Interaction of integrin α7β1 in C2C12 myotubes and in solution with laminin," *Experimental Cell Research*, vol. 240, no. 1. pp. 86–94, 1998.
[136] I. Boraschi-Diaz, J. Wang, J. S. Mort, and S. V. Komarova, "Collagen type i as a ligand for receptor-mediated signaling," *Front. Phys.*, vol. 5, no. MAY, pp. 1–11, 2017.
[137] N. Davidenko *et al.*, "Evaluation of cell binding to collagen and gelatin: a study of the effect of 2D and 3D architecture and surface chemistry," *J. Mater. Sci. Mater. Med.*, vol. 27, no. 10, 2016.
[138] C. C. Yao, B. L. Ziober, A. E. Sutherland, D. L. Mendrick, and R. H. Kramer, "Laminins promote the locomotion of skeletal myoblasts via the alpha 7 integrin receptor," *J. Cell Sci.*, vol. 109, no. 13, pp. 3139–3150, 1996.
[139] Gorgieva Selestina; Kokol Vanja; Pignatello Rosario, "Collagen- vs. Gelatine-Based Biomaterials and Their Biocompatibility: Review and Perspectives, Biomaterials Applications for Nanomedicine," *IntechOpen*, pp. 1–36, 2011.
[140] E. Ugarte-Berzal, J. Vandooren, E. Bailón, G. Opdenakker, and A. García-Pardo, "Inhibition of MMP-9-dependent degradation of gelatin, but not other MMP-9 substrates, by the MMP-9 hemopexin domain blades 1 and 4," *J. Biol. Chem.*, vol. 291, no. 22, pp. 11751–11760, 2016.
[141] Gentian Lluri and Diane M. Jaworski, "Regulation of TIMP-2, MT1-MMP, and MMP-2 expression during C2C12 differentiation," *Nat Rev Mol Cell Biol.*, vol. 10 (2), no. 1, pp. 116–125, 2009.
[142] N. Jaccard *et al.*, "Automated method for the rapid and precise estimation of adherent cell culture characteristics from phase contrast microscopy images," *Biotechnol. Bioeng.*, vol. 111, no. 3, pp. 504–517, 2014.

[143] B. Sun, K. Xie, T. H. Chen, and R. H. W. Lam, "Preferred cell alignment along concave microgrooves," *RSC Adv.*, vol. 7, no. 11, pp. 6788–6794, 2017.
[144] W. W. Ahmed *et al.*, "Myoblast morphology and organization on biochemically micro-patterned hydrogel coatings under cyclic mechanical strain," *Biomaterials*, vol. 31, no. 2, pp. 250–258, 2010.
[145] R. M. Smeal, R. Rabbitt, R. Biran, and P. A. Tresco, "Substrate curvature influences the direction of nerve outgrowth," *Ann. Biomed. Eng.*, vol. 33, no. 3, pp. 376–382, 2005.
[146] S. J. P. Callens, R. J. C. Uyttendaele, L. E. Fratila-Apachitei, and A. A. Zadpoor, "Substrate curvature as a cue to guide spatiotemporal cell and tissue organization," *Biomaterials*, vol. 232, no. December 2019, p. 119739, 2020.
[147] M. Rumpler, A. Woesz, J. W. C. Dunlop, J. T. Van Dongen, and P. Fratzl, "The effect of geometry on three-dimensional tissue growth," *J. R. Soc. Interface*, vol. 5, no. 27, pp. 1173–1180, 2008.
[148] W. Xi, S. Sonam, T. Beng Saw, B. Ladoux, and C. Teck Lim, "Emergent patterns of collective cell migration under tubular confinement," *Nat. Commun.*, vol. 8, no. 1, 2017.
[149] V. Hosseini *et al.*, "Fiber-Assisted Molding (FAM) of Surfaces with Tunable Curvature to Guide Cell Alignment and Complex Tissue Architecture," 2014.
[150] S. Romanazzo *et al.*, "Substrate stiffness affects skeletal myoblast differentiation in vitro," vol. 13, 2012.
[151] M. Levy-Mishali, J. Zoldan, and S. Levenberg, "Effect of Scaffold Stiffness on Myoblast Differentiation," *Tissue Eng. Part A*, vol. 15, no. 4, pp. 935–944, Apr. 2009.
[152] J. Joshi, G. Mahajan, and C. R. Kothapalli, "Three-dimensional collagenous niche and azacytidine selectively promote time-dependent cardiomyogenesis from human bone marrow-derived MSC spheroids," *Biotechnology and Bioengineering*, vol. 115, no. 8. pp. 2013–2026, 2018.
[153] M. Lama *et al.*, "Biomimetic Tough Gels with Weak Bonds Unravel the Role of Collagen from Fibril to Suprafibrillar Self-Assembly," *Macromol. Biosci.*, vol. 21, no. 6, pp. 1–10, 2021.
[154] A. S. Williams, L. Kang, and D. H. Wasserman, "The extracellular matrix and insulin resistance," *Trends Endocrinol. Metab.*, vol. 26, no. 7, pp. 357–366, Jul. 2015.
[155] P. S. Zammit, "Function of the myogenic regulatory factors Myf5, MyoD, Myogenin and MRF4 in skeletal muscle, satellite cells and regenerative myogenesis," *Semin. Cell Dev. Biol.*, vol. 72, pp. 19–32, 2017.
[156] S. Schiaffino and C. Reggiani, "Fiber types in Mammalian skeletal muscles," *Physiol. Rev.*, vol. 91, no. 4, pp. 1447–1531, 2011.
[157] E. van der Wal *et al.*, "Large-Scale Expansion of Human iPSC-Derived Skeletal Muscle Cells for Disease Modeling and Cell-Based Therapeutic Strategies," *Stem Cell Reports*, vol. 10, no. 6, pp. 1975–1990, 2018.
[158] R. Michna, M. Gadde, A. Ozkan, M. DeWitt, and M. Rylander, "Vascularized microfluidic platforms to mimic the tumor microenvironment," *Biotechnol. Bioeng.*, vol. 115, no. 11, pp. 2793–2806, 2018.
[159] W. J. Polacheck, M. L. Kutys, J. B. Tefft, and C. S. Chen, *Microfabricated blood vessels for modeling the vascular transport barrier*, vol. 14, no. 5. Springer US, 2019.
[160] I. K. Zervantonakis, S. K. Hughes-Alford, J. L. Charest, J. S. Condeelis, F. B. Gertler, and R. D. Kamm, "Three-dimensional microfluidic model for tumor cell intravasation and endothelial barrier function," *Proc. Natl. Acad. Sci. U. S. A.*, vol. 109, no. 34, pp. 13515–13520, 2012.
[161] S. Kim, H. Lee, M. Chung, and N. L. Jeon, "Engineering of functional, perfusable 3D microvascular networks on a chip," *Lab Chip*, vol. 13, no. 8, pp. 1489–1500, 2013.
[162] J. Kim, M. Chung, S. Kim, D. H. Jo, J. H. Kim, and N. L. Jeon, "Engineering of a biomimetic pericyte-covered 3D microvascular network," *PLoS One*, vol. 10, no. 7, pp. 1–15, 2015.
[163] J. S. Miller *et al.*, "Rapid casting of patterned vascular networks for perfusable engineered

three-dimensional tissues," *Nat. Mater.*, vol. 11, no. 9, pp. 768–774, 2012.
[164] A. M. A. O. Pollet, "Recapitulating the Vasculature Using Organ-On-Chip Technology," pp. 1–18, 2020.
[165] C. F. Buchanan, S. S. Verbridge, P. P. Vlachos, and M. N. Rylander, "Flow shear stress regulates endothelial barrier function and expression of angiogenic factors in a 3D microfluidic tumor vascular model," *Cell Adhes. Migr.*, vol. 8, no. 5, pp. 517–524, 2014.
[166] S. Chatterjee, "Endothelial mechanotransduction, redox signaling and the regulation of vascular inflammatory pathways," *Front. Physiol.*, vol. 9, no. JUN, pp. 1–16, 2018.
[167] G. M. Price and J. Tien, "Methods for Forming Human Microvascular Tubes In Vitro and Measuring Their Macromolecular Permeability," in *Dialogue*, vol. 671, no. 1, 2011, pp. 281–293.
[168] V. Van Duinen *et al.*, "96 Perfusable Blood Vessels To Study Vascular Permeability in Vitro," *Sci. Rep.*, vol. 7, no. 1, pp. 1–11, 2017.
[169] W. J. Polacheck *et al.*, "A non-canonical Notch complex regulates adherens junctions and vascular barrier function," *Nature*, vol. 552, no. 7684, pp. 258–262, 2017.
[170] W. J. Polacheck, M. L. Kutys, J. B. Tefft, and C. S. Chen, *Microfabricated blood vessels for modeling the vascular transport barrier*, vol. 14, no. 5. Springer US, 2019.
[171] J. J. Chiu and S. Chien, "Effects of disturbed flow on vascular endothelium: Pathophysiological basis and clinical perspectives," *Physiol. Rev.*, vol. 91, no. 1, pp. 327–387, 2011.
[172] C. M. Warboys, N. Amini, A. De Luca, and P. C. Evans, "The role of blood flow in determining the sites of atherosclerotic plaques," *F1000 Med. Rep.*, vol. 3, no. 1, pp. 1–8, 2011.
[173] D. A. Chistiakov, A. N. Orekhov, and Y. V. Bobryshev, "Effects of shear stress on endothelial cells: go with the flow," *Acta Physiol.*, vol. 219, no. 2, pp. 382–408, 2017.
[174] D. Gholobova *et al.*, "Endothelial Network Formation Within Human Tissue-Engineered Skeletal Muscle," *Tissue Eng. Part A*, vol. 21, no. 19–20, pp. 2548–2558, 2015.
[175] A. L. Mackey, M. Magnan, B. Chazaud, and M. Kjaer, "Human skeletal muscle fibroblasts stimulate in vitro myogenesis and in vivo muscle regeneration," *J. Physiol.*, vol. 595, no. 15, pp. 5115–5127, 2017.
[176] M. R. Hicks, T. V. Cao, D. H. Campbell, and P. R. Standley, "Mechanical strain applied to human fibroblasts differentially regulates skeletal myoblast differentiation," *J. Appl. Physiol.*, vol. 113, no. 3, pp. 465–472, 2012.
[177] B. K. Pedersen, A. Steensberg, and P. Schjerling, "Muscle-derived interleukin-6: Possible biological effects," *J. Physiol.*, vol. 536, no. 2, pp. 329–337, 2001.
[178] X. Liu *et al.*, "Type i collagen promotes the migration and myogenic differentiation of C2C12 myoblasts: Via the release of interleukin-6 mediated by FAK/NF-κB p65 activation," *Food and Function*, vol. 11, no. 1. pp. 328–338, 2020.
[179] W. Zhao, X. Wang, K. H. Sun, and L. Zhou, "A-Smooth Muscle Actin Is Not a Marker of Fibrogenic Cell Activity in Skeletal Muscle Fibrosis," *PLoS ONE*, vol. 13, no. 1. 2018.
[180] I. A. Darby, N. Zakuan, F. Billet, and A. Desmoulière, "The myofibroblast, a key cell in normal and pathological tissue repair," *Cell. Mol. Life Sci.*, vol. 73, no. 6, pp. 1145–1157, 2016.
[181] Y. H. Yen *et al.*, "Curcumin accelerates cutaneous wound healing via multiple biological actions: The involvement of TNF-α, MMP-9, α-SMA, and collagen," *Int. Wound J.*, vol. 15, no. 4, pp. 605–617, 2018.
[182] M. A. Bakooshli *et al.*, "A three-dimensional culture model of innervated human skeletal muscle enables studies of the adult neuromuscular junction and disease modeling," *bioRxiv*, pp. 1–29, 2018.
[183] R. R. Besser *et al.*, "A Chemically Defined Common Medium for Culture of C2C12 Skeletal Muscle and Human Induced Pluripotent Stem Cell Derived Spinal Spheroids," *Cell. Mol. Bioeng.*, vol. 13, no. 3, 2020.

[184] S. E. Park, A. Georgescu, J. M. Oh, K. W. Kwon, and D. Huh, "Polydopamine-Based Interfacial Engineering of Extracellular Matrix Hydrogels for the Construction and Long-Term Maintenance of Living Three-Dimensional Tissues," *ACS Appl. Mater. Interfaces*, vol. 11, no. 27, pp. 23919–23925, 2019.
[185] Y. H. Ding, M. Floren, and W. Tan, "Mussel-inspired polydopamine for bio-surface functionalization," *Biosurface and Biotribology*, vol. 2, no. 4, pp. 121–136, 2016.
[186] D. Salvatore, W. S. Simonides, M. Dentice, A. M. Zavacki, and P. R. Larsen, "Thyroid hormones and skeletal muscle - New insights and potential implications," *Nat. Rev. Endocrinol.*, vol. 10, no. 4, pp. 206–214, 2014.
[187] D. A. Stoltz, D. K. Meyerholz, and M. J. Welsh, "Origins of Cystic Fibrosis Lung Disease," *N. Engl. J. Med.*, vol. 372, no. 4, pp. 351–362, 2015.
[188] R. Plebani *et al.*, "Modeling pulmonary cystic fibrosis in a human lung airway-on-a-chip: Cystic fibrosis airway chip," *J. Cyst. Fibros.*, no. xxxx, 2021.
[189] K. Shik Mun *et al.*, "Patient-derived pancreas-on-a-chip to model cystic fibrosis-related disorders," *Nat. Commun.*, vol. 10, no. 1, 2019.

RÉSUMÉ

L'essor de la microfluidique en biologie a conduit la communauté scientifique à développer des modèles in vitro de différents organes, initiant ainsi le domaine des organes sur puce. Ceux-ci ont but d'apporter un modèle biomimétique complémentaire aux systèmes traditionnels, avec une transposition plus fiable des résultats chez l'Homme. Nous nous sommes plus particulièrement intéressés au muscle squelettique. Le muscle squelettique in vivo se compose de longues cellules musculaires, alignées dans l'axe longitudinal du muscle, regroupées en fascicules. Plusieurs fascicules forment le muscle. La matrice extracellulaire (MEC) principalement composée de collagène I segmente ces parties et abrite d'autres types cellulaires. Reproduire un muscle squelettique in vitro requiert donc un pré alignement des cellules dans un hydrogel bio compatible. L'objectif était de déterminer les éléments clefs nécessaires à la génération d'un tissu musculaire squelettique biomimétique en système microfluidique tubulaire. Nous avons donc développé une puce microfluidique, composée de tubes parallèles et indépendants en collagène I. Pour des tubes en collagène de 200 µm de diamètre, l'ensemencement des cellules C2C12 suspendues dans du milieu de culture ne permettait pas de reproduire l'architecture du muscle, les cellules musculaires s'organisant sous forme de lumen. Afin de modifier l'auto-organisation cellulaire, nous avons évalué l'effet d'un ensemencement en présence de MEC permettant une adhésion des cellules dans toute la section du tube, mais aussi une approche d'ensemencement séquentiel permettant aux cellules de reposer sur un matériau de rigidité appropriée. Bien que cette dernière approche permettait un meilleur alignement des myotubes, l'organisation en lumen persistait pour ces deux conditions. Puis nous avons évalué l'effet d'un substrat de courbure trois fois supérieure (75 µm de diamètre) sur l'organisation cellulaire. Dans ce cas, les cellules colonisaient l'intégralité du volume disponible du tube en collagène. Comme précédemment, différentes conditions d'ensemencement ont été évaluées. Nos résultats ont montré ici que les cellules ensemencées dans du milieu de culture permettaient un meilleur alignement des myotubes le long de l'axe, un meilleur alignement des noyaux parallèles aux myotubes, la formation de myotubes striés, ainsi qu'une augmentation des gènes de différentiation musculaire. En revanche, les cellules ensemencées en présence de MEC généraient des myotubes ramifiés d'aspect hétérogène, avec un indicateur de fusion cellulaire et un diamètre moyen significativement plus grands. Ces caractéristiques sont retrouvées dans certaines myopathies. En parallèle, nous avons montré la versatilité de notre système en développant un vaisseau sur puce de 200 µm de diamètre en utilisant des cellules primaires endothéliales humaines, l'objectif étant de reproduire l'écosystème musculaire et notamment les autres types cellulaires. L'intégrité morphologique et fonctionnelle de ce vaisseau sur puce a été caractérisée par immunomarquage des jonctions adhérentes, par des études de perméabilité vasculaire, d'adhésion leucocytaire et de biologie moléculaire par RT-qPCR. Cependant, les premiers essais de co-culture avec les C2C12 se sont heurtés à une incompatibilité des milieux de cultures. Nous avons également mis en œuvre la co-culture des C2C12 avec la lignée fibroblastique NIH 3T3 permettant la génération de myotubes ayant la même maturation sur le plan morphologique, que ceux générés précédemment en mono culture dans les tubes en collagène de 75 µm. Néanmoins, la co-culture permettait une meilleure maturation sur le plan moléculaire, avec une expression augmentée des gènes de différentiation musculaire. Les perspectives à venir seront d'y cultiver des cellules primaires/souches induites, permettant de créer des modèles de pathologies et d'étudier l'influence sur le tissu musculaire de traitements perfusés dans le vaisseau sur puce.

MOTS CLÉS

Organe-sur-puce, microfluidique, ingénierie tissulaire, myopathies, vascularisation, microfabrication

ABSTRACT

Advances in microfluidics and especially in biology prompted scientists to develop in vitro organs models, thus initiating the organ-on-chip technology. The aim is to bring complementary biomimetic models to traditional ones with results more faithfully transposable to Human. We were particularly interested in the skeletal muscle. In vivo skeletal muscle is made of long muscle cells, aligned parallel to the longitudinal axis, gathered into fascicles. Several fascicules constitute the whole muscle. Extracellular matrix (ECM), mainly composed of collagen I, compartmentalizes those structures and hosts many other cell types. Recapitulating a skeletal muscle in vitro therefore required cell pre alignment, embedded in a bio compatible hydrogel. The objective was to determine the key cues required to generate a biomimetic skeletal muscle in a tubular system. We developed a microfluidic chip, composed of independent and parallel collagen I hollow tubes. Within 200 µm diameter collagen tubes, seeding C2C12 cells in growth medium did not faithfully recapitulate the skeletal muscle architecture, cells organizing into in a lumen structure. To modify muscle cells self-organization, we investigated the effect of cell seeding in the presence of ECM, allowing cells to adhere through the whole collagen tube section, as well as a sequential seeding approach, giving to cells an appropriate substrate stiffness. The lumen organization still remained when seeding cells mixed with ECM or for sequential seeding. However, this latest seeding condition resulted in a higher myotubes alignment toward the long axis of the collagen tube. We then evaluated the effect of a substrate with 3-folds higher curvature (tube of 75 µm) on cell self-organization. In this case, muscle cells colonized the whole available volume of the collagen tube. Seeding cells suspended in growth medium resulted in a better cell organization with higher aligned myotubes toward the long axis, a better nuclei alignment parallel to the myotubes, the formation of striated myotubes, and an upregulation of muscle differentiation genes. On the other hand, cells mixed with ECM generated branched and heterogeneous myotubes, with larger diameter and higher fusion indicator. This is similar to what we find in some myopathies. In parallel, we demonstrated the versatility of our system by generating a micro vessel-on-chip of 200 µm diameter using human primary endothelial cells, the objective being to recapitulate the skeletal muscle ecosystem and the other cell types. Investigations by immunostaining of adherent junction (VE-cadherin), vascular permeability, leukocytes adhesion and molecular biology with RT-qPCR showed the morphological and functional integrity of the vessel-on-chip. However, the first results of co-culture with C2C12 cells encountered medium incompatibility, leading to a high cell death. We also performed co-cultures of C2C12 with NIH 3T3 fibroblast cell line, allowing the generation of myotubes with the same morphological maturation as the one generated previously in mono culture within 75 µm collagen tubes. However, this co-culture allowed a better myotubes maturation on a molecular point of view, with an upregulation of the muscle differentiation genes.

This micro device is promising and future perspectives include cultivating primary cells or induced pluripotent stem cells. This would allow us to create diseases models and to study the impact of perfused drugs through the vessel, on the muscle-construct.

KEYWORDS

Organ-on-chip, microfluidics, tissue engineering, myopathies, vascularization, mirofabrication.